



# Investigation of non-equilibrium crystallization of mixed gas clathrates hydrates : an experimental study compared to thermodynamic modeling with and without flash calculations

Quang-Du Le

## ► To cite this version:

Quang-Du Le. Investigation of non-equilibrium crystallization of mixed gas clathrates hydrates : an experimental study compared to thermodynamic modeling with and without flash calculations. Other. Université de Lyon, 2016. English. NNT : 2016LYSEM002 . tel-01665152

**HAL Id: tel-01665152**

**<https://theses.hal.science/tel-01665152>**

Submitted on 15 Dec 2017

**HAL** is a multi-disciplinary open access archive for the deposit and dissemination of scientific research documents, whether they are published or not. The documents may come from teaching and research institutions in France or abroad, or from public or private research centers.

L'archive ouverte pluridisciplinaire **HAL**, est destinée au dépôt et à la diffusion de documents scientifiques de niveau recherche, publiés ou non, émanant des établissements d'enseignement et de recherche français ou étrangers, des laboratoires publics ou privés.



NNT: **2016LYSEM002**

## **THÈSE**

présentée par

**Quang-Du LE**

pour obtenir le grade de

Docteur de l'École Nationale Supérieure des Mines de Saint-Étienne

Spécialité : Génie des Procédés

# **INVESTIGATION DE LA CRISTALLISATION HORS-ÉQUILIBRE DES CLATHRATES HYDRATES DE GAZ MIXTES: UNE ÉTUDE EXPÉRIMENTALE COMPARÉE À LA MODÉLISATION THERMODYNAMIQUE AVEC ET SANS CALCULS FLASH**

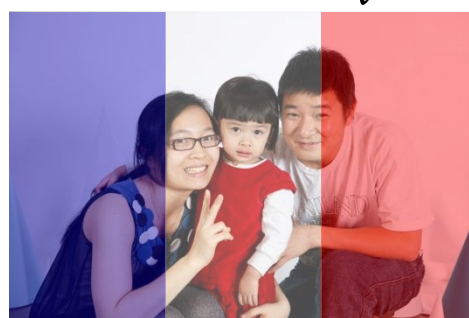
soutenue à Saint-Étienne, le 09 mars 2016

Membres du jury

Rapporteurs:	<b>Ryo OHMURA</b>	Keio University, Yokohama, Japan
	<b>Karine BALLERAT-BUSSEROLLES</b>	Université Blaise-Pascal, Ingénieure de Recherche CNRS
Examineurs:	<b>Eric CHASSEFIERE</b>	Université Paris-Sud
	<b>Pierre DUCHET-SUCHAUX</b>	TOTAL SA, Paris
	<b>Baptiste BOUILLOT</b>	EMSE, Co-Encadrant
	<b>Jean-Michel HERRI</b>	EMSE, Encadrant HDR
Invité:	<b>Freddy GARCIA</b>	TOTAL SA, Paris

Spécialités doctorales	Responsables :		Spécialités doctorales	Responsables
SCIENCES ET GENIE DES MATERIAUX	K. Wolski Directeur de recherche		MATHEMATIQUES APPLIQUEES	O. Roustant, Maître-assistant
MECANIQUE ET INGENIERIE	S. Drapier, professeur		INFORMATIQUE	O. Boissier, Professeur
GENIE DES PROCEDES	F. Gruy, Maître de recherche		IMAGE, VISION, SIGNAL	JC. Pinoli, Professeur
SCIENCES DE LA TERRE	B. Guy, Directeur de recherche		GENIE INDUSTRIEL	A. Dolgui, Professeur
SCIENCES ET GENIE DE L'ENVIRONNEMENT	D. Graillot, Directeur de recherche		MICROELECTRONIQUE	S. Dauzere Peres, Professeur
<b>EMSE : Enseignants-chercheurs et chercheurs autorisés à diriger des thèses de doctorat (titulaires d'un doctorat d'État ou d'une HDR)</b>				
ABSI	Nabil	CR	Génie industriel	CMP
AVRIL	Stéphane	PR2	Mécanique et ingénierie	CIS
BALBO	Flavien	PR2	Informatique	FAYOL
BASSEREAU	Jean-François	PR	Sciences et génie des matériaux	SMS
BATTALA-GUSCHINSKAYA	Olga	CR	Génie industriel	FAYOL
BATTON-HUBERT	Mireille	PR2	Sciences et génie de l'environnement	FAYOL
BERGER DOUCE	Sandrine	PR2	Sciences de gestion	FAYOL
BIGOT	Jean Pierre	MR(DR2)	Génie des Procédés	SPIN
BILAL	Essaïd	DR	Sciences de la Terre	SPIN
BLAYAC	Sylvain	MA(MDC)	Microélectronique	CMP
BOISSIER	Olivier	PR1	Informatique	FAYOL
BONNEFOY	Olivier	MA(MDC)	Génie des Procédés	SPIN
BORBELY	Andras	MR(DR2)	Sciences et génie des matériaux	SMS
BOUCHER	Xavier	PR2	Génie Industriel	FAYOL
BRODHAG	Christian	DR	Sciences et génie de l'environnement	FAYOL
BRUCHON	Julien	MA(MDC)	Mécanique et ingénierie	SMS
BURLAT	Patrick	PR1	Génie Industriel	FAYOL
COURNIL	Michel	PR0	Génie des Procédés	DIR
DAUZERE-PERES	Stéphane	PR1	Génie Industriel	CMP
DEBAYLE	Johan	CR	Image Vision Signal	CIS
DELAFOSSSE	David	PR0	Sciences et génie des matériaux	SMS
DELORME	Xavier	MA(MDC)	Génie industriel	FAYOL
DESRAYAUD	Christophe	PR1	Mécanique et ingénierie	SMS
DOLGUI	Alexandre	PR0	Génie Industriel	FAYOL
DRAPIER	Sylvain	PR1	Mécanique et ingénierie	SMS
FAVERGEON	Loïc	CR	Génie des Procédés	SPIN
FEILLET	Dominique	PR1	Génie Industriel	CMP
FRACZKIEWICZ	Anna	DR	Sciences et génie des matériaux	SMS
GARCIA	Daniel	MR(DR2)	Génie des Procédés	SPIN
GAVET	Yann	MA(MDC)	Image Vision Signal	CIS
GERINGER	Jean	MA(MDC)	Sciences et génie des matériaux	CIS
GOEURIOT	Dominique	DR	Sciences et génie des matériaux	SMS
GONDRAN	Natacha	MA(MDC)	Sciences et génie de l'environnement	FAYOL
GRAILLOT	Didier	DR	Sciences et génie de l'environnement	SPIN
GROSSEAU	Philippe	DR	Génie des Procédés	SPIN
GRUY	Frédéric	PR1	Génie des Procédés	SPIN
GUY	Bernard	DR	Sciences de la Terre	SPIN
HAN	Woo-Suck	MR	Mécanique et ingénierie	SMS
HERRI	Jean Michel	PR1	Génie des Procédés	SPIN
KERMOUCHE	Guillaume	PR2	Mécanique et Ingénierie	SMS
KLOCKER	Helmut	DR	Sciences et génie des matériaux	SMS
LAFOREST	Valérie	MR(DR2)	Sciences et génie de l'environnement	FAYOL
LERICHE	Rodolphe	CR	Mécanique et ingénierie	FAYOL
LI	Jean-Michel		Microélectronique	CMP
MALLIARAS	Georges	PR1	Microélectronique	CMP
MAURINE	Philippe	Ingénieur de recherche	Microélectronique	CMP
MOLIMARD	Jérôme	PR2	Mécanique et ingénierie	CIS
MONTHEILLET	Frank	DR	Sciences et génie des matériaux	SMS
MOUTTE	Jacques	CR	Génie des Procédés	SPIN
NEUBERT	Gilles	PR	Génie industriel	FAYOL
NIKOLOVSKI	Jean-Pierre	Ingénieur de recherche		CMP
NORTIER	Patrice	PR1		SPIN
OWENS	Rosin	MA(MDC)	Microélectronique	CMP
PICARD	Gauthier	MA(MDC)	Informatique	FAYOL
PIJOLAT	Christophe	PR0	Génie des Procédés	SPIN
PIJOLAT	Michèle	PR1	Génie des Procédés	SPIN
PINOLI	Jean Charles	PR0	Image Vision Signal	CIS
POURCHEZ	Jérémy	MR	Génie des Procédés	CIS
ROBISSON	Bruno	Ingénieur de recherche	Microélectronique	CMP
ROUSSY	Agnès	MA(MDC)	Génie industriel	CMP
ROUSTANT	Olivier	MA(MDC)	Mathématiques appliquées	FAYOL
ROUX	Christian	PR	Image Vision Signal	CIS
STOLARZ	Jacques	CR	Sciences et génie des matériaux	SMS
TRIA	Assia	Ingénieur de recherche	Microélectronique	CMP
VALDIVIESO	François	PR2	Sciences et génie des matériaux	SMS
VIRICELLE	Jean Paul	DR	Génie des Procédés	SPIN
WOLSKI	Krzystof	DR	Sciences et génie des matériaux	SMS
XIE	Xiaolan	PR1	Génie industriel	CIS
YUGMA	Gallian	CR	Génie industriel	CMP
<b>ENISE : Enseignants-chercheurs et chercheurs autorisés à diriger des thèses de doctorat (titulaires d'un doctorat d'État ou d'une HDR)</b>				
BERGHEAU	Jean-Michel	PU	Mécanique et Ingénierie	ENISE
BERTRAND	Philippe	MCF	Génie des procédés	ENISE
DUBUJET	Philippe	PU	Mécanique et Ingénierie	ENISE
FEULVARCH	Eric	MCF	Mécanique et Ingénierie	ENISE
FORTUNIER	Roland	PR	Sciences et Génie des matériaux	ENISE
GUSSAROV	Andrey	Enseignant contractuel	Génie des procédés	ENISE
HAMDI	Hédi	MCF	Mécanique et Ingénierie	ENISE
LYONNET	Patrick	PU	Mécanique et Ingénierie	ENISE
RECH	Joël	PU	Mécanique et Ingénierie	ENISE
SMUROV	Igor	PU	Mécanique et Ingénierie	ENISE
TOSCANO	Rosario	PU	Mécanique et Ingénierie	ENISE
ZAHOUANI	Hassan	PU	Mécanique et Ingénierie	ENISE

*À ma famille*







## Remerciements

« La vie, c'est comme le vent »

Il y a 3 ans, pendant l'hiver 2012, j'ai décidé d'amener ma petite famille, et de quitter mon pays pour commencer une nouvelle vie, celle de thésard en France, à 10 000 km du Vietnam. Je savais qu'il y aurait beaucoup de difficulté et j'étais préparé à faire le plus d'efforts possibles.

Cette thèse a été réalisée au sein de l'équipe Hydrate du centre Sciences des Processus Industriels et Naturels (SPIN) de l'école Nationale Supérieure des Mines de Saint-Étienne.

En premier lieu, je remercie chaleureusement mon directeur de thèse M. Jean-Michel HERRI pour m'avoir accueilli dans son équipe, m'avoir encadré et m'avoir conseillé tout au long de ces trois années de thèse. Il m'a apporté son soutien scientifique.

J'adresse aussi sincèrement mes remerciements à mon Co-encadrant, M. Baptiste BOUILLOT qui m'a accompagné et m'a apporté le soutien nécessaire pour mener à bien ce travail. Il a été aussi encadrant de ma femme quand elle faisait un master à l'école. Nous lui devons donc beaucoup. Je remercie vivement Mme. Ana CAMEIRAO, qui m'a apporté le soutien nécessaire pour mener à bien ce travail.

Je tiens à remercier les membres du jury de ma soutenance. Je remercie M. Eric CHASSEFIERE d'avoir accepté de présider mon jury de thèse. Je remercie également M. Ryo OHMURA et Mme. Karine BALLERAT-BUSSEROLLES d'avoir accepté d'être rapporteur de mon jury de thèse et je remercie aussi M. Pierre DUCHET-SUCHAUX et M. Freddy GARCIA d'avoir accepté de participer à mon jury de thèse.

Je souhaite remercier aussi messieurs Fabien CHAUVY, Alain LALLEMAND, Jean-Pierre POYET, Richard DROGO et M. Marc ROUVIERE, pour leur aide technique pendant ma thèse. Sans eux, les travaux présentés dans ce manuscrit n'auraient pas pu être réalisés. J'ai également une pensée pour Alain LALLEMAND qui a pris sa retraite il y a peu de temps.

J'adresse également mes remerciements au personnel administratif, particulièrement Carole BIGOURAUX, Joëlle GUELON, Fabienne DEMEURE, Christine VENDEVILLE et Andrée-Aimée TOUCAS qui m'ont accompagnée tout au long de cette thèse dans mes besoins administratifs.

Je voudrais remercier tous les membres de l'équipe Hydrate qui m'ont très bien accueilli et pour tous les moments qu'on a passé ensemble pendant ces longues années de thèse: Jérôme, Fatima, Jérôme, Aurélie, Yamina, Matthias, Pedro, Kien, Aline, Saheb, Son.

Je remercie vivement toutes les personnes de l'EMSE-SE, doctorants, enseignants chercheurs. Grâce à vous, ma thèse a été une expérience enrichissante et agréable à la fois.

Je voudrais dire un « gros » remercie à mes parents qui m'ont toujours soutenu et à la famille de LE-QUANG Duyen, mon grand frère qui m'a aidé beaucoup dans les premiers jours où j'étais en France.

Enfin, un très grand remerciement à mes amours: ma femme Phuong-Anh et ma fille Phuong-Linh pour leurs présences dans ma vie, particulièrement dans ces moments importants. Sans elles, rien n'aurait été possible.

Et bien sûr, bien évidemment, merci à ma famille au Vietnam, surtout mes parents.

## Résumé:

L'activité scientifique du sujet porte sur l'acquisition de données expérimentales et la modélisation de la composition des clathrates hydrates de gaz. Les domaines d'application concernent la séparation et le stockage de gaz, la purification de l'eau, et le stockage d'énergie par matériaux à changement de phase.

L'équipe a mis en évidence il y a quelques années que la composition des hydrates de gaz était sensible aux conditions de cristallisation, et que le phénomène de formation se produisait en dehors de l'équilibre thermodynamique.

Le travail de thèse a permis d'explorer plusieurs modes de cristallisation à partir de solutions de même composition initiale pour observer les différences concernant l'état final, compositions notamment, et les relier à la vitesse de cristallisation.

Suivant le mode de cristallisation, lent ou rapide, l'acquisition des données expérimentales peut prendre de quelques jours à plusieurs semaines. Les expériences sont réalisées en réacteur pressurisé dans lequel nous mesurons en ligne la composition de la phase gaz et de la phase liquide, pour calculer par bilan de matière la composition de la phase hydrate.

Nous avons bien mis en évidence des variations dans la composition de la phase hydrate suivant le mode de cristallisation. Nous avons dû établir un modèle thermodynamique donnant la composition de la phase hydrate à l'équilibre pour des mélanges de gaz qui n'avaient jamais été traité par la littérature, et qui ont donc nécessité des campagnes de mesure extrêmement lentes et donc longues pour être sûr de l'état thermodynamique à l'équilibre.

Nous sommes en cours d'établir un modèle cinétique pour modéliser les écarts à cet état d'équilibre de référence pour nos expériences réalisées à vitesse de cristallisation rapide.

**Mots-clés:** Clathrate hydrates, Captage et Stockage du CO<sub>2</sub>, Thermodynamique, Cinétique, Cristallisation, Flow assurance, Phase équilibrais, Flash calculations.



## Summary:

The scientific goal of this thesis is based on the acquisition of experimental data and the modeling of the composition of clathrates gas hydrate. The domains of application concern the gas separation and storage, water purification, and energy storage using change phase materials (PCMs).

Our research team has recently demonstrated that the composition of gas hydrates was sensitive to the crystallization conditions, and that the phenomenon of formation was out of thermodynamic equilibrium.

During this thesis, we have investigated several types of crystallization, which are based on the same initial states. The goal is to point out the differences between the initial solution composition and the final solution composition, and to establish a link between the final state and the crystallization rate.

Depending on the rate of crystallization (slow or fast), the acquisition time of experimental data lasted from a few days to several weeks. The experimental tests were performed inside a stirred batch reactor (autoclave, 2.44 or 2.36 litre) cooled with a double jacket. Real-time measurements of the composition of the gas and the liquid phases have been performed, in order to calculate the composition of the hydrate phase using mass balance calculations. Depending on the crystallization mode, we have identified several variations of the composition of the hydrate phase and final hydrate volume.

We have established a successful thermodynamic model, which indicates the composition of the hydrate phase and hydrate volume in thermodynamic equilibrium state using a gas mixture which had never been used before in the literature. So this thermodynamic model has required an extremely slow experimental test. These tests were also long in order to be sure of the thermodynamic equilibrium state.

We are currently establishing a kinetics model in order to model the deviations from the reference point of equilibrium of our experimental tests which were carried out at a high crystallization rate.

**Key-words:** Gas Hydrates, Thermodynamic, Kinetic, Crystallization, CO<sub>2</sub> capture and storage, Flow assurance, Phase equilibria, Flash calculations



## LIST OF FIGURE

Figure 1: Water molecules forming cages corresponding to hydrate structures, sI, sII and sH .....	26
Figure 2: Comparison of guest molecule sizes and cavities occupied as simple hydrates. Modified from (Carroll, 2014) .....	28
Figure 3: Lattice parameters versus temperature for various sI Hydrates, modified from (Hester et al., 2007).....	29
Figure 4: Lattice parameters versus temperature for various sII Hydrates, modified from (Hester et al., 2007).....	29
Figure 5: Phase diagrams of methane clathrate hydrates (with P: pressure; T: temperature) (Adisasmito et al., 1991; De Roo et al., 1983; Deaton and Frost, 1946; Falabella, 1975; Galloway et al., 1970; Jhaveri and Robinson, 1965; Kobayashi et al., 1949; Makogon and Sloan, 1994; Marshall et al., 1964; McLeod and Campbell, 1961; Roberts et al., 1940; Thakore and Holder, 1987; Verma, 1974; Yang et al., 2001). .....	34
Figure 6: CH-V Equilibrium of single CO <sub>2</sub> at temperature below the ice point. The simulation curve is obtained with the GasHyDyn simulator, implemented with reference parameters from Table 25 (Dharmawardhana et al., 1980) and Table 26. (Page. 63) and Kihara parameters given in Table 28. (Page. 75).....	36
Figure 7: CH-V Equilibrium of single CH <sub>4</sub> at temperature below the ice point. The simulation of SI structure is obtained with the GasHyDyn simulator, implemented with reference parameters from Table 25 (Dharmawardhana et al., 1980) and Table 26. (Page. 63) and Kihara parameters given in Table 28. (Page. 75).....	37
Figure 8: CH-V and CH_SI-V-Lw Equilibrium of single C <sub>2</sub> H <sub>6</sub> . The simulation of SI Structure is obtained with the GasHyDyn simulator, implemented with reference parameters from Table 25 (Dharmawardhana et al., 1980) and Table 26. (Page. 63) and Kihara parameters given in Table 28. (Page. 75).....	38
Figure 9: CH-V and CH_SII-V-Lw Equilibrium of single C <sub>3</sub> H <sub>8</sub> . The simulation of SII Structure is obtained with the GasHyDyn simulator, implemented with	



reference parameters from Table 25 (Dharmawardhana et al., 1980) and Table 26. (Page. 63) and Kihara parameters given in Table 28. (Page. 75).	39
Figure 10: Schematic of the principle to referring at a hypothetical reference state in order to write the equilibrium between the clathrate hydrate phase and the liquid phase.	58
Figure 11: Procedure to optimise the kihara parameters	65
Figure 12: Deviation (in %, from Eq.20) between experimental equilibrium data of pure CO <sub>2</sub> hydrate Experimental data are from (Yasuda and Ohmura, 2008), (Adisasmito et al., 1991), (Falabella, 1975), (Miller and Smythe, 1970) which cover a range of temperature from 151.52K to 282.9K and a pressure range from 0.535kPa to 4370kPa.	67
Figure 13 : $\varepsilon/k$ versus $\sigma$ at the minimum deviation with experimental data. a value is taken from Table 27. Pressure and temperature equilibrium data for CO <sub>2</sub> hydrate are taken from (Yasuda and Ohmura, 2008), (Adisasmito et al., 1991), (Falabella, 1975), (Miller and Smythe, 1970) which cover a range of temperature from 151.52K to 282.9K and a pressure range from 0.535kPa to 4370kPa.	68
Figure 14 : $\varepsilon/k$ versus $\sigma$ at the minimum deviation with experimental data. a value is taken from Table 27. Pressure and temperature equilibrium data for CH <sub>4</sub> hydrate are taken from (Fray et al., 2010), (Yasuda and Ohmura, 2008), (Adisasmito et al., 1991) which cover a range of temperature from 145.75 to 286.4K and a pressure range from 2.4kPa to 10570kPa.	69
Figure 15 : $\varepsilon/k$ versus $\sigma$ at the minimum deviation with experimental data. a value is taken from Table 27. Pressure and temperature equilibrium data for C <sub>2</sub> H <sub>6</sub> hydrate are taken , from (Roberts et al., 1940), (Deaton and Frost, 1946), (Reamer et al., 1952), (Falabella, 1975), (Yasuda and Ohmura, 2008), (Mohammadi and Richon, 2010a, 2010b), which cover a wide range of temperature from 200.08 to 287.4K and a pressure range from 8.3kPa to 3298kPa.	70
Figure 16 : $\varepsilon/k$ versus $\sigma$ at the minimum deviation with experimental data. a value is taken from Table 27. Pressure and temperature equilibrium data for C <sub>3</sub> H <sub>8</sub> hydrate are taken from (Deaton and Frost, 1946), (Yasuda and Ohmura, 2008) and (Nixdorf and Oellrich, 1997) which cover a wide range of temperature from 245 to 278.5K and a pressure range from 41kPa to 567kPa	71

Figure 17 : $\varepsilon/k$ versus $\sigma$ at the minimum deviation with experimental data. a value is taken from Table 27. Pressure and temperature equilibrium data for CH <sub>4</sub> -C <sub>3</sub> H <sub>8</sub> hydrate are taken from (Verma et al., 1974) and (Verma, 1974). .....	72
Figure 18 : $\varepsilon/k$ versus $\sigma$ at the minimum deviation with experimental data. SII is assumed. a value is taken from Table 27. Pressure and temperature equilibrium data for Xe- C <sub>3</sub> H <sub>8</sub> hydrate is taken from (Tohidi et al., 1993). .....	73
Figure 19: $\varepsilon/k$ versus $\sigma$ at the minimum deviation with experimental data. SI is assumed. a value is taken from Table 27. Pressure and temperature equilibrium data for Xe-C <sub>3</sub> H <sub>8</sub> hydrate is taken from (Tohidi et al., 1993). .....	73
Figure 20: $\varepsilon/k$ versus $\sigma$ at the minimum deviation with experimental data. a value is taken from Table 27. Pressure and temperature equilibrium data for CO <sub>2</sub> -C <sub>3</sub> H <sub>8</sub> hydrate is taken from (Adisasmito and Sloan, 1992). .....	74
Figure 21: Schematic of the concentration profiles in the environment of a particle in a liquid bulk.....	78
Figure 22 : Influence of the stirring rate on the rate of methane dissolution in a stirred batch reactor (Herri et al., 1999a) .....	80
Figure 23 : Shape of the Gibbs energy function during formation of a cluster of n entities, depending on supersaturation (Herri, 1996) .....	85
Figure 24: Induction time versus supersaturation during nucleation of methane hydrate in pure water, at 1°C (Herri et al., 1999b) .....	86
Figure 25: The factor $\psi$ versus angle according to Eq. (45) .....	89
Figure 26: Association of clusters .....	90
Figure 27: Molar fraction of clusters at equilibrium. The index n refers to the number of elementary units of the cluster. S is the value of the supersaturation.....	93
Figure 28 : Elementary steps of gas integration in the vicinity of the growing hydrate surface (Herri and Kwaterski, 2012). .....	96
Figure 29: Double procedure of convergence to calculate the gas hydrate growing rate G, and the gas composition $x_{j,int}$ around the growing hydrate.....	107
Figure 30: Molar composition of the hydrate phase as a function of the intrinsic growth rates. The liquid phase is supposed to be in equilibrium with a gas phase composed of an equimolar CO <sub>2</sub> -N <sub>2</sub> mixture, at a pressure of 4 MPa and temperature of 1 °C .....	111

Figure 31 : Growth rate of the hydrate phase as a function of the intrinsic growth rate. The liquid phase is assumed to be in equilibrium with a gas phase composed of an equimolar CO <sub>2</sub> -N <sub>2</sub> mixture at a temperature of 1 °C and a pressure of 4 MPa .....	111
Figure 32: The system of Milli-Q®-AdvantageA10 at SPIN center laboratory .....	113
Figure 33: Experimental set-up .....	116
Figure 34: Schematic of Electromagnetic version of the ROLSITM Sampler injector. ....	117
Figure 35: Schematic of the VARIAN chromatograph (Model 3800 GC) equipped with a TCD detector. ....	118
Figure 36: The system of the ionic chromatography at SPIN laboratory .....	119
Figure 37: The procedure of the high crystallization rate .....	121
Figure 38: P– T evolution during equilibria experiments at high crystallization rate. ....	121
Figure 39: The procedure of the low crystallization rate.....	122
Figure 40: P – T evolution during equilibrium experiment at low crystallization rate. ....	122
Figure 41: Chromatogram of a liquid sample - Analysis of Lithium .....	123
Figure 42: Calibration curve of the ionic chromatography .....	124
Figure 43: GC principle .....	124
Figure 44: Calibration curve of gas chromatograph .....	127
Figure 45: Chromatogram of a sample of CO <sub>2</sub> -N <sub>2</sub> mixtures .....	129
Figure 46: Experimental equilibrium data of CO <sub>2</sub> -N <sub>2</sub> gas hydrate at high driving force compared with GasHyDyn predictions.....	139
Figure 47: Experimental equilibrium data of CO <sub>2</sub> -CH <sub>4</sub> -C <sub>2</sub> H <sub>4</sub> gas hydrate at high driving force compare with GasHyDyn predictions .....	141
Figure 48: Experimental equilibrium data of CO <sub>2</sub> -CH <sub>4</sub> -C <sub>2</sub> H <sub>4</sub> gas hydrate at low driving force compare with GasHyDyn predictions .....	142
Figure 49: Experimental equilibrium data of CH <sub>4</sub> -C <sub>3</sub> H <sub>8</sub> gas hydrate at high and low driving force .....	145
Figure 50: Experimental equilibrium data of CH <sub>4</sub> -C <sub>2</sub> H <sub>6</sub> -C <sub>3</sub> H <sub>8</sub> gas hydrate at low driving force .....	147
Figure 51: Example of Flash algorithm ( $\theta$ =mass flow ratio between phases).....	153

Figure 52: Basic hydrate flash algorithm. ....	155
Figure 53: Thermodynamic path (Bouillot and Herri, 2016). ....	156
Figure 54: Algorithm to perform hydrate flash calculation with no reorganization of the crystal phase (framework I) (Bouillot and Herri, 2016). ....	159
Figure 55: Mixed hydrate growth (no reorganization) (Bouillot and Herri, 2016). ....	160
Figure 56: Algorithm to perform hydrate flash calculation with reorganization of the hydrate phase during crystallization (framework II) (Bouillot and Herri, 2016). .....	161
Figure 57: Hydrate growth with crystal phase reorganization (framework II*) (Bouillot and Herri, 2016). ....	162
Figure 58: PT diagram of experimental and predicted results of the reference case (CO <sub>2</sub> -CH <sub>4</sub> -C <sub>2</sub> H <sub>6</sub> ) at different temperatures from the same initial state. ....	164
Figure 59: Predicted and experimental thermodynamic paths (Pressure vs temperature during crystallization) in the reference case (left: all frameworks at different numbers of iterations; right: framework I, N=7). ....	167
Figure 60: Schematic of the calculation of the Volume of Reactor. ....	201
Figure 61: Schematic of calibration of Gas Chromatography (GC) ....	203
Figure 62: Calibration curve of gas chromatograph of CO <sub>2</sub> -N <sub>2</sub> gas mixture. ....	205
Figure 63: Calibration curve of gas chromatograph of CH <sub>3</sub> -C <sub>3</sub> H <sub>8</sub> gas mixture. ....	206
Figure 64: Calibration curve of the gas chromatograph for CO <sub>2</sub> -CH <sub>4</sub> . ....	207
Figure 65: Calibration curve of the gas chromatograph for C <sub>2</sub> H <sub>6</sub> -CH <sub>4</sub> ....	207
Figure 66: Algorithm of calculation on the molar composition ....	209



## LIST OF TABLE

Table 1: Structure of gas hydrates .....	27
Table 2: Molar Masses of Some Hydrates at 0°C .....	30
Table 3: Densities of Some Hydrates at 0°C (Carroll, 2014) .....	32
Table 4: CH <sub>4</sub> -SI-V-Lw Equilibrium of CO <sub>2</sub> -CH <sub>4</sub> from (Bouchemoua et al., 2009). The simulation curve is obtained with the GasHyDyn simulator, implemented with reference parameters from Table 25 (Dharmawardhana et al., 1980) and Table 26. (Page. 63) and Kihara parameters given in Table 28. (Page. 75).....	40
Table 5: CH <sub>4</sub> -SI-V-Lw Equilibrium of CO <sub>2</sub> -CH <sub>4</sub> from (Le Quang, 2013). The simulation curve is obtained with the GasHyDyn simulator, implemented with reference parameters from Table 25 (Dharmawardhana et al., 1980) and Table 26. (Page. 63) and Kihara parameters given in Table 28. (Page. 75).....	40
Table 6: CH <sub>4</sub> -SI-V-Lw Equilibrium of CO <sub>2</sub> -CH <sub>4</sub> from (Belandria et al., 2011). The simulation curve is obtained with the GasHyDyn simulator, implemented with reference parameters from Table 25 (Dharmawardhana et al., 1980) and Table 26. (Page. 63) and Kihara parameters given in Table 28. (Page. 75).....	41
Table 7: CH <sub>4</sub> -SI-V-Lw Equilibrium of CO <sub>2</sub> -CH <sub>4</sub> from (Seo et al., 2000). The simulation curve is obtained with the GasHyDyn simulator, implemented with reference parameters from Table 25 (Dharmawardhana et al., 1980) and Table 26. (Page. 63) and Kihara parameters given in Table 28. (Page. 75).....	42
Table 8: CH <sub>4</sub> -SI-V-Lw Equilibrium of CO <sub>2</sub> -CH <sub>4</sub> from (Fan and Guo, 1999). The simulation curve is obtained with the GasHyDyn simulator, implemented with reference parameters from Table 25 (Dharmawardhana et al., 1980) and Table 26. (Page. 63) and Kihara parameters given in Table 28. (Page. 75).....	43
Table 9: CH <sub>4</sub> -SI-V-Lw Equilibrium of CO <sub>2</sub> -CH <sub>4</sub> from (Ohgaki et al., 1996). The simulation curve is obtained with the GasHyDyn simulator, implemented with reference parameters from Table 25 (Dharmawardhana et al., 1980) and Table 26. (Page. 63) and Kihara parameters given in Table 28. (Page. 75).....	43
Table 10: CH <sub>4</sub> -SI-V-Lw Equilibrium of CO <sub>2</sub> -CH <sub>4</sub> from (Adisasmito et al., 1991). The simulation curve is obtained with the GasHyDyn simulator, implemented with	

reference parameters from Table 25 (Dharmawardhana et al., 1980) and Table 26. (Page. 63) and Kihara parameters given in Table 28. (Page. 75). .....	44
Table 11: CH_SI-V-Lw Equilibrium of CO <sub>2</sub> -CH <sub>4</sub> from (Hachikubo et al., 2002). The simulation curve is obtained with the GasHyDyn simulator, implemented with reference parameters from Table 25 (Dharmawardhana et al., 1980) and Table 26. (Page. 63) and Kihara parameters given in Table 28. (Page. 75). .....	45
Table 12: CH_SI-V-Lw Equilibrium of CO <sub>2</sub> -CH <sub>4</sub> from (Unruh and Katz, 1949). The simulation curve is obtained with the GasHyDyn simulator, implemented with reference parameters from Table 25 (Dharmawardhana et al., 1980) and Table 26. (Page. 63) and Kihara parameters given in Table 28. (Page. 75). .....	46
Table 13 : CH_SI-V-Lw Equilibrium of CH <sub>4</sub> -C <sub>2</sub> H <sub>6</sub> from (Adisasmito and Sloan, 1992). The simulation curve is obtained with the GasHyDyn simulator, implemented with reference parameters from Table 25 (Dharmawardhana et al., 1980) and Table 26. (Page. 63) and Kihara parameters given in Table 28. (Page. 75). .....	46
Table 14: CH-V-Lw Equilibrium of CH <sub>4</sub> -C <sub>3</sub> H <sub>8</sub> from (Verma et al., 1974). The simulation curve is obtained with the GasHyDyn simulator, implemented with reference parameters from Table 25 (Dharmawardhana et al., 1980) and Table 26. (Page. 63) and Kihara parameters given in Table 28. (Page. 75). .....	47
Table 15: CH-V-Lw Equilibrium of CH <sub>4</sub> -C <sub>3</sub> H <sub>8</sub> from (Deaton and Frost, 1946). The simulation curve is obtained with the GasHyDyn simulator, implemented with reference parameters from Table 25 (Dharmawardhana et al., 1980) and Table 26. (Page. 63) and Kihara parameters given in Table 28. (Page. 75). .....	48
Table 16: CH-V-Lw Equilibrium of CH <sub>4</sub> -C <sub>3</sub> H <sub>8</sub> from (McLeod and Campbell, 1961). The simulation curve is obtained with the GasHyDyn simulator, implemented with reference parameters from Table 25 (Dharmawardhana et al., 1980) and Table 26. (Page. 63) and Kihara parameters given in Table 28. (Page. 75). .....	49
Table 17: CH-V-Lw Equilibrium of CH <sub>4</sub> -C <sub>3</sub> H <sub>8</sub> from (Thakore and Holder, 1987). The simulation curve is obtained with the GasHyDyn simulator, implemented with reference parameters from Table 25 (Dharmawardhana et al., 1980) and Table 26. (Page. 63) and Kihara parameters given in Table 28. (Page. 75). .....	50
Table 18: CH-V-Lw Equilibrium of C <sub>2</sub> H <sub>6</sub> -C <sub>3</sub> H <sub>8</sub> from (Mooijer-Van den Heuvel, 2004). The simulation curve is obtained with the GasHyDyn simulator, implemented	

with reference parameters from Table 25 (Dharmawardhana et al., 1980) and Table 26. (Page. 63) and Kihara parameters given in Table 28. (Page. 75).	51
Table 19: CH-V-Lw Equilibrium of CO <sub>2</sub> -CH <sub>4</sub> -C <sub>2</sub> H <sub>6</sub> from (Le Quang, 2013). The simulation curve is obtained with the GasHyDyn simulator, implemented with reference parameters from Table 25 (Dharmawardhana et al., 1980) and Table 26. (Page. 63) and Kihara parameters given in Table 28. (Page. 75).	52
Table 20: CH-V-Lw Equilibrium of CO <sub>2</sub> -CH <sub>4</sub> -C <sub>2</sub> H <sub>6</sub> from (Kvenvolden et al., 1984). The simulation curve is obtained with the GasHyDyn simulator, implemented with reference parameters from Table 25 (Dharmawardhana et al., 1980) and Table 26. (Page. 63) and Kihara parameters given in Table 28. (Page. 75).	53
Table 21: CH-V-Lw Equilibrium of CH <sub>4</sub> -C <sub>2</sub> H <sub>6</sub> -C <sub>3</sub> H <sub>8</sub> from (Le Quang, 2013). The simulation curve is obtained with the GasHyDyn simulator, implemented with reference parameters from Table 25 (Dharmawardhana et al., 1980) and Table 26. (Page. 63) and Kihara parameters given in Table 28. (Page. 75).	53
Table 22: CH-V-Lw Equilibrium of CH <sub>4</sub> -C <sub>2</sub> H <sub>6</sub> -C <sub>3</sub> H <sub>8</sub> C <sub>4</sub> H <sub>10</sub> (-1) from (Le Quang, 2013). The simulation curve is obtained with the GasHyDyn simulator, implemented with reference parameters from Table 25 (Dharmawardhana et al., 1980) and Table 26. (Page. 63) and Kihara parameters given in Table 28. (Page. 75).	54
Table 23 : CH-V-Lw Equilibrium of CH <sub>4</sub> -C <sub>2</sub> H <sub>6</sub> -C <sub>3</sub> H <sub>8</sub> C <sub>4</sub> H <sub>10</sub> (-1) from (Le Quang, 2013). The simulation curve is obtained with the GasHyDyn simulator, implemented with reference parameters from Table 25 (Dharmawardhana et al., 1980) and Table 26. (Page. 63) and Kihara parameters given in Table 28. (Page. 75).	55
Table 24: Correlations to calculate the $\varepsilon$ , $\sigma$ , and $a$ .kihara parameters as a function of the pitzer acentric factor $\omega$ and critical coordinates $P_c$ , $T_c$ and $V_c$	60
Table 25: Mascroscopic parameters of hydrates and Ice (Sloan, 1998; Sloan and Koh, 2007)	63
Table 26: Reference properties of hydrates from (Sloan, 1998; Sloan and Koh, 2007)	63
Table 27: Kihara parameters after optimisation on experimental data (Herri et al., 2011) and compared to litterature	66
Table 28: Kihara parameters, after optimisation from experimental data with the GasHyDyn simulator, implemented with reference parameters from Table 25 (Dharmawardhana et al., 1980) and Table 26.	75



Table 29: Nucleation of cluster of n building units, in homogeneous condition (a), at the surface of foreign surface or parent surface (b), at a gas/liquid interface (c). $\psi$ is a factor between 0 and 1 to quantify the decrease in the critical Gibbs Energy. $\gamma$ is the interfacial energy between the phases, <i>hyd</i> =hydrate phase, <i>liq</i> =liq solution, <i>gas</i> =gas, <i>solid</i> =foreign or parent phase (Kashchiev and Firoozabadi, 2002a, 2002b).....	88
Table 30: Occupancy factor of enclathrated molecules as a function of the composition in the liquid phase. The equations of the right-hand column are obtained from the classical Langmuir expressions from Eq. (73) (left column) upon replacing $x_j$ by the expression of Eq. (93) (right column).....	103
Table 31: Purity of Helium gas used in our experiments.....	113
Table 32 : The physical properties of Lithium nitrate (LiNO <sub>3</sub> ).....	114
Table 33: Molar composition of the experiments gas mixtures (standard deviation about 3%) .....	115
Table 34 : Operating conditions of the chromatogram.....	126
Table 35: SRK parameters .....	130
Table 36: Constants for calculating Henry's constant (Holder et al., 1980).....	133
Table 37: Molar composition of the studied gas mixtures and initial conditions of experiments. ....	137
Table 38: CH <sub>4</sub> -SI-V-Lw Equilibrium of CO <sub>2</sub> -N <sub>2</sub> at quick crystallization rate procedure versus predicted results.....	138
Table 39: CH <sub>4</sub> -SI-V-Lw Equilibrium of CO <sub>2</sub> -CH <sub>4</sub> -C <sub>2</sub> H <sub>6</sub> at high crystallization rate procedure versus predicted results.....	140
Table 40: CH <sub>4</sub> -SI-V-Lw Equilibrium of CO <sub>2</sub> -CH <sub>4</sub> -C <sub>2</sub> H <sub>6</sub> at low crystallization rate procedure versus predicted results.....	142
Table 41: CH <sub>4</sub> -SI-V-Lw Equilibrium of CH <sub>4</sub> -C <sub>3</sub> H <sub>8</sub> at high crystallization rate procedure.....	143
Table 42: CH <sub>4</sub> -SI-V-Lw Equilibrium of CH <sub>4</sub> -C <sub>3</sub> H <sub>8</sub> at low crystallization rate procedure.....	144
Table 43: Experimental and predicted pressures for the first data obtained in each experiments (CH <sub>4</sub> -C <sub>3</sub> H <sub>8</sub> ).....	146
Table 44 : CH <sub>4</sub> -SI-V-Lw Equilibrium of CH <sub>4</sub> -C <sub>2</sub> H <sub>6</sub> -C <sub>3</sub> H <sub>8</sub> at high crystallization rate (Le Quang, 2013).....	148

Table 45: CH <sub>4</sub> -SI-V-Lw Equilibrium of CH <sub>4</sub> -C <sub>2</sub> H <sub>6</sub> -C <sub>3</sub> H <sub>8</sub> at low crystallization rate procedure.....	148
Table 46: Quick Kihara parameters optimization of CO <sub>2</sub> , CH <sub>4</sub> and C <sub>2</sub> H <sub>6</sub> on a few experimental data (Adisasmito et al., 1991; Avlonitis, 1988; Dyadin, 1996; Y. A. Dyadin et al., 1996; Yurii A. Dyadin et al., 1996; Englezos and Bishnoi, 1991; Larson, 1955; Le Quang et al., n.d.; Nixdorf and Oellrich, 1997; Thakore and Holder, 1987; Yasuda and Ohmura, 2008) (* data from (Sloan and Koh, 2007))	163
Table 47: Experimental versus predicted results for the reference case (CO <sub>2</sub> , CH <sub>4</sub> and C <sub>2</sub> H <sub>6</sub> ) from classic thermodynamic calculations assuming a SI structure.....	164
Table 48: Experimental versus predicted results for the reference case (CO <sub>2</sub> , CH <sub>4</sub> and C <sub>2</sub> H <sub>6</sub> ) from classic thermodynamic calculations assuming a SI structure.....	166
Table 49: Influence of the Kihara parameters uncertainties on the flash hydrate results (framework I, reference case). .....	167
Table 50: Framework I ( <i>n</i> =5 and 20) and II* predictions compared to experimental results at quick crystallization (gas 1-2 from CO <sub>2</sub> -CH <sub>4</sub> mixtures and 3-4-5 from CO <sub>2</sub> -CH <sub>4</sub> -C <sub>2</sub> H <sub>6</sub> mixtures) and slow crystallization (reference case of the present study).....	169
Table 51: Constants necessary for the calculation of the compressibility factor.....	200
Table 52: Experiment data .....	202
Table 53: The results of the calculation.....	202
Table 54: Experiment results .....	204



## TABLE OF CONTENTS

1. INTRODUCTION.....	21
2. GAS HYDRATES .....	25
2.1. STRUCTURE OF GAS HYDRATES .....	25
2.2. PHYSICAL PROPERTIES OF GAS HYDRATES.....	30
2.2.1 Molar Mass	30
2.2.2 Density	31
2.2.3 Volume of Gas in Hydrate	32
2.2.4 The Hydration Number	33
2.2.5 Phase diagrams of the hydrates	33
3. EQUILIBRIUM DATA.....	35
3.1. PURE HYDRATES.....	36
3.1.1 CO <sub>2</sub> Clathrate Hydrate equilibrium data	36
3.1.2 CH <sub>4</sub> Clathrate Hydrate equilibrium data	37
3.1.3 C <sub>2</sub> H <sub>6</sub> Clathrate Hydrate equilibrium data	38
3.1.4 C <sub>3</sub> H <sub>8</sub> Clathrate Hydrate equilibrium data	39
3.2. MIXED HYDRATES .....	40
3.2.1 CO <sub>2</sub> -CH <sub>4</sub> Clathrate Hydrate equilibrium data	40
3.2.2 CO <sub>2</sub> -C <sub>2</sub> H <sub>6</sub> Clathrate Hydrate equilibrium data	46
3.2.3 CH <sub>4</sub> -C <sub>3</sub> H <sub>8</sub> Clathrate Hydrate equilibrium data	47
3.2.4 C <sub>2</sub> H <sub>6</sub> -C <sub>3</sub> H <sub>8</sub> Clathrate Hydrate equilibrium data	51
3.2.5 CO <sub>2</sub> -CH <sub>4</sub> -C <sub>2</sub> H <sub>6</sub> Clathrate Hydrate equilibrium data	52
3.2.6 CH <sub>4</sub> -C <sub>2</sub> H <sub>6</sub> -C <sub>3</sub> H <sub>8</sub> Clathrate Hydrate equilibrium data	53
3.2.7 CH <sub>4</sub> -C <sub>2</sub> H <sub>6</sub> -C <sub>3</sub> H <sub>8</sub> C <sub>4</sub> H <sub>10</sub> (-1) Clathrate Hydrate equilibrium data	54
4. THERMODYNAMIC OF GAS HYDRATES .....	57
4.1. MODELLING OF $\Delta\mu_w^{H-\beta}$ .....	57
4.2. MODELLING OF $\Delta\mu_w^{p-\beta}$ .....	61
4.3. ADJUSTMENT OF MODELS PARAMETERS.....	63
4.3.1 Determination of the reference parameters	64
4.3.2 Determination of the kihara parameters	66
5. HYDRATES UNDER NON EQUILIBRIUM CONDITIONS .....	77

5.1.	INTRODUCTION .....	77
5.2.	GENERALITIES ABOUT THE CRYSTALLIZATION OF GAS HYDRATES.....	78
5.3.	MODELLING THE GAS/LIQUID TRANSFER IN A BATCH REACTOR .....	79
5.4.	MODELLING THE NUCLEATION .....	80
5.4.1	Primary nucleation from the model of Volmer and Weber (1926)	81
5.4.2	Primary nucleation from a rigorous kinetic approach	89
5.4.3	Primary nucleation for chemical engineers	93
5.4.4	Secondary nucleation	94
5.5.	MODELLING THE GROWTH.....	95
5.5.1	Enclathration during crystallisation	98
5.5.2	Discussion	108
5.5.3	Numerical application	109
5.6.	Conclusion.....	112
6.	MATERIALS AND METHODS .....	113
6.1.	CHEMICALS .....	113
6.1.1	Deionized water (H <sub>2</sub> O)	113
6.1.2	Helium (He)	113
6.1.3	Lithium Nitrate (LiNO <sub>3</sub> )	114
6.1.4	Gas mixtures (CO <sub>2</sub> , N <sub>2</sub> , CH <sub>4</sub> , C <sub>2</sub> H <sub>6</sub> , C <sub>3</sub> H <sub>8</sub> )	114
6.2.	EXPERIMENTAL DEVICE .....	115
6.3.	EXPERIMENTAL PROCEDURE .....	120
6.3.1	High crystallization rate	120
6.3.2	Low crystallization rate	121
6.4.	OPERATING PROTOCOLS .....	123
6.4.1	Determination of the concentration of lithium by ionic chromatography.	123
6.4.2	Calibrating the gas chromatograph (TCD)	124
6.4.3	Mass balance calculation	129
7.	EXPERIMENTALS RESULTS AND DISCUSSIONS.....	137
7.1.	CO <sub>2</sub> -N <sub>2</sub> GAS MIXTURES.....	138
7.2.	CO <sub>2</sub> -CH <sub>4</sub> -C <sub>2</sub> H <sub>6</sub> GAS MIXTURE .....	139

7.3.	CH <sub>4</sub> -C <sub>3</sub> H <sub>8</sub> GAS MIXTURES .....	143
7.4.	CH <sub>4</sub> -C <sub>2</sub> H <sub>4</sub> -C <sub>3</sub> H <sub>8</sub> GAS MIXTURES.....	147
7.5.	Conclusion .....	149
8.	FLASH CALCULATION .....	151
8.1.	INTRODUCTION .....	151
8.2.	STATE OF THE ART .....	152
8.2.1	Usual flash calculations .....	152
8.2.2	Flash hydrate modeling .....	153
8.3.	BASIC ALGORITHM .....	154
8.4.	HYDRATE FLASH ALGORITHM WITHOUT CRYSTAL REORGANIZATION.....	157
8.5.	HYDRATE FLASH ALGORITHM WITH CRYSTAL REORGANIZATION.....	161
8.6.	KIHARA PARAMETERS OPTIMIZATION .....	162
8.7.	RESULTS .....	163
8.7.1.	Thermodynamic equilibrium .....	163
8.7.2.	Flash results .....	165
8.8.	KIHARA UNCERTAINTIES .....	167
8.9.	MIXED HYDRATE CRYSTALLIZATION .....	168
8.10.	CONCLUSION .....	170
9.	CONCLUSION .....	173
10.	LIST OF SYMBOLS.....	175
11.	REFERENCES.....	183
12.	APPENDIX 1: CALCULATION OF THE VOLUME OF REACTOR.....	199
13.	APPENDIX 2: CALIBRATION OF GAS CHROMATOGRAPHY .....	203
14.	APPENDIX 3: EVALUATION OF ERRORS CALCULATION .....	209



## 1. INTRODUCTION

The Gas hydrates are encountered in many systems where the pressure is high enough and the temperature low enough to crystallize the liquid water and the gas phase in a solid called clathrate hydrate.

Applications of gas hydrate formation are numerous and a complete reviewing has been achieved in the framework of the French ANR national program called SECOHYA coordinated by our team: - gas production from methane hydrate bearing sediments and CO<sub>2</sub> injection, - natural gas storage and transportation under the form of pellets, - thermal storage by using slurries of semi-clathrate hydrates from quaternary ammonium salts, - separation of gases: methane, nitrogen, carbon dioxide, - food preservation by using ozone clathrates. The applications currently developed in our team are Air conditioning ([Darbouret et al., 2005](#); [Douzet et al., 2013](#)), CO<sub>2</sub> capture ([Duc et al., 2007](#); [Galfré et al., 2014](#); [Herri et al., 2014, 2011](#); [Herslund et al., 2013](#)), and Methane hydrate bearing sediments for gas production ([Tonnet and Herri, 2009](#)). We collaborate also with other teams to develop science on Food preservation ([Muromachi et al., 2013](#)), Sequestration ([Burnol et al., 2015](#)) or technology on Waste Water treatment.

On other hand, gas hydrate formation is a main concern as a risk in the oil production, especially in deep sea pipelines where they can plug the facilities by forming both a crust on the pipelines, and also increasing the viscosity of fluids. This subject has been a main concern for our team and still continues to be ([Cameirao et al., 2012](#); [Fidel-Dufour et al., 2005](#); [Herri et al., 2009](#); [Leba et al., 2010](#)).

Lastly, Gas Hydrates are a concern in astrophysics and planetary sciences as its formation, even at very low pressure conditions, is still possible due to the exceptional low temperature. For example, our team is collaborating on the possible methane enclathration during seasonal cycles on Mars. It could explain the anormal preservation of methane in the Martian atmosphere ([Chassefière et al., 2013](#); [Herri and Chassefière, 2012](#)).

In each of the applications, the experimentations and modelling imply to develop knowledge about thermodynamics and kinetics. In fact, the process of crystallization of gas hydrates involves many elementary steps such as nucleation, growth, agglomeration, attrition.... Each of the steps is depending on a driving force (i.e. super-saturation) in between equilibrium conditions (thermodynamic) actual conditions. Actual conditions are governed in the end by mass transfers of gases from the gas phase to the hydrate structure. For example, in a liquid bulk solution, the gas fraction in the liquid is dependent, on one side of the rate of gas dissolution at the Gas/liquid interface, and dependent on the other side of the gas consumption



rate by hydrate crystallization (to be more precise, dependent at the first order of the growth rate).

My work is a contribution to evaluate the composition of gas hydrate under a null-driving force (experiments at pseudo equilibrium) and under high driving force. In fact, from theoretical speculations, (Herri and Kwaterski, 2012) has justified that the composition could not only fixed by thermodynamic, but could be also dependent on the relative rates of mass transfers of the different gases.

It opened for my team, a new field of research, because it allows orientating the crystallization in a favorable direction, for example in gas separation process such as the capture of CO<sub>2</sub>, and it introduces the possibility to modify the crystallization with the use of kinetic additives or specific geometries.

For my proper concern, the possibility to form hydrate under un-equilibrium conditions opened a main question irrelative to the flow assurance management for oil production. In fact the volume of hydrates that are formed could be badly evaluated from simulators working at equilibrium conditions.

This manuscript is organized as following:

The first part of the document deals with structure (Chapter 2), composition (Chapter 3) and thermodynamic modeling (Chapter 4) of gas hydrates. It gives the fundamentals to model equilibrium conditions.

As said before, my work has been conducted half under equilibrium conditions, and half under non equilibrium conditions. Chapter 5 is a focus to couple kinetics and thermodynamics and to show how much the composition of gas hydrate could be not only dependent on thermodynamics but also on kinetics.

Following is my first personal contribution. It has been to monitor experimentally the compositions of hydrates under equilibrium and non-equilibrium conditions (Chapters 6 and 7) by using an original experimental protocol developed in the our laboratory during the Ph.D. work of A. Bouchemoua (Herri et al., 2011). On my side, I designed two experimental procedures, under low rate or high rate of cristallisation, and I observed the difference in the composition of the hydrates that are formed from a same mixture. The gas mixture has been choiced to be representative of the oil production industry, CO<sub>2</sub>, CH<sub>4</sub>, C<sub>2</sub>H<sub>6</sub>, C<sub>3</sub>H<sub>8</sub>.

My second concern has been to support the modelling approach from two points of view:

- Firstly, I gave equilibrium data to implement our in-house simulation software, called GasHyDyn (presented at the beginning of section §3 Page 21).

In the document, we show the difficulty in retrieving thermodynamic parameters from the experiments, because of the difficulty to be sure that the data are at equilibrium, and/or because of the necessity to run complex mixtures as some gas hydrate formers can not form pure gas hydrates.

- Secondly, I gave non-equilibrium data and supported a new approach to model the composition of hydrates from a flash calculation (Chapter 8), and to understand the composition of hydrates not from a kinetic modelling as given in Chapter 5, but from a succession of quasi-equilibrium.

As a conclusion of this work, we emphasize that equilibrium of hydrate from gas mixture needs to perform experiments at a very low rate, and so during very long time of experiments, from weeks to months.



## 2. GAS HYDRATES

### 2.1. STRUCTURE OF GAS HYDRATES

The clathrates are ice-like compounds in the sense that they correspond to a re-organisation of the water molecules to form a solid. The crystallographic structure is based on H-bonds. The clathrates of water are also designated improperly as “porous ice” because the water molecules build a solid network of cavities in which gases, volatile liquids or other small molecules could be captured.

The clathrates of gases, called gas hydrates, have been studied intensively due to their occurrence in deep sea pipelines where they cause serious problems of flow assurance.

There are two structures of hydrates commonly encountered in the petroleum business (Sloan and Koh, 2007). These are called structure I and structure II, sometimes referred to as type I and II. A third structure of hydrate that also may be encountered is structure H (structures I and II hydrates can form in the presence of a single hydrate former, but structure H requires two formers to be present, a small molecule, such as methane, and a larger type H forming molecule), but it is less commonly encountered (Carroll, 2014). Each structure is a combination of different types of polyhedra sharing faces between them. (Jeffrey, 1984) suggested the nomenclature (*ef*) to describe the polyhedra to form the primitive cells (where (*e*) is the number of edges, and (*f*) the number of faces). Currently, three different structures have been established precisely, called I, II and H (Sloan, 1998; Sloan and Koh, 2007). The three structures are formed by a total of five different water cavities are the  $5^{12}$ ,  $5^{12}6^2$ ,  $5^{12}6^4$ ,  $5^{12}6^8$  and the  $4^35^66^3$  (Sloan, 1998; Sloan and Koh, 2007). A schematic of these cavities may be found in Figure 1 which shows the polyhedra involved in structure I, II and H. On this figure, the water molecule is on the corner of the polyhedral. The edges represent hydrogen bonds. The physical properties of the hydrate cavities and unit cells are provided in Table 1. Structures I, II, and H will be reviewed in more detail throughout this part. In its pure form, the unit cell of the structure I (sI) hydrate contains two small  $5^{12}$  and six large  $5^{12}6^2$  cavities, in which only methane, ethane and carbon dioxide of the natural gas components stabilize the structure. Structure II (sII) hydrate contains sixteen small  $5^{12}$  cavities and eight large  $5^{12}6^4$  cavities. The large cavity in sII can contain larger molecules (up to 6.6 Å, see in Figure 2). This means that propane and iso-butane can stabilize this large cavity. Alternatively, small cavities can be filled with methane, which means that natural gas with propane or iso-butane typically forms sII hydrates. Methane will form sI hydrate by filling both the large and the small cavities, but not sII because the molecules are too small to stabilize the large cavities in sII. Both of these unit cell lattice structures belong to the cubic type. The structure H (sH) hydrate is contains three  $5^{12}$ , two  $4^35^66^3$  and one  $5^{12}6^8$  cavities, being significantly more complex (Sum et

al., 2009). This hydrate structure forms a hexagonal unit cell. A given hydrate structure is typically determined by the size and shape of the guest molecule. Each cavity may encapsulate one or in rare cases more guest molecules of proper sizes. Of course, the presence of the guest molecule is necessary to stabilize the crystalline water structure at temperatures well above the normal freezing point.

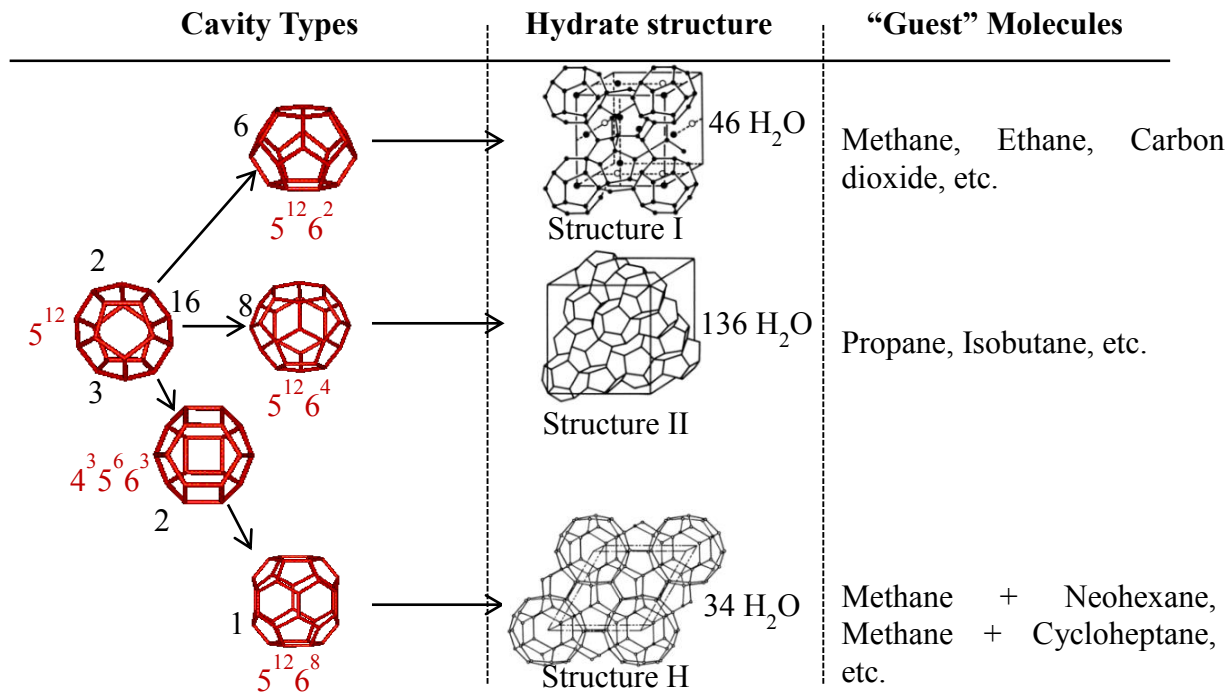


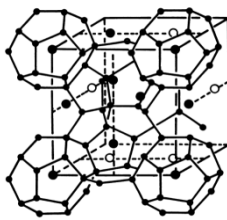
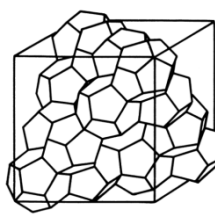
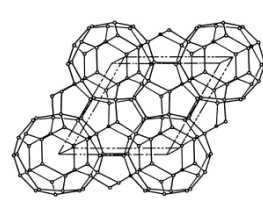
**Figure 1:** Water molecules forming cages corresponding to hydrate structures, sI, sII and sH

Based on the knowledge about the hydrate structure for a given gas composition, it is possible to calculate the relative water/guest ratio known as the ideal hydration number:

$$n_{hyd} = \frac{\text{number of water molecules}}{\text{number of gas molecules}} \quad (1)$$

Pure methane will occupy the 2 small and the 6 large cavities of sI. With 46 water molecules in a unit cell, the ideal hydration number becomes 5.75. For an natural gas mixture of methane, ethane and propane, where propane and ethane stabilize the 8 large cavities of sII, methane enter the 16 small cavities, and the unit cell has 136 water molecules, the ideal hydration number becomes 5.67 (Figure 1 and Figure 2).

**Table 1: Structure of gas hydrates**

	SI		SII		SH																				
																									
Cavity	5 <sup>12</sup>	5 <sup>12</sup> 6 <sup>2</sup>	5 <sup>12</sup>	5 <sup>12</sup> 6 <sup>4</sup>	5 <sup>12</sup>	4 <sup>3</sup> 5 <sup>6</sup> 6 <sup>3</sup>	5 <sup>12</sup> 6 <sup>8</sup>																		
Type of cavity ( <i>j</i> : indexing number)	1	2	1	3	1	5	4																		
Typical formers	CH <sub>4</sub> , C <sub>2</sub> H <sub>6</sub> , H <sub>2</sub> S, CO <sub>2</sub>		N <sub>2</sub> , C <sub>3</sub> H <sub>8</sub> , i-C <sub>4</sub> H <sub>10</sub>		See below <sup>o</sup>																				
Number of cavities ( <i>m<sub>j</sub></i> )	2	6	16	8	3	2	1																		
Average cavity radius (nm)(1)	0.395	0.433	0.391	0.473	0.391	0.406	0.571																		
Variation in radius, % (2)	3.4	14.4	5.5	1.73																					
Coordination number	20	24	20	28	20	20	36																		
Number of water molecules	42		136		134																				
Cell parameters (nm)	<i>a</i> <sub>0</sub> = 1.1956 (3)		<i>a</i> <sub>0</sub> = 1.7315 (4)		a = 1.2217, b = 1.0053 (5)																				
Thermal expansivity $\alpha = \frac{1}{a} \left( \frac{\partial a}{\partial T} \right)$ (6)	$\alpha = a_1 + a_2 (T - T_0) + a_3 (T - T_0)^2$ $\frac{a - a_0}{a_0} + 1 = \exp \left[ a_1 (T - T_0) + \frac{a_2}{2} (T - T_0)^2 + \frac{a_3}{3} (T - T_0)^3 \right]$ <table> <tr> <td><i>a</i><sub>1</sub></td> <td>=</td> <td>1.1280 10<sup>-4</sup></td> <td><i>a</i><sub>1</sub></td> <td>=</td> <td>6.7659 10<sup>-5</sup></td> </tr> <tr> <td><i>a</i><sub>2</sub>/2</td> <td>=</td> <td>1.8003 10<sup>-7</sup></td> <td><i>a</i><sub>2</sub>/2</td> <td>=</td> <td>6.1706 10<sup>-8</sup></td> </tr> <tr> <td><i>a</i><sub>3</sub>/3</td> <td>=</td> <td>-1.5898 10<sup>-11</sup></td> <td><i>a</i><sub>3</sub>/3</td> <td>=</td> <td>-6.2649 10<sup>-11</sup></td> </tr> </table>							<i>a</i> <sub>1</sub>	=	1.1280 10 <sup>-4</sup>	<i>a</i> <sub>1</sub>	=	6.7659 10 <sup>-5</sup>	<i>a</i> <sub>2</sub> /2	=	1.8003 10 <sup>-7</sup>	<i>a</i> <sub>2</sub> /2	=	6.1706 10 <sup>-8</sup>	<i>a</i> <sub>3</sub> /3	=	-1.5898 10 <sup>-11</sup>	<i>a</i> <sub>3</sub> /3	=	-6.2649 10 <sup>-11</sup>
<i>a</i> <sub>1</sub>	=	1.1280 10 <sup>-4</sup>	<i>a</i> <sub>1</sub>	=	6.7659 10 <sup>-5</sup>																				
<i>a</i> <sub>2</sub> /2	=	1.8003 10 <sup>-7</sup>	<i>a</i> <sub>2</sub> /2	=	6.1706 10 <sup>-8</sup>																				
<i>a</i> <sub>3</sub> /3	=	-1.5898 10 <sup>-11</sup>	<i>a</i> <sub>3</sub> /3	=	-6.2649 10 <sup>-11</sup>																				
Cell volume (nm <sup>3</sup> )	1.709 (3)		5.192 (4)		1.22994 (5)																				

(1) From (Sloan, 1998, p. 33)

(2) Variation in distance of oxygen atoms from centre of cages (Sloan, 1998, p. 33).

(3) For ethane hydrate, from (Udachin et al., 2002).

(4) For tetrahydrofuran hydrate, from (Udachin et al., 2002).

(5) For methylcyclohexane-methane hydrate, from (Udachin et al., 2002).

(6) From (Hester et al., 2007).

- o 2-methylbutane, 2,2-dimethylbutane, 2,3-dimethylbutane, 2,2,3-trimethylbutane, 2,2-dimethylpentane, 3,3-dimethylpentane, methylcyclopentane, ethylcyclopentane, methylcyclohexane, cycloheptane, and cyclooctane. Most of these components are not commonly found in natural gas.

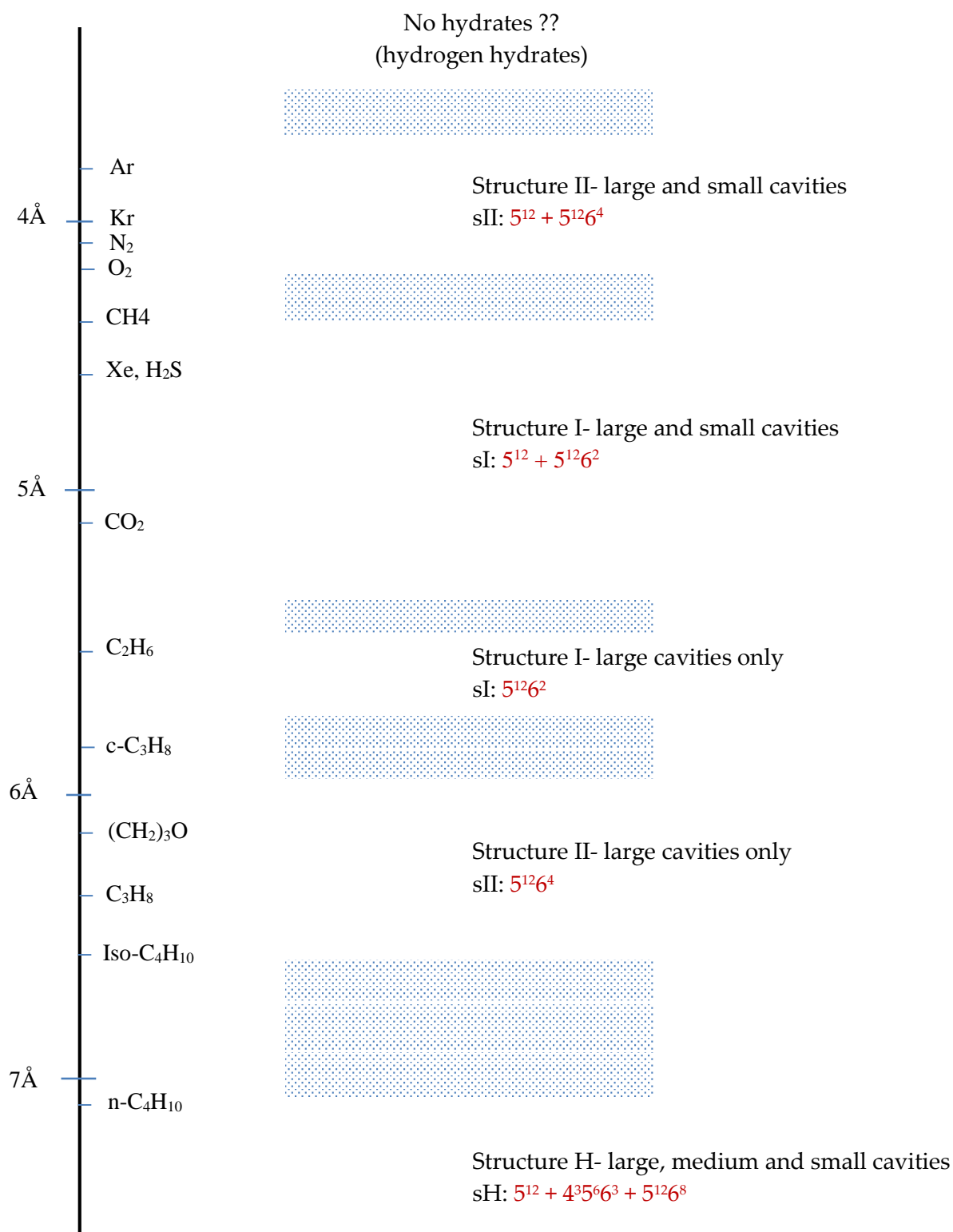


**Figure 2:** Comparison of guest molecule sizes and cavities occupied as simple hydrates. Modified from (Carroll, 2014)

More details about the cell parameters can be found in (Hester et al., 2007). They measured the hydrate lattice parameters for four Structure I (C<sub>2</sub>H<sub>6</sub>, CO<sub>2</sub>, 47% C<sub>2</sub>H<sub>6</sub> + 53% CO<sub>2</sub>, and 85% CH<sub>4</sub> + 15% CO<sub>2</sub>) and seven Structure II (C<sub>3</sub>H<sub>8</sub>, 60% CH<sub>4</sub> + 40%

C<sub>3</sub>H<sub>8</sub>, 30% C<sub>2</sub>H<sub>6</sub> + 70% C<sub>3</sub>H<sub>8</sub>, 18% CO<sub>2</sub> + 82% C<sub>3</sub>H<sub>8</sub>, 87.6% CH<sub>4</sub> + 12.4% i-C<sub>4</sub>H<sub>10</sub>, 95% CH<sub>4</sub> + 5% C<sub>5</sub>H<sub>10</sub>O, and a natural gas mixture). The measurements have been compared to literature data with Structure I (Figure 3) from EtO (Rondinone et al., 2003), CD<sub>4</sub> (Gutt et al., 2000), CO<sub>2</sub> (Ikeda et al., 1999), Xe (Ikeda et al., 2000), TMO-d6 (Rondinone et al., 2003), CH<sub>4</sub> (Ogienko et al., 2006; Shpakov et al., 1998), CH<sub>4</sub>+CO<sub>2</sub> (Takeya et al., 2006), and Structure II (Figure 4) from THF (Tse, 1987), TMO-d6 (Rondinone et al., 2003), C<sub>3</sub>H<sub>8</sub> (Chakoumakos et al., 2003; Hester et al., 2007; Jones et al., 2003), CH<sub>4</sub>+C<sub>2</sub>H<sub>6</sub> (Rawn et al., 2003), Air (Takeya et al., 2000), THF-d8 (Jones et al., 2003). (Hester et al., 2007) conclude that both sI and sII hydrates, with a few exceptions, had a common thermal expansivity, independent of hydrate guest, following the correlation given in Table 1.

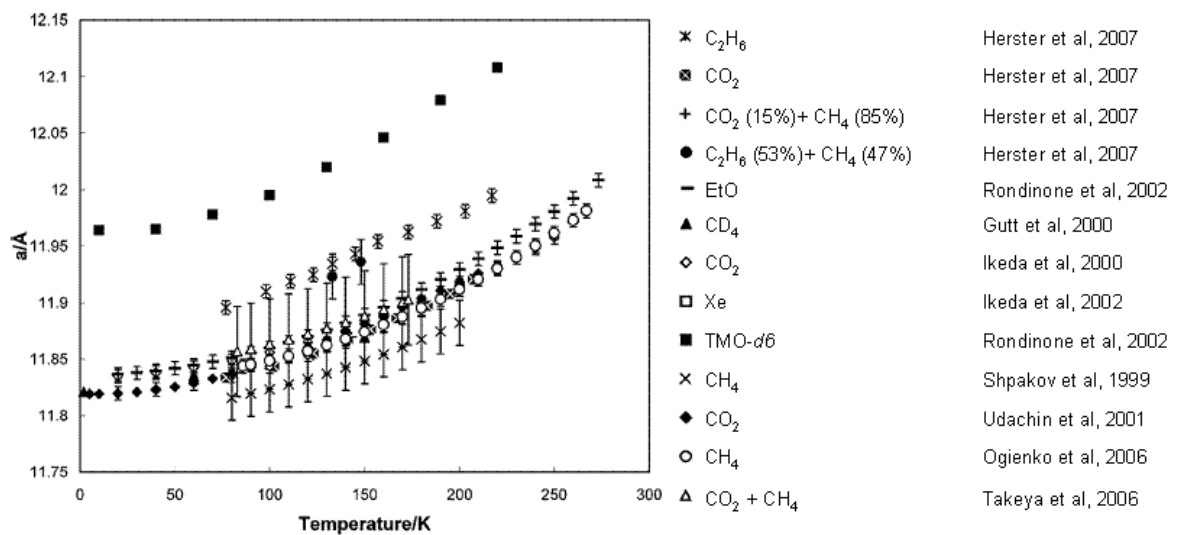


**Figure 3:** Lattice parameters versus temperature for various sI Hydrates, modified from (Hester et al., 2007)

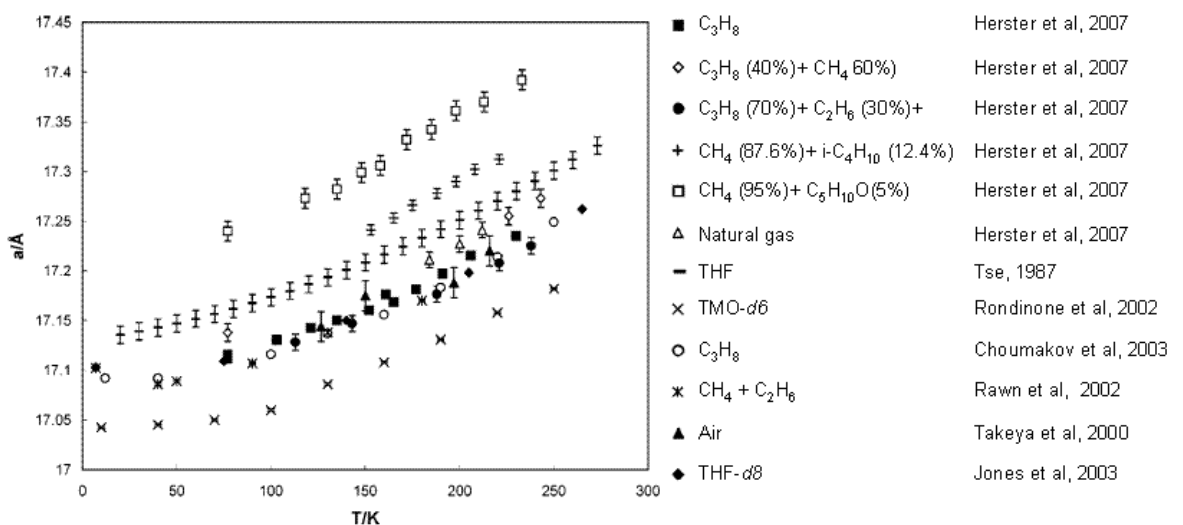


**Figure 4:** Lattice parameters versus temperature for various sII Hydrates, modified from (Hester et al., 2007)



## 2.2. PHYSICAL PROPERTIES OF GAS HYDRATES

### 2.2.1 MOLAR MASS

The molar mass (molecular weight) of a hydrate can be determined from its crystal structure and the degree of saturation (An exception is CSMHYD, which does give saturation values). Then, the newer CSMGEM gives composition of the hydrate phase, but not specifically the cell saturation). The molar mass of the hydrate,  $M$ , is expressed as follow (Carroll, 2014):

$$M = \frac{N_w M_w + \sum_{j=1}^c \sum_{i=1}^n Y_{ij} v_i M_j}{N_w + \sum_{j=1}^c \sum_{i=1}^n Y_{ij} v_i} \quad (2)$$

where  $N_w$  is the number of water molecules per unit cell (46 for Structure I, 136 for Structure II, and 34 for Structure H, (see on Table 1)),  $M_w$  is the molar mass of water,  $Y_{ij}$  is the fractional occupancy of cavities of structure  $i$  by component  $j$ ,  $v_i$  is the number of structure  $i$  cavities,  $n$  is the number of cavities of structure  $i$  (two for both Structure I and II, but is three for Structure H), and  $c$  is the number of components in the cell.

Although this equation looks fairly complicated, it is just accounting for all of the molecules present and then using a number average to get the molar mass.

**Table 2:** Molar Masses of Some Hydrates at 0°C

(Note: calculated using Eq. (2). The saturation values were calculated using CSMHYD)

Gas	Hydrate structures	Saturation		Molar mass (g/mol)
		Small	Large	
Methane	I	0.8723	0.9730	17.74
Ethane	I	0.0000	0.9864	19.39
Propane	II	0.0000	0.9987	19.46
Iso-Butane	II	0.0000	0.9987	20.24
CO <sub>2</sub>	I	0.7295	0.9813	21.59

On Table 2 summarizes the molar masses of a few hydrate formers. It is a little surprising that the molar masses of all six components are approximately around

equal (17÷22g/mol). This is because the hydrate is composed mostly of water (18.015 g/mol).

It is interesting that the molar masses of hydrates are a function of the temperature and the pressure, since the degree of saturation is a function of these variables. We usually think of molar masses as being constants for a given substance.

### 2.2.2 DENSITY

The density of a hydrate,  $\rho$ , can be calculated using the following formula below (Carroll, 2014):

$$\rho = \frac{N_w M_w + \sum_{j=1}^c \sum_{i=1}^n Y_{ij} v_i M_j}{N_A V_{cell}} \quad (3)$$

Where  $N_A$  is Avogadro's number ( $6.023 \cdot 10^{23}$  molecules/mole),  $V_{cell}$  is the volume of the unit cell (Table 1),  $N_w$  is the number of water molecules per unit cell),  $M_w$  is the molar mass of water,  $Y_{ij}$  is the fractional occupancy of cavities of structure  $i$  by component  $j$ ,  $v_i$  is the number of structure  $i$  cavities,  $n$  is the number of cavities of structure  $i$  (two for both Structure I and II, but is three for Structure H), and  $c$  is the number of components in the cell.

Eq. (3) can be reduced for a single component in either a Structure I or Structure II hydrate to:

$$\rho = \frac{N_w M_w + (Y_1 v_1 + Y_2 v_2) M_j}{N_A V_{cell}} \quad (4)$$

Again, although Eq. (3) and (4) look complicated, they are just accounting for the number of molecules in a unit cell of hydrate. The mass of all these molecules divided by the unit volume of the crystal gives the density of the hydrate.

The densities of some pure hydrates at 0°C are given in Table 3. Note that the densities of the hydrates of the hydrocarbons are similar to ice.

At last, for an empty hydrate structure, the formula is simple:

$$M = \frac{N_w M_w}{N_A V_{cell}} \quad (5)$$

**Table 3:** Densities of Some Hydrates at 0°C (Carroll, 2014)

	Hydrate structure (I, II, or H)	Density (g/cm <sup>3</sup> )
Methane	I	0.913
Ethane	I	0.967
Propane	II	0.899
Isobutane	II	0.934
CO <sub>2</sub>	I	1.107
Ice	-	0.917
Water	-	1.000

This equation gives a density of 790 kg/m<sup>3</sup> for structure I and 785kg/m<sup>3</sup> for structure II. It is a usefull equation to calculate the hydrate volume from the crystallized mass of water.

### 2.2.3 VOLUME OF GAS IN HYDRATE

Some interesting properties of methane hydrate at 0°C: the density is 913 kg/m<sup>3</sup>, the molar mass (molecular weight) is 17.74 kg/kmol, and methane concentration is 14.1 mol percent-this means there are 141 molecules of methane per 859 molecules of water in the methane hydrate.

This information can be used to determine the volume of gas in the methane hydrate. From the density, 1 m<sup>3</sup> of hydrate has a mass of 913 kg. Converting this to moles, 913/17.74 = 51.45 kmol of hydrate, of which 7.257 kmol are methane.

Ideal gas law can be used to calculate the volume of gas when expanded to standard conditions (15 °C and 1 atm or 101.325 kPa)

$$V = \frac{nRT}{P} = \frac{(7.257)(8.314)(15 + 273.15)}{101.325} = 171.5 \text{ (Sm}^3\text{)} \quad (6)$$

Therefore, 1 m<sup>3</sup> of hydrate contains about ~170 Sm<sup>3</sup> of methane gas at standard conditions (15 °C and 1 atm or 101.325 kPa). According to Kvenvolden (Kvenvolden, 1993) 1m<sup>3</sup> gas hydrate may release about 164 m<sup>3</sup> methane and 0.8 m<sup>3</sup> of water under standard temperature and pressure (STP) condition.

#### 2.2.4 THE HYDRATION NUMBER

An important property is the hydration number. This value describes the relationship between the water molecules and molecules (Thiam, 2008). The knowledge of this property directly provides information which corresponds to a correct structure is given by Eq. (1) (section §2.1. Page. 25).

If all the cavities were completely occupied, the hydration number corresponds to the ratio between the number of water molecules, and the number of cavities. However, experience shows that the cavities are partially occupied, and that we must define an occupancy rate, to which we return more detail in the section on Thermodynamics modelling. The actual number of hydration is given by:

$$n_{hyd} = \frac{\text{number of water molecules per unit cell}}{\sum_{j=1}^{C_T} \sum_{i=1}^{N_T} v_i \theta_j^i} \quad (7)$$

Where  $v_i$  is the number of cavities of the type  $i$  per molecule of water,  $\theta_j^i$  is the occupancy rate of cavities  $i$  by each gas  $j$  (the occupancy rate is a function of thermodynamic conditions (pressure and temperature) and specific physical properties to the gas molecule, such as size, shape, or its mode of interaction with host molecules),  $C_T$  is the number of species of present gases,  $N_T$  is the number of different cavities in the elementary network. If we know the number of hydration and the formed structure, can then determine other physical quantities such that the molar volume or density.

#### 2.2.5 PHASE DIAGRAMS OF THE HYDRATES

Phase diagrams define stability regions of gas hydrates and the existing phases in the system. Usually, these phase diagrams represent the liquid-hydrate equilibrium in pressure vs temperature. Indeed, for a given temperature, knowing the pressure is directly linked to the knowledge of the gas solubility (thus the gas molecule concentration in the liquid phase). Figure 5 shows the phase diagram of methane from literature.

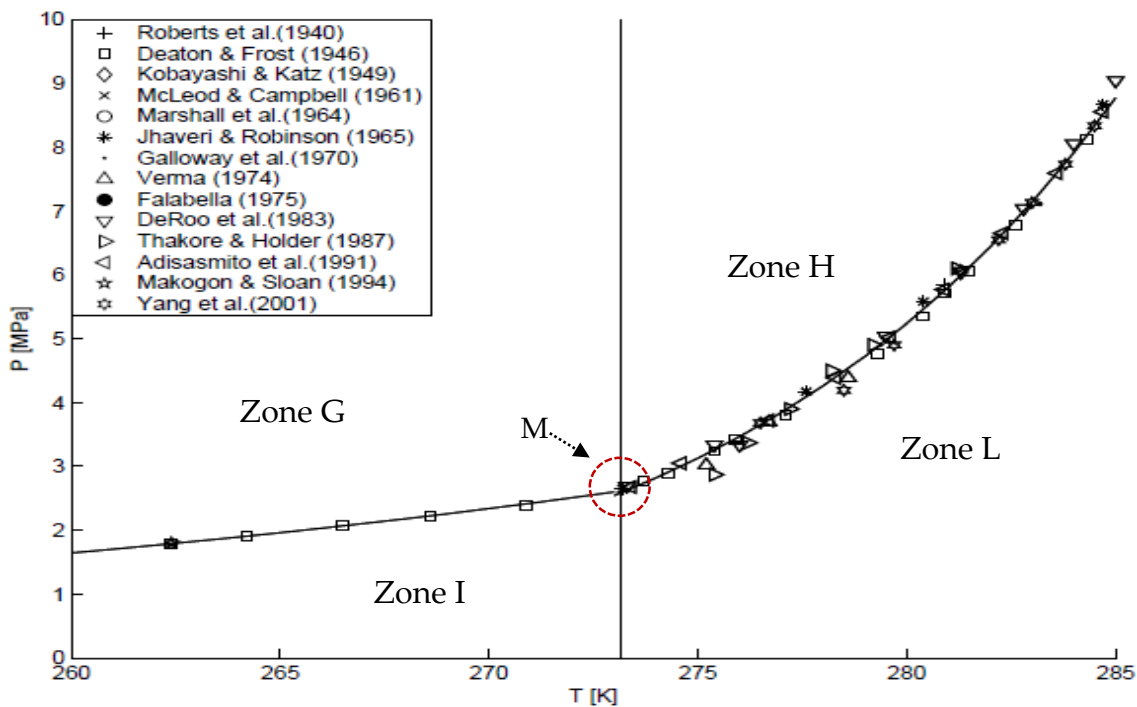


**Figure 5:** Phase diagrams of methane clathrate hydrates (with P: pressure; T: temperature) (Adisasmito et al., 1991; De Roo et al., 1983; Deaton and Frost, 1946; Falabella, 1975; Galloway et al., 1970; Jhaveri and Robinson, 1965; Kobayashi et al., 1949; Makogon and Sloan, 1994; Marshall et al., 1964; McLeod and Campbell, 1961; Roberts et al., 1940; Thakore and Holder, 1987; Verma, 1974; Yang et al., 2001).

On this figure, four different phases coexist around point M: ice, liquid water, gas, and hydrate. The lower left side (zone I) corresponds to the ice phase. The upper left side (zone G) corresponds to hydrate phase. Between the two zones is the ice-hydrate equilibrium curve. The bottom right area (zone L) is the liquid aqueous phase, and the upper right the hydrate phase again (zone H). Between zone L and H is the liquid-hydrate equilibrium. Between zones I and L is the ice-liquid equilibrium.

Based on the model of (Klauda and Sandler, 2005), a prediction for the distribution of methane hydrate in ocean sediment is presented on a  $1^\circ$  latitude by  $1^\circ$  longitude ( $1^\circ \times 1^\circ$ ) global grid. From that detailed prediction, it is estimated that the global gas hydrates in marine sediments contain  $1.2 \times 10^{17} \text{ m}^3$  of methane gas (expanded to atmospheric conditions), or, equivalently, 74 400 Gt of  $\text{CH}_4$  in ocean hydrates, which is 3 orders of magnitude larger than worldwide conventional natural gas reserves. Of this number, (Klauda and Sandler, 2005) estimated that  $4.4 \times 10^{16} \text{ m}^3$  of methane expanded to Standard Temperature and Pressure (STP) exists on the continental margins, which represents one of the largest sources of hydrocarbon on Earth.

### 3. EQUILIBRIUM DATA

The NIST Standard Reference Database #156 is an open access data base which gives the equilibrium data in multiphase systems with Clathrate Hydrates (CH), Vapor (V), Liquid water ( $L_w$ ) or Ice (I), Liquid hydrocarbon ( $L_{HC}$ ) for many pure components or mixtures. This data base extends the data from (Sloan, 2005, 1998): (<http://gashydrates.nist.gov/>).

The data base implemented in our in-house software, GasHyDyn, also offers a free access to many equilibrium data. All the following equilibrium data are extracted from this data base. The GasHyDyn database has been completed from the NIST database, literature survey and our own experimental data.

Gashydyn software is developed at Saint-Etienne School of Mines by The Hydrate team. It is based on classic Van der Waals and Plateeuw model for the prediction of gas hydrate equilibria with the constant of Parrish and Prausnitz. This software predicts the thermodynamics and the cage occupancy of stable hydrate structures (sI, sII, and sH) from a given pressure or temperature and gas phase composition: (<http://www.emse.fr>). This software can also be used for both pure and mixed gas hydrates. The software allows takes in account constants  $\Delta\mu_w^0$ ,  $\Delta C_p^0$ ,  $\Delta h_w^0$  and  $a$ ,  $\Delta v_w^0$ ,  $\Delta\mu_w^0$ ,  $\Delta C_p^0$ ,  $\Delta h_w^0$  from different authors. More details can be founded in section of the thermodynamic (presented in section §4. Page. 57).

In the next subsection will be provided pure and mixed hydrate equilibrium data. These data are relevant to this work since the same gas molecules were used.

### 3.1. PURE HYDRATES

#### 3.1.1 CO<sub>2</sub> CLATHRATE HYDRATE EQUILIBRIUM DATA

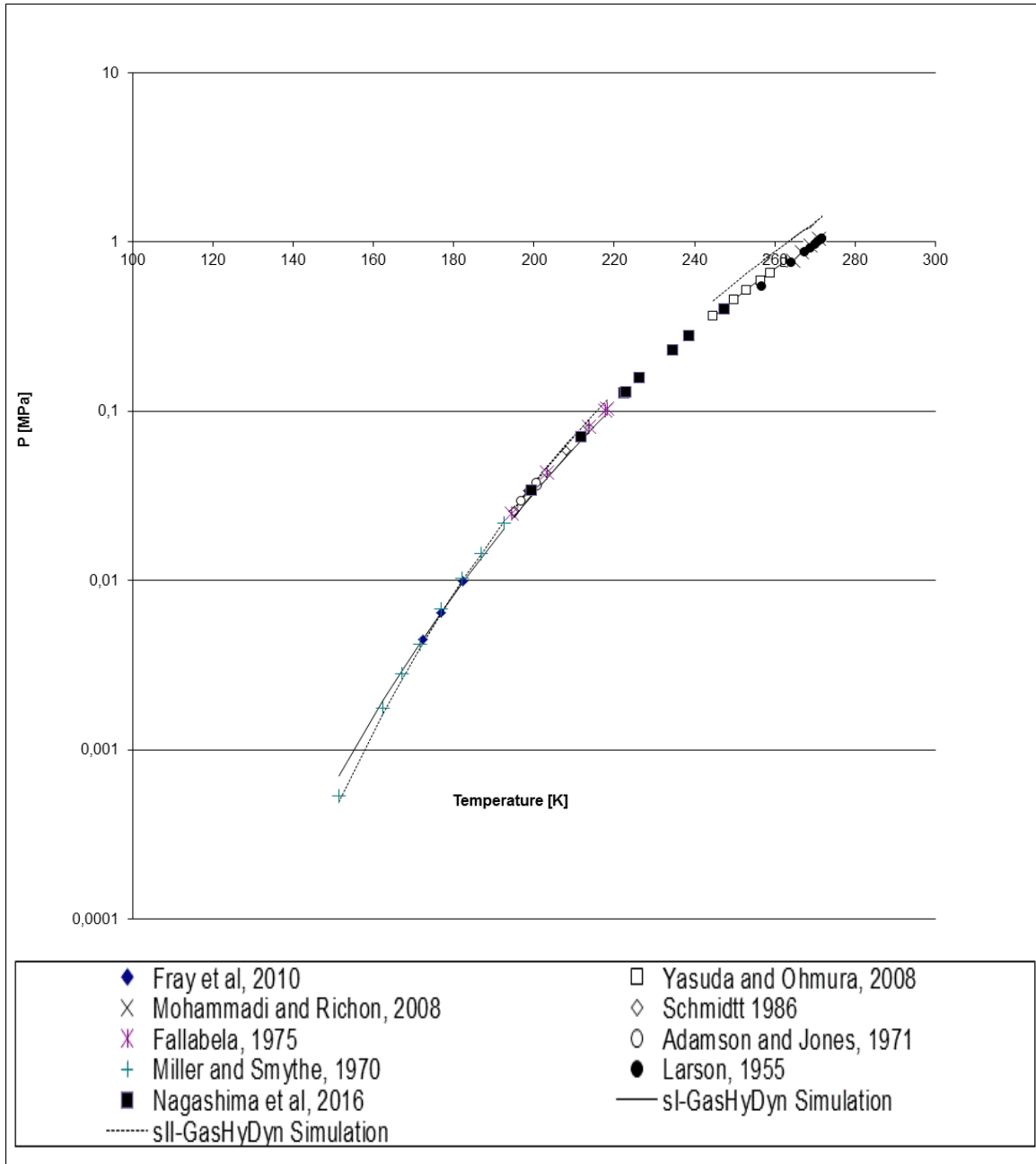


**Figure 6:** CH-V Equilibrium of single CO<sub>2</sub> at temperature below the ice point. The simulation curve is obtained with the GasHyDyn simulator, implemented with reference parameters from [Table 25 \(Dharmawardhana et al., 1980\)](#) and [Table 26. \(Page. 63\)](#) and Kihara parameters given in [Table 28. \(Page. 75\).](#)

### 3.1.2 CH<sub>4</sub> CLATHRATE HYDRATE EQUILIBRIUM DATA

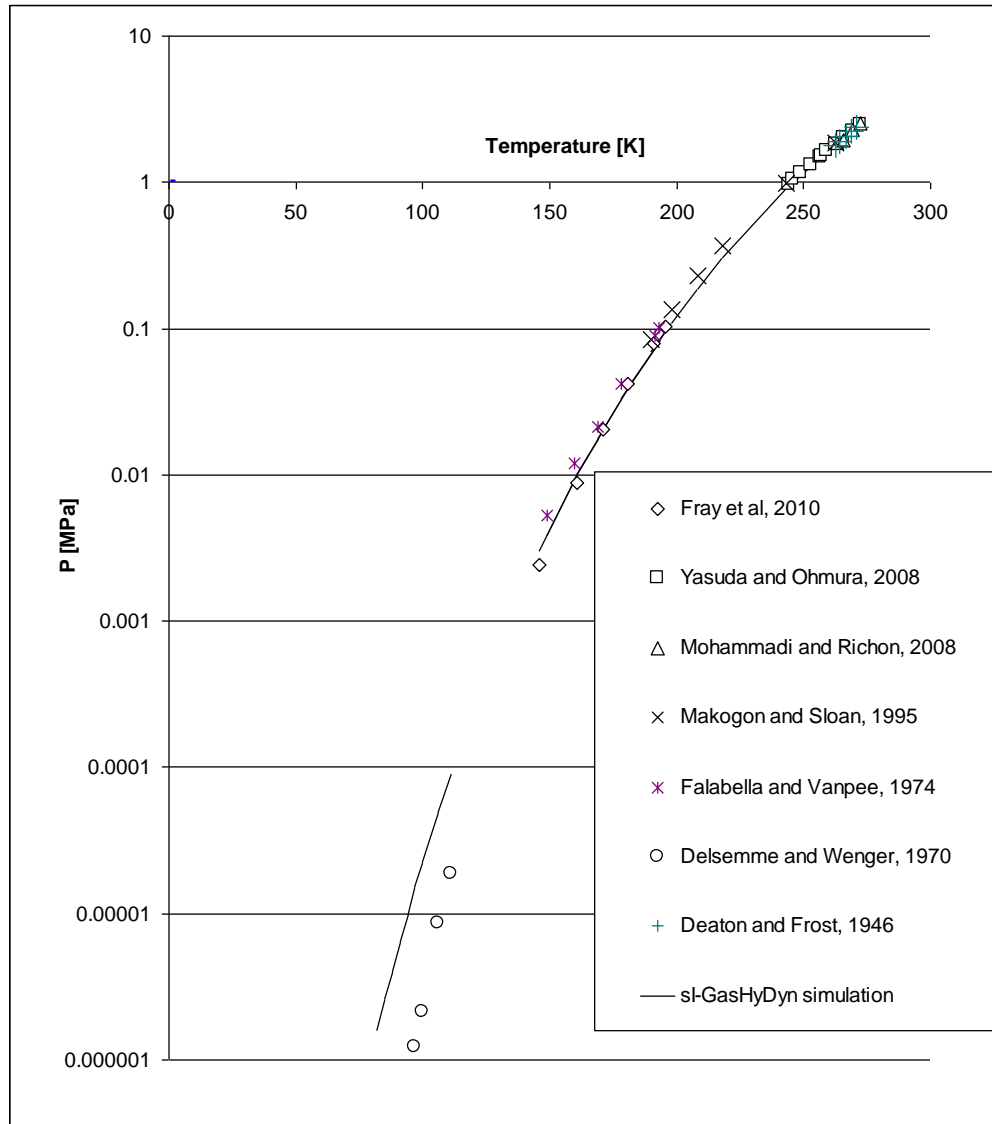


**Figure 7:** CH-V Equilibrium of single CH<sub>4</sub> at temperature below the ice point. The simulation of SI structure is obtained with the GasHyDyn simulator, implemented with reference parameters from [Table 25](#) (Dharmawardhana et al., 1980) and [Table 26](#). (Page. 63) and Kihara parameters given in [Table 28](#). (Page. 75).



### 3.1.3 C<sub>2</sub>H<sub>6</sub> CLATHRATE HYDRATE EQUILIBRIUM DATA

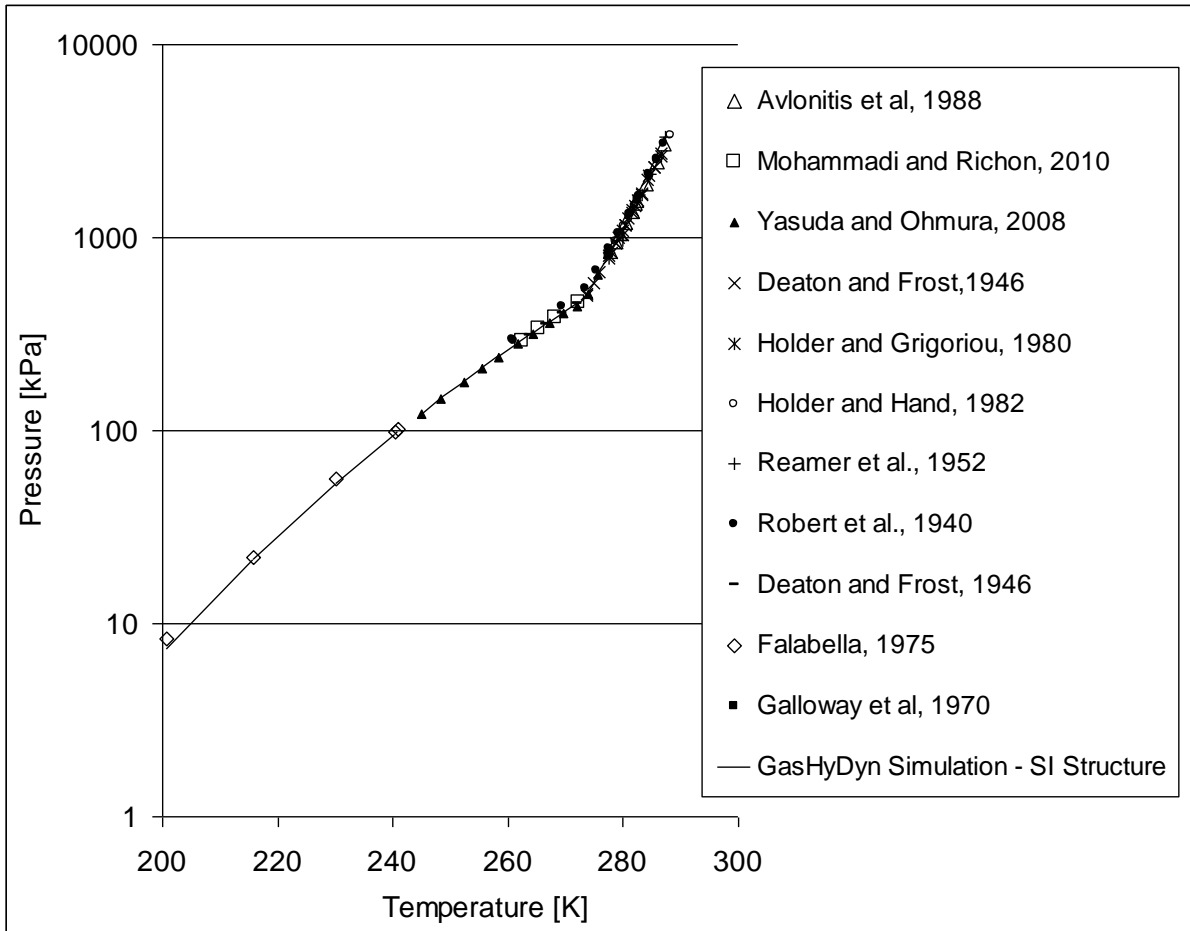


**Figure 8:** CH-V and CH\_SI-V-L<sub>w</sub> Equilibrium of single C<sub>2</sub>H<sub>6</sub>. The simulation of SI Structure is obtained with the GasHyDyn simulator, implemented with reference parameters from [Table 25 \(Dharmawardhana et al., 1980\)](#) and [Table 26. \(Page. 63\)](#) and Kihara parameters given in [Table 28. \(Page. 75\)](#).

### 3.1.4 C<sub>3</sub>H<sub>8</sub> CLATHRATE HYDRATE EQUILIBRIUM DATA

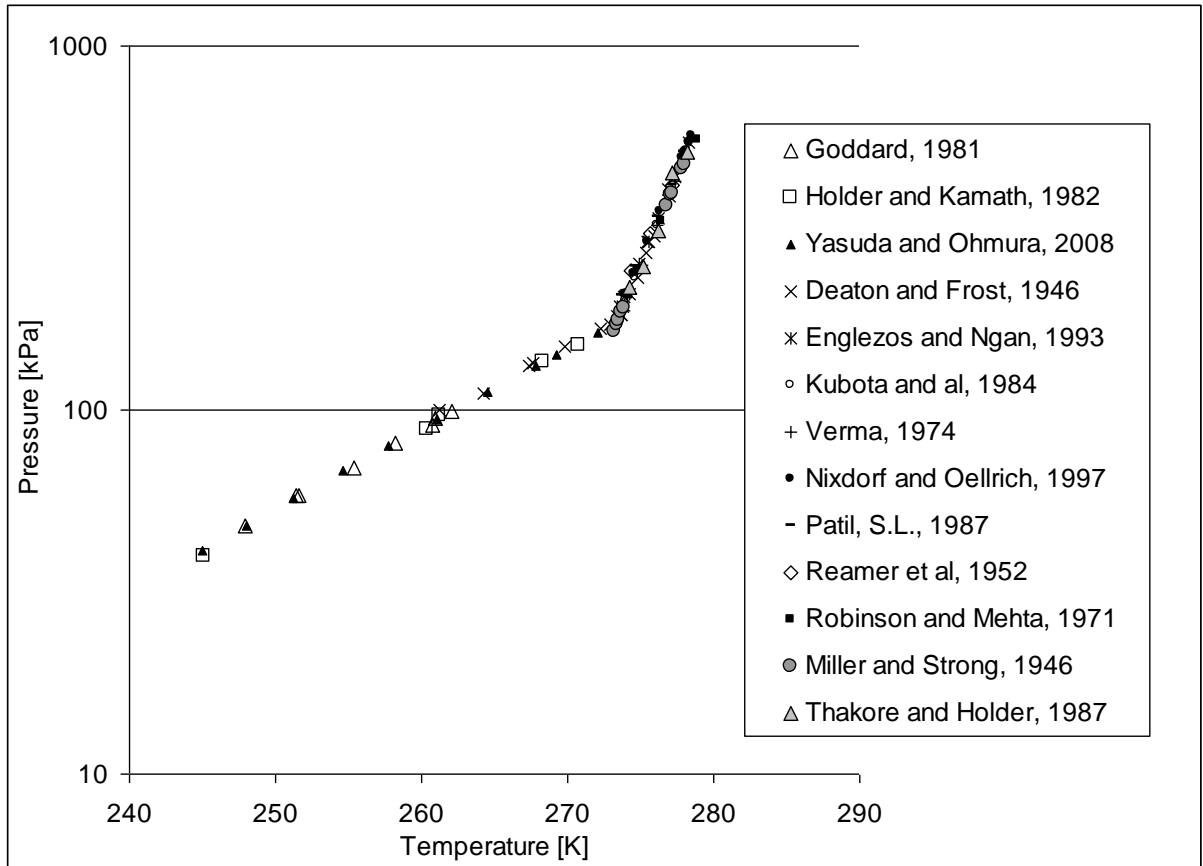


**Figure 9:** CH-V and CH<sub>SII</sub>-V-L<sub>w</sub> Equilibrium of single C<sub>3</sub>H<sub>8</sub>. The simulation of SII Structure is obtained with the GasHyDyn simulator, implemented with reference parameters from [Table 25](#) (Dharmawardhana et al., 1980) and [Table 26](#). (Page. 63) and Kihara parameters given in [Table 28](#). (Page. 75).

### 3.2. MIXED HYDRATES

#### 3.2.1 CO<sub>2</sub>-CH<sub>4</sub> CLATHRATE HYDRATE EQUILIBRIUM DATA

**Table 4:** CH<sub>SI</sub>-V-Lw Equilibrium of CO<sub>2</sub>-CH<sub>4</sub> from (Bouchemoua et al., 2009). The simulation curve is obtained with the GasHyDyn simulator, implemented with reference parameters from Table 25 (Dharmawardhana et al., 1980) and Table 26. (Page 63) and Kihara parameters given in Table 28. (Page. 75).

Experimental Equilibrium Data						Simulation			
T °C (±0.2)	P MPa (±0.02)	Gas composition (±0.003)		Hydrate composition (±0.0003)		S	P MPa (±0.02)	Hydrate composition (±0.001)	
		CO <sub>2</sub>	CH <sub>4</sub>	CO <sub>2</sub>	CH <sub>4</sub>			CO <sub>2</sub>	CH <sub>4</sub>
4	2.04	1.000	0.000	1.000	0.000	SI	2.03	1.000	0.000
4	2.36	0.639	0.361	0.767	0.233	SI	2.45	0.771	0.229
4	2.55	0.523	0.477	0.677	0.323	SI	2.63	0.678	0.322
4	2.8	0.364	0.636	0.535	0.465	SI	2.92	0.527	0.473
4	3.55	0.112	0.888	0.214	0.786	SI	3.55	0.202	0.798
4	3.9	0.000	1.000	0.000	1.000	SI	3.94	0.000	1.000
Mean Deviation (%)							2.14	1.98	1.37

**Table 5:** CH<sub>SI</sub>-V-Lw Equilibrium of CO<sub>2</sub>-CH<sub>4</sub> from (Le Quang, 2013). The simulation curve is obtained with the GasHyDyn simulator, implemented with reference parameters from Table 25 (Dharmawardhana et al., 1980) and Table 26. (Page. 63) and Kihara parameters given in Table 28. (Page. 75).

Experimental Equilibrium Data						Simulation			
T °C (±0.2)	P MPa (±0.02)	Gas composition (±0.003)		Hydrate composition (±0.0003)		S	P MPa (±0.02)	Hydrate composition (±0.001)	
		CO <sub>2</sub>	CH <sub>4</sub>	CO <sub>2</sub>	CH <sub>4</sub>			CO <sub>2</sub>	CH <sub>4</sub>
2.2	1.92	0.655	0.345	0.760	0.240	SI	1.99	0.789	0.211
2.9	2.05	0.776	0.224	0.640	0.360	SI	2.00	0.870	0.130
4	2.26	0.659	0.341	0.760	0.240	SI	2.42	0.786	0.214
4.5	2.44	0.665	0.335	0.760	0.240	SI	2.53	0.789	0.211
5.5	2.71	0.670	0.330	0.760	0.240	SI	2.86	0.789	0.211
6.5	3.01	0.678	0.322	0.740	0.260	SI	3.20	0.791	0.209
7.3	3.31	0.682	0.318	0.730	0.270	SI	3.53	0.790	0.210
2.2	2.91	0.120	0.880	0.290	0.710	SI	2.93	0.219	0.781
2.5	2.97	0.129	0.871	0.280	0.720	SI	3.00	0.232	0.768
3.6	3.18	0.135	0.865	0.280	0.720	SI	3.33	0.239	0.761
4.5	3.47	0.147	0.853	0.260	0.740	SI	3.63	0.254	0.746
5.2	3.8	0.162	0.838	0.200	0.800	SI	3.85	0.274	0.726
2.2	2.52	0.296	0.704	none	none	SI	2.53	0.459	0.541
3.1	2.59	0.454	0.546	none	none	SI	2.49	0.620	0.380
3.9	2.81	0.407	0.593	none	none	SI	2.80	0.572	0.428
4.7	3.02	0.334	0.666	none	none	SI	3.21	0.492	0.508

5.6	3.29	0.340	0.660	none	none	SI	3.52	0.495	0.505
6.6	3.53	0.345	0.655	none	none	SI	3.93	0.495	0.505
7.3	3.87	0.350	0.650	none	none	SI	4.25	0.497	0.503
3.4	3.33	0.127	0.873	0.311	0.689	SI	3.29	0.227	0.773
4.4	3.53	0.134	0.866	0.309	0.691	SI	3.62	0.235	0.765
4.9	3.71	0.141	0.859	0.308	0.692	SI	3.80	0.244	0.756
5.8	4.03	0.151	0.849	0.304	0.696	SI	4.14	0.256	0.744
6.8	4.45	0.163	0.837	0.295	0.705	SI	4.57	0.270	0.730
7.8	4.93	0.175	0.825	0.260	0.740	SI	5.06	0.283	0.717
2.2	2.91	0.120	0.880	0.290	0.710	SI	2.93	0.219	0.781
2.5	2.97	0.129	0.871	0.280	0.720	SI	3.00	0.232	0.768
3.6	3.18	0.135	0.865	0.280	0.720	SI	3.33	0.239	0.761
4.5	3.47	0.147	0.853	0.260	0.740	SI	3.63	0.254	0.746
5.2	3.8	0.162	0.838	0.200	0.800	SI	3.85	0.274	0.726
Mean Deviation (%)							3.8	15.7	11.5

**Table 6:** CH<sub>4</sub>-SI-V-Lw Equilibrium of CO<sub>2</sub>-CH<sub>4</sub> from (Belandria et al., 2011). The simulation curve is obtained with the GasHyDyn simulator, implemented with reference parameters from Table 25 (Dharmawardhana et al., 1980) and Table 26. (Page. 63) and Kihara parameters given in Table 28. (Page. 75).

Experimental Equilibrium Data						Simulation			
T °C	P MPa	Gas composition (±0.003)		Hydrate composition (±0.003)		S	P MPa	Hydrate composition (±0.001)	
(±0.2)	(±0.02)	CO <sub>2</sub>	CH <sub>4</sub>	CO <sub>2</sub>	CH <sub>4</sub>		(±0.02)	CO <sub>2</sub>	CH <sub>4</sub>
0.45	2.234	0.141	0.859	none	none	SI	2.41	0.255	0.745
0.45	2.416	0.125	0.875	none	none	SI	2.43	0.230	0.770
0.45	2.44	0.081	0.919	0.096	0.904	SI	2.55	0.156	0.844
0.45	1.844	0.345	0.655	0.549	0.451	SI	2.03	0.520	0.480
0.45	1.941	0.288	0.712	0.392	0.608	SI	2.12	0.455	0.545
0.45	2.048	0.220	0.780	0.294	0.706	SI	2.24	0.369	0.631
0.45	1.51	0.630	0.370	0.884	0.116	SI	1.67	0.775	0.225
0.45	1.607	0.545	0.455	0.801	0.199	SI	1.77	0.708	0.292
2.05	2.583	0.166	0.834	0.338	0.662	SI	2.77	0.289	0.711
2.05	2.712	0.129	0.871	none	none	SI	2.84	0.233	0.767
2.05	2.766	0.086	0.914	0.179	0.821	SI	2.98	0.162	0.838
2.05	2.123	0.384	0.616	0.650	0.350	SI	2.33	0.556	0.444
2.05	2.22	0.302	0.698	0.586	0.414	SI	2.48	0.466	0.534
2.05	2.4	0.228	0.772	0.366	0.634	SI	2.63	0.375	0.625
2.05	1.792	0.657	0.343	0.831	0.169	SI	1.96	0.790	0.210
2.05	1.865	0.565	0.435	0.752	0.248	SI	2.07	0.720	0.280
2.95	2.813	0.179	0.821	0.264	0.736	SI	3.00	0.306	0.694
2.95	3.025	0.134	0.866	0.239	0.761	SI	3.12	0.239	0.761
2.95	3.027	0.096	0.904	0.238	0.762	SI	3.23	0.178	0.822
2.95	2.318	0.405	0.595	0.644	0.356	SI	2.43	0.575	0.425
2.95	2.503	0.315	0.685	0.400	0.600	SI	2.70	0.478	0.522
2.95	2.69	0.232	0.768	0.312	0.688	SI	2.88	0.377	0.623
2.95	1.985	0.669	0.331	0.877	0.123	SI	2.14	0.797	0.203

2.95	2.174	0.579	0.421	0.784	0.216	SI	2.26	0.728	0.272
4.95	3.416	0.202	0.798	0.233	0.767	SI	3.64	0.331	0.669
4.95	3.631	0.139	0.861	0.225	0.775	SI	3.83	0.241	0.759
4.95	3.802	0.103	0.897	0.148	0.852	SI	3.95	0.185	0.815
4.95	3.037	0.323	0.677	0.457	0.543	SI	3.33	0.479	0.521
4.95	3.319	0.233	0.767	0.273	0.727	SI	3.55	0.372	0.628
4.95	2.45	0.694	0.306	none	none	SI	2.65	0.808	0.192
4.95	2.58	0.609	0.391	0.786	0.214	SI	2.77	0.745	0.255
6.05	3.565	0.202	0.798	0.266	0.734	SI	4.09	0.327	0.673
7.05	4.486	0.147	0.853	0.307	0.693	SI	4.76	0.246	0.754
7.05	4.655	0.108	0.892	0.245	0.755	SI	4.90	0.188	0.812
7.05	3.541	0.344	0.656	0.727	0.273	SI	4.14	0.492	0.508
7.05	4.109	0.235	0.765	0.339	0.661	SI	4.46	0.365	0.635
7.05	3.139	0.620	0.380	0.860	0.140	SI	3.53	0.744	0.256
7.05	3.481	0.490	0.510	0.788	0.212	SI	3.75	0.635	0.365
9.05	5.767	0.114	0.886	0.276	0.724	SI	6.08	0.191	0.809
11.05	7.19	0.115	0.885	0.107	0.893	SI	7.65	0.184	0.816
Mean Deviation (%)							7.8	18.8	21.4

**Table 7:** CH<sub>4</sub>-SI-V-Lw Equilibrium of CO<sub>2</sub>-CH<sub>4</sub> from (Seo et al., 2000). The simulation curve is obtained with the GasHyDyn simulator, implemented with reference parameters from Table 25 (Dharmawardhana et al., 1980) and Table 26. (Page. 63) and Kihara parameters given in Table 28. (Page. 75).

Experimental Equilibrium Data						Simulation			
T °C	P MPa	Gas composition (±0.003)		Hydrate composition (±0.003)		S	P MPa (±0.02)	Hydrate composition (±0.001)	
(±0.2)	(±0.02)	CO <sub>2</sub>	CH <sub>4</sub>	CO <sub>2</sub>	CH <sub>4</sub>			CO <sub>2</sub>	CH <sub>4</sub>
-0.05	2	0.284	0.716	0.915	0.085	SI	1.92	0.453	0.547
0.95	2	0.403	0.597	0.936	0.064	SI	2.03	0.579	0.421
2.25	2	0.608	0.392	0.982	0.018	SI	2.06	0.753	0.247
3.15	2	0.794	0.206	0.997	0.003	SI	2.04	0.881	0.119
0.65	2.6	0.129	0.871	0.662	0.338	SI	2.48	0.236	0.764
1.75	2.6	0.234	0.766	0.847	0.153	SI	2.54	0.384	0.616
3.15	2.6	0.415	0.585	0.927	0.073	SI	2.56	0.583	0.417
4.35	2.6	0.641	0.359	0.981	0.019	SI	2.55	0.772	0.228
4.95	2.6	0.834	0.166	0.994	0.006	SI	2.46	0.902	0.098
3.45	3.5	0.133	0.867	0.647	0.353	SI	3.29	0.236	0.764
4.45	3.5	0.252	0.748	0.733	0.267	SI	3.32	0.397	0.603
5.85	3.5	0.419	0.581	0.890	0.110	SI	3.45	0.575	0.425
6.75	3.5	0.611	0.389	0.952	0.048	SI	3.43	0.738	0.262
7.35	3.5	0.834	0.166	0.993	0.007	SI	3.30	0.896	0.104
Mean Deviation (%)							3.3	34.8	866.5

**Table 8:** CH<sub>4</sub>-SI-V-Lw Equilibrium of CO<sub>2</sub>-CH<sub>4</sub> from (Fan and Guo, 1999). The simulation curve is obtained with the GasHyDyn simulator, implemented with reference parameters from Table 25 (Dharmawardhana et al., 1980) and Table 26. (Page. 63) and Kihara parameters given in Table 28. (Page. 75).

Experimental Equilibrium Data						Simulation			
T °C (±0.2)	P MPa (±0.02)	Gas composition (±0.003)		Hydrate composition (±0.003)		S	P MPa (±0.02)	Hydrate composition (±0.001)	
		CO <sub>2</sub>	CH <sub>4</sub>	CO <sub>2</sub>	CH <sub>4</sub>			CO <sub>2</sub>	CH <sub>4</sub>
0.35	1.1	0.965	0.035	none	none	SI	1.37	0.982	0.018
0.45	1.16	0.965	0.035	none	none	SI	1.38	0.982	0.018
0.55	1.2	0.965	0.035	none	none	SI	1.40	0.982	0.018
4.05	1.95	0.965	0.035	none	none	SI	2.07	0.981	0.019
4.45	1.94	0.965	0.035	none	none	SI	2.17	0.981	0.019
4.75	2.05	0.965	0.035	none	none	SI	2.25	0.981	0.019
7.25	3	0.965	0.035	none	none	SI	3.07	0.979	0.021
8.55	3.73	0.965	0.035	none	none	SI	3.65	0.978	0.022
9.15	4.8	0.965	0.035	none	none	SI	3.98	0.977	0.023
Mean Deviation (%)							12.2	none	none

**Table 9:** CH<sub>4</sub>-SI-V-Lw Equilibrium of CO<sub>2</sub>-CH<sub>4</sub> from (Ohgaki et al., 1996). The simulation curve is obtained with the GasHyDyn simulator, implemented with reference parameters from Table 25 (Dharmawardhana et al., 1980) and Table 26. (Page. 63) and Kihara parameters given in Table 28. (Page. 75).

Experimental Equilibrium Data						Simulation			
T °C (±0.2)	P MPa (±0.02)	Gas composition (±0.003)		Hydrate composition (±0.003)		S	P MPa (±0.02)	Hydrate composition (±0.001)	
		CO <sub>2</sub>	CH <sub>4</sub>	CO <sub>2</sub>	CH <sub>4</sub>			CO <sub>2</sub>	CH <sub>4</sub>
7.15	3.04	1.000	0.000	1.000	0.000	SI	2.98	1.000	0.000
7.15	3.24	0.683	0.317	0.840	0.160	SI	3.46	0.792	0.208
7.15	3.38	0.585	0.415	0.800	0.200	SI	3.55	0.717	0.283
7.15	3.6	0.488	0.512	0.670	0.330	SI	3.85	0.632	0.368
7.15	3.64	0.450	0.550	0.690	0.310	SI	3.93	0.598	0.402
7.15	3.67	0.448	0.552	0.680	0.320	SI	3.93	0.596	0.404
7.15	3.71	0.429	0.571	0.610	0.390	SI	3.98	0.578	0.422
7.15	3.77	0.384	0.616	0.600	0.400	SI	4.09	0.533	0.467
7.15	3.86	0.357	0.643	0.590	0.410	SI	4.16	0.505	0.495
7.15	4.22	0.241	0.759	0.440	0.560	SI	4.49	0.372	0.628
7.15	4.31	0.215	0.785	0.390	0.610	SI	4.57	0.339	0.661
7.15	4.32	0.217	0.783	0.360	0.640	SI	4.57	0.342	0.658
7.15	4.34	0.203	0.797	0.370	0.630	SI	4.61	0.323	0.677
7.15	4.37	0.203	0.797	0.350	0.650	SI	4.61	0.323	0.677
7.15	4.37	0.183	0.817	0.360	0.640	SI	4.68	0.297	0.703
7.15	4.44	0.179	0.821	0.360	0.640	SI	4.70	0.291	0.709
7.15	4.5	0.169	0.831	0.350	0.650	SI	4.73	0.277	0.723
7.15	4.57	0.144	0.856	0.320	0.680	SI	4.82	0.242	0.758

7.15	3.98	0.302	0.698	0.530	0.470	SI	4.31	0.445	0.555
7.15	4	0.310	0.690	0.520	0.480	SI	4.29	0.454	0.546
7.15	4.01	0.311	0.689	0.550	0.450	SI	4.28	0.455	0.545
7.15	4.06	0.288	0.712	0.510	0.490	SI	4.35	0.429	0.571
7.15	4.07	0.293	0.707	0.520	0.480	SI	4.33	0.434	0.566
7.15	4.15	0.268	0.732	0.470	0.530	SI	4.41	0.405	0.595
7.15	4.2	0.245	0.755	0.450	0.550	SI	4.48	0.377	0.623
7.15	4.58	0.141	0.859	0.320	0.680	SI	4.83	0.237	0.763
7.15	4.63	0.143	0.857	0.290	0.710	SI	4.83	0.240	0.760
7.15	4.75	0.104	0.896	0.240	0.760	SI	4.96	0.181	0.819
7.15	4.85	0.090	0.910	0.230	0.770	SI	5.03	0.159	0.841
7.15	4.99	0.065	0.935	0.160	0.840	SI	5.14	0.118	0.882
7.15	5.46	0.000	1.000	0.000	1.000	SI	5.44	0.000	1.000
Mean Deviation (%)							5.9	15.4	14.4

**Table 10:** CH<sub>4</sub>-SI-V-Lw Equilibrium of CO<sub>2</sub>-CH<sub>4</sub> from (Adisasmito et al., 1991). The simulation curve is obtained with the GasHyDyn simulator, implemented with reference parameters from Table 25 (Dharmawardhana et al., 1980) and Table 26. (Page. 63) and Kihara parameters given in Table 28. (Page. 75).

Experimental Equilibrium Data						Simulation			
T °C (±0.2)	P MPa (±0.02)	Gas composition (±0.003)		Hydrate composition (±0.003)		S	P MPa (±0.02)	Hydrate composition (±0.001)	
		CO <sub>2</sub>	CH <sub>4</sub>	CO <sub>2</sub>	CH <sub>4</sub>			CO <sub>2</sub>	CH <sub>4</sub>
0.55	2.52	0.100	0.900	none	none	SI	2.53	0.189	0.811
2.65	3.1	0.090	0.910	none	none	SI	3.15	0.168	0.832
4.65	3.83	0.080	0.920	none	none	SI	3.90	0.148	0.852
7.05	4.91	0.080	0.920	none	none	SI	5.02	0.143	0.857
10.05	6.8	0.080	0.920	none	none	SI	6.98	0.135	0.865
11.95	8.4	0.080	0.920	none	none	SI	8.71	0.130	0.870
14.05	10.76	0.090	0.910	none	none	SI	11.20	0.136	0.864
1.45	2.59	0.140	0.860	none	none	SI	2.67	0.252	0.748
3.75	3.24	0.130	0.870	none	none	SI	3.40	0.231	0.769
5.95	4.18	0.130	0.870	none	none	SI	4.28	0.225	0.775
8.45	5.38	0.130	0.870	none	none	SI	5.57	0.217	0.783
10.85	7.17	0.130	0.870	none	none	SI	7.40	0.207	0.793
12.95	9.24	0.120	0.880	none	none	SI	9.60	0.183	0.817
14.25	10.95	0.130	0.870	none	none	SI	11.30	0.189	0.811
0.65	2.12	0.250	0.750	none	none	SI	2.24	0.408	0.592
6.25	3.96	0.220	0.780	none	none	SI	4.13	0.350	0.650
10.25	6.23	0.220	0.780	none	none	SI	6.51	0.329	0.671
12.05	7.75	0.210	0.790	none	none	SI	8.16	0.304	0.696
14.45	10.44	0.250	0.750	none	none	SI	11.10	0.327	0.673
0.55	1.81	0.440	0.560	none	none	SI	1.92	0.616	0.384
3.75	2.63	0.420	0.580	none	none	SI	2.73	0.585	0.415
7.55	4.03	0.400	0.600	none	none	SI	4.24	0.547	0.453
9.95	5.43	0.390	0.610	none	none	SI	5.70	0.519	0.481
11.95	6.94	0.390	0.610	none	none	SI	7.42	0.499	0.501

14.25	9.78	0.390	0.610	none	none	SI	10.41	0.465	0.535
2.45	1.99	0.500	0.500	none	none	SI	2.25	0.664	0.336
5.35	2.98	0.470	0.530	none	none	SI	3.15	0.626	0.374
7.75	4.14	0.400	0.600	none	none	SI	4.34	0.545	0.455
8.65	4.47	0.410	0.590	none	none	SI	4.76	0.550	0.450
11.95	6.84	0.440	0.560	none	none	SI	7.29	0.546	0.454
14.25	9.59	0.450	0.550	none	none	SI	10.23	0.517	0.483
1.45	1.66	0.730	0.270	none	none	SI	1.75	0.842	0.158
3.25	2.08	0.700	0.300	none	none	SI	2.13	0.818	0.182
5.05	2.58	0.680	0.320	none	none	SI	2.70	0.798	0.202
7.05	3.28	0.680	0.320	none	none	SI	3.43	0.790	0.210
8.85	4.12	0.670	0.330	none	none	SI	4.33	0.772	0.228
0.55	1.45	0.790	0.210	none	none	SI	1.54	0.883	0.117
2.75	1.88	0.780	0.220	none	none	SI	1.97	0.873	0.127
4.65	2.37	0.760	0.240	none	none	SI	2.47	0.855	0.145
6.45	2.97	0.750	0.250	none	none	SI	3.07	0.843	0.157
8.45	3.79	0.740	0.260	none	none	SI	3.97	0.827	0.173
9.55	4.37	0.850	0.150	none	none	SI	4.41	0.898	0.102
Mean Deviation (%)							4.5	none	none

**Table 11:** CH<sub>4</sub>-SI-V-Lw Equilibrium of CO<sub>2</sub>-CH<sub>4</sub> from (Hachikubo et al., 2002). The simulation curve is obtained with the GasHyDyn simulator, implemented with reference parameters from Table 25 (Dharmawardhana et al., 1980) and Table 26. (Page. 63) and Kihara parameters given in Table 28. (Page. 75).

Experimental Equilibrium Data						Simulation			
T °C (±0.2)	P MPa (±0.02)	Gas composition (±0.003)		Hydrate composition (±0.003)		S	P MPa (±0.02)	Hydrate composition (±0.001)	
		CO <sub>2</sub>	CH <sub>4</sub>	CO <sub>2</sub>	CH <sub>4</sub>			CO <sub>2</sub>	CH <sub>4</sub>
0.78	1.349	1.000	0.000	1.000	0.000	SI	1.41	1.000	0.000
3.65	1.806	1.000	0.000	1.000	0.000	SI	1.94	1.000	0.000
4.9	2.204	1.000	0.000	1.000	0.000	SI	2.25	1.000	0.000
-9.98	0.774	1.000	0.000	1.000	0.000	SI	0.79	1.000	0.000
-5.04	0.921	1.000	0.000	1.000	0.000	SI	0.96	1.000	0.000
-1.92	1.029	1.000	0.000	1.000	0.000	SI	1.09	1.000	0.000
4.13	2.187	1.000	0.000	1.000	0.000	SI	2.06	1.000	0.000
-4.75	2.324	0.000	1.000	0.000	1.000	SI	2.23	0.000	1.000
-1.87	2.527	0.000	1.000	0.000	1.000	SI	2.45	0.000	1.000
-1.9	1.271	0.770	0.230	none	none	SI	1.25	0.873	0.127
-1.74	1.434	0.500	0.500	none	none	SI	1.52	0.676	0.324
-1.78	2.022	0.250	0.750	none	none	SI	1.87	0.413	0.587
Mean Deviation (%)							4.6	none	none



**Table 12:** CH<sub>4</sub>-SI-V-Lw Equilibrium of CO<sub>2</sub>-CH<sub>4</sub> from (Unruh and Katz, 1949). The simulation curve is obtained with the GasHyDyn simulator, implemented with reference parameters from Table 25 (Dharmawardhana et al., 1980) and Table 26. (Page. 63) and Kihara parameters given in Table 28. (Page. 75).

Experimental Equilibrium Data						Simulation			
T °C	P MPa	Gas composition (±0.003)		Hydrate composition (±0.003)		S	P MPa (±0.02)	Hydrate composition (±0.001)	
(±0.2)	(±0.02)	CO <sub>2</sub>	CH <sub>4</sub>	CO <sub>2</sub>	CH <sub>4</sub>			CO <sub>2</sub>	CH <sub>4</sub>
5.75	3.46	0.300	0.700	none	none	SI	3.69	0.449	0.551
5.75	3.43	0.360	0.640	none	none	SI	3.45	0.516	0.484
7.75	4.24	0.320	0.680	none	none	SI	4.56	0.461	0.539
9.75	5.17	0.280	0.720	none	none	SI	5.91	0.404	0.596
11.55	6.47	0.230	0.770	none	none	SI	7.50	0.332	0.668
2.35	1.99	0.600	0.400	none	none	SI	2.09	0.747	0.253
6.05	3.08	0.440	0.560	none	none	SI	3.48	0.594	0.406
3.25	3.2	0.125	0.875	none	none	SI	3.25	0.224	0.776
5.25	3.95	0.085	0.915	none	none	SI	4.13	0.155	0.845
7.85	5.1	0.070	0.930	none	none	SI	5.52	0.125	0.875
10.65	6.89	0.055	0.945	none	none	SI	7.61	0.094	0.906
6.45	3	0.710	0.290	none	none	SI	3.13	0.814	0.186
9.05	4.27	0.610	0.390	none	none	SI	4.57	0.723	0.277
10.65	5.27	0.520	0.480	none	none	SI	5.88	0.633	0.367
12.35	6.89	0.410	0.590	none	none	SI	7.70	0.514	0.486
12.55	7	0.410	0.590	none	none	SI	8.00	0.510	0.490
Mean Deviation (%)							8.2	none	None

### 3.2.2 CO<sub>2</sub>-C<sub>2</sub>H<sub>6</sub> CLATHRATE HYDRATE EQUILIBRIUM DATA

**Table 13 :** CH<sub>4</sub>-SI-V-Lw Equilibrium of CH<sub>4</sub>-C<sub>2</sub>H<sub>6</sub> from (Adisasmito and Sloan, 1992). The simulation curve is obtained with the GasHyDyn simulator, implemented with reference parameters from Table 25 (Dharmawardhana et al., 1980) and Table 26. (Page. 63) and Kihara parameters given in Table 28. (Page. 75).

Experimental Equilibrium Data						Simulation			
T °C	P MPa	Gas composition (±0.003)		Hydrate composition (±0.003)		S	P MPa (±0.02)	Hydrate composition (±0.001)	
(±0.2)	(±0.02)	CO <sub>2</sub>	C <sub>2</sub> H <sub>6</sub>	CO <sub>2</sub>	C <sub>2</sub> H <sub>6</sub>			CO <sub>2</sub>	CO <sub>2</sub> H <sub>6</sub>
0.55	0.57	0.220	0.780	none	none	SI	0.49	0.192	0.808
2.45	0.70	0.202	0.798	none	none	SI	0.60	0.189	0.811
4.35	0.87	0.189	0.811	none	none	SI	0.75	0.189	0.811
6.15	1.09	0.193	0.807	none	none	SI	0.92	0.198	0.802
7.95	1.41	0.246	0.754	none	none	SI	1.13	0.230	0.770
9.75	1.75	0.256	0.744	none	none	SI	1.39	0.241	0.759
11.95	2.39	0.317	0.683	none	none	SI	1.83	0.275	0.725
3.35	0.85	0.428	0.572	none	none	SI	0.73	0.299	0.701

5.25	1.08	0.417	0.583	none	none	SI	0.89	0.300	0.700
7.05	1.35	0.406	0.594	none	none	SI	1.08	0.300	0.700
8.85	1.72	0.400	0.600	none	none	SI	1.32	0.303	0.697
10.65	2.19	0.402	0.598	none	none	SI	1.63	0.309	0.691
12.65	2.83	0.389	0.611	none	none	SI	2.05	0.309	0.691
14.65	3.83	0.398	0.602	none	none	SI	2.64	0.321	0.679
0.55	0.57	0.220	0.780	none	none	SI	0.49	0.192	0.808
Mean Deviation (%)							19.9	none	none

### 3.2.3 CH<sub>4</sub>-C<sub>3</sub>H<sub>8</sub> CLATHRATE HYDRATE EQUILIBRIUM DATA

**Table 14:** CH-V-Lw Equilibrium of CH<sub>4</sub>-C<sub>3</sub>H<sub>8</sub> from (Verma et al., 1974). The simulation curve is obtained with the GasHyDyn simulator, implemented with reference parameters from Table 25 (Dharmawardhana et al., 1980) and Table 26. (Page. 63) and Kihara parameters given in Table 28. (Page. 75).

Experimental Equilibrium Data						Simulation			
T °C (±0.2)	P MPa (±0.02)	Gas composition (±0.003)		Hydrate composition (±0.003)		S	P MPa (±0.02)	Hydrate composition (±0.001)	
		CH <sub>4</sub>	C <sub>3</sub> H <sub>8</sub>	CH <sub>4</sub>	C <sub>3</sub> H <sub>8</sub>			CH <sub>4</sub>	C <sub>3</sub> H <sub>8</sub>
1.75	0.263	0.2375	0.7625	none	none	SI	0.34	0.119	0.881
3.25	0.35	0.2375	0.7625	none	none	SI	0.40	0.127	0.873
4.65	0.443	0.2375	0.7625	none	none	SI	0.48	0.135	0.865
5.95	0.56	0.2375	0.7625	none	none	SI	0.56	0.142	0.858
7.05	0.689	0.2375	0.7625	none	none	SI	0.65	0.149	0.851
8.25	0.83	0.2375	0.7625	none	none	SI	0.75	0.156	0.844
1.25	0.27	0.371	0.629	none	none	SI	0.35	0.159	0.841
2.75	0.343	0.371	0.629	none	none	SI	0.42	0.167	0.833
3.95	0.419	0.371	0.629	none	none	SI	0.49	0.174	0.826
5.45	0.536	0.371	0.629	none	none	SI	0.58	0.182	0.818
7.05	0.691	0.371	0.629	none	none	SI	0.71	0.191	0.809
9.15	0.945	0.371	0.629	none	none	SI	0.92	0.202	0.798
Mean Deviation (%)							12.6	none	None
1.75	0.26	0.238	0.763	none	none	SII	0.19	0.324	0.676
3.25	0.35	0.238	0.763	none	none	SII	0.25	0.353	0.647
4.65	0.44	0.238	0.763	none	none	SII	0.30	0.379	0.621
5.95	0.56	0.238	0.763	none	none	SII	0.37	0.403	0.597
7.05	0.69	0.238	0.763	none	none	SII	0.44	0.422	0.578
8.25	0.83	0.238	0.763	none	none	SII	0.52	0.441	0.559
1.25	0.27	0.371	0.629	none	none	SII	0.17	0.382	0.618
2.75	0.34	0.371	0.629	none	none	SII	0.22	0.408	0.592
3.95	0.42	0.371	0.629	none	none	SII	0.26	0.427	0.573
5.45	0.54	0.371	0.629	none	none	SII	0.32	0.450	0.550
7.05	0.69	0.371	0.629	none	none	SII	0.40	0.472	0.528
9.15	0.95	0.371	0.629	none	none	SII	0.52	0.498	0.502
Mean Deviation (%)							36.3	none	None

**Table 15:** CH-V-Lw Equilibrium of CH<sub>4</sub>-C<sub>3</sub>H<sub>8</sub> from (Deaton and Frost, 1946). The simulation curve is obtained with the GasHyDyn simulator, implemented with reference parameters from Table 25 (Dharmawardhana et al., 1980) and Table 26. (Page. 63) and Kihara parameters given in Table 28. (Page. 75).

Experimental Equilibrium Data						Simulation			
T °C	P MPa	Gas composition (±0.003)		Hydrate composition (±0.003)		S	P MPa (±0.02)	Hydrate composition (±0.001)	
(±0.2)	(±0.02)	CH <sub>4</sub>	C <sub>3</sub> H <sub>8</sub>	CH <sub>4</sub>	C <sub>3</sub> H <sub>8</sub>			CH <sub>4</sub>	C <sub>3</sub> H <sub>8</sub>
1.65	0.27	0.362	0.638	none	none	SI	0.37	0.159	0.841
4.45	0.44	0.362	0.638	none	none	SI	0.51	0.174	0.826
7.25	0.69	0.362	0.638	none	none	SI	0.72	0.189	0.811
1.65	0.37	0.712	0.288	none	none	SI	0.61	0.274	0.726
4.45	0.54	0.712	0.288	none	none	SI	0.85	0.288	0.712
7.25	0.80	0.712	0.288	none	none	SI	1.18	0.302	0.698
10.05	1.15	0.712	0.288	none	none	SI	1.67	0.318	0.682
1.65	0.55	0.883	0.117	none	none	SI	1.08	0.412	0.588
4.45	0.78	0.883	0.117	none	none	SI	1.49	0.431	0.569
7.25	1.11	0.883	0.117	none	none	SI	2.10	0.453	0.547
10.05	1.56	0.883	0.117	none	none	SI	2.99	0.481	0.519
1.65	0.81	0.952	0.048	none	none	SI	1.73	0.592	0.408
4.45	1.14	0.952	0.048	none	none	SI	2.38	0.618	0.382
7.25	1.59	0.952	0.048	none	none	SI	3.31	0.649	0.351
10.05	2.23	0.952	0.048	none	none	SI	4.66	0.685	0.315
1.65	1.15	0.974	0.026	none	none	SI	2.17	0.720	0.280
4.45	1.59	0.974	0.026	none	none	SI	2.96	0.745	0.255
7.25	2.19	0.974	0.026	none	none	SI	4.08	0.773	0.227
10.05	3.01	0.974	0.026	none	none	SI	5.67	0.804	0.196
1.65	1.63	0.990	0.010	none	none	SI	2.67	0.868	0.132
4.45	2.25	0.990	0.010	none	none	SI	3.59	0.883	0.117
4.45	2.26	0.990	0.010	none	none	SI	3.59	0.883	0.117
7.25	3.12	0.990	0.010	none	none	SI	4.87	0.900	0.100
9.95	4.36	0.990	0.010	none	none	SI	6.61	0.917	0.083
Mean Deviation (%)							71.76	none	none
1.65	0.27	0.362	0.638	none	none	SII	0.18	0.385	0.615
4.45	0.44	0.362	0.638	none	none	SII	0.28	0.432	0.568
7.25	0.69	0.362	0.638	none	none	SII	0.41	0.472	0.528
1.65	0.37	0.712	0.288	none	none	SII	0.21	0.504	0.496
4.45	0.54	0.712	0.288	none	none	SII	0.30	0.531	0.469
7.25	0.80	0.712	0.288	none	none	SII	0.42	0.554	0.446
10.05	1.15	0.712	0.288	none	none	SII	0.59	0.573	0.427
1.65	0.55	0.883	0.117	none	none	SII	0.29	0.561	0.439
4.45	0.78	0.883	0.117	none	none	SII	0.40	0.578	0.422
7.25	1.11	0.883	0.117	none	none	SII	0.55	0.593	0.407
10.05	1.56	0.883	0.117	none	none	SII	0.76	0.606	0.394
1.65	0.81	0.952	0.048	none	none	SII	0.30	0.574	0.426
4.45	1.14	0.952	0.048	none	none	SII	0.56	0.608	0.392
7.25	1.59	0.952	0.048	none	none	SII	0.76	0.618	0.382

10.05	2.23	0.952	0.048	none	none	SII	1.04	0.627	0.373
1.65	1.15	0.974	0.026	none	none	SII	0.51	0.614	0.386
4.45	1.59	0.974	0.026	none	none	SII	0.70	0.624	0.376
7.25	2.19	0.974	0.026	none	none	SII	0.91	0.631	0.369
10.05	3.01	0.974	0.026	none	none	SII	1.31	0.640	0.360
1.65	1.63	0.990	0.010	none	none	SII	0.74	0.641	0.359
4.45	2.25	0.990	0.010	none	none	SII	1.01	0.649	0.351
4.45	2.26	0.990	0.010	none	none	SII	1.01	0.649	0.351
7.25	3.12	0.990	0.010	none	none	SII	1.38	0.657	0.343
9.95	4.36	0.990	0.010	none	none	SII	1.87	0.664	0.336
Mean Deviation (%)							50.5	none	none

**Table 16:** CH-V-Lw Equilibrium of CH<sub>4</sub>-C<sub>3</sub>H<sub>8</sub> from (McLeod and Campbell, 1961). The simulation curve is obtained with the GasHyDyn simulator, implemented with reference parameters from Table 25 (Dharmawardhana et al., 1980) and Table 26. (Page. 63) and Kihara parameters given in Table 28. (Page. 75).

Experimental Equilibrium Data						Simulation			
T °C	P MPa	Gas composition (±0.003)		Hydrate composition (±0.003)		S	P MPa (±0.02)	Hydrate composition (±0.001)	
(±0.2)	(±0.02)	CH <sub>4</sub>	C <sub>3</sub> H <sub>8</sub>	CH <sub>4</sub>	C <sub>3</sub> H <sub>8</sub>			CH <sub>4</sub>	C <sub>3</sub> H <sub>8</sub>
17.35	6.93	0.965	0.035	none	none	SI	14.89	0.868	0.132
30.55	62.47	0.965	0.035	none	none	SI	86.02	0.899	0.101
31.25	68.98	0.965	0.035	none	none	SI	92.61	0.895	0.105
25.95	34.51	0.965	0.035	none	none	SI	50.26	0.913	0.087
23.45	20.86	0.965	0.035	none	none	SI	36.27	0.912	0.088
28.45	48.37	0.965	0.035	none	none	SI	68.09	0.908	0.092
30.55	62.29	0.965	0.035	none	none	SI	86.02	0.899	0.101
21.35	13.89	0.965	0.035	none	none	SI	27.05	0.905	0.095
20.15	10.45	0.965	0.035	none	none	SI	22.70	0.897	0.103
17.55	6.93	0.965	0.035	none	none	SI	15.35	0.871	0.129
19.95	7.41	0.945	0.055	none	none	SI	20.47	0.846	0.154
19.65	7.41	0.945	0.055	none	none	SI	19.61	0.843	0.157
27.45	34.58	0.945	0.055	none	none	SI	57.76	0.871	0.129
29.55	48.37	0.945	0.055	none	none	SI	73.46	0.863	0.137
31.75	62.23	0.945	0.055	none	none	SI	92.51	0.848	0.152
25.35	23.62	0.945	0.055	none	none	SI	44.48	0.874	0.126
23.05	13.89	0.945	0.055	none	none	SI	32.63	0.870	0.130
17.35	6.93	0.965	0.035	none	none	SI	14.89	0.868	0.132
Mean Deviation (%)							85	none	none
17.35	6.93	0.965	0.035	none	none	SII	2.68	0.651	0.349
30.55	62.47	0.965	0.035	none	none	SII	19.73	0.690	0.310
31.25	68.98	0.965	0.035	none	none	SII	22.49	0.693	0.307
25.95	34.51	0.965	0.035	none	none	SII	8.33	0.671	0.329
23.45	20.86	0.965	0.035	none	none	SII	5.75	0.664	0.336
28.45	48.37	0.965	0.035	none	none	SII	12.99	0.680	0.320
30.55	62.29	0.965	0.035	none	none	SII	19.73	0.690	0.310
21.35	13.89	0.965	0.035	none	none	SII	4.26	0.659	0.341

20.15	10.45	0.965	0.035	none	none	SII	3.65	0.657	0.343
17.55	6.93	0.965	0.035	none	none	SII	2.75	0.652	0.348
19.95	7.41	0.945	0.055	none	none	SII	3.05	0.649	0.351
19.65	7.41	0.945	0.055	none	none	SII	2.94	0.648	0.352
27.45	34.58	0.945	0.055	none	none	SII	8.36	0.665	0.335
29.55	48.37	0.945	0.055	none	none	SII	12.11	0.671	0.329
31.75	62.23	0.945	0.055	none	none	SII	18.75	0.679	0.321
25.35	23.62	0.945	0.055	none	none	SII	6.08	0.660	0.340
23.05	13.89	0.945	0.055	none	none	SII	4.47	0.655	0.345
17.35	6.93	0.965	0.035	none	none	SII	2.68	0.651	0.349
Mean Deviation (%)							68	none	none

**Table 17:** CH-V-Lw Equilibrium of CH<sub>4</sub>-C<sub>3</sub>H<sub>8</sub> from (Thakore and Holder, 1987). The simulation curve is obtained with the GasHyDyn simulator, implemented with reference parameters from Table 25 (Dharmawardhana et al., 1980) and Table 26. (Page. 63) and Kihara parameters given in Table 28. (Page. 75).

Experimental Equilibrium Data						Simulation			
T °C (±0.2)	P MPa (±0.02)	Gas composition (±0.003)		Hydrate composition (±0.003)		S	P MPa (±0.02)	Hydrate composition (±0.001)	
		CH <sub>4</sub>	C <sub>3</sub> H <sub>8</sub>	CH <sub>4</sub>	C <sub>3</sub> H <sub>8</sub>			CH <sub>4</sub>	C <sub>3</sub> H <sub>8</sub>
2	0.42	0.765	0.235	none	none	SI	0.73	0.304	0.696
2	0.39	0.727	0.273	none	none	SI	0.66	0.283	0.717
2	0.37	0.700	0.300	none	none	SI	0.62	0.271	0.729
2	0.30	0.516	0.484	none	none	SI	0.45	0.206	0.794
2	0.28	0.420	0.580	none	none	SI	0.30	0.161	0.839
2	0.28	0.366	0.634	none	none	SI	0.38	0.162	0.838
2	0.27	0.352	0.648	none	none	SI	0.38	0.158	0.842
2	0.25	0.190	0.810	none	none	SI	0.34	0.102	0.898
2	0.25	0.083	0.917	none	none	SI	0.32	0.053	0.947
2	0.25	0.081	0.919	none	none	SI	0.32	0.052	0.948
2	0.25	0.054	0.946	none	none	SI	0.31	0.037	0.963
2	0.25	0.046	0.954	none	none	SI	0.31	0.032	0.968
2	0.25	0.037	0.963	none	none	SI	0.31	0.026	0.974
2	0.25	0.021	0.979	none	none	SI	0.31	0.015	0.985
2	0.26	0.000	1.000	none	none	SI	0.31	0.000	1.000
5	1.31	0.956	0.044	none	none	SI	2.63	0.643	0.357
5	1.14	0.947	0.053	none	none	SI	2.43	0.602	0.398
5	0.85	0.894	0.106	none	none	SI	1.67	0.453	0.547
5	0.63	0.768	0.232	none	none	SI	1.04	0.321	0.679
5	0.50	0.530	0.470	none	none	SI	0.66	0.225	0.775
5	0.49	0.510	0.490	none	none	SI	0.64	0.219	0.781
5	0.48	0.502	0.498	none	none	SI	0.63	0.217	0.783
5	0.48	0.468	0.532	none	none	SI	0.61	0.207	0.793
5	0.48	0.412	0.588	none	none	SI	0.58	0.191	0.809
5	0.46	0.394	0.606	none	none	SI	0.57	0.186	0.814
5	0.46	0.390	0.610	none	none	SI	0.56	0.185	0.815
5	0.48	0.030	0.970	none	none	SI	0.46	0.028	0.972

5	0.48	0.026	0.974	none	none	SI	0.46	0.024	0.976
5	0.51	0.000	1.000	none	none	SI	0.46	0.000	1.000
Mean Deviation (%)							41.4	none	none
2	0.67	0.903	0.097	none	none	SII	0.32	0.571	0.429
2	0.42	0.765	0.235	none	none	SII	0.23	0.523	0.477
2	0.39	0.727	0.273	none	none	SII	0.22	0.512	0.488
2	0.37	0.700	0.300	none	none	SII	0.22	0.504	0.496
2	0.30	0.516	0.484	none	none	SII	0.20	0.448	0.552
2	0.28	0.420	0.580	none	none	SII	0.19	0.415	0.585
2	0.28	0.366	0.634	none	none	SII	0.19	0.393	0.607
2	0.27	0.352	0.648	none	none	SII	0.19	0.387	0.613
2	0.25	0.190	0.810	none	none	SII	0.21	0.297	0.703
2	0.25	0.083	0.917	none	none	SII	0.23	0.188	0.812
2	0.25	0.081	0.919	none	none	SII	0.23	0.184	0.816
2	0.25	0.054	0.946	none	none	SII	0.24	0.141	0.859
2	0.25	0.046	0.954	none	none	SII	0.25	0.126	0.874
2	0.25	0.037	0.963	none	none	SII	0.25	0.107	0.893
2	0.25	0.021	0.979	none	none	SII	0.26	0.067	0.933
2	0.26	0.000	1.000	none	none	SII	0.28	0.000	1.000
5	1.31	0.956	0.044	none	none	SII	0.61	0.612	0.388
5	1.14	0.947	0.053	none	none	SII	0.57	0.607	0.393
5	0.85	0.894	0.106	none	none	SII	0.43	0.583	0.417
5	0.63	0.768	0.232	none	none	SII	0.34	0.550	0.450
5	0.50	0.530	0.470	none	none	SII	0.29	0.491	0.509
5	0.49	0.510	0.490	none	none	SII	0.29	0.484	0.516
5	0.48	0.502	0.498	none	none	SII	0.29	0.483	0.517
5	0.48	0.468	0.532	none	none	SII	0.29	0.474	0.526
5	0.48	0.412	0.588	none	none	SII	0.30	0.457	0.543
5	0.46	0.394	0.606	none	none	SII	0.30	0.451	0.549
5	0.46	0.390	0.610	none	none	SII	0.30	0.450	0.550
5	0.48	0.030	0.970	none	none	SII	0.47	0.138	0.862
5	0.48	0.026	0.974	none	none	SII	0.48	0.125	0.875
Mean Deviation (%)							27.4	none	none

### 3.2.4 C<sub>2</sub>H<sub>6</sub>-C<sub>3</sub>H<sub>8</sub> CLATHRATE HYDRATE EQUILIBRIUM DATA

**Table 18:** CH-V-Lw Equilibrium of C<sub>2</sub>H<sub>6</sub>-C<sub>3</sub>H<sub>8</sub> from (Mooijer-Van den Heuvel, 2004). The simulation curve is obtained with the GasHyDyn simulator, implemented with reference parameters from Table 25 (Dharmawardhana et al., 1980) and Table 26. (Page. 63) and Kihara parameters given in Table 28. (Page. 75).

Experimental Equilibrium Data						Simulation			
T °C	P MPa	Gas composition (±0.003)		Hydrate composition (±0.003)		S	P MPa (±0.02)	Hydrate composition (±0.001)	
(±0.2)	(±0.02)	CH <sub>4</sub>	C <sub>3</sub> H <sub>8</sub>	CH <sub>4</sub>	C <sub>3</sub> H <sub>8</sub>			CH <sub>4</sub>	C <sub>3</sub> H <sub>8</sub>
3.88	0.54	0.299	0.701	none	none	SI	0.47	0.190	0.810
4.28	0.58	0.299	0.701	none	none	SI	0.49	0.191	0.809

4.63	0.63	0.299	0.701	none	none	SI	0.52	0.192	0.808
4.84	0.66	0.299	0.701	none	none	SI	0.53	0.193	0.807
5.02	0.67	0.299	0.701	none	none	SI	0.54	0.193	0.807
3.91	0.81	0.501	0.499	none	none	SI	0.53	0.356	0.644
4.75	0.81	0.501	0.499	none	none	SI	0.59	0.360	0.640
4.81	0.86	0.501	0.499	none	none	SI	0.60	0.360	0.640
4.88	0.86	0.501	0.499	none	none	SI	0.60	0.360	0.640
4.97	0.96	0.501	0.499	none	none	SI	0.61	0.361	0.639
5.03	0.91	0.501	0.499	none	none	SI	0.61	0.361	0.639
3.88	0.54	0.299	0.701	none	none	SI	0.47	0.190	0.810
Mean Deviation (%)							25.5	none	none
3.88	0.54	0.299	0.701	none	none	SII	0.63	0.016	0.984
4.28	0.58	0.299	0.701	none	none	SII	0.69	0.017	0.983
4.63	0.63	0.299	0.701	none	none	SII	0.76	0.018	0.982
4.84	0.66	0.299	0.701	none	none	SII	0.80	0.019	0.981
5.02	0.67	0.299	0.701	none	none	SII	0.84	0.019	0.981
3.91	0.81	0.501	0.499	none	none	SII	0.94	0.038	0.962
4.75	0.81	0.501	0.499	none	none	SII	1.19	0.044	0.956
4.81	0.86	0.501	0.499	none	none	SII	1.21	0.044	0.956
4.88	0.86	0.501	0.499	none	none	SII	1.24	0.045	0.955
4.97	0.96	0.501	0.499	none	none	SII	1.27	0.046	0.954
5.03	0.91	0.501	0.499	none	none	SII	1.30	0.046	0.954
Mean Deviation (%)							29.4	none	none

### 3.2.5 CO<sub>2</sub>-CH<sub>4</sub>-C<sub>2</sub>H<sub>6</sub> CLATHRATE HYDRATE EQUILIBRIUM DATA

**Table 19:** CH-V-Lw Equilibrium of CO<sub>2</sub>-CH<sub>4</sub>-C<sub>2</sub>H<sub>6</sub> from (Le Quang, 2013). The simulation curve is obtained with the GasHyDyn simulator, implemented with reference parameters from Table 25 (Dharmawardhana et al., 1980) and Table 26. (Page. 63) and Kihara parameters given in Table 28. (Page. 75).

Experimental Equilibrium Data								Simulation				
T °C	P MPa	Gas composition (±0.003)			Hydrate composition (±0.003)				P MPa (±0.02)	Hydrate composition (±0.001)		
(±0.2)	(±0.02)	CO <sub>2</sub>	CH <sub>4</sub>	C <sub>2</sub> H <sub>6</sub>	CO <sub>2</sub>	CH <sub>4</sub>	C <sub>2</sub> H <sub>6</sub>			CO <sub>2</sub>	CH <sub>4</sub>	C <sub>2</sub> H <sub>6</sub>
2.75	3.54	0.059	0.916	0.026	0.144	0.769	0.087	SI	2.72	0.097	0.739	0.164
3.65	3.81	0.065	0.906	0.030	0.144	0.769	0.087	SI	2.90	0.103	0.717	0.180
5.15	4.23	0.071	0.892	0.038	0.141	0.774	0.085	SI	3.22	0.106	0.683	0.210
6.55	4.56	0.073	0.884	0.043	0.141	0.777	0.082	SI	3.64	0.107	0.669	0.224
7.80	5.12	0.078	0.876	0.046	0.135	0.777	0.089	SI	4.11	0.112	0.662	0.226
9.25	5.99	0.090	0.865	0.045	0.049	0.804	0.148	SI	4.83	0.127	0.661	0.211
Mean Deviation (%)									21.7	48.18	11.4	119.2
2.75	3.54	0.059	0.916	0.026	0.144	0.769	0.087	S2	2.45	0.071	0.833	0.096
3.65	3.81	0.065	0.906	0.030	0.144	0.769	0.087	S2	2.65	0.076	0.819	0.105
5.15	4.23	0.071	0.892	0.038	0.141	0.774	0.085	S2	3.03	0.081	0.798	0.121
6.55	4.56	0.073	0.884	0.043	0.141	0.777	0.082	S2	3.46	0.082	0.790	0.128
7.80	5.12	0.078	0.876	0.046	0.135	0.777	0.089	S2	3.94	0.086	0.785	0.129
9.25	5.99	0.090	0.865	0.045	0.049	0.804	0.148	S2	4.63	0.098	0.780	0.122
Mean Deviation (%)									26.5	53.3	3.9	32.1



**Table 20:** CH-V-Lw Equilibrium of CO<sub>2</sub>-CH<sub>4</sub>-C<sub>2</sub>H<sub>6</sub> from (Kvenvolden et al., 1984). The simulation curve is obtained with the GasHyDyn simulator, implemented with reference parameters from Table 25 (Dharmawardhana et al., 1980) and Table 26. (Page. 63) and Kihara parameters given in Table 28. (Page. 75).

Experimental Equilibrium Data								Simulation				
T °C	P MPa	Gas composition (±0.003)			Hydrate composition (±0.003)				P MPa (±0.02)	Hydrate composition (±0.001)		
(±0.2)	(±0.02)	CO <sub>2</sub>	CH <sub>4</sub>	C <sub>2</sub> H <sub>6</sub>	CO <sub>2</sub>	CH <sub>4</sub>	C <sub>2</sub> H <sub>6</sub>			CO <sub>2</sub>	CH <sub>4</sub>	C <sub>2</sub> H <sub>6</sub>
-4	3.79	0.002	0.997	0.001	none	none	none	SI	2.25	0.004	0.984	0.011
-4	3.62	0.002	0.991	0.007	none	none	none	SI	2.14	0.005	0.932	0.063
-4	3.50	0.003	0.995	0.003	none	none	none	SI	2.22	0.006	0.970	0.024
-4	3.22	0.002	0.995	0.002	none	none	none	SI	2.23	0.005	0.973	0.023
-4	2.78	0.003	0.994	0.003	none	none	none	SI	2.22	0.007	0.970	0.024
-4	2.04	0.003	0.995	0.003	none	none	none	SI	2.23	0.005	0.971	0.024
-4	1.20	0.005	0.992	0.003	none	none	none	SI	2.21	0.010	0.962	0.027
Mean Deviation (%)									37.4	none	none	none
-4	3.79	0.002	0.997	0.001	none	none	none	SII	1.79	0.003	0.990	0.007
-4	3.62	0.002	0.991	0.007	none	none	none	SII	1.74	0.003	0.959	0.038
-4	3.50	0.003	0.995	0.003	none	none	none	SII	1.77	0.004	0.981	0.015
-4	3.22	0.002	0.995	0.002	none	none	none	SII	1.78	0.003	0.983	0.014
-4	2.78	0.003	0.994	0.003	none	none	none	SII	1.78	0.004	0.981	0.014
-4	2.04	0.003	0.995	0.003	none	none	none	SII	1.77	0.004	0.982	0.014
-4	1.20	0.005	0.992	0.003	none	none	none	SII	1.77	0.007	0.977	0.017
Mean Deviation (%)									37.4	none	none	none

### 3.2.6 CH<sub>4</sub>-C<sub>2</sub>H<sub>6</sub>-C<sub>3</sub>H<sub>8</sub> CLATHRATE HYDRATE EQUILIBRIUM DATA

**Table 21:** CH-V-Lw Equilibrium of CH<sub>4</sub>-C<sub>2</sub>H<sub>6</sub>-C<sub>3</sub>H<sub>8</sub> from (Le Quang, 2013). The simulation curve is obtained with the GasHyDyn simulator, implemented with reference parameters from Table 25 (Dharmawardhana et al., 1980) and Table 26. (Page. 63) and Kihara parameters given in Table 28. (Page. 75).

Experimental Equilibrium Data								Simulation				
T °C	P MPa	Gas composition (±0.003)			Hydrate composition (±0.003)				P MPa (±0.02)	Hydrate composition (±0.001)		
(±0.2)	(±0.02)	CH <sub>4</sub>	C <sub>2</sub> H <sub>6</sub>	C <sub>3</sub> H <sub>8</sub>	CH <sub>4</sub>	C <sub>2</sub> H <sub>6</sub>	C <sub>3</sub> H <sub>8</sub>			CH <sub>4</sub>	C <sub>2</sub> H <sub>6</sub>	C <sub>3</sub> H <sub>8</sub>
2.45	3.13	0.980	0.003	0.017	0.870	0.070	0.060	SI	2.58	0.784	0.018	0.198
3.15	3.36	0.979	0.004	0.017	0.855	0.079	0.067	SI	2.78	0.786	0.023	0.191
4.15	3.55	0.978	0.005	0.017	0.840	0.087	0.073	SI	3.07	0.788	0.028	0.184
4.95	3.67	0.976	0.007	0.018	0.833	0.089	0.078	SI	3.31	0.784	0.039	0.177
6.30	3.78	0.973	0.009	0.018	0.832	0.088	0.080	SI	3.75	0.778	0.050	0.172
7.70	3.94	0.968	0.012	0.020	0.828	0.087	0.085	SI	4.27	0.769	0.064	0.167
9.10	4.21	0.962	0.018	0.021	0.813	0.083	0.104	SI	4.81	0.755	0.086	0.159



10.10	4.34	0.958	0.020	0.022	0.808	0.081	0.111	SI	5.33	0.750	0.092	0.158
11.15	4.50	0.953	0.023	0.024	0.804	0.071	0.124	SI	5.88	0.742	0.101	0.157
Mean Deviation (%)									15.0	7.3	44.2	113.8
2.45	3.13	0.980	0.003	0.017	0.870	0.070	0.060	SII	0.66	0.628	0.000	0.372
3.15	3.36	0.979	0.004	0.017	0.855	0.079	0.067	SII	0.71	0.630	0.001	0.369
4.15	3.55	0.978	0.005	0.017	0.840	0.087	0.073	SII	0.80	0.633	0.001	0.366
4.95	3.67	0.976	0.007	0.018	0.833	0.089	0.078	SII	0.86	0.635	0.001	0.364
6.30	3.78	0.973	0.009	0.018	0.832	0.088	0.080	SII	0.99	0.638	0.001	0.361
7.70	3.94	0.968	0.012	0.020	0.828	0.087	0.085	SII	1.13	0.640	0.002	0.358
9.10	4.21	0.962	0.018	0.021	0.813	0.083	0.104	SII	1.30	0.642	0.003	0.355
10.10	4.34	0.958	0.020	0.022	0.808	0.081	0.111	SII	1.42	0.643	0.003	0.354
11.15	4.50	0.953	0.023	0.024	0.804	0.071	0.124	SII	1.55	0.644	0.003	0.353
Mean Deviation (%)									73.3	23.3	97.9	338.9

### 3.2.7 CH<sub>4</sub>-C<sub>2</sub>H<sub>6</sub>-C<sub>3</sub>H<sub>8</sub> C<sub>4</sub>H<sub>10</sub>(-1) CLATHRATE HYDRATE EQUILIBRIUM DATA

**Table 22:** CH-V-Lw Equilibrium of CH<sub>4</sub>-C<sub>2</sub>H<sub>6</sub>-C<sub>3</sub>H<sub>8</sub> C<sub>4</sub>H<sub>10</sub>(-1) from (Le Quang, 2013). The simulation curve is obtained with the GasHyDyn simulator, implemented with reference parameters from Table 25 (Dharmawardhana et al., 1980) and Table 26. (Page. 63) and Kihara parameters given in Table 28. (Page. 75).

Experimental Equilibrium Data										Simulation					
T °C	P MPa	Gas composition (±0.003)				Hydrate composition (±0.003)					P MPa (±0.02)	Hydrate composition (±0.001)			
(±0.2)	(±0.02)	CH <sub>4</sub>	C <sub>2</sub> H <sub>6</sub>	C <sub>3</sub> H <sub>8</sub>	C <sub>3</sub> H <sub>8</sub> -1	CH <sub>4</sub>	C <sub>2</sub> H <sub>6</sub>	C <sub>3</sub> H <sub>8</sub>	C <sub>3</sub> H <sub>8</sub> -1			CH <sub>4</sub>	C <sub>2</sub> H <sub>6</sub>	C <sub>3</sub> H <sub>8</sub>	C <sub>3</sub> H <sub>8</sub> -1
2.40	2.28	0.971	0.017	0.004	0.008	0.721	0.111	0.118	0.051	SI	2.80	0.833	0.117	0.050	0.000
3.45	2.31	0.967	0.019	0.005	0.008	0.723	0.109	0.118	0.050	SI	3.04	0.818	0.125	0.057	0.000
7.60	2.75	0.942	0.035	0.008	0.015	0.696	0.104	0.149	0.051	SI	4.21	0.748	0.182	0.069	0.000
9.15	2.97	0.930	0.041	0.012	0.017	0.677	0.103	0.169	0.052	SI	4.76	0.723	0.193	0.084	0.000
9.90	3.05	0.923	0.044	0.015	0.018	0.679	0.099	0.171	0.051	SI	4.99	0.704	0.194	0.101	0.000
10.80	3.12	0.915	0.046	0.020	0.019	0.686	0.097	0.167	0.050	SI	5.34	0.688	0.191	0.122	0.000
11.70	3.22	0.906	0.048	0.026	0.021	0.692	0.096	0.163	0.049	SI	5.70	0.670	0.186	0.144	0.000
12.65	3.34	0.896	0.050	0.032	0.022	0.703	0.093	0.155	0.048	SI	6.13	0.654	0.182	0.164	0.000
13.65	3.46	0.888	0.052	0.037	0.023	0.711	0.091	0.150	0.048	SI	6.79	0.650	0.178	0.173	0.000
Mean Deviation (%)											62.1	7.3	73.6	34.8	100
2.40	2.28	0.971	0.017	0.004	0.008	0.721	0.111	0.118	0.051	SII	1.11	0.671	0.010	0.304	0.014
3.45	2.31	0.967	0.019	0.005	0.008	0.723	0.109	0.118	0.050	SII	1.17	0.667	0.009	0.310	0.013
7.60	2.75	0.942	0.035	0.008	0.015	0.696	0.104	0.149	0.051	SII	1.55	0.660	0.012	0.314	0.014
9.15	2.97	0.930	0.041	0.012	0.017	0.677	0.103	0.169	0.052	SII	1.65	0.655	0.010	0.323	0.012
9.90	3.05	0.923	0.044	0.015	0.018	0.679	0.099	0.171	0.051	SII	1.64	0.650	0.009	0.331	0.010
10.80	3.12	0.915	0.046	0.020	0.019	0.686	0.097	0.167	0.050	SII	1.62	0.646	0.008	0.338	0.009
11.70	3.22	0.906	0.048	0.026	0.021	0.692	0.096	0.163	0.049	SII	1.66	0.643	0.006	0.344	0.007
12.65	3.34	0.896	0.050	0.032	0.022	0.703	0.093	0.155	0.048	SII	1.70	0.641	0.005	0.348	0.006
13.65	3.46	0.888	0.052	0.037	0.023	0.711	0.091	0.150	0.048	SII	1.81	0.640	0.005	0.349	0.006
Mean Deviation (%)											47.6	6.47	91.7	120.7	79.8

**Table 23 :** CH-V-Lw Equilibrium of CH<sub>4</sub>-C<sub>2</sub>H<sub>6</sub>-C<sub>3</sub>H<sub>8</sub> C<sub>4</sub>H<sub>10</sub>(-1) from (Le Quang, 2013). The simulation curve is obtained with the GasHyDyn simulator, implemented with reference parameters from Table 25 (Dharmawardhana et al., 1980) and Table 26. (Page. 63) and Kihara parameters given in Table 28. (Page. 75).

Experimental Equilibrium Data										Simulation					
T °C	P MPa	Gas composition (±0.003)				Hydrate composition (±0.003)					P MPa (±0.02)	Hydrate composition (±0.001)			
(±0.2)	(±0.02)	CH <sub>4</sub>	C <sub>2</sub> H <sub>6</sub>	C <sub>3</sub> H <sub>8</sub>	C <sub>3</sub> H <sub>8</sub> -1	CH <sub>4</sub>	C <sub>2</sub> H <sub>6</sub>	C <sub>3</sub> H <sub>8</sub>	C <sub>3</sub> H <sub>8</sub> -1			CH <sub>4</sub>	C <sub>2</sub> H <sub>6</sub>	C <sub>3</sub> H <sub>8</sub>	C <sub>3</sub> H <sub>8</sub> -1
2.75	2.14	0.954	0.024	0.007	0.014	0.718	0.082	0.159	0.041	SI	2.68	0.769	0.151	0.080	0.000
4.30	2.16	0.955	0.024	0.007	0.014	0.717	0.082	0.160	0.041	SI	3.16	0.780	0.146	0.074	0.000
4.85	2.18	0.952	0.025	0.009	0.014	0.718	0.082	0.159	0.041	SI	3.28	0.768	0.144	0.088	0.000
5.90	2.21	0.951	0.025	0.010	0.014	0.716	0.082	0.160	0.042	SI	3.64	0.767	0.141	0.091	0.000
6.80	2.26	0.948	0.027	0.011	0.014	0.715	0.082	0.162	0.042	SI	3.92	0.757	0.143	0.100	0.000
7.45	2.36	0.939	0.030	0.015	0.016	0.713	0.079	0.166	0.042	SI	3.95	0.726	0.154	0.121	0.000
9.20	2.53	0.926	0.035	0.022	0.017	0.709	0.077	0.172	0.042	SI	4.53	0.692	0.156	0.151	0.000
11.05	2.82	0.905	0.042	0.032	0.021	0.704	0.070	0.186	0.040	SI	5.12	0.651	0.164	0.185	0.000
18.15	3.72	0.845	0.050	0.078	0.027	0.926	0.043	0.020	0.011	SI	12.34	0.668	0.128	0.203	0.000
Mean Deviation (%)											79.9	8.4	101.3	130.6	100
2.75	2.14	0.954	0.024	0.007	0.014	0.718	0.082	0.159	0.041	SII	0.95	0.651	0.008	0.324	0.016
4.30	2.16	0.955	0.024	0.007	0.014	0.717	0.082	0.160	0.041	SII	1.13	0.656	0.009	0.319	0.016
4.85	2.18	0.952	0.025	0.009	0.014	0.718	0.082	0.159	0.041	SII	1.12	0.652	0.008	0.328	0.013
5.90	2.21	0.951	0.025	0.010	0.014	0.716	0.082	0.160	0.042	SII	1.21	0.652	0.007	0.329	0.012
6.80	2.26	0.948	0.027	0.011	0.014	0.715	0.082	0.162	0.042	SII	1.27	0.650	0.007	0.333	0.011
7.45	2.36	0.939	0.030	0.015	0.016	0.713	0.079	0.166	0.042	SII	1.24	0.645	0.006	0.340	0.009
9.20	2.53	0.926	0.035	0.022	0.017	0.709	0.077	0.172	0.042	SII	1.32	0.640	0.005	0.347	0.007
11.05	2.82	0.905	0.042	0.032	0.021	0.704	0.070	0.186	0.040	SII	1.41	0.637	0.005	0.353	0.006
18.15	3.72	0.845	0.050	0.078	0.027	0.926	0.043	0.020	0.011	SII	2.33	0.638	0.003	0.356	0.003
Mean Deviation (%)											47.1	11.7	91.7	275.6	72.6



## 4. THERMODYNAMIC OF GAS HYDRATES

The (van der Waals and Platteeuw, 1959) describes the hydrate phase by means of statistical thermodynamics based on the following assumptions:

- Each cavity contains at most one guest (gas) molecule
- The interaction between guest and water molecules can be described by a pair potential function of the pair gas-molecule, and the cavity can be treated as perfectly spherical
- The free energy contribution of the water molecules is independent of the modes of occupancy of guest molecules. This assumption means that the gas molecules do not deform cavities
- There is no interaction between the guests molecules in different cavities, gas molecules interact only with the nearest water molecules.

From the previous hypotheses, statistical thermodynamics allows for the description of the different parameters of the system and link them to quantities like temperature, volume and chemical potential.

In the case of hydrates, in thermodynamic equilibrium, the equality of chemical potentials of water in the liquid phase and in the hydrate phase can be written. This relationship can be rewritten by introducing reference states. For both liquid and hydrate phases, the reference state used in the van der Waals and Platteeuw model is a hypothetical phase  $\beta$  which corresponds to the empty hydrate:

$$\Delta\mu_w^{H-\beta} = \Delta\mu_w^{L-\beta} \quad (8)$$

Where  $\Delta\mu_w^{H-\beta}$  and  $\Delta\mu_w^{L-\beta}$  are the differences of the chemical potentials between water in hydrate and liquid phase and water in the  $\beta$  statephase,  $\Delta\mu_w^{H-\beta}$  is determined from statistical thermodynamics whereas  $\Delta\mu_w^{L-\beta}$  is determined by means of relations from classical thermodynamics (Gibbs-Duhem equation).

### 4.1. MODELLING OF $\Delta\mu_w^{H-\beta}$

The hydrate term is expressed as follow:

$$\Delta\mu_w^{H-\beta} = RT \sum_i v_i \ln \left( 1 - \sum_j \theta_j^i \right) \quad (9)$$

In Eq. (9)  $v_i$  is the number of cavities of type  $i$  per mole of water (Table 1) and  $\theta_j^i$  is the occupancy factor ( $\theta_j^i \in [0,1]$ ) of the cavities of type  $i$  by the gas molecule  $j$ . This

last parameter is very important to define the thermodynamic equilibrium and to determine the hydrate properties.

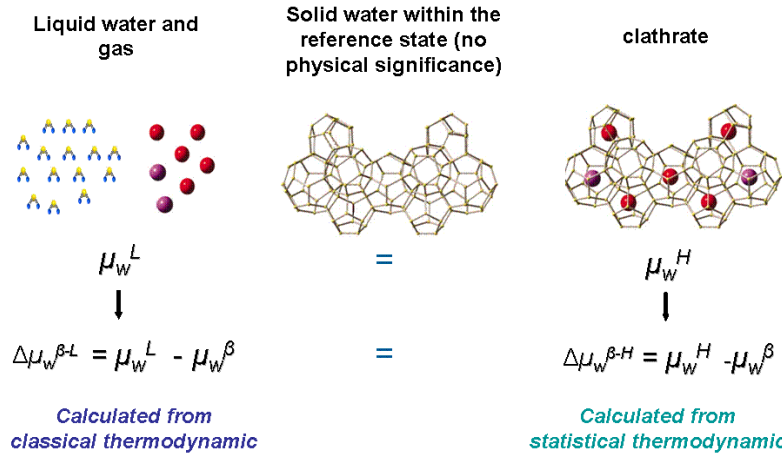


**Figure 10:** Schematic of the principle to referring at a hypothetical reference state in order to write the equilibrium between the clathrate hydrate phase and the liquid phase.

The occupancy factor is described by a model based on ideas considering the analogy between the gas adsorption in the 3-dimensional hydrate structure and the 2-dimensional Langmuir adsorption:

- The guest molecule is adsorbed at the surface
- The adsorption energy is independent from the presence of other adsorbed molecules
- The maximum amount of adsorbed gas corresponds to one molecule per site (one molecule par cavity)

The expression of the occupancy factor  $\theta_j^i$  is given by:

$$\theta_j^i = \frac{C_{f,ji} f_j(T, P)}{1 + \sum_j C_{f,ji} f_j(T, P)} \quad (10)$$

Eq.(9) can be rewritten as:

$$\Delta\mu_w^{H-\beta} = RT \sum_i v_i \ln \left( 1 - \sum_j C_{f,ji} f_j(T, P) \right) \quad (11)$$

Where  $C_{f,ji}$  is the Langmuir constant of component  $j$  in the cavity  $i$ . It describes the interaction potential between the encaged guest molecule and the surrounding water molecules evaluated by assuming a spherically symmetrical cage that can be described by a spherical symmetrical potential:

$$C_j^i = \frac{4\pi}{kT} \int_0^\infty \exp\left(-\frac{w(r)}{kT}\right) r^2 dr \quad (12)$$

Where  $w(r)$  is the interaction potential between the cavity and the gas molecule according to the distance  $r$  between the guest molecule and the water molecules over the structure. The interaction potential can be determined by different models such as e.g. the (van der Waals and Platteeuw, 1959), the (Parrish and Prausnitz, 1972) or the so-called Kihara model. The latter, being the most precise (McKoy and Sinanoğlu, 1963),  $w(r)$  can be expressed as follow:

$$w(r) = 2z\varepsilon \left[ \frac{\sigma^{12}}{R^{11}r} \left( \delta^{10} + \frac{a}{R} \delta^{11} \right) - \frac{\sigma^6}{R^5 r} \left( \delta^4 + \frac{a}{R} \delta^5 \right) \right] \quad (13)$$

$$\delta^N = \frac{1}{N} \left[ \left( 1 - \frac{r}{R} - \frac{a}{R} \right)^{-N} - \left( 1 + \frac{r}{R} - \frac{a}{R} \right)^{-N} \right] \quad (14)$$

The gas parameters  $\varepsilon$ ,  $\sigma$  and  $a$  are the so-called Kihara parameters and can be calculated from experimental data by fitting the model equations to corresponding hydrate equilibrium experimental data.  $\varepsilon$  accounts for the maximum attractive potential,  $\sigma$  to the distance from the cavity center, and  $a$  to the hard-core radius. The first two terms are fitted from PT data (if possible), while the hard-core radius  $a$  is usually taken from the literature (geometrical term). In this description, the interaction potential becomes only dependent on the properties of gases (*via* the Kihara parameters), and dependent of geometrical properties of the cavities (*via* their coordination number  $z$  and radius  $R$ , Table 1).

### Comment on the geometric description of the cavity

Theoretically, in Eq. (12), the interaction potential  $w(r)$  needs to be integrated from 0 to infinity. It means that the gas molecule interacts with the overall structure, not only with its first hydration shell (i.e. the water molecules of the cavity inside which the gas molecule is encapsulated), but also interacts with other molecules localized away from it. In fact, (John and Holder, 1982a, 1982b) have showed that 2<sup>nd</sup> and 3<sup>rd</sup> hydration shells contribute significantly to the Langmuir constant with a resulting change of this Langmuir constant by 1-2 orders of magnitudes (Sparks and Tester, 1992). Also, even with a rigorous integration of the interaction potential over all the hydration shells, the (John and Holder, 1982a, 1982b) can give rigorous results only for spherical molecules (such as Kr, Ar, CH<sub>4</sub>...). (John et al., 1985) have introduced a correction factor to take into account the asymmetry of the encapsulated molecules. All these refinement methods tend to give a physical signification to the interaction potential  $w(r)$  and Kihara parameters but results in a time consuming calculation.

For this reason, we have retained an integration of the cell potential over the first hydration shell.

Another comment concerns the size of the cavities. (Hester et al., 2007) did an experimental investigation of lattice parameters for sI and sII structure and different gases (Figure 3 and Figure 4). From one gas to another one, it is showed the lattice parameter can differ from 1%. It has been demonstrated previously via statistical mechanics that a minor change in the lattice parameter (0.5%) can lead to a major change in the predicted hydrate formation (e.g. > 15% at >100MPa for methane). So, from a theoretical point of view, the size of the cavities needs to be adapted to the component. But, this adaptation can be shifted to the kihara parameter by modifying artificially the  $\varepsilon$  parameter. So, in modelling, a unique cell dimension can be retained for all gases, and the adjustment of the model will be obtained by fitting the kihara parameters once again.

Kihara parameters for pure substances can be evaluated from measurement of the viscosity, calculated from second viriel coefficient, or from both (Tee et al., 1966a), or evaluated from Henry constants (Uno et al., 1975). The Table 24 gives the correlations to evaluate the kihara parameters, assuming a (6,12) Lennard-Jones potential (Tee et al., 1966b), and interaction between pair of molecules.

These Kihara parameters can not be used directly to model the gas hydrate equilibrium. In fact, in the gas hydrate modelling, the kihara potential is assumed to be the one from (McKoy and Sinanoğlu, 1963) in Eq. (13) and (14). Also, and more important, and in respect to the previous comment: the interaction potential Eq. (12) is a pseudo pair potential between a molecule on one hand, and pseudo other molecule on the other hand consisting on the overall structure.

So, the so-called Kihara parameters need to be re-optimised on experimental data, following a procedure given in Chapter 4 in §4.3. Page. 63.

**Table 24:** Correlations to calculate the  $\varepsilon$ ,  $\sigma$ , and  $a$ .kihara parameters as a function of the pitzer acentric factor  $\omega$ , and critical coordinates  $P_c$ ,  $T_c$  and  $V_c$

		$a^* = \frac{2a}{\sigma - 2a}$	$\sigma \left( \frac{P_c}{T_c} \right)^{1/3}$	$\sigma(V_c)^{1/3}$	$\frac{\varepsilon}{kT_c}$
(Tee et al., 1966a)	based on viscosity	$0.1501 + 2.3724 \omega$	$2.2802 + 0.2487 \omega$		$0.9736 - 0.4317 \omega$
	based on second virial coefficient	$0.1527 + 1.9809 \omega$	$2.2639 + 0.2487 \omega$		$1.0042 + 3.0454 \omega$
	based on second virial coefficient	$0.1495 + 1.8428 \omega$	$2.2631 - 0.3278 \omega$		$1.0070 + 2.2450 \omega$
	and viscosity	$0.1495 + 1.8428$		$0.7864 - 0.0527 \omega$	$1.0030 + 2.2329 \omega$
(Uno et al., 1975)	based on gas solubility	$0.240 + 2.20 \omega$		$0.676 + 0.0788 \omega$	$1.03 + 1.61 \omega$

From Eq. (10), we can write the average occupancy of component in the overall structure  $\theta_j$  where  $v_i$  is the stoichiometry of the cavities given in:

$$\theta_j \sum_i v_i = \sum_i v_i \frac{C_{f,ji} f_j(T,P)}{1 + \sum_j C_{f,ji} f_j(T,P)} \quad (15)$$

If we consider the case of a binary gas mixture of two components ( $j=1, 2$ ) of respective gas composition  $(x, 1-x)$

$$\theta_j \sum_i v_i = \sum_i v_i \frac{C_{f,ji} f_j(T,P)}{1 + \sum_j C_{f,ji} f_j(T,P)} \quad (16)$$

#### 4.2. MODELLING OF $\Delta\mu_w^{\varphi-\beta}$

The chemical potential of water in the aqueous phase is calculated by means of the Gibbs-Duhem equation of classical thermodynamics which expresses the variation of the chemical potential with temperature and pressure. The reference conditions are the temperature  $T_0 = 273.15$  K and the pressure  $P_0 = 1$  bar. The difference of the chemical potential of water between the reference phase (liquid in our case, but it could be ice or vapour phase) and the (hypothetical) empty hydrate phase  $\beta$ ,  $\Delta\mu_w^{\varphi-\beta}$ , can be written as follows:

$$\Delta\mu_w^{\text{L}-\beta} = T \frac{\Delta\mu_w^{\text{L}-\beta} \big|_{T^0, P^0}}{T^0} - T \int_{T^0}^T \frac{\Delta h_w^{\text{L}-\beta} \big|_{P^0}}{T^2} dT + \int_{P^0}^P \Delta v_w^{\text{L}-\beta} \big|_T dP - RT \ln a_w^{\text{L}} \big|_{T,P} \quad (17)$$

- The activity of water in the liquid phase,  $a_w^{\text{L}}$ , is the product of the mole fraction of water,  $x_w$ , and its activity coefficient,  $\gamma_w^{\text{L}}$ , hence  $a_w^{\text{L}} = x_w \gamma_w^{\text{L}}$ . In a good approximation, the aqueous phase can be regarded as ideal and the activity coefficient can therefore be set to 1, resulting in  $a_w^{\text{L}} \cong x_w$ . However, in the presence of polar molecules, or even salts, the system usually shows strong deviations from ideality. In that case,  $\gamma_w^{\text{L}}$  needs an appropriate description, as provided e.g. by an activity coefficient model. In the specific case of salts, a simple Pitzer-Debye-Hückel model (Ananthaswamy and Atkinson, 1984; Pitzer, 1977) accounting for the long term electrostatic interactions only, or a



more elaborate model like the eNRTL (Chen et al., 1982; Chen and Evans, 1986) or the Pitzer model (Pitzer, 1980, 1973) can be used to describe the long (and short) range electrostatic forces. Nevertheless, in the present work, there is no need for introducing this kind of model to describe  $\gamma_w^L$  since the liquid phases encountered in these experiments can be treated as pure liquid water. From a practical point of view,  $a_w^L$  is a second order parameter compared to the three following:  $\Delta v_w^{L-\beta}|_T$ ,  $\Delta h_w^{L-\beta}|_{p^0}$  and  $\Delta \mu_w^{L-\beta}|_{T^0, p^0}$ .

- The value of  $\Delta v_w^{L-\beta}|_T$  is a first order parameter. It has been measured with high accuracy by (Stackelberg and Müller, 1951) from X ray diffraction. Since that data are believed to be very reliable, the parameter  $\Delta v_w^{L-\beta}|_T$  was taken from this source.
- The value of  $\Delta h_w^{L-\beta}|_{p^0}$  is a first order parameter as well. A refinement of the model is given by (Sloan, 1998; Sloan and Koh, 2007) that takes into account the temperature dependence of  $\Delta h_w^{L-\beta}|_{p^0}$  using the well-known classical thermodynamic relationship

$$\Delta h_w^{L-\beta}|_{p^0} = \Delta h_w^{L-\beta}|_{T^0, p^0} + \int_{T^0}^T \Delta c_{p, w}^{L-\beta}|_{p^0} dT \quad (18)$$

assuming a linear dependence of  $\Delta c_{p, w}^{L-\beta}|_{p^0}$  on temperature according to:

$$\Delta c_{p, w}^{L-\beta}|_{p^0} = \Delta c_{p, w}^{L-\beta}|_{T^0, p^0} + b_{p, w}^{L-\beta}(T - T^0) \quad (19)$$

The model becomes first order dependent on  $\Delta h_w^{L-\beta}|_{T^0, p^0}$  (hereafter referred as  $\Delta h_w^{L-\beta, 0}$ ) and second order dependent on  $\Delta c_{p, w}^{L-\beta}|_{T^0, p^0}$  (hereafter abbreviated as  $\Delta c_{p, w}^{L-\beta, 0}$ ) and  $b_{p, w}^{L-\beta}$ .

- The last first order parameter of the equation is  $\Delta \mu_w^{L-\beta}|_{T^0, p^0}$  (hereafter referred to as  $\Delta \mu_w^{L-\beta, 0}$ )

**Table 25:** Mascroscopic parameters of hydrates and Ice (Sloan, 1998; Sloan and Koh, 2007)

Structure I		Structure II		
$\Delta\mu_w^{L-\beta,0}$	$\Delta h_w^{I-\beta,0}$	$\Delta\mu_w^{L-\beta,0}$	$\Delta h_w^{I-\beta,0}$	
J/mol	J/mol	J/mol	J/mol	
699	0	820	0	(van der Waals and Platteeuw, 1959)
1255.2	753	795	837	(Child, 1964)
1297	1389	937	1025	(Dharmawardhana et al., 1980) ..... model 1(*)
1120	931	1714	1400	(John et al., 1985)..... model 2(*)
1287	931	1068	764	(Handa and Tse, 1986) ..... model 3(*)

$\Delta h_w^{L-\beta,0} = \Delta h_w^{I-\beta,0} - 6011$ , where 6011 is the enthalpy of fusion of Ice (J/mol)

(\*) model refers to the model in which the  $\Delta\mu_w^{L-\beta,0}$  and  $\Delta h_w^{L-\beta,0}$  reference parameters are implemented as described in the next part of the work.

**Table 26:** Reference properties of hydrates from (Sloan, 1998; Sloan and Koh, 2007)

	Unit	Structure I	Structure II
$\Delta h_w^{L-\beta,0}$	J mol	$\Delta h_w^{I-\beta} \Big _{T^0, P^0, SI} - 6011$	$\Delta h_w^{I-\beta} \Big _{T^0, P^0, SII} - 6011$
$\Delta v_w^{L-\beta} \Big _{T^0}$	10 <sup>-6</sup> m <sup>3</sup> /mol	4.5959	4.99644
$\Delta c_{p,w}^{L-\beta,0}$	J/(mol K <sup>-1</sup> )	-38.12	-38.12
$b_{p,w}^{L-\beta}$	J/(mol K <sup>-2</sup> )	0.141	0.141

### 4.3. ADJUSTMENT OF MODELS PARAMETERS

The phase equilibrium between the water in the hydrate and the water in the liquid phase is described by Eq.(8).

The calculation implies to choice a set of set of Kihara parameters  $\varepsilon_j$ ,  $\sigma_j$ , and  $a_j$  for each of components  $j$ , and to select the correct set of reference parameters.

Then, at a given temperature (resp. a given Pressure), and assuming a value of the pressure (resp. the temperature), it allows the calculation of the interaction potential in Eq.(14), then the constants of Langmuir Eq.(12), and finally  $\Delta\mu_w^{H-\beta}$  in Eq.(11). Also, it provides  $\Delta\mu_w^{\varphi-\beta}$  from Eq.(17). The calculated equilibrium pressure  $P_{calc}$  (resp. the calculated equilibrium temperature  $T_{calc}$ ) corresponds to the value at which  $\Delta\mu_w^{H-\beta} = \Delta\mu_w^{L-\beta}$ .

A special attention (**first step**) has to be paid when assigning value for  $\Delta\mu_w^{L-\beta} \Big|_{T^0, P^0}$  and  $\Delta h_w^{L-\beta} \Big|_{T^0, P^0}$  since the corresponding data found in the literature vary strongly

from one author to the other, mainly due to the difficulties arising when determining these quantities experimentally. The values can be found in the open literature as cited by (Sloan, 1998; Sloan and Koh, 2007) and some of them are reported in Table 25. The other quantities  $\Delta h_w^{L-\beta,0}$ ,  $\Delta v_w^{L-\beta}|_T$ ,  $\Delta c_{p,w}^{L-\beta,0}$ , and  $b_{p,w}^{L-\beta}$  are taken from Table 26.

The **second step** is to choose the Kihara parameters in order to fit with equilibrium data. The number of Kihara parameters is 3:  $\varepsilon_j$ ,  $\sigma_j$ , and  $a_j$ .

(Mehta and Sloan, 1996) propose to fix the kihara  $a$  value first, for example by using the correlation established by (Tee et al., 1966a, 1966b). As said previously,  $a$  is a geometric parameter, and the volume of the molecule is supposed to be spherical. It can be assumed it is a conservative value in the different models describing interaction potentials.

Then, for a given set of Kihara parameters  $\varepsilon_j$  and  $\sigma_j$ , it is possible to evaluate the deviation between the model and a set of experimental data.:

$$F(\varepsilon_j, \sigma_j) = \sum_{l=1}^N \left| \frac{P_{calc}}{P_{exp}} - 1 \right| \rightarrow \min \text{ (resp. } F(\varepsilon_j, \sigma_j) = \sum_{l=1}^N \left| \frac{T_{calc}}{T_{exp}} - 1 \right| \rightarrow \min \text{ )} \quad (20)$$

In Eq.(20), the index  $l$  assigns the specific data point and the summation has to be performed over all  $N$  data of the set. It presents a simplified version of the deviation function, based on deviation between the (Pressure, Temperature) coordinates at equilibrium. Eq.(20) can be enriched to additional data such as deviation to composition if the data are available (much harder to obtain with accuracy).

In the end, the Kihara parameters remain adjustable parameters. As it has been claimed by (John et al., 1985) and reported by (Mehta and Sloan, 1996): the wrong kihara parameters, wrong cell potential, wrong Langmuir constants (and we can add from (Herri et al., 2011), the wrong reference parameters) could still lead to “right” dissociation pressures.

#### 4.3.1 DETERMINATION OF THE REFERENCE PARAMETERS

As we mentioned before, the values for  $\Delta \mu_w^{L-\beta}|_{T^0, P^0}$  and  $\Delta h_w^{L-\beta}|_{T^0, P^0}$  strongly differ from one author to another (Table 26). A previous work consisted in determining the best values to use. It implied to test them against experimental results in a thermodynamic model.

- 1) Choice of a set of macroscopic parameters as literature input from Table 25 and Table 26.
- 2) Under the assumption of a SI and SII structure, respectively, retrieve the best Kihara parameters by adjusting  $\varepsilon$  and  $\sigma$  ( $a$  value are taken from (Sloan, 2005, 1998), by using the correlation established by (Tee et al., 1966a, 1966b), given in Table 24).

These best values of parameters minimize the mean standard deviation between the experimental data and the corresponding data calculated from the model (see §4.3.2).

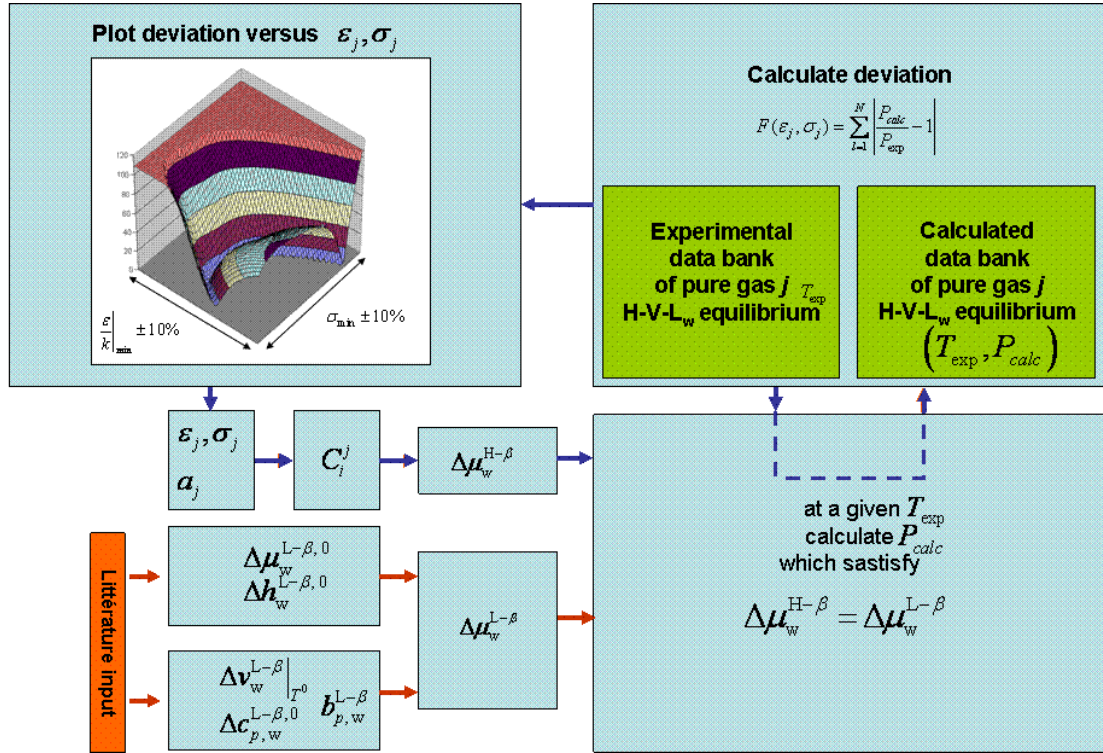


**Figure 11:** Procedure to optimise the kihara parameters

(Herri et al., 2011) determined the sensibility of the kihara parameters to the values for  $\Delta\mu_w^{L-\beta}|_{T^0, P^0}$  and  $\Delta h_w^{L-\beta}|_{T^0, P^0}$ . Table 27 shows the best kihara parameters to predict complex H-L<sub>w</sub>-V equilibrium, not only on pure CO<sub>2</sub>, N<sub>2</sub> and CH<sub>4</sub> gas, but also on CO<sub>2</sub>-N<sub>2</sub>, CH<sub>4</sub>-N<sub>2</sub> and CO<sub>2</sub>-CH<sub>4</sub> gas mixtures, giving not only the (Pressure, Temperature, Gas mixture composition) at equilibrium but also the Hydrate composition at equilibrium. It can be observed that the kihara parameters are dependent on values of  $\Delta\mu_w^{L-\beta}|_{T^0, P^0}$  and  $\Delta h_w^{L-\beta}|_{T^0, P^0}$ . Also, (Herri et al., 2011) showed that a better simulation is performed as the model is implemented with parameters from (Handa and Tse, 1986).

**Table 27:** Kihara parameters after optimisation on experimental data (Herri et al., 2011) and compared to literature

Kihara parameters regressed from experimental results from (Herri et al., 2011) and implemented in model 1,2,3 with macroscopic parameters from Table 25. -(1) (Dharmawardhana et al., 1980) - (2) (John et al., 1985) – (3) (Handa and Tse, 1986)									
	CO <sub>2</sub>			CH <sub>4</sub>			N <sub>2</sub>		
	$\frac{\varepsilon}{k}$	$\sigma$	$a$	$\frac{\varepsilon}{k}$	$\sigma$	$a$	$\frac{\varepsilon}{k}$	$\sigma$	$a$
Model 1	170.00	2.9855	0.6805	157.85	3.1439	0.3834	126.98	3.0882	0.3526
Model 2	164.56	2.9824	0.6805	154.47	3.1110	0.3834	166.38	3.0978	0.3526
Model 3	171.41	2.9830	0.6805	158.71	3.1503	0.3834	138.22	3.0993	0.3526
<b>Kihara parameters from literature</b>									
(Sloan, 1998; Sloan and Koh, 2007)	168.77	2.9818	0.6805	154.54	3.1650	0.3834	125.15	3.0124	0.3526
	175.405	2.97638	0.6805	155.593	3.14393	0.3834	127.426	3.13512	0.3526

#### 4.3.2 DETERMINATION OF THE KIHARA PARAMETERS

The reference parameters  $\Delta\mu_w^{L-\beta}|_{T^0, P^0}$  and  $\Delta h_w^{L-\beta}|_{T^0, P^0}$  are taken from (Handa and Tse, 1986) in Table 25. The other reference parameters  $\Delta h_w^{L-\beta, 0}$ ,  $\Delta v_w^{L-\beta}|_{T^0}$ ,  $\Delta c_{p, w}^{L-\beta, 0}$  and  $b_{p, w}^{L-\beta}$  are taken from (Sloan, 1998; Sloan and Koh, 2007) (Table 26).  $\Delta\mu_w^{L-\beta}$  can be calculated (Eq. 17) provided the water activity can be calculated.  $\Delta\mu_w^{H-\beta}$  can be calculated (§4.1) provided the kihara parameters are known. As it has been mentioned in the previous section (§4.3.1), the determination of the kihara parameters implies to optimise them so that the condition of equilibrium is achieved (Eq.8) following the procedure summarized on Figure 11. It also implies to minimize the deviation between experimental results from a data bank and simulated results.

##### • CO<sub>2</sub> Kihara parameters

In the work of (Herri and Chassefière, 2012), the Kihara parameters have been retrieved for pure CO<sub>2</sub> clathrate hydrate by assuming a SI structure. It corresponds to the values of Kihara parameters which minimise the deviation given in Eq.(20). It is an optimal situation because the equilibrium data are numerous. The study compares 32 experimental results from (Yasuda and Ohmura, 2008), (Adisasmito et al., 1991), (Falabella, 1975), (Miller and Smythe, 1970) which cover a range of temperature from 151.52K to 282.9K and a pressure range from 0.535kPa to 4370kPa.

In [Figure 12](#), we can see that the  $\varepsilon/k$  and  $\sigma$  values which minimize the deviation are located in a deep valley. The [Figure 13](#) plots the  $\varepsilon/k$  and  $\sigma$  values in the valley, and the corresponding deviation. We can see that the deviation presents a clear minimum which can be considered as the best values of  $\varepsilon/k$  and  $\sigma$  (reported in [Table 28](#)).

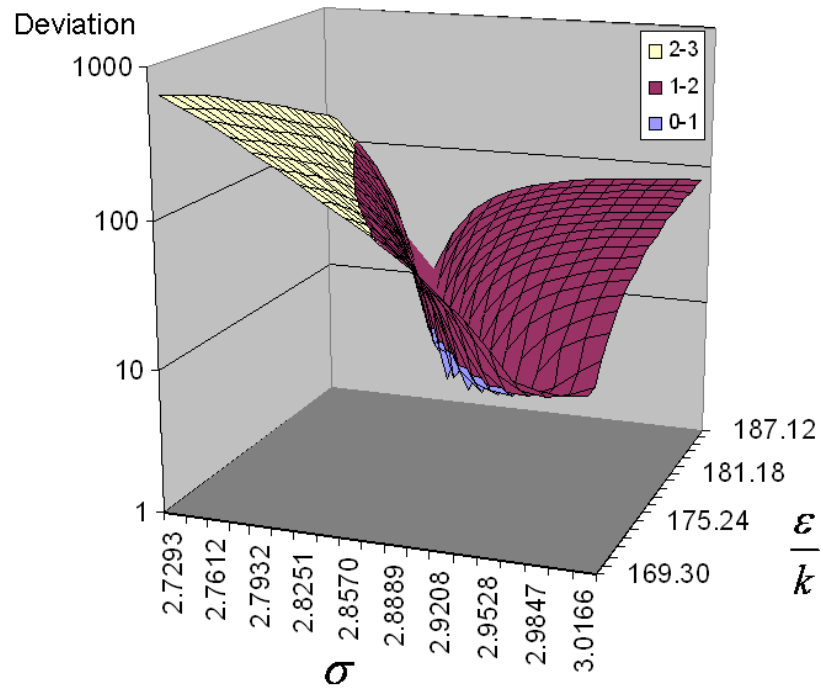


**Figure 12:** Deviation (in %, from Eq.20) between experimental equilibrium data of pure CO<sub>2</sub> hydrate Experimental data are from ([Yasuda and Ohmura, 2008](#)), ([Adisasmito et al., 1991](#)), ([Falabella, 1975](#)), ([Miller and Smythe, 1970](#)) which cover a range of temperature from 151.52K to 282.9K and a pressure range from 0.535kPa to 4370kPa.

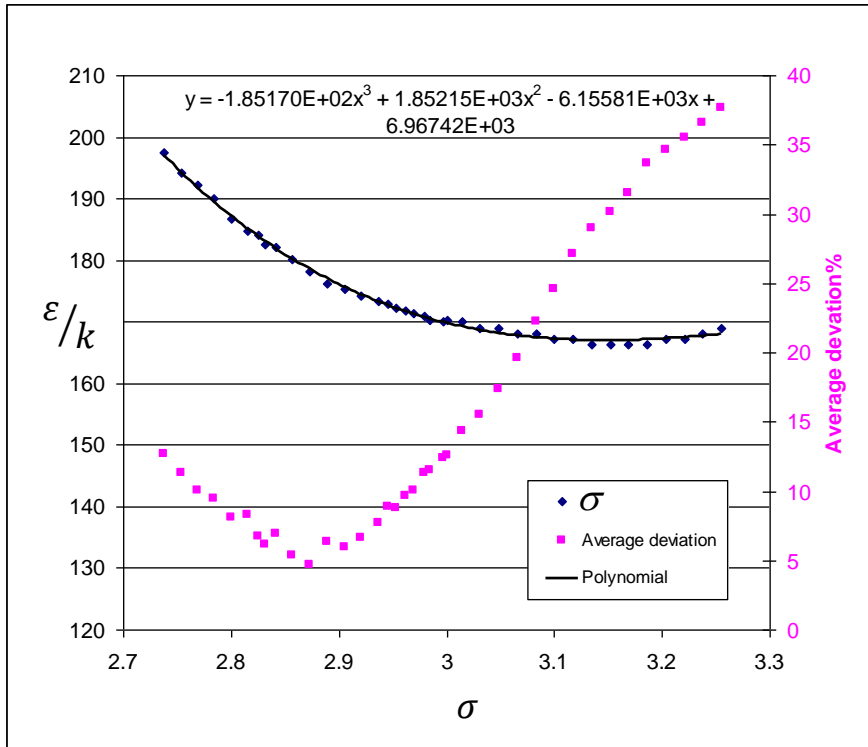


**Figure 13 :**  $\varepsilon/k$  versus  $\sigma$  at the minimum deviation with experimental data.  $a$  value is taken from [Table 27](#). Pressure and temperature equilibrium data for CO<sub>2</sub> hydrate are taken from ([Yasuda and Ohmura, 2008](#)), ([Adisasmito et al., 1991](#)), ([Falabella, 1975](#)), ([Miller and Smythe, 1970](#)) which cover a range of temperature from 151.52K to 282.9K and a pressure range from 0.535kPa to 4370kPa.

- *CH<sub>4</sub> Kihara parameters*

The Kihara parameters have been retrieved for pure CH<sub>4</sub> clathrate hydrate ([Herri and Chassefière, 2012](#)) by assuming a SI structure. The equilibrium data are numerous. The study used a set of 27 experimental results from ([Fray et al., 2010](#)), ([Yasuda and Ohmura, 2008](#)), ([Adisasmito et al., 1991](#)) which cover a range of temperature from 145.75 to 286.4K and a pressure range from 2.4kPa to 10570kPa. On [Figure 14](#), the deviation presents a clear minimum which can be considered as the best values of  $\varepsilon/k$  and  $\sigma$  (reported in [Table 28](#)).

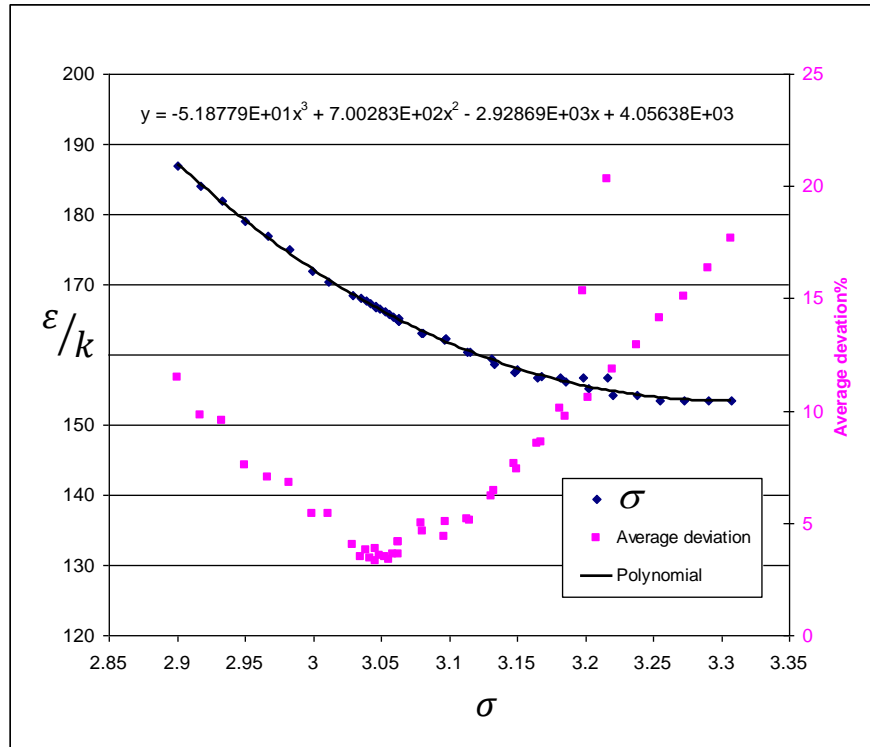


**Figure 14 :**  $\varepsilon/k$  versus  $\sigma$  at the minimum deviation with experimental data.  $a$  value is taken from [Table 27](#). Pressure and temperature equilibrium data for  $\text{CH}_4$  hydrate are taken from ([Fray et al., 2010](#)), ([Yasuda and Ohmura, 2008](#)), ([Adisasmito et al., 1991](#)) which cover a range of temperature from 145.75 to 286.4K and a pressure range from 2.4kPa to 10570kPa.

- *$\text{C}_2\text{H}_6$  Kihara parameters*

The Kihara parameters have been retrieved for pure ethane clathrate hydrate by assuming a SI structure. The equilibrium data are numerous ([Figure 8](#)) and 61 experimental results have been retained for the optimisation, from ([Roberts et al., 1940](#)), ([Deaton and Frost, 1946](#)), ([Reamer et al., 1952](#)), ([Falabella, 1975](#)), ([Yasuda and Ohmura, 2008](#)), ([Mohammadi and Richon, 2010a, 2010b](#)), which cover a wide range of temperature from 200.08 to 287.4K and a pressure range from 8.3kPa to 3298kPa. On [Figure 15](#), the deviation presents a clear minimum which can be considered as the best values of  $\varepsilon/k$  and  $\sigma$  (reported in [Table 28](#)).



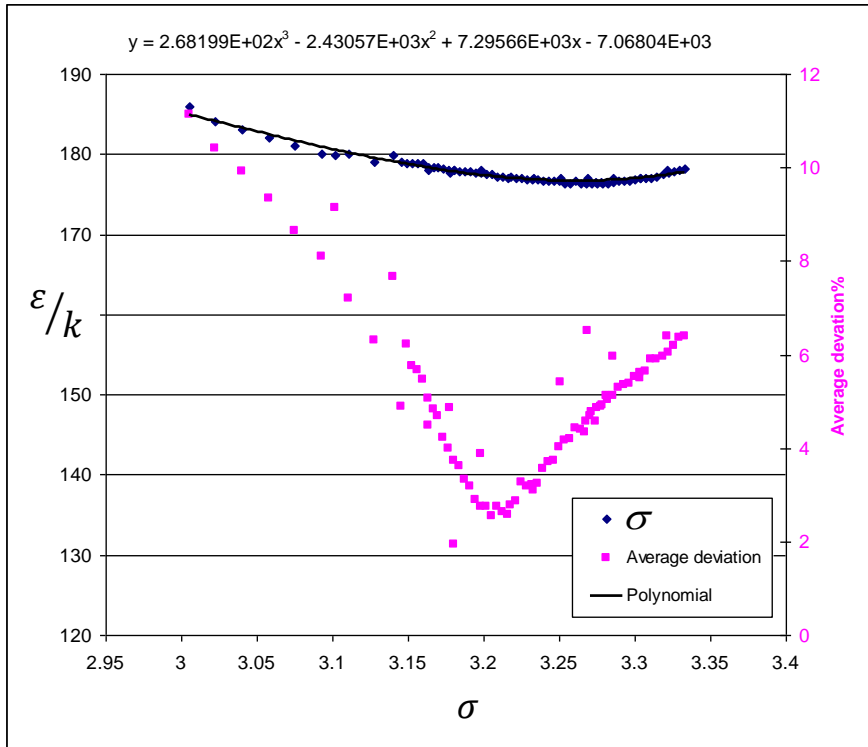


**Figure 15 :**  $\varepsilon/k$  versus  $\sigma$  at the minimum deviation with experimental data.  $a$  value is taken from [Table 27](#). Pressure and temperature equilibrium data for  $C_2H_6$  hydrate are taken , from ([Roberts et al., 1940](#)), ([Deaton and Frost, 1946](#)), ([Reamer et al., 1952](#)), ([Falabella, 1975](#)), ([Yasuda and Ohmura, 2008](#)), ([Mohammadi and Richon, 2010a, 2010b](#)), which cover a wide range of temperature from 200.08 to 287.4K and a pressure range from 8.3kPa to 3298kPa.

- *$C_3H_8$  Kihara parameters*

Popane Kihara parameters have been retrieved from different sources and equilibriua. First pure propane clathrate hydrate has been considered assuming a SII structure. The equilibrium data are numerous ([Figure 9, page 39](#)) but do not cover a wide temperature range. 41 experimental results have been retained for the parameters optimisation from ([Deaton and Frost, 1946](#)), ([Yasuda and Ohmura, 2008](#)) and ([Nixdorf and Oellrich, 1997](#)) which cover a range of temperature from 245 to 278.5K and a pressure range from 41kPa to 567kPa. On [Figure 16](#), the deviation does not present a minimum, and the best set of kihara parameters can not be found directly from this curve.

The experimental data bank needs to be extended to equilibrium data on two components gas mixtures, with a second gas which kihara parameters is well known, for example  $CO_2$ ,  $CH_4$ , Kr, Xe. Of course, the experimental data on these mixed hydrates have to be accurate.

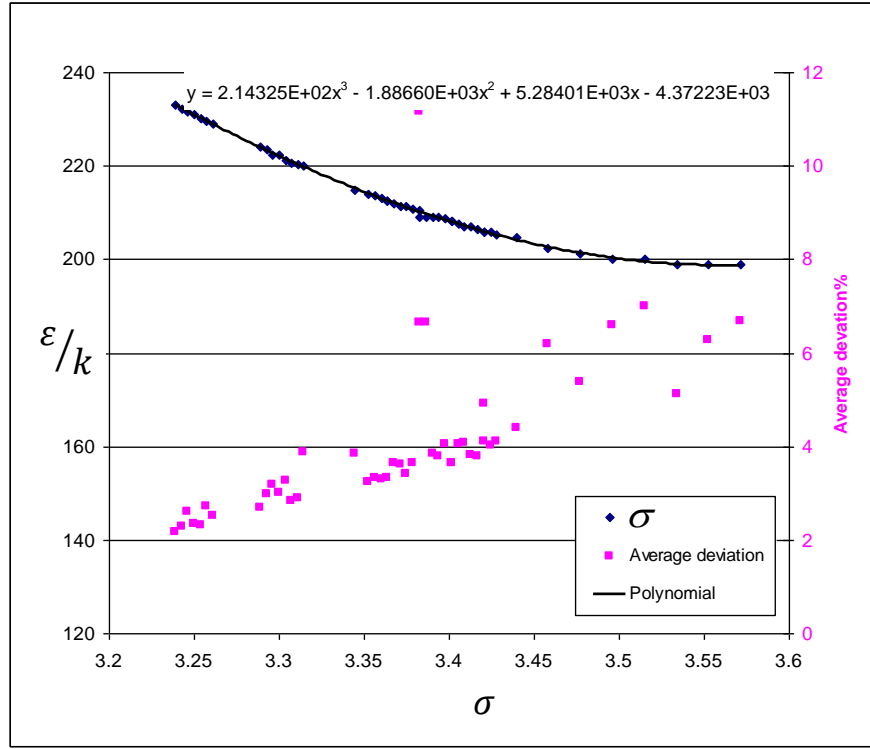


**Figure 16:**  $\varepsilon/k$  versus  $\sigma$  at the minimum deviation with experimental data.  $a$  value is taken from [Table 27](#). Pressure and temperature equilibrium data for  $C_3H_8$  hydrate are taken from ([Deaton and Frost, 1946](#)), ([Yasuda and Ohmura, 2008](#)) and ([Nixdorf and Oellrich, 1997](#)) which cover a wide range of temperature from 245 to 278.5K and a pressure range from 41kPa to 567kPa

First, binary methane-propane clathrate hydrate equilibrium data have been considered. 12 equilibrium points have been chosen in temperature range of [274.9K-282.3K], pressure range of [0.26MPa-0.95MPa] and  $CH_4$  molar composition range of [0.24-0.37] ([Verma, 1971](#)), ([Verma et al., 1974](#)) and assuming both a SI and SII structure ([Table 14](#)). The [Figure 17](#) shows that the best ( $\varepsilon/k$ ,  $\sigma$ ) parameters by assuming a SI Structure. We observe that  $\varepsilon/k$  and  $\sigma$  parameters are very close to the ones determined on the single propane clathrate hydrate froming a Structure II. It confirms that the  $CH_4$ - $C_3H_8$  here forms a Structure I Hydrates. The average deviation curve does not present a clear minimum. The comparison between the curves does not allow retrieving a best set of kihara parameters.

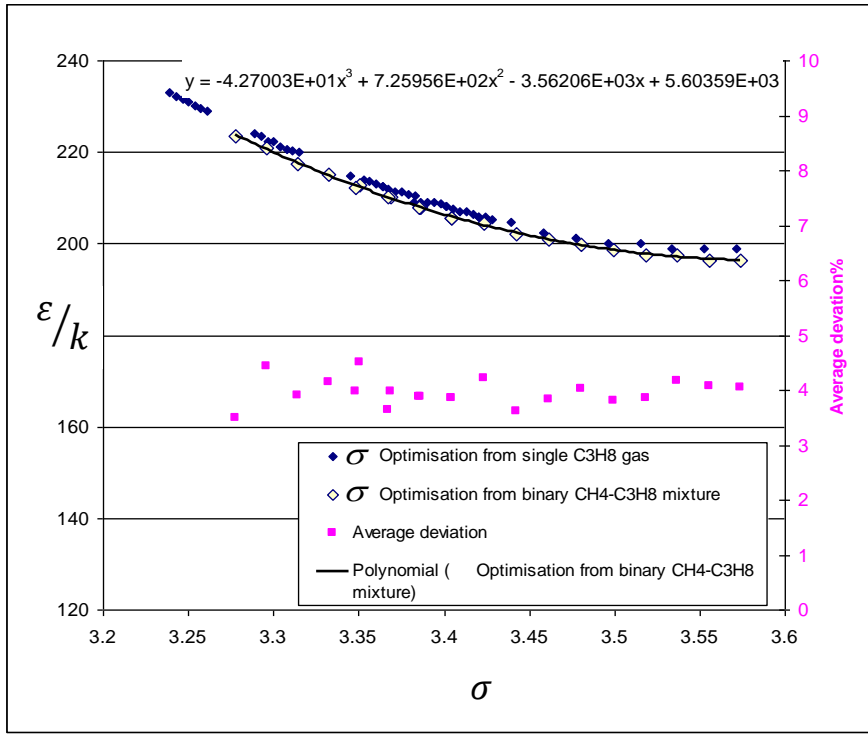


**Figure 17:**  $\varepsilon/k$  versus  $\sigma$  at the minimum deviation with experimental data.  $a$  value is taken from [Table 27](#). Pressure and temperature equilibrium data for  $\text{CH}_4\text{-C}_3\text{H}_8$  hydrate are taken from [\(Verma et al., 1974\)](#) and [\(Verma, 1974\)](#).

[Figure 18](#) and [Figure 19](#) show another tentative to retrieve the propane kihara parameters by doing an optimisation based on a  $\text{Xe-C}_3\text{H}_8$  gas mixture, respectively by assuming that  $\text{Xe-C}_3\text{H}_8$  gas mixture forms a SII and SI Structure. The literature data concerns only one equilibrium point from [\(Tohidi et al., 1993\)](#) but it gives not only the pressure, temperature, gas composition in the gas phase, but also the gas composition in the hydrate phase. It is then possible to calculate a mean deviation not only based on the deviation between the experimental and calculated pressure, but also on the hydrate phase composition.

$\text{Xe}$  is a Structure II former, as well as  $\text{C}_3\text{H}_8$ . If we assume that the gas mixture forms a Structure II ([Figure 18](#)), we observe that the  $(\varepsilon/k, \sigma, F)$  curves of the pure propane and  $\text{Xe-C}_3\text{H}_8$  mixture does not present any intersection points. It is a different situation from [Figure 17](#) where the  $(\varepsilon/k, \sigma)$  curves of the pure propane and  $\text{CH}_4\text{-C}_3\text{H}_8$  mixture are identical and provide an infinite set of equivalent  $(\varepsilon/k, \sigma)$  values. In this case both pure propane as a Structure II former and  $\text{CH}_4\text{-propane}$  as a Structure SI former equilibria can be simulated. In the case of  $\text{Xe-propane}$  mixture, there is no  $(\varepsilon/k, \sigma)$  value which allows simulating both the equilibrium of pure propane as a Structure II former and  $\text{Xe-C}_3\text{H}_8$  as a Structure SII former. But, if we assume that the  $\text{Xe-C}_3\text{H}_8$  mixture forms an unexpected Structure I hydrate ([Figure 19](#)), it becomes possible to find a unique solution for  $(\varepsilon/k, \sigma)$  which satisfies both the simulation of the pure  $\text{C}_3\text{H}_8$  and  $\text{Xe-C}_3\text{H}_8$  mixture.

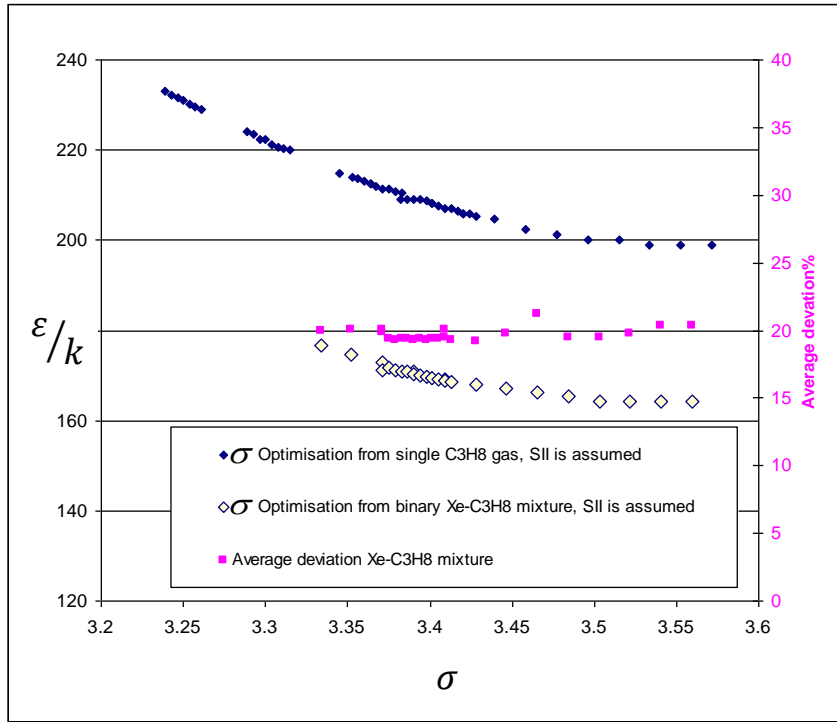


**Figure 18:**  $\varepsilon/k$  versus  $\sigma$  at the minimum deviation with experimental data. SII is assumed.  $a$  value is taken from [Table 27](#). Pressure and temperature equilibrium data for Xe- C<sub>3</sub>H<sub>8</sub> hydrate is taken from ([Tohidi et al., 1993](#)).

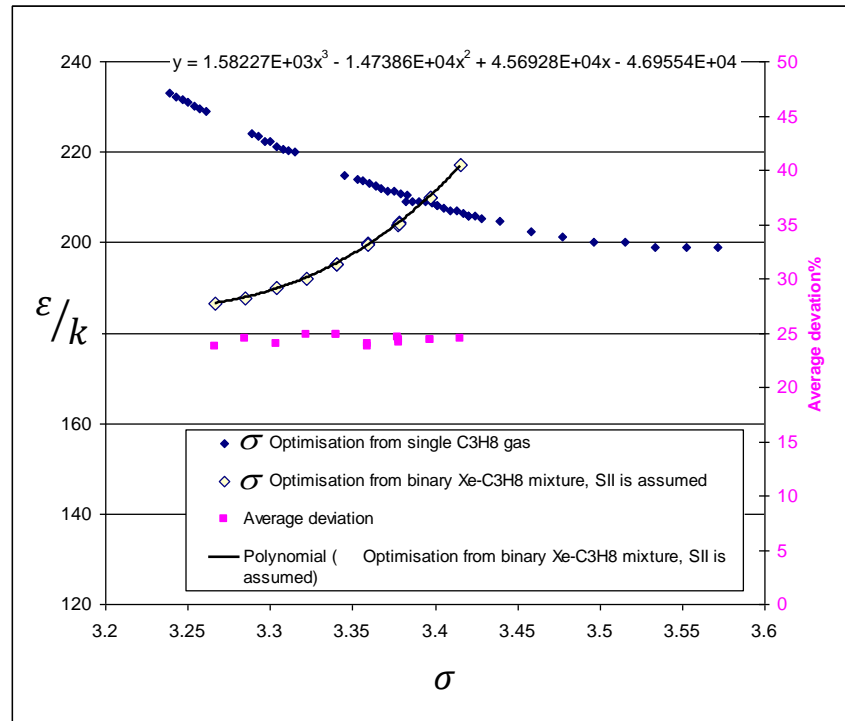


**Figure 19:**  $\varepsilon/k$  versus  $\sigma$  at the minimum deviation with experimental data. SI is assumed.  $a$  value is taken from [Table 27](#). Pressure and temperature equilibrium data for Xe-C<sub>3</sub>H<sub>8</sub> hydrate is taken from ([Tohidi et al., 1993](#)).

To confirm this value, On [Figure 20](#) presents the optimisation of the propane kihara parameters based on a CO<sub>2</sub>-C<sub>3</sub>H<sub>8</sub> gas mixture, from experimental data of ([Adisasmito and Sloan, 1992](#)) providing 55 equilibrium points in the temperature range of [273.7K-282.0K], pressure range of [0.22MPa-3.64MPa] and range of CO<sub>2</sub> gas fraction of [0.1-0.99]. The average deviation is a mean deviation between the calculated and experimental pressures at the temperature and gas composition in the gas phase given by ([Adisasmito and Sloan, 1992](#)). The mean deviation is important (15%) and does not present a minimum. But the ( $\varepsilon/k, \sigma$ ) curves of the pure propane and CO<sub>2</sub>-C<sub>3</sub>H<sub>8</sub> mixture present also a single point in common at the same value of  $\sigma \approx 3.39$ , which confirms the previously obtained value from Xe-C<sub>3</sub>H<sub>8</sub> gas mixture.

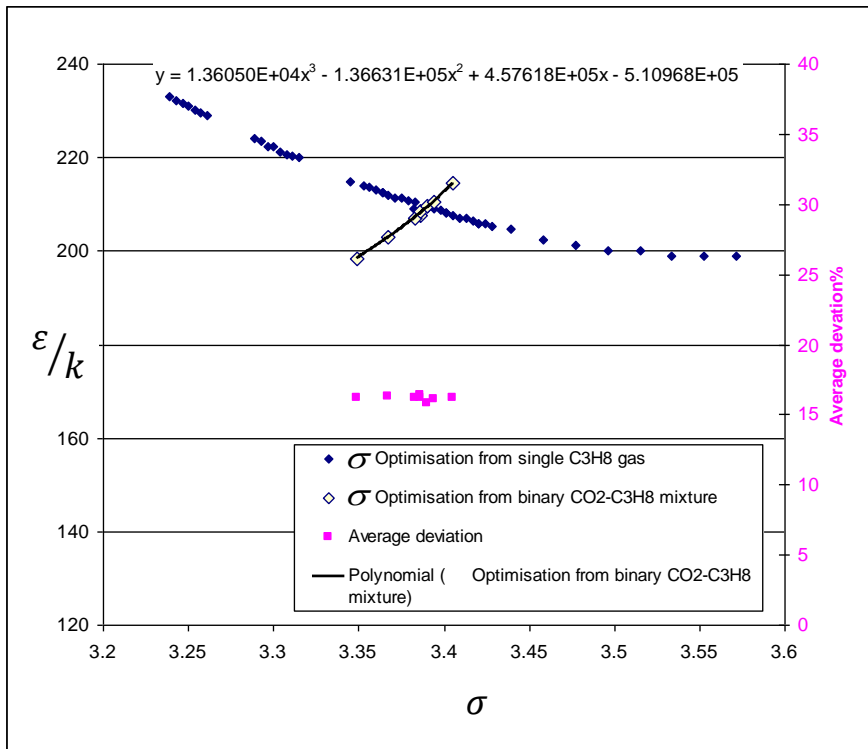


**Figure 20:**  $\varepsilon/k$  versus  $\sigma$  at the minimum deviation with experimental data.  $a$  value is taken from [Table 27](#). Pressure and temperature equilibrium data for CO<sub>2</sub>-C<sub>3</sub>H<sub>8</sub> hydrate is taken from ([Adisasmito and Sloan, 1992](#)).

**Table 28:** Kihara parameters, after optimisation from experimental data with the GasHyDyn simulator, implemented with reference parameters from [Table 25](#) (Dharmawardhana et al., 1980) and [Table 26](#).

Gas	$\frac{\varepsilon}{k}$	$a$	$\sigma$
CO <sub>2</sub>	178.21 <sup>(*)</sup>	0.6805 <sup>(+)</sup>	2.873 <sup>(*)</sup>
CH <sub>4</sub>	166.36 <sup>(*)</sup>	0.3834 <sup>(+)</sup>	3.050 <sup>(*)</sup>
C <sub>2</sub> H <sub>6</sub>	177.46 <sup>(*)</sup>	0.5651 <sup>(+)</sup>	3.205
C <sub>3</sub> H <sub>8</sub>	209.20 <sup>(*)</sup>	0.6502 <sup>(+)</sup>	3.390 <sup>(*)</sup>
<sup>(*)</sup> -regressed from experimental data, <sup>(+)</sup> -from (Sloan, 2005, 1998), <sup>(-)</sup> -(Barrer and Edge, 1967a, 1967b)			



## 5. HYDRATES UNDER NON EQUILIBRIUM CONDITIONS

### 5.1. INTRODUCTION

The laboratory has faced during the last decade experimental data, generally from complex gas mixtures, which can hardly be modeled using the classical thermodynamic approach given in the previous chapter (§3 Page 35).

A new approach has been attempted to give a fundamental explanation by re-considering the (van der Waals and Platteeuw, 1959), which is fundamentally a kinetic approach, but at equilibrium, where the hydrate finds its equilibrium as the rate of enclathration of new species at its surface is equal to the rate of desorption of the same species.

This approach has been extended by (Herri and Kwaterski, 2012) to non equilibrium conditions that is to say when the fugacities of components in all the phases are not equal, giving a driving force to start the elementary steps of the cristallisation.

Understanding the crystallization processes, especially nucleation and growth, are essential in the modelling.

The historical model of (Volmer and Weber, 1926a) (§5.4.1) is an approach from the thermodynamic collectivity where the kinetics is understood as an energetic barrier to cross away. Kashchiev and Firoozabadi on their side (§5.4.2) (Kashchiev and Firoozabadi, 2003, 2002a, 2002b) have applied to hydrates the backroung of the collectivity that considers nucleation as a continuous mechanisms of clusters aggregations considered individually as reactions. In the end, the collectivity of chemical engineers (§5.4.3) has developed correlations to implement the nucleation in a simple way in complex crystallization models.

But whatever the approach, each of the models define a driving force, as a temperature difference, or a pressure ratio, or a concentration profile in between the actual operative conditions and the equilibrium conditions. Based on an expression of the driving force given as a concentration grandiant at the vicinity of the growing particles, we conclude this chapter (§5.5) by enlighting that clathrate hydrates, because they are non defined compounds, can encapsulate chemicals at a composition that is not constrained by thermodynamics, but constrained by mass transfers.

In the end, the composition of gas hydrates is geometric depending on the reactor in which is operated the crystallization.

This chapter presents reviews of the elementary steps of the crystallization, and the models given by the collectivity working in this field. Especially, theory of mass transfer phenomena, nucleation and crystal growth are presented.



## 5.2. GENERALITIES ABOUT THE CRYSTALLIZATION OF GAS HYDRATES

The simplest situation corresponds to the crystallization of gas hydrate in a single liquid phase, composed of pure water. In this case, gas molecules have to cross only the gas/liquid interface, and the bulk phase.

If the reaction is operated in a stirred reactor, or a bubble reactor, the bulk solution can be considered as homogeneous. Supersaturation ratio is defined as  $S=C/C_{eq}$  in which  $C$  is the concentration in dissolved gas and  $C_{eq}$  is the equilibrium concentration. We define supersaturation for each gas component. Three zones can be distinguished as pointed by (Vysniauskas and Bishnoi, 1983):

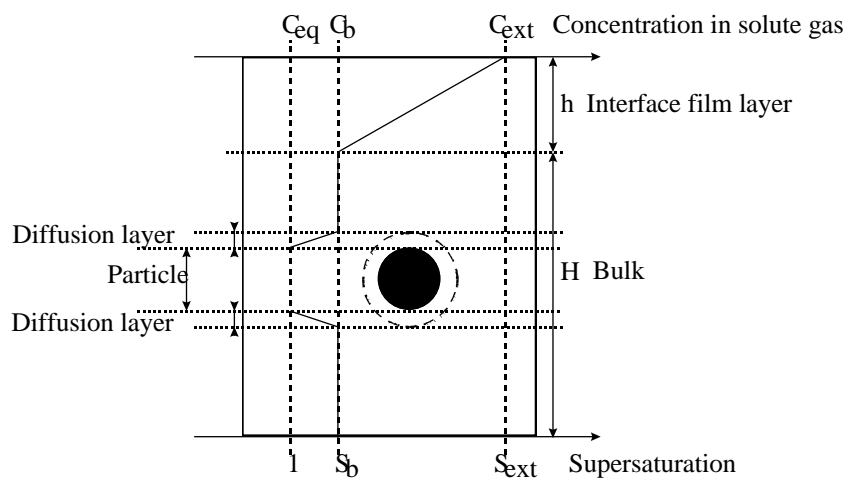


**Figure 21:** Schematic of the concentration profiles in the environment of a particle in a liquid bulk

- The first zone is the interface film layer. In the investigated system, its thickness is about tens of micrometer. Because of the high supersaturation level of this zone compared to the rest of the reactor, primary nucleation (§5.4) is particularly active in the interfacial film which acts most of the time as a source of nuclei for the bulk of the reactor.
- The second zone is the bulk zone in which the concentration is supposed to be uniform. This zone is supposed to be the main place of the crystallisation process in which we can find all the classical steps of growth, agglomeration, and secondary nucleation.
- The third zone is the solid/liquid interface. The crystal is assumed to be surrounded by two successive layers: an integration layer and a diffusion layer. The integration layer is the region of volume in which a transition between the solid state and the liquid state occurs. The integration layer can be considered as a solidification layer.

First works were developed in Canada by (Vysniauskas and Bishnoi, 1983) and then completed by (Englezos et al., 1987a, 1987b). The authors identified a mass transfer

limiting step at the gas liquid interface, or a growth rate limiting step at the vicinity of the elementary particles, depending on the stirring rate. In 1994 (Per Skovborg and Rasmussen, 1994; P. Skovborg and Rasmussen, 1994) analyzed again those results and demonstrated that the limiting step remains the gas/liquid mass transfer, whatever the stirring rate. This conclusion has been supported by (Herri et al., 1999a) and (PIC et al., 2000) from experimental results obtained by using a new particle size analysis tool (Herri et al., 1999b).

So, even in the simplest situation, the principal teams working on the subject propose different approach. The degree of precision of the model is widely dependent on the possibility to monitor the population of particles. So, this modeling has been driven for decades by the development of new sensors adapted to the high pressure conditions during crystallization. First experiments have consisted in studying the gas consumption rate coupled with a population balance in order to propose a model between the size/number of crystals, and the quantity of gas consumed.

So, it can be said that, even in the simplest case consisting in crystallizing gas hydrates in pure water, the authors doesn't agree on the limiting step. A fruitful reading is the reviewing from (Ribeiro Jr. and Lage, 2008).

### 5.3. MODELLING THE GAS/LIQUID TRANSFER IN A BATCH REACTOR

The Gas/Liquid transfer through the interface liquid film layer of thickness (Figure 21) is a first order law consistent with the well-known relation (Mehta and Sharma, 1971; Sridharan and Sharma, 1976):

$$r_i = k_L^i a (C_{i,ext} - C_{i,bulk}) V_{L+G} \quad (21)$$

$r_i [mol.s^{-1}]$  is the dissolution rate of component  $i$ ,  $a [m^{-1}]$  is the mass transfer surface area per unit of volume of liquid and  $k_L [m.s^{-1}]$  the mass transfer coefficient,  $C_{i,bulk} [mol.m^{-3}]$  is the gaz component  $i$  concentration in the liquid bulk,  $C_{i,ext} [mol.m^{-3}]$  is the interfacial concentration, and  $V_{L+G}$  is the liquid volume plus the volume of gas that is eventually dispersed.

The Figure 22 plots the experimental determination of the  $k_L^i a$  value in the case of methane.

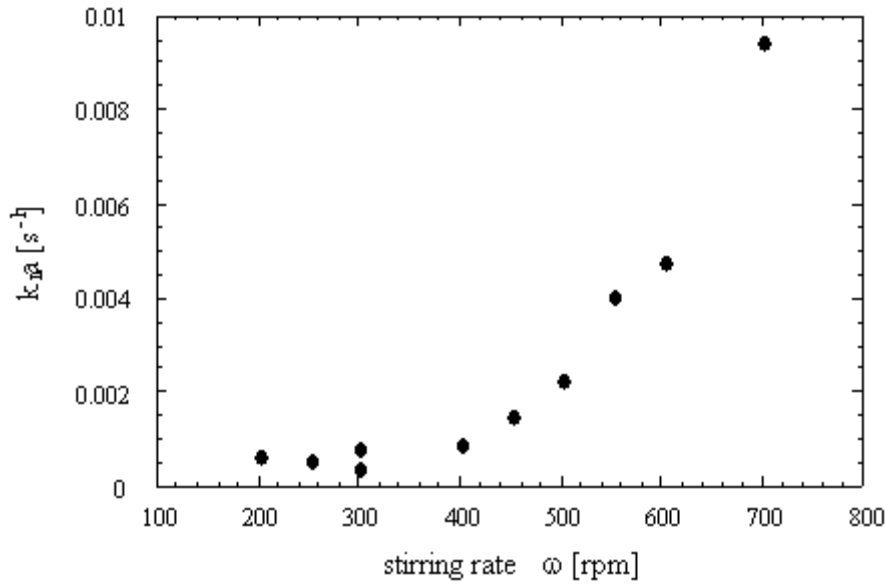


**Figure 22 :** Influence of the stirring rate on the rate of methane dissolution in a stirred batch reactor (Herri et al., 1999a)

#### 5.4. MODELLING THE NUCLEATION

The nucleation is the process in which a new phase appears, here the crystal clathrate hydrate (or semi clathrate hydrate). The nucleation is qualified as primary if there is parent crystal. If a crystal is already present, it can help the nucleation process, and the nucleation is qualified as secondary.

Both the primary and secondary nucleation are dependent on the level of supersaturation of the reactants. The supersaturation ratio is defined as the ratio in between the “concentration” of the reactant and the “equilibrium concentration”.

The composition of the liquid phase with respect to  $j=1,\dots,N_g$  species is characterised by a vector of generalised concentrations  $\vec{\zeta} = (\zeta_1, \dots, \zeta_{N_g})^T$ . For chemical engineering applications, especially applications concerning crystallisation processes in liquids, liquid phase non-idealities are often neglected and the fugacity is replaced by a concentration variable  $\zeta_j$ . In this section, and in the remaining parts of this manuscript, the variable  $\zeta$  will characterise the composition while the concentration of the guest species is chosen to be the mole fraction  $x$ .

So, the supersaturation ratio is defined as the ratio between the mole fraction of reactant  $j$  in the bulk ( $x_{j, \text{bulk}}$ ) and the mole fraction at equilibrium ( $x_j$ )

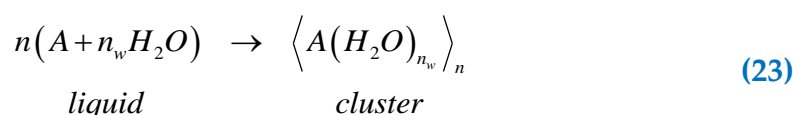
$$S = \frac{x_{j, \text{bulk}}}{x_j} \quad (22)$$

(Kashchiev and Firoozabadi, 2002a) have given different ways to express the driving force for hydrates from a rigorous approach based on thermodynamic considerations (difference of chemical potentials). Then, (Noguera et al., 2006a, 2006b) have extended the work to precipitation, vapour condensation and crystallization in the melt.

#### 5.4.1 PRIMARY NUCLEATION FROM THE MODEL OF VOLMER AND WEBER (1926)

The original model of (Volmer and Weber, 1926a, 1926b, 1926c, 1926d) is the reference model which gives the basement for the interpretation of the primary nucleation mechanism. The original experiment deals with the nucleation of water droplets in a supersaturated gas phase. (Volmer, 1929) considered that a local fluctuation of density initiates a water droplet which size can be lower than critical size, and that this droplet then dissociates. If its size is bigger than the critical size, and the droplet continues to growth. This approach can be extrapolated to the nucleation in solution, and especially the nucleation of clathrate hydrates.

The solution is a liquid solution of water, and gas in solution, here called A.  $n_w$  is the hydration number. The liquid  $n_w$  water molecules and the gas molecules A can associate to form a cluster:



$n$  is the number of A molecules which aggregate with water to form a cluster. The formation of the cluster is accompanied with a variation of the Gibbs energy  $\Delta G_n$ , corresponding to the formation of the new volume  $V_n$ , and a new interface of surface  $S_n$  of:

$$\Delta G_n^{\text{liq to solid}} = \frac{V_n}{v_{\langle \text{cluster} \rangle}} \Delta \mu + S_n \gamma \quad (24)$$

The first term is equal to the difference  $\Delta \mu$  between the chemical potentials of  $n$  nucleation units in solution and in the solid. The second term is a surface term, proportional to the particle surface energy.  $v_{\langle \text{cluster} \rangle}$  is the molar volume of the cluster,

the volume of  $N_{\text{Av}}$  (number of Avogadro) unities of cluster  $\langle A(H_2O)_{n_w} \rangle$ . It is equal to  $n_w v_{\langle w \rangle}$  where  $v_{\langle w \rangle}$  is the molar volume of clathrate per mole of water molecule.

$\Delta\mu$  is the partial Gibbs energy. It can be expressed in the following form:

$$\Delta\mu = \mu_{\langle cluster \rangle} - \mu_{(A)} - n_w \mu_{(w)} \quad (25)$$

The chemical potential of solute A is:

$$\mu_{(A)} = \mu_{(A)}^0 + RT \ln a_{(A)} \quad (26)$$

In a first approximation, the activity coefficient of solute A in solution can be evaluated by its mole fraction  $x_{A, \text{bulk}}$ .

The chemical potential of water in liquid solution is:

$$\mu_{(w)} = \mu_{(w)}^0 + RT \ln a_{(w)} \quad (27)$$

In a first approximation, the activity of water is  $(1 - x_{A, \text{bulk}})$ , and in a second approximation, equal to 1.

The chemical potential of the cluster is assumed to be the value at the reference state:

$$\mu_{\langle cluster \rangle} = \mu_{\langle cluster \rangle}^0 \quad (28)$$

So, finally:

$$\Delta\mu = \mu_{\langle cluster \rangle}^0 - \mu_{(A)}^0 - n_w \mu_{(w)}^0 - RT \ln x_{A, \text{bulk}} \quad (29)$$

And at thermodynamic equilibrium

$$0 = \mu_{\langle cluster \rangle}^0 - \mu_{(A)}^0 - n_w \mu_{(w)}^0 - RT \ln x_A \quad (30)$$

And finally, combining Eq. (29) and Eq. (30), it gives:

$$\Delta\mu = RT \ln \frac{x_{A, \text{bulk}}}{x_A} = RT \ln S \quad (31)$$

After combination of Eq. (24) and Eq. (31), we obtain a general expression to calculate the variation of the Gibbs energy during the formation of a cluster of  $n$  basic unities  $\langle A(H_2O)_{n_w} \rangle$ :

$$\Delta G_n^{\text{liq to solid}} = V_n \frac{RT}{n_w v_{\langle w \rangle}} \ln S + S_n \gamma \quad (32)$$

If the cluster is assumed to be spherical, and diameter  $l$ :

$$V_n = \frac{\pi}{6} l^3 = \frac{n}{N_{\text{Av}}} v_{\langle \text{cluster} \rangle} = \frac{n}{N_{\text{Av}}} n_w v_{\langle w \rangle} \quad (33)$$

$$l = \left( \frac{6}{\pi} \frac{n}{N_{\text{Av}}} n_w v_{\langle w \rangle} \right)^{\frac{1}{3}} \quad (34)$$

$$S_n = \pi \left( \frac{6}{\pi} \frac{n}{N_{\text{Av}}} n_w v_{\langle w \rangle} \right)^{\frac{2}{3}} = \left( 36\pi n_w^2 v_{\langle w \rangle}^2 \frac{1}{N_{\text{Av}}^2} \right)^{\frac{1}{3}} n^{\frac{2}{3}} \quad (35)$$

$$\Delta G_n^{\text{liq to solid}} = -RT \ln S \cdot \frac{n}{N_{\text{Av}}} + \gamma \left( 36\pi n_w^2 v_{\langle w \rangle}^2 \right)^{\frac{1}{3}} \left( \frac{n}{N_{\text{Av}}} \right)^{\frac{2}{3}} \quad (36)$$

Figure 23 shows the variation of the Gibbs energy of formation, in respect to the value of the supersaturation. The first observation is the shape of each curve, with a maximum. It depicts the existence of a cluster critical size. Below the value of the critical size, the clusters which are formed are not stable, because their tendency is to decrease their size to diminish their Gibbs energy, and dissociate. But, following the interpretation of (Volmer and Weber, 1926a), the fluctuations which generate clusters with a size above the critical allow to form stable crystals. In fact, the clusters can continue to grow by decreasing their value of Gibbs energy.

The size of the critical cluster is given by:

$$\frac{d\Delta G_n}{dn} = 0 \quad (37)$$

$$l^* = \frac{-4\gamma}{\Delta g} \quad (38)$$

From Eq. (32) and assuming cluster to be spherical, we got:

$$l^* = \frac{-4\gamma}{\Delta\mu} = \frac{-4n_w v_{\langle w \rangle} \gamma}{RT \ln S} \quad (39)$$

The Eq. (39) shows that the critical size decreases as the supersaturation increases.

The maximum (or critical) Gibbs energy, corresponding to the critical size, is a barrier of formation. From Eqs. (32 - 35), we can calculate its value:

$$\Delta G_{\text{homogeneous}}^* = \frac{-16\pi\gamma^3 n_w^2 v_{\langle w \rangle}^2}{3R^2 T^2 \ln^2 S} \quad (40)$$

On Figure 23, we can observe the decrease of the critical size Eq. (39) and decrease of the maximum Gibbs energy Eq. (40) as the superstation is increased.

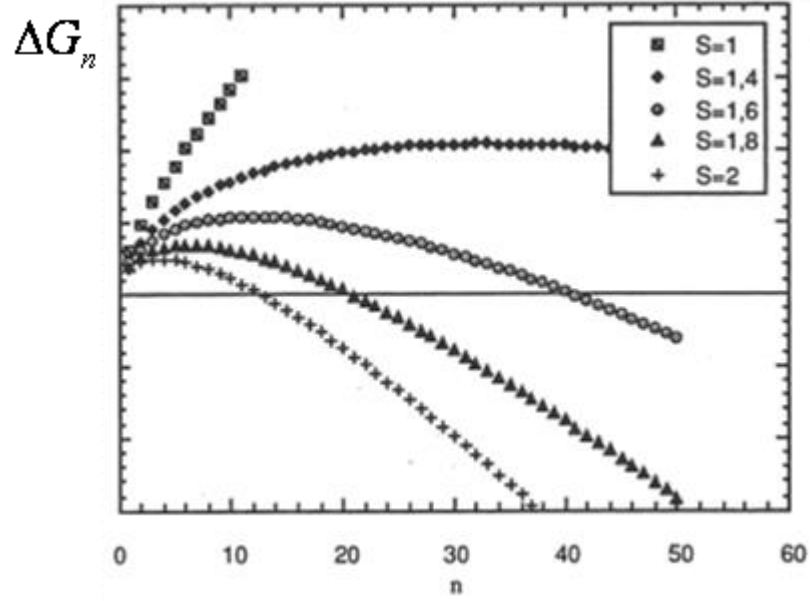


**Figure 23 :** Shape of the Gibbs energy function during formation of a cluster of  $n$  entities, depending on supersaturation (Herri, 1996)

From Eq. (40), (Volmer and Weber, 1926a) has proposed to consider the maximum Gibbs energy as an activation energy. As a consequence, it is possible to propose a kinetic interpretation of Eq. (40), and to give a simple expression of the nucleation rate  $B_I$  (i.e. the number of nuclei produced per unit volume and unit time) under the form:

$$B_I = k_1 \exp\left(\frac{\Delta G^*}{RT}\right) = k_1 \exp\left(\frac{-16\pi\gamma^3 n_w^2 v_w^2}{3R^3 T^3 \ln^2 S}\right) \quad (41)$$

in which  $k_1$  is a constant.

The rate of primary nucleation can not be measured experimentally easily. In fact, the size of the critical nuclei, about tens of nanometers, remains inaccessible to the majority of particle sizers.

But, the nucleation rate can be indirectly quantified because it is inversely proportional to the induction time. The induction time is the duration between the moment at which the solution is considered to be supersaturated, and the moment at which the first crystals are observed:



$$t_{ind} \propto \exp \left( \frac{16\pi\gamma^3 n_w^2 v_w^2}{3R^3 T^3 \ln^2 S} \right) \quad (42)$$

For gas hydrate in pure water, the supersaturation can be controlled via the operative pressure. The following Figure 24 shows the shape of the induction time as function of the operative pressure. The shape is very typical. It shows the existence of the minimum supersaturation under which the operator has to wait an infinite time before observing the nucleation, but above which the nucleation time decreases and becomes null.

From an experimental point of view, Eq. (42) explains the fact that the nucleation can be experimentally observed, only if a minimum level of supersaturation is applied.

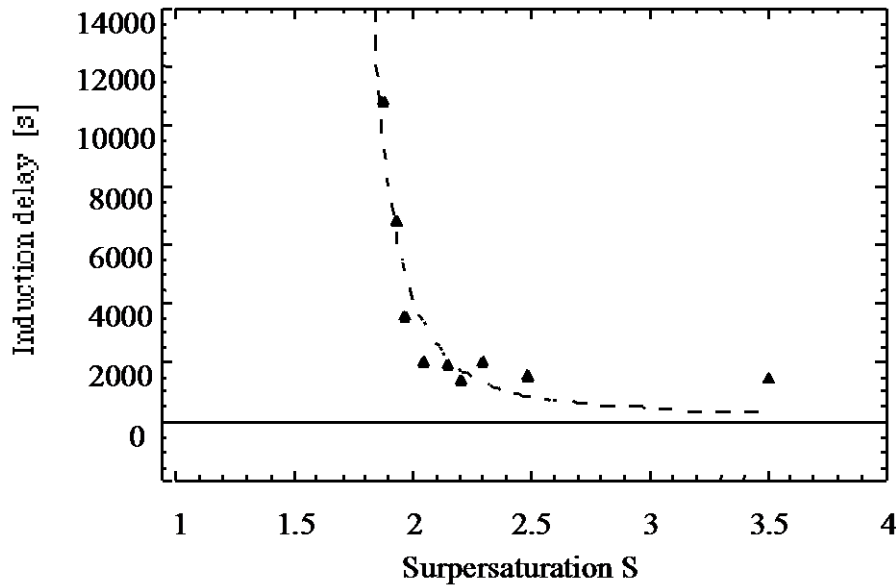


**Figure 24:** Induction time versus supersaturation during nucleation of methane hydrate in pure water, at 1°C (Herri et al., 1999b)

From Eq. (42) and Figure 24, it is possible to estimate the value of the interfacial energy  $\gamma = 5.3 \text{ mJ.m}^{-2}$  between the hydrate and the liquid water. This value is inferior to the value of the interfacial energy between ice and liquid water ( $\gamma = 28 \text{ mJ.m}^{-2}$ ).

The difference can be a true difference in respect to physical difference between the ice and the clathrate hydrate. But also, it can be explained from the consideration that nucleation is not homogeneous, but heterogeneous. In a heterogeneous mechanism of nucleation, the formation of the critical nuclei takes place at an interface. It can be a solid surface such as the wall of the reactor, or a dust. Also, it can be a gas/liquid interface. The shape of the critical nuclei moves from a spherical

geometry (homogeneous nucleation) to a complex form, such as a cap-shaped cluster (heterogeneous nucleation at a solid interface), or a lens-shaped cluster (heterogeneous nucleation at a gas/liquid interface). The shape depends on the relative interfacial energy  $\gamma$  between the phases. The respective  $\gamma$  values fix the angles at the heterogeneous junctions in respect to the Young equation (Eqs. 44, 46 and 47). The different situations are summarised in Table 29, from an original work of (Vysniauskas and Bishnoi, 1985) summarised and extended by (Kashchiev and Firoozabadi, 2002a, 2002b).

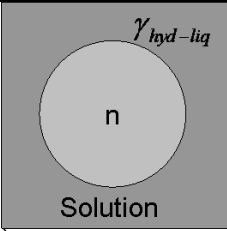
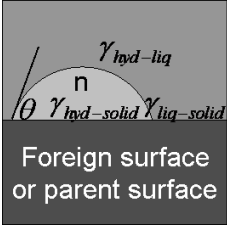
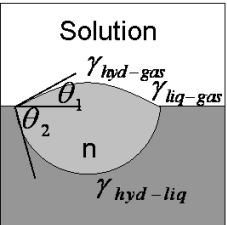
The presence of an interface results in a decrease of the critical Gibbs energy. This decrease can be quantified under the form of a factor  $\psi$  between 0 and 1 (Eqs. 45 and 48).

$$\Delta G_{\text{heterogeneous}}^* = \psi \Delta G_{\text{homogeneous}}^* \quad (43)$$

$\Delta G_{\text{homogeneous}}^*$  is given in Eq. (40).

In the case of a nucleation on a solid surface (Table 29 case b) with a formation of a cap-shaped cluster, the shape of the value of  $\psi$  is given on Figure 25 as a function of the contact angle.

**Table 29:** Nucleation of cluster of n building units, in homogeneous condition (a), at the surface of foreign surface or parent surface (b), at a gas/liquid interface (c).  $\psi$  is a factor between 0 and 1 to quantify the decrease in the critical Gibbs Energy.  $\gamma$  is the interfacial energy between the phases, *hyd*=hydrate phase, *liq*=liq solution, *gas*=gas, *solid*=foreign or parent phase (Kashchiev and Firoozabadi, 2002a, 2002b).

 <p>(a)</p>	
 <p>(b)</p>	$\cos \theta = \frac{\gamma_{liq-solid} - \gamma_{hyd-solid}}{\gamma_{hyd-liq}} \quad (44)$ <p>Young equation Eq.(44)</p> $4\psi = (2 + \cos \theta)(1 - \cos \theta)^2 \quad (45)$
 <p>(c)</p>	$\cos \theta_1 = \frac{\gamma_{liq-gas}^2 + \gamma_{hyd-liq}^2 - \gamma_{hyd-gas}^2}{2\gamma_{liq-gas}\gamma_{hyd-liq}} \quad (46)$ $\cos \theta_2 = \frac{\gamma_{liq-gas}^2 - \gamma_{hyd-liq}^2 + \gamma_{hyd-gas}^2}{2\gamma_{liq-gas}\gamma_{hyd-gas}} \quad (47)$ $4\psi = (2 + \cos \theta_2)(1 - \cos \theta_2)^2 + (2 + \cos \theta_1)(1 - \cos \theta_1)^2 \times (\sin \theta_1 / \sin \theta_2)^3 \quad (48)$

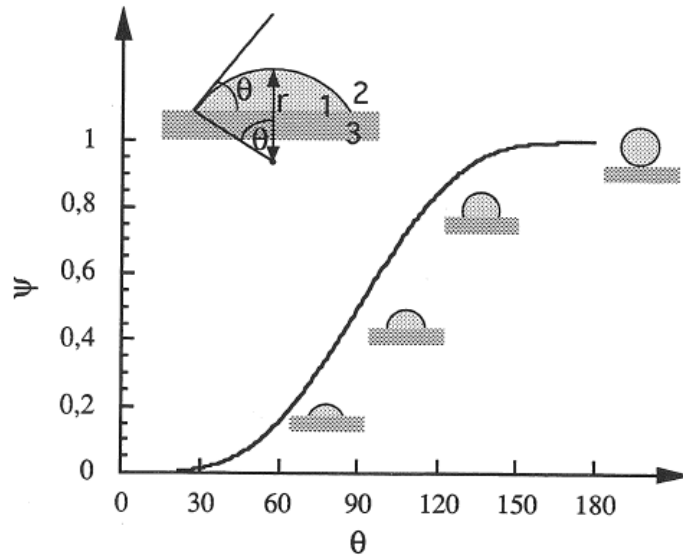


**Figure 25:** The factor  $\psi$  versus angle according to Eq. (45)

If the formulation of (Volmer and Weber, 1926a) has the advantage of simplicity and can depict many experimental facts such the induction time and it is based on a simplified assumption. It considers that primary nucleation is the event which transforms instantaneously of volume of solution from a state (here the liquid with supersaturated gas) to another state (the hydrate phase). For the specific case of gas hydrates, a rigorous approach of primary nucleation from Volmer and Weber theory has been proposed by (Kashchiev and Firoozabadi, 2003).

#### 5.4.2 PRIMARY NUCLEATION FROM A RIGOROUS KINETIC APPROACH

The modelling of primary nucleation can be considered from another point of view. It is possible to consider that nucleation is a continuous process, similar to agglomeration or polymerisation, during which the nuclei are growing step by step to reach a stable size (Becker and Döring, 1935; Cournil and Gohar, 1989; Dunning, 1955; Farkas, 1927; Kashchiev, 1984; Katz and Spaepen, 1978; Katz and Wiedersich, 1977; Zettlemoyer, 1969).

The nucleation is observed as a significant flow of new particles can be detected. The existence of clusters of molecules has been proven experimentally in gas. But the presence of such clusters in liquid solutions is remained a postulate for years. The more advanced works have been developed in the team of (Myerson and Lo, 1990) and also (Mohan et al., 2000). Today, the existence of clusters in supersaturated solutions or in non saturated solutions has showed evidences: new Raman frequencies appearing in supersaturated solution, concentration gradients in

stagnant zones induced by the differential sedimentation of clusters, drop of the diffusion constant in electrolytes or non electrolytes solutions.

The size of the clusters has been measured to be 2, 50 and 100 elementary units respectively in Glycine solution, potassium sulphate solution and citric acid solution.

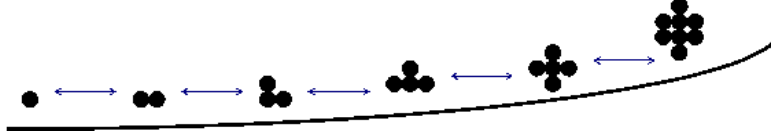
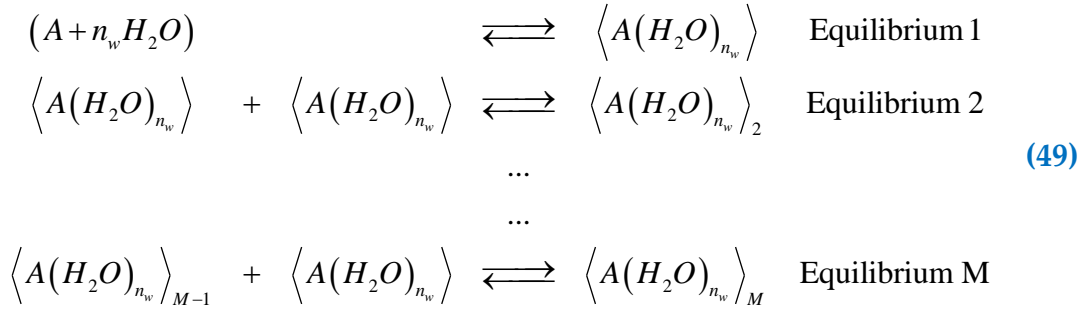
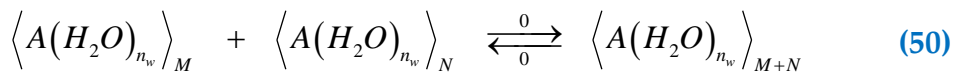


**Figure 26:** Association of clusters



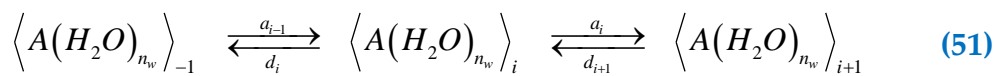
This approach needs to be completed with three remarks

- 1) The agglomeration between clusters is supposed to be low enough to be neglected,



The opposite reaction of dissociation of a cluster into two clusters is also supposed to be negligible.

- 2) The notion of nucleation rate is defined as a reaction. The nucleation is a succession of condensations with individual rates:



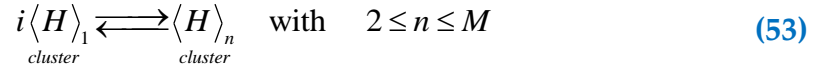
The system is completely defined if the constants of condensation ( $a_i$ ) and dissociation ( $d_i$ ) are defined. The condensation constants ( $a_i$ ) can be determined from simple kinetic consideration (Farkas, 1927). Unfortunately, there is no model available to evaluation the constant of dissociation ( $a_i$ ). The problem can be partially solved by introducing a stationary reference state:

$$0 = J_{i-1} - J_i \quad (52)$$

$J_i$  is the number of cluster of  $i$  unities which condensate (per unit of time and volume) to form a cluster of  $(i+1)$  unities. Equation Eq. (52) implies that the concentration of clusters is constant. (Kashchiev, 1984) showed that the establishment of this stationary regime is very rapid.

3) The nucleation rate allows defining a nucleation time. It corresponds to the duration for the biggest clusters of size  $M$  to reach a size and a concentration that could be detected by the operator.

Each cluster is supposed to be at thermodynamic equilibrium. In the following equation, the elementary cluster unit  $\langle A(H_2O)_{n_w} \rangle$  is renamed as  $\langle H \rangle$ .



$$\mu_{\langle H \rangle_i} = \frac{n}{N_{Av}} \cdot \mu_{(H)} \quad (54)$$

$$\frac{x_{\langle H \rangle_n, bulk}}{\left( x_{\langle H \rangle_1, bulk} \right)^{n/N_{Av}}} = K_n \quad (55)$$

$K_i$  is a constant of equilibrium:

$$K_n = \exp \frac{-\Delta G_n^{cluster \text{ to } cluster, 0}}{RT} \quad (56)$$

The expression of  $\Delta G_n^{cluster\ to\ cluster,0}$  is decomposed in a volume contribution and a surface contribution.

$$\Delta G_n^{cluster\ to\ cluster} = \frac{n}{N_{Av}} \Delta \mu^0 + S_n \gamma \quad (57)$$

$\Delta \mu^0$  is the variation of chemical potential to transform a monomer at the liquid state to a monomer at the cluster state, following Equilibrium 1 in Eq. (49). is the volume contribution to  $\Delta G_n^{cluster\ to\ cluster}$  and corresponds to the transformation of  $n$  monomers at the liquid state to an agglomerate of  $n$  associated monomers at the cluster state.

Following Eq. (30), it can be write

$$0 = \Delta \mu^0 - RT \ln x_{(H)} \quad (58)$$

And from Eq. (35)

$$\Delta G_n^{cluster\ to\ cluster} = n \frac{RT}{N_{Av}} \ln x_{(H)} + \gamma \left( 36\pi n_w^2 v_{(w)}^2 \frac{1}{N_{Av}^2} \right)^{\frac{1}{3}} n^{\frac{2}{3}} \quad (59)$$

From Eq. (59), Eq. (55) and Eq. (56), we obtain

$$\frac{x_{\langle H \rangle_n, bulk}}{(x_{\langle H \rangle_1, bulk})^{n/N_{Av}}} = \frac{1}{x_{(H)}^{n/N_{Av}}} \exp \left[ \frac{\gamma}{RT} \left( 36\pi n_w^2 v_{(w)}^2 \frac{1}{N_{Av}^2} \right)^{\frac{1}{3}} n^{\frac{2}{3}} \right] \quad (60)$$

$$x_{\langle H \rangle_n, bulk} = S^{n/N_{Av}} \exp \left[ \frac{\gamma}{RT} \left( 36\pi n_w^2 v_{(w)}^2 \right)^{\frac{1}{3}} (n/N_{Av})^{\frac{2}{3}} \right] \quad (61)$$

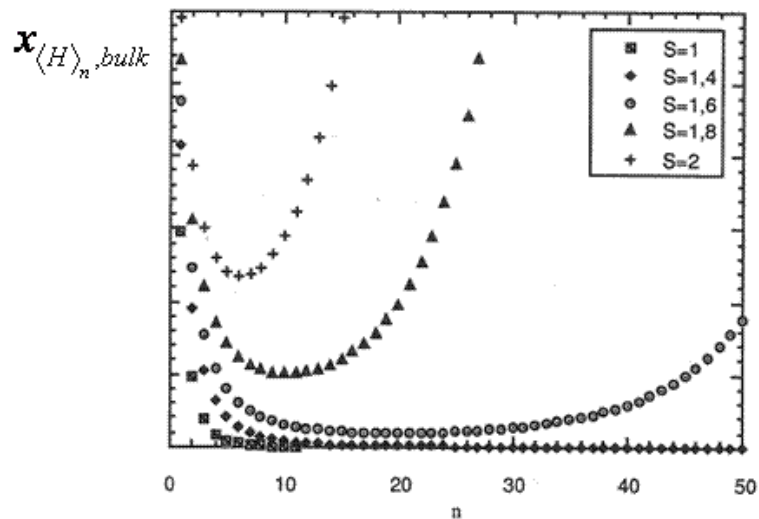


**Figure 27:** Molar fraction of clusters at equilibrium. The index  $n$  refers to the number of elementary units of the cluster.  $S$  is the value of the supersaturation

The [Figure 27](#) shows the shape of the concentration profiles (here the molar fraction) of the cluster in the supersaturated solution:

- For the unsaturated solution, up to a supersaturation of 1, the concentration profile is continuously decreasing,
- For the supersaturation above the value of 1, the concentration profile is firstly decreasing down to a plateau, and then increasing. The value of the concentration at the plateau increases as the supersaturation increases. It depicts the fact that the concentration of clusters increases as the supersaturation is increased.

#### 5.4.3 PRIMARY NUCLEATION FOR CHEMICAL ENGINEERS

It needs to be said the modelling of nucleation remains incomplete in respect to many facts: 1) the extrapolation of macroscopic thermodynamic to small clusters encounters a limit in the definition of the elementary energetic constants such as specific energetic surface, 2) it is difficult to observe experimentally the nucleation in respect to the small size of nuclei, 3) the nucleation is generally stochastic.

So, it is useful to express the primary nucleation in a simplified analytical form, taking into account the driving force directly, ([Cournil and Herri, 2003](#)) (Eq. [62](#)) or indirectly from another variable that is also dependent on the driving force, for example the growth rate  $G$ , ([PIC et al., 2000](#)) (Eq. [63](#)):



$$B_I \propto_1 (S-1)^{s_1} \quad (62)$$

$$B_I \propto_1 G^g \quad (63)$$

In such formulations,  $s_1$  and  $g$  are adjustable parameters

#### 5.4.4 SECONDARY NUCLEATION

During the crystallization, after the appearance of the first crystal, new mechanisms of nucleation are introduced in respect to the presence of parent crystals. Nucleation can be observed at level of supersaturation in which primary nucleation is not possible. These new mechanisms of nucleation are qualified as secondary nucleation. (Botsaris, 1975) proposes to distinguish three different cases:

- **Initial breeding:** In industrial crystallization, it is useful to force the nucleation by introducing parent crystals in the supersaturated solution. After introduction, it is observed a sudden and massive nucleation induced by the crystal dusts dispersed in the solution from the parent crystal surface.
- **Catalytic nucleation:** the parent crystal, under growing, can generate some clusters or nuclei at their surface. If they are scarpered from the surface, for example in reason of the local turbulence or chocks in between particles, they constitute sorts of elementary pieces that can reach a stable size more easily. Also, the presence of the parent crystal is a surface on which the primary nucleation can be activated from a catalytic mechanism. The catalytic nucleation is only possible in a supersaturated solution.
- **Attrition:** the reactor in which is operated the crystallisation is a stirred volume, with mechanical chocks in between the particles, or in between the particles and walls or stirrer blades. The particles can be broken into different pieces. If the crystal is broken in pieces of comparable sizes, the process is qualified as fragmentation. If very small particles are generated, the process is qualified as attrition, and can be regarded as a generation of new nuclei.

It is difficult to propose a mechanism for each situation. (Mersmann et al., 1992) proposes to model the secondary nucleation under a general formulation:

$$B_{II} \propto (S-1)^{p_3} S_p^s \omega^w \quad (64)$$

## 5.5. MODELLING THE GROWTH

The classical approach of (van der Waals and Platteeuw, 1959) provides a description of the thermodynamics of equilibrium involving clathrate hydrate phases. In this approach, the encapsulation of gas molecules in the empty cavities is described similarly to the adsorption of molecules on a two dimensional surface. The model assumptions lead to a Langmuir type of equation for describing this “adsorption” of guest species onto the empty lattice sites.

During crystallisation (here in a liquid system), the crystal is assumed to be surrounded by two successive layers: an integration layer and a diffusion layer. The integration layer is the region of volume in which a transition between the solid state and the liquid state occurs. Following the approach of (Svandal et al., 2006), the integration layer can be considered as a solidification layer. It is described by means of the scalar phase field and a composition variable. At the interface between the solid and the integration layer, the scalar phase field assumes the value 1 (solid state). Furthermore, local equilibrium is assumed. The local equilibrium composition is characterised by the set of mole fractions  $x_j$  for all  $j \in S_g$ . Then, in the direction of the second interface, between the integration layer and the diffusion layer, the scalar field varies from 1 (solid state) to 0 (liquid state), and the composition varies from  $x_j$  to  $x_{j,\text{int}}$ . The whole model is described by (Herri and Kwaterski, 2012) and hereafter. In contrast to (Svandal et al., 2006), a model description of the profiles of the scalar phase field or the composition variables is not given in this work. We only assume that they exist and simplify the problem by introducing Eq. (77) which is described below.

The modelling of the diffusion layer is easier, since it is a liquid, though continuous, phase throughout. The composition varies from  $x_{j,\text{int}}$  at the interface between the integration layer and the diffusion layer to  $x_{j,\text{bulk}}$  at the interface between the diffusion layer and the liquid bulk phase. A schematic representation of the different regions surrounding the hydrate phase under formation conditions is given in Figure 28.

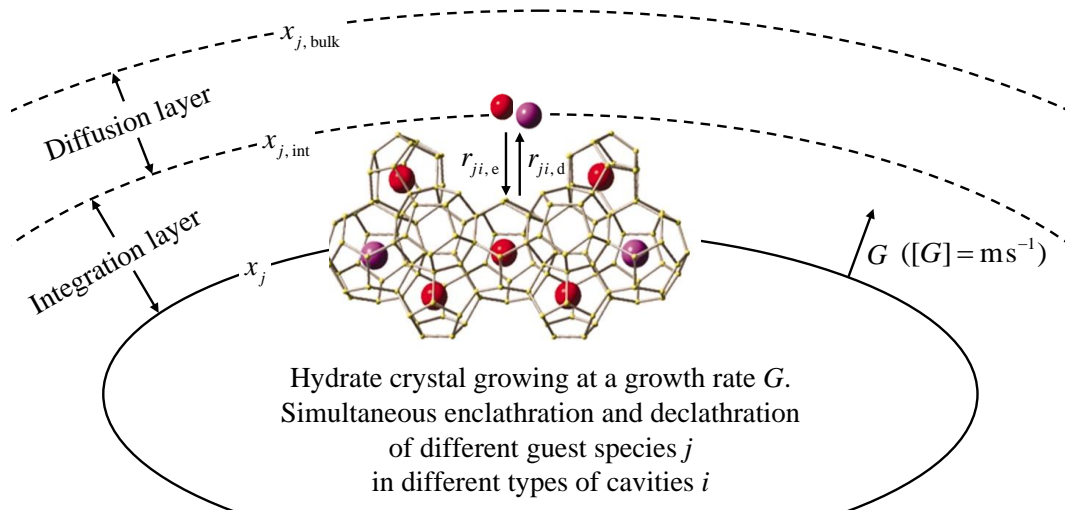


**Figure 28 :** Elementary steps of gas integration in the vicinity of the growing hydrate surface (Herri and Kwaterski, 2012).

In such a system, the different species  $j$  are enclosed by the sites in proportion to their relative affinity. The rate of enclathration,  $r_{ji,e}$ , is directly proportional to the product of the mole fraction  $x_{j,int}$  of  $j$  and the fraction of empty cavities,  $1-\theta_i$ , according to

$$r_{ji,e} = k_{x,ji,e} x_{j,int} (1-\theta_i) \quad (65)$$

where  $k_{x,ji,e}$  is the corresponding kinetic rate constant of enclathration of species  $j$  in a cavity of type  $i$ . The subscript  $x$  at the symbol  $k$  refers to the mole fraction as the particular concentration variable chosen for  $\zeta$ .

The liberation of guest species  $j$  from the cavities of type  $i$  due to the declathration process can be described by the following rate law

$$r_{ji,d} = k_{ji,d} \theta_{ji} \quad (66)$$

In other words, the corresponding molar rate  $r_{ji,d}$  is directly proportional to the occupancy factor  $\theta_{ji}$ , i.e. the fraction of cavities  $i$  which are filled with guest species  $j$ .

As a result, we can define a local flow rate of component  $j$  which results from the unbalance between adsorption and desorption:

$$F_{ji} = r_{ji,e} - r_{ji,d} = k_{x,ji,e} x_{j,int} (1 - \theta_i) - k_{ji,d} \theta_{ji} \quad (67)$$

Eq. (67) can be rewritten as:

$$F_{ji} = r_{ji,e} - r_{ji,d} = k_{ji,d} \left( \frac{k_{x,ji,e}}{k_{ji,d}} x_{j,int} (1 - \theta) - \theta_j \right) \quad (68)$$

### Particular case of equilibrium

At equilibrium,  $F_{ji} = 0$ , and the following relation is derived from Eq. (68), holding for all  $j \in S_g$ , taking into account that  $x_{j,bulk} \equiv x_{j,int} \equiv x_j$ :

$$k_{ji,d} \left( \frac{k_{x,ji,e}}{k_{ji,d}} x_j (1 - \theta) - \theta_j \right) = 0 \quad (69)$$

With the Langmuir constants  $C_{x,ji}$  defined as the ratio between the rate of enclathration and declathration according to:

$$C_{x,ji} = \frac{k_{x,ji,e}}{k_{ji,d}} \quad (70)$$

Eq. (69), can be re-written as:

$$\forall_{i \in S_{cav}} \quad \forall_{j \in S_g} \quad (C_{x,ji} x_j (1 - \theta_i) - \theta_{ji} = 0) \quad (71)$$

Summing up Eq. (71) over all guest species leads to

$$\theta_i = \frac{\sum_{j' \in S_g} C_{x,ji'} x_{j'}}{1 + \sum_{j' \in S_g} C_{x,ji'} x_{j'}} \Leftrightarrow 1 - \theta_i = \frac{1}{1 + \sum_{j' \in S_g} C_{x,ji'} x_{j'}} \quad (72)$$

Finally, by inserting Eq. (71) into Eq. (72), the following relation is derived for  $\theta_{ji}$

$$\theta_{ji} = \frac{C_{x,ji}x_j}{1 + \sum_{j' \in S_g} C_{x,j'i}x_{j'}} \quad (73)$$

### 5.5.1 ENCLATHRATION DURING CRYSTALLISATION

The surface of crystal is supposed to be covered with cavities under formation, which can be regarded as “opened cavities” or active sites. They are assumed to cover the surface and we can define a concentration  $\Gamma_i$  (number of moles of active cavities of type  $i$  per unit of surface area,  $[\Gamma_i] = \text{mol m}^{-2}$ ). Each type of opened cavity  $i$  is exposed to a rate  $F_{ji}$  (mole of component  $j$ /mole of cavity of type  $i$ /unit of time). During the growth of the crystals, the rate by which the gas molecules  $j$  (mole per unit of time) are incorporated into the cavities of the newly created volume is given by:

$$F_{ji}\Gamma_i A_s \quad (74)$$

Where  $A_s$  denotes the total surface area of the growing crystals. The crystal is assumed to grow at a rate  $G$  ( $[G] = \text{m s}^{-1}$ ). The increase in volume of the quantity of solid newly formed per element of time  $dt$  is given by

$$\frac{dV}{dt} = GA_s \quad (75)$$

The volume of the newly formed solid is composed of water molecules which build a network of cavities of different types  $i$ . Their molar volumetric concentration is  $c_i$  (moles of cavity of type  $i$  per unit of volume) and they are occupied by gas molecules of type  $j$ . The occupancy is given by  $\theta_{ji}$  (mole of component  $j$ /mole of cavity  $i$ ). The flow rate by which the gas molecules  $j$  (mole per unit of time) are incorporated in the cavities of the new volume is:

$$c_i \theta_{ji} \frac{dV}{dt} = c_i \theta_{ji} GA_s \quad (76)$$

From Eq. (74) and Eq. (76), it follows for all  $i \in S_{\text{cav}}$  and all  $j \in S_g$  that

$$\Gamma_i F_{ji} = c_i \theta_{ji} G \quad (77)$$

Summing up Eq.(77) over all  $j \in S_g$  leads to

$$\Gamma_i F_i = c_i \theta_i G \quad (78)$$

A general consideration to be taken into account is the following relationship that for each cavity  $i$ , but for two different molecular adsorbents  $j$  and  $j'$ , is obtained from Eq. (77):

$$\forall_{j \in S_g} \forall_{j' \in S_g} \forall_{i \in S_{cav}} \left( \frac{F_{ji}}{F_{j'i}} = \frac{\theta_{ji}}{\theta_{j'i}} \Leftrightarrow \frac{F_{j'i}}{\theta_{j'i}} = \frac{F_{ji}}{\theta_{ji}} \right) \quad (79)$$

From Eq. (79) it follows that a characteristic constant  $a_i$  can be defined according to:

$$\forall_{j \in S_g} \forall_{i \in S_{cav}} \left( a_i = \frac{F_{ji}}{\theta_{ji}} \right) \quad (80)$$

After summation over all guest species  $j$ , the total flow rate  $F_i$  of guest molecules arriving at the cavity  $i$  under construction is

$$F_i = \sum_{j \in S_g} F_{ji} = \sum_{j \in S_g} a_i \theta_{ji} = a_i \sum_{j \in S_g} \theta_{ji} = a_i \theta_i \Leftrightarrow a_i = \frac{F_i}{\theta_i} \quad (81)$$

Thus, with Eq. (78) it can be found from Eq. (81) that for all  $i \in S_{cav}$

$$a_i = \frac{c_i}{\Gamma_i} G \quad (82)$$

During crystallisation, the cavities of the crystals under formation can encapsulate components in consideration of the unbalance between the declathration and enclathration rate. Therefore, from Eq. (68) and (70), the overall rate  $F_{ji}$  by which molecules of type  $j$  are accumulated in the cavities of type  $i$  is given by

$$F_{ji} = r_{ji,e} - r_{ji,d} = k_{ji,d} (C_{x,ji} x_{j,int} (1 - \theta_i) - \theta_{ji}) \geq 0 \quad (83)$$

However, once it has been formed and because it has been formed, the hydrate can be considered being in equilibrium with the integration layer at composition  $x_j$ . For this phase, all of the conditions characterising a state of equilibrium and especially:

$$\theta_{ji} = C_{x,ji} x_j (1 - \theta_i) \quad (84)$$

are assumed to hold. Therefore, upon substituting the right hand side of Eq. (84) for  $\theta_{ji}$  in Eq. (83) one arrives at

$$F_{ji} = r_{ji,e} - r_{ji,d} = k_{ji,d} C_{x,ji} (x_{j,int} - x_j) (1 - \theta_i) \quad (85)$$

Another way to describe the problem is to start again from Eq. (83) and to write it in the form

$$\frac{F_{ji}}{k_{ji,d}} = C_{x,ji} x_{j,int} (1 - \theta_i) - \theta_{ji} \quad (86)$$

Combining Eq. (86) with

$$\theta_{ji} = \frac{F_{ji}}{a_i} \quad (87)$$

leads to the following identity

$$\left( \frac{1}{k_{ji,d}} + \frac{1}{a_i} \right) F_{ji} = C_{x,ji} x_{j,int} (1 - \theta_i) \Leftrightarrow F_{ji} = \frac{C_{x,ji} x_{j,int} (1 - \theta_i)}{1/k_{ji,d} + 1/a_i} \quad (88)$$

being valid for all  $j \in S_g$  and  $i \in S_{cav}$ . The equality of Eq. (85) and Eq. (88) reads

$$\frac{C_{x,ji}x_{j,int}}{1/k_{ji,d} + 1/a_i} = k_{ji,d}C_{x,ji}(x_{j,int} - x_j) \quad (89)$$

which is equivalent to

$$x_{j,int} - x_j = \frac{x_{j,int}}{1 + k_{ji,d}/a_i} \quad (90)$$

Eq. (90) has a strong consequence. The left member of the equality in Eq. (90) is a driving force, expressed here by a difference of the mole fraction of the species to be integrated in the structure under growing. This driving force is the same for any cavities. It means that the right member of the equality in Eq. (90) is also independent of the cavity. It can be stated more specifically that the ratio  $k_{ji,d}/a_i$  is independent of the nature of the cavity. Upon expressing  $a_i$  by means of Eq. (82) in terms of  $c_i$ ,  $\Gamma_i$  and  $G$ , the ratio  $k_{ji,d}/a_i$  is given by

$$\frac{k_{ji,d}}{a_i} = \frac{k_{ji,d}\Gamma_i}{Gc_i} \quad (91)$$

The independence of  $k_{ji,d}/a_i$  of the nature of the cavity  $i$  gives rise to the definition of a kinetic constant  $k_j$ , which is to be regarded as an intrinsic kinetic constant of component  $j$

$$k_j = k_{ji,d} \frac{\Gamma_i}{c_i} \quad (92)$$

By expressing  $k_{ji,d}/a_i$  in Eq. (90) by means of Eq. (91) and (92) in terms of  $k_j$  and  $G$  and solving for  $x_j$ , the following relationship is obtained

$$x_j = x_{j,int} \frac{k_j/G}{1 + k_j/G} \quad (93)$$



It summarises the relations that allow for the calculation of the hydrate composition as a function of the composition of the liquid phase in the vicinity of the growing hydrate crystal. The expressions are dependent on the composition  $x_{j,\text{int}}$  at the interface between the integration layer and the diffusion layer.

To composition can be evaluated from a mass balance in Eq. (94) giving the equality between the integration rate due to the Langmuir type of enclathration (left-hand-side), and the gas diffusion around (right-hand-side):

$$\forall_{j \in S_g} \left( GA_s \sum_{i \in S_{\text{cav}}} c_i \theta_{ji} = d_j^* A_s (x_{j,\text{bulk}} - x_{j,\text{int}}) \frac{\rho_w^\circ}{M_w} \right) \quad (94)$$

Where  $x_{j,\text{bulk}}$  is the mole fraction of  $j$  in the bulk phase, and  $d_j^*$  ( $[d_j^*] = \text{ms}^{-1}$ ) the mass transfer coefficient of the guest species  $j$  around the crystal, respectively.  $\rho_w^\circ$  and  $M_w$ , respectively, stands for the density ( $[\rho_w^\circ] = \text{kg m}^{-3}$ ) and the molar mass ( $[M_w] = \text{g mol}^{-1}$ ) of the solvent (water), respectively.  $d_i^*$  can be estimated from a classical correlation between the dimensionless Reynolds, Sherwood and Schmidt numbers of/around the crystal particle (index “p”),  $\text{Re}_p$ ,  $\text{Sh}_p$  and  $\text{Sc}$ , as for example by the one of (Armenante and Kirwan, 1989) which can be retained

$$\text{Sh}_p = 2 + 0.52 \text{Re}_p^{0.52} \text{Sc}^{1/3} \quad (95)$$

$$\text{Sh}_p = \frac{d_j^* l}{D_j}, \text{Re}_p = \frac{l^{4/3} \varepsilon^{1/3}}{\nu}, \text{Sc} = \frac{\nu}{D_j} \quad (96)$$

In the equations compiled in Eq. (96),  $l$  is the diameter of the crystals under growing and  $\nu$  the kinematic viscosity of the liquid phase, approximated by the kinematic viscosity of the pure solvent, i.e. water.  $D_j$  ( $[D_j] = \text{m}^2 \text{s}^{-1}$ ) denotes the diffusivity of the gas in the solvent. It can be extrapolated from the value at a given temperature by using the correlation of (Wilke and Chang, 1955) in which  $D_j \eta / T = \text{const}$ .  $\eta$  is the dynamic viscosity at temperature  $T$ ,  $\varepsilon$  stands for the energy dissipation rate per unit mass of the fluid, here water. For the case of a stirred reactor equipped with a four blades impeller, the following relationship for  $\varepsilon$  is provided by (Baldi et al., 1978).

$$\varepsilon = \frac{(\text{stirring rate})^5 (\text{impeller diameter})^3}{\text{liquid volume}} \quad (97)$$

**Table 30:** Occupancy factor of enclathrated molecules as a function of the composition in the liquid phase. The equations of the right-hand column are obtained from the classical Langmuir expressions from Eq. (73) (left column) upon replacing  $x_j$  by the expression of Eq. (93) (right column).

	Thermodynamic equilibrium <sup>a</sup>	Local equilibrium resulting from a kinetic equilibrium <sup>a</sup>
$\theta_{ji}$	$\frac{C_{x,ji}x_j}{1 + \sum_{j' \in S_g} C_{x,j'i}x_{j'}}$	$\frac{K_j C_{x,ji}x_{j,int}/(1+k_j/G)}{1 + \sum_{j' \in S_g} K_{j'} C_{x,j'i}x_{j',int}/(1+k_{j'}/G)}$
$\theta_i$	$\frac{\sum_{j \in S_g} C_{x,ji}x_j}{1 + \sum_{j' \in S_g} C_{x,j'i}x_{j'}}$	$x_j = x_{j,int} \frac{\frac{k_j}{G}}{1 + \frac{k_j}{G}} \frac{\sum_{j \in S_g} K_j C_{x,ji}x_{j,int}/(1+k_j/G)}{1 + \sum_{j' \in S_g} K_{j'} C_{x,j'i}x_{j',int}/(1+k_{j'}/G)}$
$1-\theta_i$	$\frac{1}{1 + \sum_{j \in S_g} C_{x,ji}x_j}$	$\frac{1}{1 + \sum_{j \in S_g} K_j C_{x,ji}x_{j,int}/(1+k_j/G)}$

<sup>a</sup> The Langmuir coefficient is usually calculated by using a modified Kihara approach in which the mole fraction  $x_j$  of the guest component  $j$  is replaced by the corresponding fugacity  $f_j$ . Expressing the relation between the Langmuir coefficients  $C_{x,ji}$  and  $C_{f,ji} = C_{ji}$  as  $C_{x,ji}x_j = C_{ji}f_i$ , an approximate relation can be derived for calculating  $C_{x,ji}$  as a function of  $C_{ji}$  by using a simplified version of Henry's law in the form of  $f_j = x_j k_{H,jw}^\infty \exp(pV_{m,j}^\infty/RT)$ , where liquid phase non-idealities expressed by means of the activity coefficient as well as the pressure dependence of  $V_{m,j}^\infty$ , the partial molar volume of  $j$  at infinite dilution, are neglected. In this relationship  $k_{H,jw}^\infty$  is Henry's constant of the guest species  $j$  in the solvent water at the saturation pressure of the solvent. By proceeding in that way, the approximate relation  $C_{x,ji} = C_{ji} k_{H,jw}^\infty \exp(pV_{m,j}^\infty/RT)$  is obtained.

Thus, once numerical values for  $k_j$  ( $[k_j] = \text{ms}^{-1}$ ) and for  $G$  are assumed, the  $x_{j,int}$  values can be determined as the solution of the system of the  $N$  non-linear equations Eq. (98). This set of equations is obtained by substituting the expressions for  $\theta_{ji}$  of Table 30 into Eq (94).

$$\forall_{j \in S_g} \left( G \sum_{i \in S_{cav}} c_i \frac{K_j C_{x,ji} x_{j,int} / (1 + K_j)}{1 + \sum_{j' \in S_g} K_{j'} C_{x,j'i} x_{j',int} / (1 + K_{j'})} = d_j (x_{j,bulk} - x_{j,int}) \right) \quad (98)$$

with  $d_j = d_j^* \frac{\rho_w^\circ}{M_w}$

Where the quantity  $d_j$  has the dimension of a molar flux and thus  $[d_j] = \text{mol m}^{-2} \text{s}^{-1}$ . The last equation to be taken into account for completely solving the problem is a relation expressing the hydrate stability. The subject of this work is not to describe the physical model inherited from the model of (van der Waals and Platteeuw, 1959). For more details on that issue, see in (Sloan, 1998; Sloan and Koh, 2007). A fruitful reading could also be a previous study (Herri et al., 2011) which has motivated the work presented in here. In fact, it focuses on the inter-dependency of internal parameters (i.e. Kihara parameters versus reference state parameters) and points to the difference between the experimental data from different laboratories.

The fundamental equation expressing the hydrate stability is deduced from statistical thermodynamics. It demonstrates that the hydrates become stable once the cavities are sufficiently filled, without considering the chemical nature of the components.

$$\frac{\Delta \mu_w^{\beta-H}(T, p, \vec{\theta})}{RT} = \sum_{i \in S_{cav}} \nu_i \ln(1 - \theta_i) \quad (99)$$

In Eq. (99),  $R$  is the universal molar gas constant and  $\vec{\theta}$  is the vector of independent occupancy factors. The summation is to be performed over all types of cavities (e.g., the two types of cavities,  $5^{12}$  and  $5^{12}6^2$  in case of a sI hydrate with a stoichiometry of 2 and 6, respectively, as shown in Table 1, counted by the index  $i$ .  $\Delta \mu_w^{\beta-H}$  is the difference of the chemical potential of water in the hydrate phase and the chemical potential of water in an hypothetical empty hydrate lattice, denoted as  $\beta$ . It can be calculated since, at equilibrium, the chemical potential of water in the solid phase and in the liquid phase are equal. The difference between the chemical potential of water in the liquid phase and in the  $\beta$ -phase,  $\Delta \mu_w^{\beta-L}(T, p)$ , is calculated by means of the following relation originating from classical thermodynamics, explained in detail in (Sloan, 1998; Sloan and Koh, 2007).

$$\frac{\Delta\mu_w^{\beta-L}(T, p, \vec{x})}{RT} = \frac{\Delta\mu_w^{\beta-L}(T_0, p_0)}{RT_0} - \int_{T_0}^T \frac{\Delta H_{m,w}^{\beta-L}(T, p_0)}{RT^2} dT + \int_{p_0}^p \frac{\Delta V_{m,w}^{\beta-L}(T, p)}{RT} dp - \ln a_w^L(T, p, \vec{x}) \quad (100)$$

In Eq. (100),  $T_0$  and  $p_0$  are reference values for temperature and pressure, taken to be 273.15 K and 0 MPa, respectively, whereas  $\vec{x}$  denotes the vector of independent mole fractions in the liquid phase indicating the composition dependence of  $\mu_w^{\beta-L}$  and  $a_w^L$ , the latter of which stands for the activity of water in the liquid phase.  $\Delta V_{m,w}^{\beta-L}(T, p)$  denotes the difference in the molar volumes of water in the liquid and the  $\beta$ -phase, respectively. The latter has been measured with high accuracy by (Stackelberg and Müller, 1951). The value of  $\Delta H_{m,w}^{\beta-L}(T, p_0)$  can be expressed as temperature dependent according to (Sloan, 1998; Sloan and Koh, 2007). The last parameter of the equation is  $\Delta\mu_w^{\beta-L}(T_0, p_0)$ . Numerical values published for this parameter show strong variations among different laboratories (Herri et al., 2011). Therefore, it needs to be selected with precaution when being used in calculations of the Langmuir coefficient together with Kihara parameters which are retained on the other hand (Herri et al., 2011). Once  $\mu_w^{\beta-L}$  is calculated, which in equilibrium is equal to  $\Delta\mu_w^{\beta-H}$ , the hydrate composition needs to satisfy the identity given by Eq. (99). Hence, by eliminating  $\theta_i$  from Eq. (99) via the expression presented in Table 30, the growth rate  $G$  fulfils the equation

$$\frac{\Delta\mu_w^{\beta-H}}{RT} = - \sum_{i \in S_{cav}} \nu_i \ln \left( 1 + \sum_{j \in S_g} \frac{K_j C_{x,ji} x_{j,int}}{1 + K_j} \right) \quad (101)$$

Finally, the local equilibrium is defined when the values of  $G$  and  $x_{j,int}$  for all  $j \in S_g$  satisfy Eq. (98) and (101).

The calculation procedure is outlined in more detail in Figure 29. It is a double convergence loop. In the first loop, an iteration is performed on the growth rate in order to satisfy Eq. (101) describing the hydrate stability. From a physical point of view, the  $G$  value is the value at which the structure can grow by incorporation of solute gas to such an amount that is sufficient for stabilising the structure (i.e. the cavities are filled to a sufficient extend). The relative proportion to which the different gas molecules  $j$  are entering the structure is determined in the second convergence loop which is an indirect consequence of the competition between the diffusion rates around the crystals and integration rates in the structure. By this competition the  $x_{j,int}$  values are fixed.

Even for a system containing only a single hydrate forming component  $j \equiv A$ , it can be demonstrated that the hydrate phase does not form at equilibrium. Eq. (99) along with the expressions presented in Table 30, can be written at kinetic

equilibrium, during crystallisation, and yields to Eq. (101), and after mathematical reformulation to Eq. (102). At thermodynamic equilibrium, Eq. (99) leads to Eq.(105)

$$\exp\left(-\frac{\Delta\mu_w^{\beta-H}}{RT}\right)_{\text{crist}} = \prod_{i \in S_{\text{cav}}} \left(1 + \frac{K_j C_{x,ji} x_{j,\text{int}}}{1 + K_j}\right)^{v_i} = \prod_{i \in S_{\text{cav}}} (1 + C_{x,ji} x_j)^{v_i} \quad (102)$$

where the index “crist” indicates that the properties are calculated during crystallisation.  $x_j$  is to be calculated from  $x_{j,\text{int}}$  by means of Eq. (93). At equilibrium, the following relation holds:

$$\exp\left(-\frac{\Delta\mu_w^{\beta-H}}{RT}\right)_{\text{eq}} = \prod_{i \in S_{\text{cav}}} (1 + C_{x,ji} x_{j,\text{eq}})^{v_i} \quad (103)$$

On the other hand Eq. (100) becomes:

$$(\Delta\mu_w^{\beta-L})_{\text{cyst}} - (\Delta\mu_w^{\beta-L})_{\text{eq}} = \Delta V_{\text{m,w}}^{\beta-L}(T)(p - p_{\text{eq}}(T)) - RT \ln \frac{a_w^L(T, p)}{a_w^L(T, p_{\text{eq}}(T))} \quad (104)$$

Eq. (104) shows that in general the difference  $(\Delta\mu_w^{\beta-L})_{\text{cyst}} - (\Delta\mu_w^{\beta-L})_{\text{eq}}$  does not vanish. Since the fundamental equation describing the equilibrium condition is  $\Delta\mu_w^{L-\beta} = \Delta\mu_w^{H-\beta}$ , it follows that  $(\Delta\mu_w^{\beta-H})_{\text{cyst}} - (\Delta\mu_w^{\beta-H})_{\text{eq}}$  is also different from zero, and hence, it is found that

$$\prod_{i \in S_{\text{cav}}} (1 + C_{x,ji} x_j)^{v_i} \neq \prod_{i \in S_{\text{cav}}} (1 + C_{x,ji} x_{j,\text{eq}})^{v_i} \quad (105)$$

$$x_j \neq x_{j,\text{eq}} \quad (106)$$

Even for gas hydrate formed in a system containing a single guest component  $j \equiv A$ , the hydrate which crystallizes from the liquid solution is in kinetic equilibrium with a liquid layer the composition of which ( $x_j$ ) is not identical with the equilibrium composition  $x_{j,\text{eq}}$ .

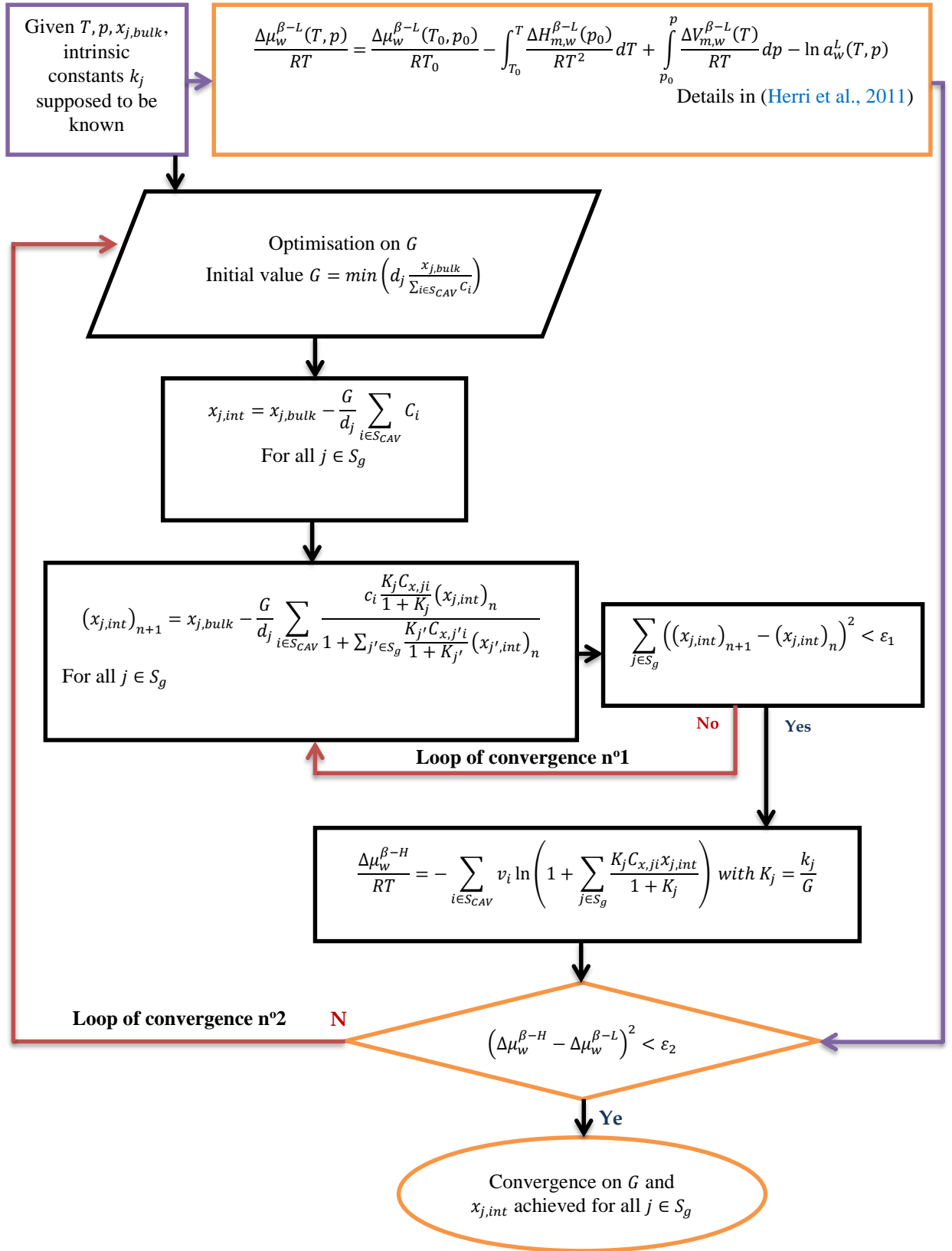


**Figure 29:** Double procedure of convergence to calculate the gas hydrate growing rate  $G$ , and the gas composition  $x_{j,int}$  around the growing hydrate.

### 5.5.2 DISCUSSION

The approach which has been developed here needs to be compared to the pioneering works of (Englezos et al., 1987a, 1987b). In contrast to our model, (Englezos et al., 1987a, 1987b) have postulated that the integration of any of the hydrate forming guest species is independent from the integration of all the other guest species. He assumed a global intrinsic reaction rate  $R$  defined according to:

$$R = \sum_{j \in S_g} K_j^* (f_j - f_{j,eq}) \quad (107)$$

Where

$$\frac{1}{K_j^*} = \frac{1}{k_j^*} + \frac{1}{D_j} \quad (108)$$

with  $K_j^*$  and  $D_j$  being, respectively, the intrinsic kinetic constant and the diffusion constant of component  $j$  around the growing crystals, respectively. The difference  $f_j - f_{j,eq}$  is the driving force, conventionally taken as the difference between the fugacity in the vicinity of the growing crystals and the fugacity of the hydrate at equilibrium. One of the important assumptions of the model of (Englezos et al., 1987b) is that the equilibrium fugacities are calculated independently, although the authors do not give a clear instruction of how they are exactly to be calculated.

For a single gas hydrate, this equation has the advantage to simplify to a popular model in crystallization, known under the acronym of BCF model (from Burton, Cabrera and Frank, 1951) (Burton et al., 1951). In this model, the linear dependence of the growth rate to the driving force corresponds to the growth of a rough surface. It can be further assumed that the overall mechanism of the coupled processes of integration and diffusion exhibits a first order dependence on the fugacity. Moreover, for a single gas, there is no competition between the different components to occupy the cavities up to the adequate filling level which stabilizes the structure physically and chemically.

For gas mixtures, the model of (Englezos et al., 1987a, 1987b) considers that the molar flux of molecules is the sum of independent individual fluxes. However, the model does not describe the local hydrate stability during crystallization as a consequence of the crystallization itself, which instead needs to be assumed independently. Neither the papers of (Englezos et al., 1987a, 1987b) are clear on that point, nor more recent work (Al-Otaibi et al., 2011) that has inherited features from

the model of (Englezos et al., 1987a, 1987b) The authors (Al-Otaibi et al., 2011) state that the hydrate composition is calculated by using a particular software (MEGHA software) without giving a detailed description of the vector of mole fractions of the guest molecules  $\vec{x} = (x_1, \dots, x_{N_g})^T$  which is being used in calculating the occupancy factors of the cavities, as for example in Eq. (72) and (73) with  $\zeta \equiv x$ .

In the approach defended here, the local hydrate stability is coupled with the crystallization itself. The competition between gas molecules, firstly at the diffusion layer scale and secondly at the integration layer scale, is considered as the fundamental rule to describe the growth rate under non-equilibrium conditions. The hydrate stability, i.e., the mole fraction at equilibrium  $x_j$ , becomes intrinsically dependent on the crystallisation mechanisms and kinetic rates. As a result, both the hydrate composition and the growth rate become dependent on the intrinsic kinetic constants (Figure 29).

### 5.5.3 NUMERICAL APPLICATION

(Herri and Kwaterski, 2012) have tested the model against CO<sub>2</sub>-N<sub>2</sub> hydrate. The underlying gas mixture is an example for a mixture as it is typically encountered in the separation of flue gases emitted in combustion processes. CO<sub>2</sub> is highly soluble in comparison to N<sub>2</sub>. The solubilities are calculated by means of a Henry's law approach as described in the monograph of (Sloan, 1998, p. 250), using the parameters of the corresponding correlation equation for CO<sub>2</sub> and N<sub>2</sub> as given in the same literature source on (Sloan, 1998, p. 253). The respective diffusion constants of the two gases in water,  $D_{\text{CO}_2}$  and  $D_{\text{N}_2}$ , at the temperature of 1 °C have been calculated from the correlation of (Wilke and Chang, 1955), using as initial values the corresponding coefficients at ambient temperature,  $D_{\text{CO}_2}(T = 298.15 \text{ K}) = 2.00 \times 10^{-5} \text{ cm}^2 \text{ s}^{-1}$  (Wilke and Chang, 1955) and  $D_{\text{N}_2}(T = 298.15 \text{ K}) = 1.9 \times 10^{-5} \text{ cm}^2 \text{ s}^{-1}$  (Green and Perry, 2007). The crystallization is supposed to be performed in a reactor containing 1 dm<sup>3</sup> of water which is agitated by means of a four blades vertical stirrer of 0.058 m diameter. The temperature is assumed to be set to 1 °C. Under such conditions we have observed (Herri et al., 1999a, 1999b) that methane hydrate particles have a mean diameter in the range of 10 µm (at a stirring rate of 400 rpm) and 24 µm (at a stirring rate of 800 rpm). For the simulation, a stirring rate of 400 rpm and a value of 10 µm for the particle diameter have been retained. Using this set of numerical values for the quantities appearing in Eqs. (95)-(98), the values  $d_{\text{CO}_2}(T = 274.15 \text{ K}) = 47.87 \text{ mol m}^{-2} \text{ s}^{-1}$  and  $d_{\text{N}_2}(T = 274.15 \text{ K}) = 45.73 \text{ mol m}^{-2} \text{ s}^{-1}$  are derived. At this stage, the knowledge of these constants allows for performing the numerical calculations with Eq. (98), corresponding to the first loop of convergence in Figure 29. This loop of convergence expresses the mass balance between the species migrating across the diffusion layer



around the particles due to diffusive transport and the species being incorporated into the particle.

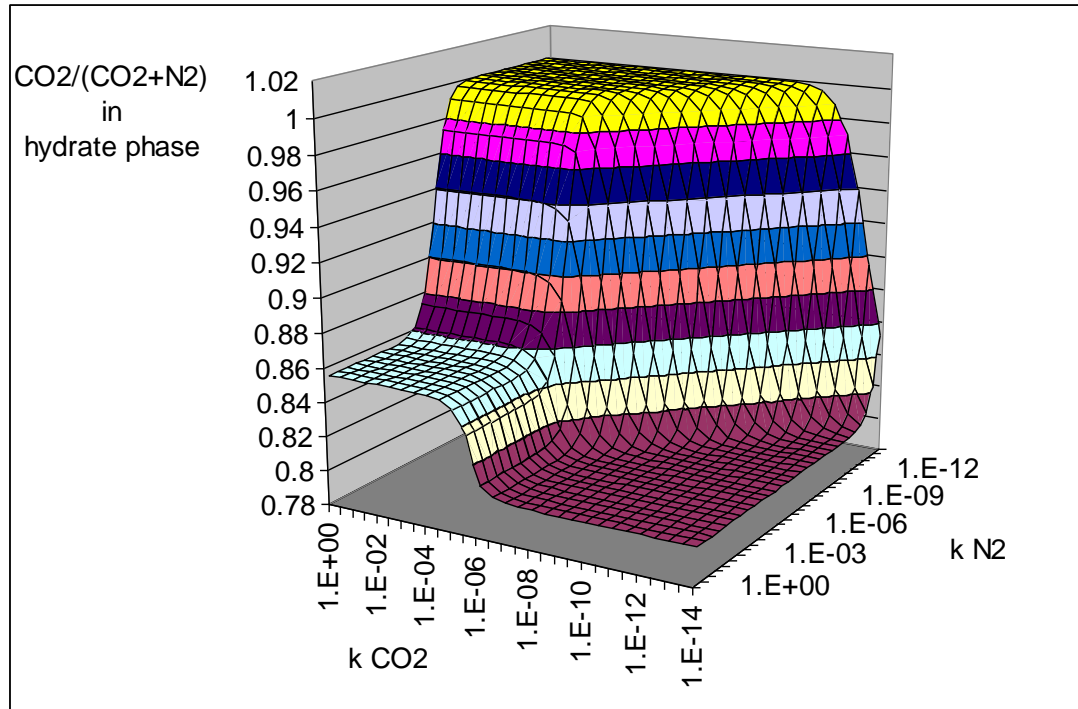
The second loop of convergence imposes the restriction that the hydrate particle is at local equilibrium with its surrounding integration layer. Therefore a thermodynamic calculation needs to be performed in which the equality of the chemical potential of water in the hydrate and the liquid phase, using the expressions given in Eqs. (100) and (101), is verified. The numerical values of the thermodynamic constants are taken from (Herri et al., 2011).

Figure 30 concerns the crystallisation of structure I gas hydrates formed from a liquid solution in equilibrium with a gas phase composed of an equimolar mixture of CO<sub>2</sub>-N<sub>2</sub>. In this example, a temperature of 1°C is assumed. The equilibrium pressure of the mixture is 2.584 MPa. The equilibrium pressure for pure CO<sub>2</sub> hydrate is 1.407 MPa, while pure N<sub>2</sub> hydrate value is 17.438 MPa. That means that a pure CO<sub>2</sub> or pure N<sub>2</sub> gas hydrate can form from the equimolar gas mixture only if the partial pressure is respectively superior to twice 1.407 MPa or twice 17.438 MPa.

The simulation is performed at a pressure of 4 MPa. Figure 30 plots the composition of the hydrate as a function of the kinetic constants  $k_{\text{CO}_2}$  and  $k_{\text{N}_2}$  as defined in Eq.(92). In Figure 31 the growth rate  $G$  is plotted.

At high values of  $k_{\text{N}_2}$  and  $k_{\text{CO}_2}$  the growth rate attains a maximum value of  $0.64 \mu\text{m s}^{-1}$  which remains constant over an extended interval of  $k_{\text{N}_2}$  and  $k_{\text{CO}_2}$  and which is limited by the diffusion around the particles. In such a case, we observe that the composition of the hydrate remains constant, close to a value of 85.5% CO<sub>2</sub>.

Decreasing the kinetic rate of integration of nitrogen or carbon dioxide in the hydrate phase ( $k_{\text{N}_2}$  or  $k_{\text{CO}_2}$ ) is equivalent to decreasing the consumption of one of those molecules. It results in an enrichment of the hydrate in the other gas. At a pressure of 4 MPa and equimolar gas composition, the pure CO<sub>2</sub> hydrate is stable. So, the deactivation of the nitrogen integration results in the formation of a pure CO<sub>2</sub> hydrate. But, at this pressure, the pure nitrogen hydrate is not stable and the deactivation of CO<sub>2</sub> integration can not lead to the formation of a pure N<sub>2</sub> hydrate. At a pressure of 4 MPa, the hydrate containing the lowest relative amount of CO<sub>2</sub> which can be formed contains 80% of CO<sub>2</sub>. The deactivation of CO<sub>2</sub> needs to be compensated on the N<sub>2</sub> side. This is achieved from both a decrease of the diffusion and growth rate, respectively, as a consequence of Eq. (98).



**Figure 30:** Molar composition of the hydrate phase as a function of the intrinsic growth rates. The liquid phase is supposed to be in equilibrium with a gas phase composed of an equimolar  $\text{CO}_2$ - $\text{N}_2$  mixture, at a pressure of 4 MPa and temperature of 1 °C

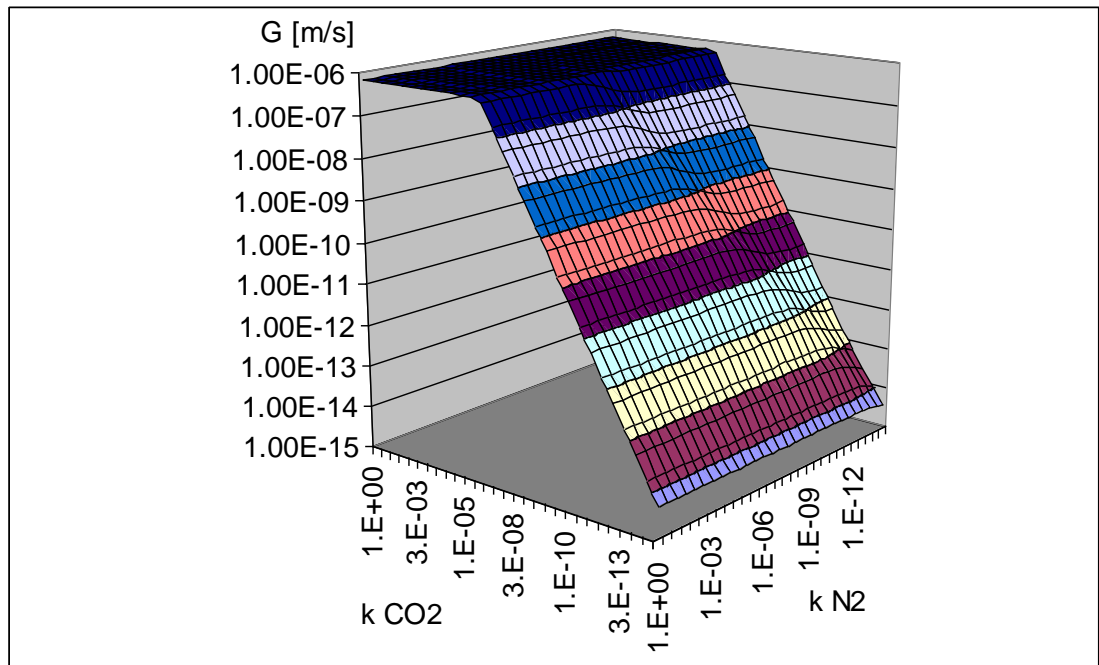


**Figure 31 :** Growth rate of the hydrate phase as a function of the intrinsic growth rate. The liquid phase is assumed to be in equilibrium with a gas phase composed of an equimolar  $\text{CO}_2$ - $\text{N}_2$  mixture at a temperature of 1 °C and a pressure of 4 MPa

## 5.6. CONCLUSION

So, it is clear that both the composition of the hydrate and the growth rate are widely dependent on the values of the intrinsic growth rate constants, except if their values are high. In such a case, the rate of gas consumption at the particle level can be evaluated only from a diffusion limiting rate in the diffusion layer around the hydrate particle. The value becomes only dependent on the diffusion coefficient in water, and the concentrations of the solute species in the bulk. The calculation has been carried out here in consideration of the equilibrium between the gas species being dissolved in the liquid phase at a concentration in with the gas phase following the Henry's law approach described earlier ([Sloan, 1998](#)). In practice, the solute concentration in the bulk, during a crystallization process, is dependent on both the gas consumption rate at the hydrate particle level and the gas diffusion rate at the gas/liquid interface.

## 6. MATERIALS AND METHODS

### 6.1. CHEMICALS

#### 6.1.1 DEIONIZED WATER (H<sub>2</sub>O)

The water used in our experiments is deionized water, it is obtained through a water purifier which is obtained from a purification system “MilliROs3” the range of Millipore® of the society Merck AG. This system is equipped with a cartridge “Milli-Q®-AdvantageA10” which lowers of the conductivity of the water to  $\sigma = 0.055 \mu S cm^{-1}$  and. The total organic carbon content is estimated at less than 5 ppb.



**Figure 32:** The system of Milli-Q®-AdvantageA10 at SPIN center laboratory

#### 6.1.2 HELIUM (He)

Helium is used as a carrier gas for chromatography analyses. It is supplied by Air Liquid B50 bottles, and by Air Product, containing around the value of 9 m<sup>3</sup>. The maximum pressure is 200 bars at 15 °C. It is substantially pure as shown in [Table 31](#).

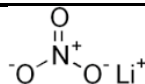

**Table 31:** Purity of Helium gas used in our experiments

Impurities	Helium Bottle (He)
C <sub>2</sub> H <sub>6</sub>	--
C <sub>n</sub> H <sub>m</sub> (n>2)	0.1 ppm
H <sub>2</sub> O	0.5 ppm
O <sub>2</sub>	0.1 ppm
H <sub>2</sub>	0.1 ppm
N <sub>2</sub>	--
CO <sub>2</sub>	0.1 ppm

### 6.1.3 LITHIUM NITRATE (LiNO<sub>3</sub>)

Lithium (see Table 30) is used herein as a liquid tracer. Cation and anion such as Li<sup>+</sup> or NO<sub>3</sub><sup>-</sup> do not fit into the structure of pure clathrate hydrates. We can track the volume of water involved in the formation of hydrates by monitoring the tracer concentration in the water liquid phase. In our study, we used lithium ion as tracer. Lithium is provided in a liquid form (100 ml samples) at mass concentration of 997 ± 5 mg / L. Then it is dissolved in our experiments at a concentration of 10 ppm mass in liquid water. So lithium is present in our solutions at so much small quantities that the physical properties of mixtures cannot be affected very significantly by the presence of this product.

**Table 32 :** The physical properties of Lithium nitrate (LiNO<sub>3</sub>)

Structure formula	
Symbol	 Flame Over Circle GHS03
Chemical formula	LiNO <sub>3</sub>
Density	2.38 g/cm <sup>3</sup>
Molar mass	68.946 g/mol
Melting point	255 °C (491 °F; 528 K)
Boiling point	600 °C (1,112 °F; 873 K) (decomposes)
Solubility in water	52.2 g/100 mL (20 °C)
	90 g/100 mL (28 °C)
	234 g/100 mL (100 °C)

### 6.1.4 GAS MIXTURES (CO<sub>2</sub>, N<sub>2</sub>, CH<sub>4</sub>, C<sub>2</sub>H<sub>6</sub>, C<sub>3</sub>H<sub>8</sub>)

In our experiments, gas compositions are given in Table 33. There are 4 gas mixtures from N<sub>2</sub>/CO<sub>2</sub>/CH<sub>4</sub>/C<sub>2</sub>H<sub>6</sub>/C<sub>3</sub>H<sub>8</sub> components. Gases were provided by Air Liquid and Air Product (CO<sub>2</sub> premium, impurities < 60ppm, nitrogen premium impurities < 6ppm, methane 3.5, ethane 2.5, propane 3.5 and n-butane 3.5). The initial compositions were determined by Gas Chromatography (Figure 35).

To prepare these initial gas mixtures, two methods were applied.

- For binary mixtures (gas 1 to 3), the mixtures were prepared from pure gas bottles directly connected to the reactor. The less volatile gas (CO<sub>2</sub> or C<sub>3</sub>H<sub>8</sub>) was first injected into the reactor. Then, the second one (N<sub>2</sub> or CH<sub>4</sub>) was injected. The mass balance is performed from the monitoring of the pressure after each injection. Gas quantity is calculated from an Equation of State (EoS), here SRK equation.

- The second method was to connect a former prepared bottle. This bottle was prepared by injecting the different gases, from the less volatile to the most volatile, and weighting the bottle after each injection. In order to have a quite homogeneous mixture, the bottle is not used before a few days after the preparation. The maximum pressure is 20% less than the gas mixture dew point to be sure avoiding any condensation.

**Table 33:** Molar composition of the experiments gas mixtures (standard deviation about 3%)

<b>Gas mixtures</b>	<b>CO<sub>2</sub> (%)</b>	<b>N<sub>2</sub> (%)</b>	<b>CH<sub>4</sub> (%)</b>	<b>C<sub>2</sub>H<sub>6</sub> (%)</b>	<b>C<sub>3</sub>H<sub>8</sub> (%)</b>	<b>n-C<sub>4</sub>H<sub>10</sub> (%)</b>
Gas 1	0.821	0.179	--	--	--	--
Gas 2	0.053	--	0.919	0.028	--	--
Gas 3	--	--	0.846	--	0.154	--
Gas 4	--	--	0.950	0.029	0.021	--

## 6.2. EXPERIMENTAL DEVICE

The reactor is a cylindrical glass vessel with diameter and height of 108 mm and 175 mm, respectively. The volume is 2.44L (ACACIA system) or 2.36L (SECOHYA system). The cylindrical glass vessel is filled in our experiments with a liquid water (deionized water plus Lithium) of 800-1100 ml volume, which corresponds to a height of liquid is 87-120 mm. The vessel is enclosed in an autoclave provided with two windows allowing a direct observation. The portholes (12cm x 2cm) allow us to check formation or dissociation of hydrates, but also to observe qualitatively the behavior, and to observe if particles are floating, or sticking at surfaces such as the stirrer. It allowed us to see that the liquid sampler is a free zone without particles.

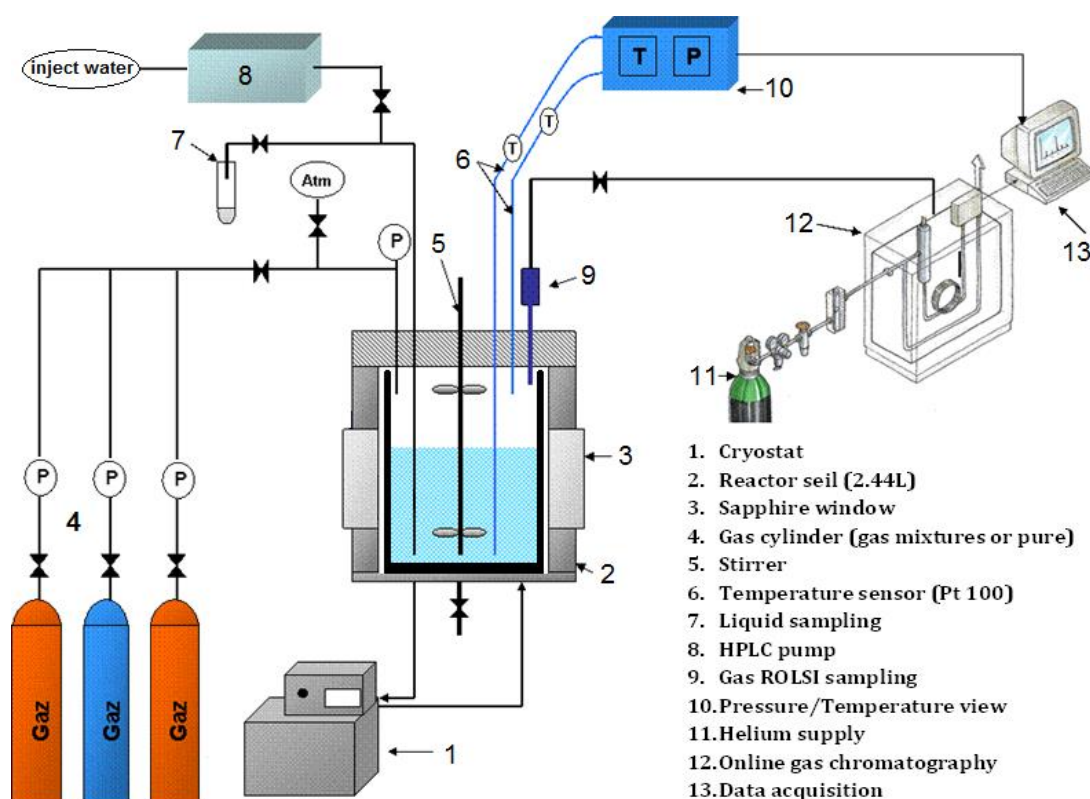


**Figure 33:** Experimental set-up

The autoclave is surrounded by a cooling jacket and cooled or heated by a cryostat (HUBERT CC-505) which temperature control is 0.02°C accuracy. The circulating refrigerant mixture consists in a mixture of water and ethanol (96% vol.) circulating into a cooling jacket. From a practical point of view, to take into account thermal losses, the cooling liquid is controlled at a temperature of 1 to 2 °C lower than the operative temperature inside the reactor.

The stirrer is a two blades impeller of 71.4 mm diameter and 10.2 mm height. It is positioned at a distance of about 25 mm from the bottom of the reactor. The stirrer is magnetically driven from 0 to 600 rpm (rotation per minute). The measurement of the stirring rate is directly done using a portable optical tachometer (Lutron DT-2236).

A JASCO PU-1587 high pressure pump can inject the liquid inside the pressurized reactor, at a rate up to 15 ml/min. The injection of the liquid is performed after the gas input.

The temperature sensor is a Pt100 probe that is immersed in the liquid reaction medium, before crystallization, and in the slurry medium during crystallization. It is linked to a WEST (8010) electronic device which converts the voltage signal into temperature, expressed in degrees Celsius. The pressure is also measured by a pressure sensor in the range 0-10 MPa. The pressure sensor is also connected to a



WEST (8010) device. The accuracy of the sensor is estimated at 0.4% over the entire pressure range. These two acquisition systems are connected to a computer and a program monitoring in LabVIEW language.

A ROLSI® (Rapid On-line Sampler-Injector) manufactured by the Paris School of Mines (Laboratory CEP/TEP) is attached to the top of the autoclave and allows gas sampling (Baba-Ahmed et al., 1999; Guilbot et al., 2000). It consists of a capillary tube of 0.1 mm inner diameter opening on one side in the gaseous headspace of the reactor and on the other side into a chamber through which is circulated the carrier gas to the Gas Chromatography. The side of the capillary connected to the sampler body is sealed by a mobile part whose upper and lower extremities consist of, respectively, a polymer part and a soft iron core, the latter being constrained by a spring. Samples are withdrawn by the action of an electromagnet which attracts the mobile part and opens the seal between the fixed capillary and the mobile part. The pressure inside the cell is higher than that in chromatographic circuit and, therefore, the sample flows through the stem of the sampling valve. After the sampling valve is closed, the sample is taken out by the carrier gas up to gas chromatograph. The amount of the withdrawn sample depends on pressure and temperature conditions and it is directly proportional to the seal opening time. This quantity obviously depends on the conditions of temperature and pressure, but the volume is of the order of 1- 5  $\mu\text{L}$ , which is negligible in comparison to the free volume of the gas that is about 1L. A heating system incorporated into the body of the ROLSI can avoid, if necessary, the condensation of the gas. This sampling system coupled to a chromatograph is a complete in-situ analysis of the gas phase system.

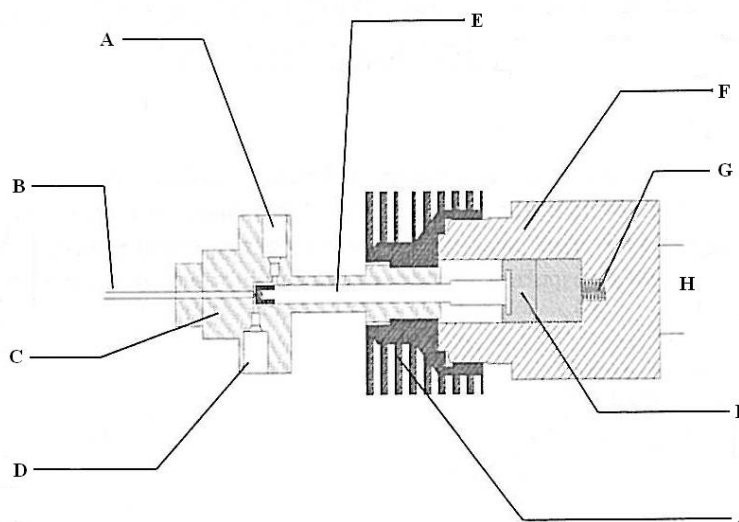


**Figure 34:** Schematic of Electromagnetic version of the ROLSI™ Sampler injector.  
**A:** carrier gas inlet; **B:** capillary; **C:** body; **D:** carrier gas outlet; **E:** moving part set in motion by the electromagnet; **F:** electromagnet; **G:** return spring; **H:** power supply coupled with a timer; **I:** soft iron core; **J:** cooling fins.



The gas samples of gas phase were analyzed by using a VARIAN chromatograph (Model 3800 GC) equipped with a TCD detector in [Figure 35](#). Chromatographic analysis is based on the principle of affinity of a solute between a moving phase (carrier gas) and a stationary phase contained in a thin and long tube. There are two types of columns depending on the nature of the stationary phase therein. We distinguish packed columns and capillary columns. The columns filled are usually made of metal, with a diameter of several millimeters and filled with a porous granule. The capillary columns are empty tubes, usually silica, where the stationary phase is deposited on the inner wall in the form of an as regular as possible film. Their diameter is less than packed columns. The injection of gas samples to the head column is realized through the ROLSI system, and pushed through the column by a carrier gas. They are going to be separated from one to another when passing through of the column according to their affinity with the stationary phase. The time taken to run through the column and reach the detector is the retention time. There are principally two types of detector: TCD (Thermal Conductivity Detector) and FID (Flame Ionization Detector). The principle of the TCD is based on the measurement of the thermal conductivity of the gas mixtures. An acquisition and data processing system is connected to the chromatographic system.



**Figure 35:** Schematic of the VARIAN chromatograph (Model 3800 GC) equipped with a TCD detector.

In our applications a double column system was specifically designed. It is two columns in parallel (PoraBOND Q and a CP-Molsieve 5A columns) for the detection and separation of a wide range of gas. PoraBOND Q is a column filled or packed with an inner diameter of 0.53 mm and a length of 50 m. It is capable of eluting compounds such as alcohols, hydrocarbons (C1-C9), H<sub>2</sub>S, CO<sub>2</sub> and other solvents. Molsieve 5A is a capillary column with an internal diameter of 0.32 mm and a length of 10 m. It is capable of holding permanent gases such as H<sub>2</sub>, N<sub>2</sub>, Neon, Ar, Krypton, O<sub>2</sub>, CH<sub>4</sub>, CO. Methane is retained in the two columns. It can therefore be used to

determine the sample sharing ratio between the two columns. An illustrative diagram of the chromatographic system is proposed in [Figure 45](#). Please note that the injector is the output of ROLSI [Figure 34](#).

The sampling system of the liquid phase consists of a tube 1/16 inch immersed in the liquid and connected to a valve. The position of the tube depends on the density of the hydrates formed. If they are lighter than the liquid, they float and the tube is then positioned toward the bottom of the reactor at a distance approximately equal to 30 mm, that is to say practically the same level as the stirrer blades. We have noticed that gas hydrates such as CO<sub>2</sub> and N<sub>2</sub> hydrates, or hydrates formed from the mixture of these two gases are floating. So it is for CH<sub>4</sub> and C<sub>3</sub>H<sub>8</sub>.

The lithium concentration in the liquid is determined by Ionic Chromatography (IC) in [Figure 36](#). The principle is substantially the same as in the gas chromatography. The fundamental difference is the nature of the mobile and stationary phases. In the case of detection of lithium (Li<sup>+</sup>, a cation), the stationary phase is a polymer with attached anionic groups (sulfonate). The eluent or mobile phase is methane sulfonic acid (HMSA). In our application, we have a DX50 chromatograph equipped with a Dionex Company CS12A column and a TCD detector. The signal obtained at the detector output is processed by a computer.

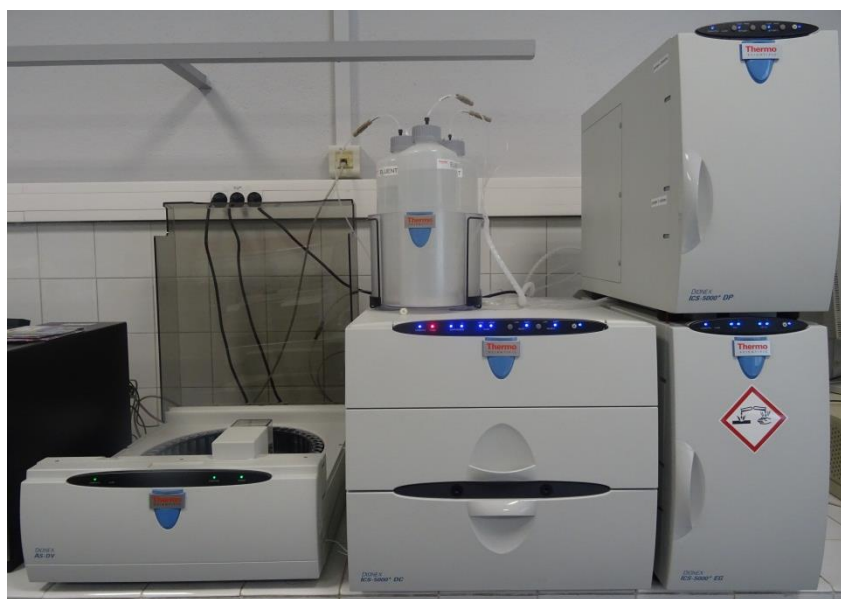


**Figure 36:** The system of the ionic chromatography at SPIN laboratory

## 6.3. EXPERIMENTAL PROCEDURE

### 6.3.1 HIGH CRYSTALLIZATION RATE

The first experimental procedure is the same as in our previous studies on gas hydrates equilibrium (Herri et al., 2011). In this procedure, the crystallization occurs at a “high rate” (or at a high supersaturation). At first, the reactor is cleaned and vacuumed (for 40-50 minutes). Then, the cell is filled with the operative gas composition either by direct injection of the various components, or from a bottle where the mixture has been prepared before.

The pressure is measured, and the temperature is set to 1°C (internal regulation of the cryostat). The gas composition in the cell is checked with GC analysis before any measurement.

A 10 mg/L water mixture of  $\text{LiNO}_3$  is prepared and injected (about 800-1000g) into the reactor thanks to the HPLC pump (n°08 on Figure 33). The water is ultrapure water (first category, 18.2 MΩ.cm). A raise of the pressure, due to the added volume of liquid, is observed. Then, the reactor is stirred at the rate of 450 rpm, on the gas upper side, and on the liquid bottom side. The gas is dissolving into the liquid phase, and after some time (induction time), the crystallization begins. Due to the exothermicity of the reaction, a brief raise of temperature is observed. At this point, we wait for the equilibrium (no more temperature and pressure time evolution). This takes about 2 to 4 days depending on the mixture and initial pressure. As the equilibrium is reached, a sample of the gas phase is taken and injected into the gas chromatograph to determine the molar composition. A liquid sample is also taken to be analyzed offline by ionic chromatography (about 4.5-5.5mg). Then, the dissociation of the hydrate is started. The temperature is increased of about 1-2°C. When the new equilibrium is reached (after 24h), new samples of the fluid phases are taken. Then, the process is repeated until there is no longer a hydrate phase into the reactor. The whole procedure is summarized on Figure 37 and Figure 38.

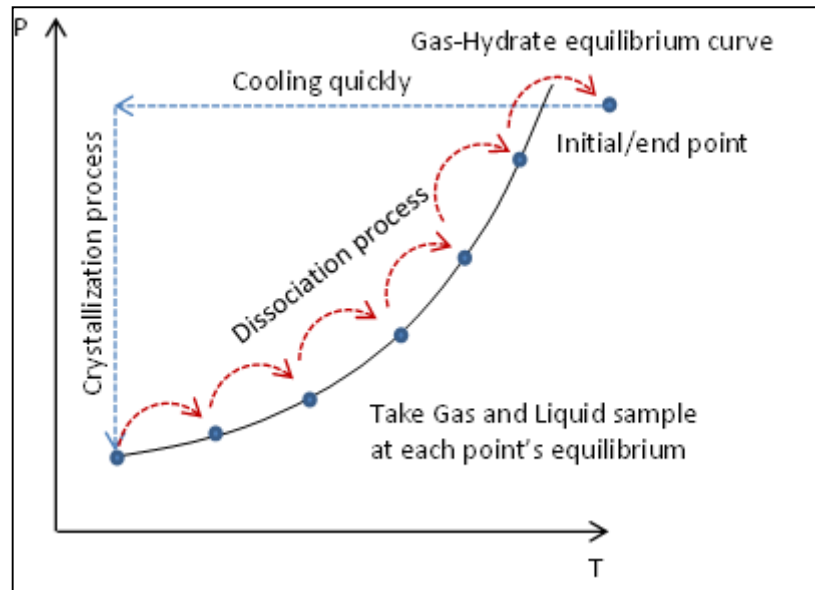


**Figure 37:** The procedure of the high crystallization rate

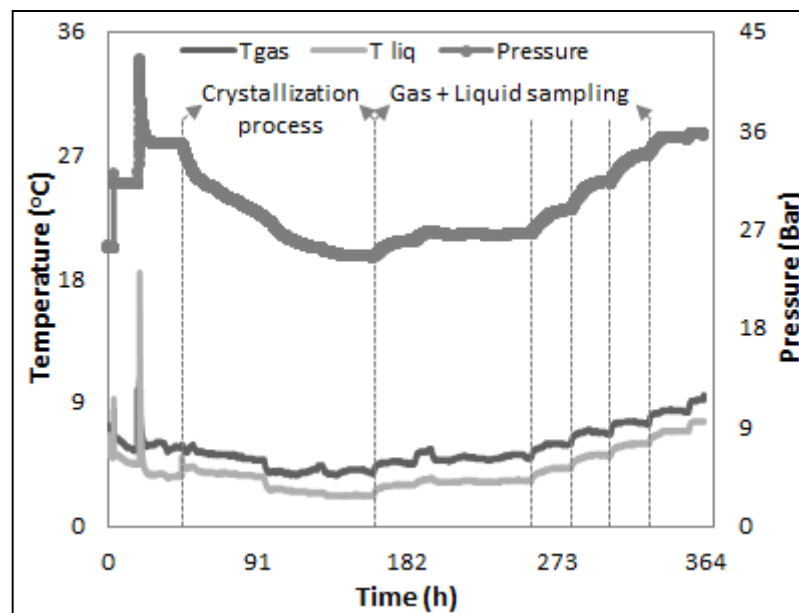


**Figure 38:** P– T evolution during equilibria experiments at high crystallization rate.

### 6.3.2 LOW CRYSTALLIZATION RATE

In this second procedure on [Figure 39](#), the objective is to focus on thermodynamic equilibrium avoiding as much as possible any kinetic effect. The objective is to stay as close as possible to the thermodynamic equilibrium curve, in order to decrease kinetic effects on crystallization.

The pressure/temperature evolution in function of the time is shown on [Figure 40](#). Instead of decreasing very quickly the temperature to the final point (between 0 and 2°C), the crystallization occurs close to the initial point in the hydrate free area. Then, the temperature is decreased very slowly (about 0.1- 0.3 °C per day). Each 1°C step, samples of the gas and liquid phases are taken and analyzed in Gas Chromatograph and Ionic Chromatography, respectively. This procedure concerns only gas mixture n°2, 3 and 4 on [Table 33](#).

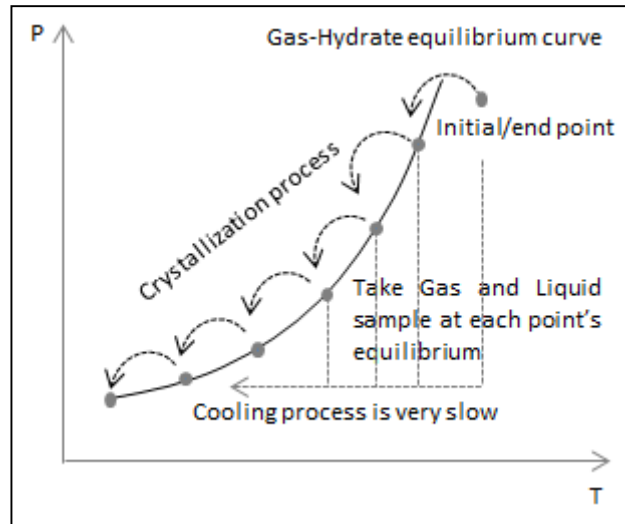


**Figure 39:** The procedure of the low crystallization rate.

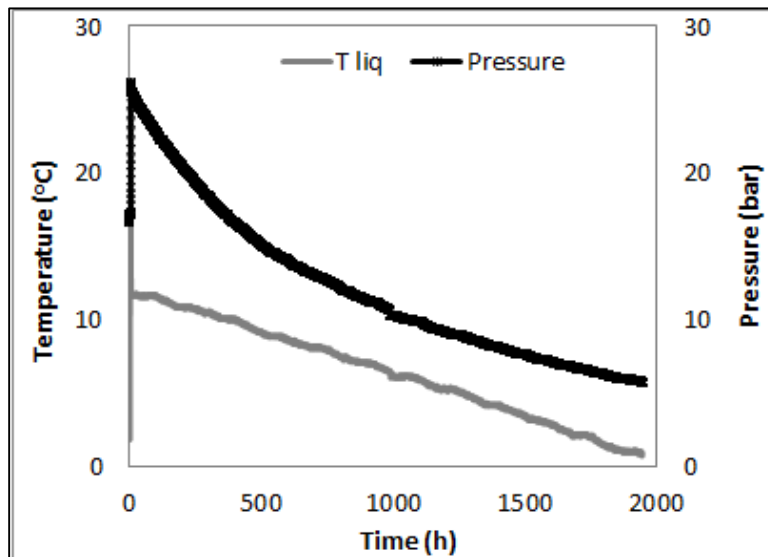


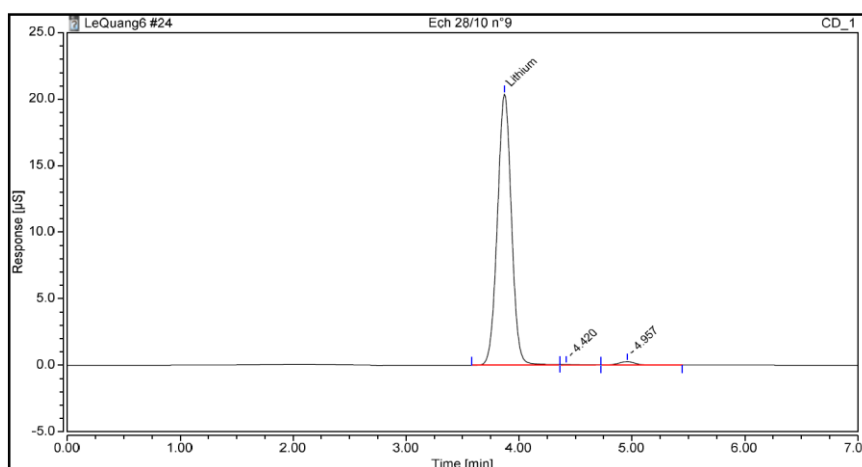
**Figure 40:** P – T evolution during equilibrium experiment at low crystallization rate.

## 6.4. OPERATING PROTOCOLS

### 6.4.1 DETERMINATION OF THE CONCENTRATION OF LITHIUM BY IONIC CHROMATOGRAPHY.

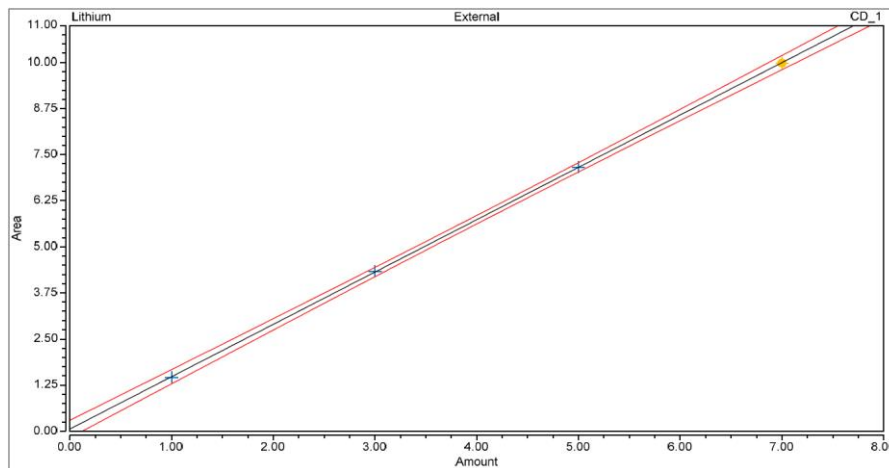
The determination of lithium ion concentration ( $\text{Li}^+$ ) is carried out by Ionic Chromatography in [Figure 36](#). The column was at ambient temperature and the TCD detector is thermostatic. The analysis protocol consists in diluting the sample by a factor in between 2 and 10, with a very high precision micropipette. This dilution is necessary because the sample to be analyzed should be 5 ml minimum whereas the volume recovered is around the value of 2 ml. In fact we need to minimize the sampling volume to avoid distorting the mass balance on the liquid. After dilution, the sample is passed through the chromatographic system, which output gives a chromatogram with peaks. This chromatogram is integrated through a computer that provides the peak areas.

[Figure 41](#) is given an example of a chromatogram of a sample from the reactor. The peak corresponding to  $\text{Li}^+$  ions is at retention time of 3.847 min and shows a good resolution. The peak corresponding to sodium is probably due to some remaining traces from a previous analysis of a solution containing sodium. The peak with a negative intensity corresponds to an artifact of measurement.



**Figure 41:** Chromatogram of a liquid sample - Analysis of Lithium

The establishment of a calibration curve is done at each series of measurements. This is explained by the fact that ambient conditions change, but also the concentration of the mobile phase is not always the same. A conventional calibration method is possible. The principle of this method is to establish a simple relationship between the concentration of  $\text{Li}^+$  and the peak area obtained by injecting standard solutions of known concentrations.



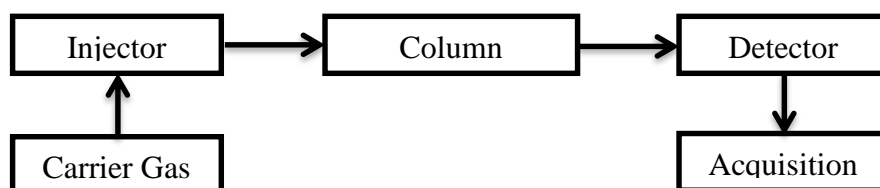
**Figure 42:** Calibration curve of the ionic chromatography

Figure 42 is showed the right chromatograph calibration for a series of measurements. On the abscissa we have  $\text{Li}^+$  ion concentration in ppm and the ordinate the peak area. We can see that the linearity relationship is well respected in the range [0-20 ppm], corresponding to our samples taken from the reactor, or after dilution.

#### 6.4.2 CALIBRATING THE GAS CHROMATOGRAPH (TCD)

A gas chromatograph (GC) is an analytical instrument that measures the content of various components in a sample. The analysis performed by a gas chromatograph is called gas chromatography. The gas chromatograph allows us to know the composition of a gas mixture. Indeed, the area of a peak given by the chromatogram is proportional to the amount of material in the sample.

Based on the laboratory experience and on the existing laboratory equipment the gas chromatography method was selected to perform the analyses. The Gas Chromatograph used is the Varian 3800 GC model on Figure 35. The chromatographic technique allows separating and quantifying the products a sample.



**Figure 43:** GC principle

The separation and the quality of the analysis is a function of the following parameters:

- Choice of the column,
- Temperature/Pressure of the oven column,
- Choice of the carrier gas,
- Flow rate of the carrier gas,
- Parameters of the detectors.

The chosen carrier gas, which has been used for most of the study, is helium (except for a set of test, where the carrier gas was nitrogen). To obtain a maximum sensitivity of the detector (thin peaks) the carrier gas flow rate is adjusted. Helium from Air Liquide (or Air Product) is pure grade with 3 ppm water trace and 0.5 ppm hydrocarbon traces (see at [Table 31](#)). To purify the carrier gas, the gas is cleaned by a molecular sieve, positioned at the outlet of the helium bottle.

Two detectors are used to perform the analyses: a Thermal Conductivity Detector (TCD) and a Flame Ionization Detector (FID), connected in series.

The TCD measures continuously the variation of the thermal conductivity of the carrier gas. The TCD is non-destructive detector. To achieve a good analysis of the samples, the thermal conductivity of each compound must be as different as possible of that of the carrier gas (see [Table 31](#)).

The FID is detector, which measures the compound capabilities to form ions when it goes through the flame. The FID is a destructive detector, thus it is connected in series, at the outlet of the TCD.

The operating conditions of the chromatograph were optimized to shorten the analysis time but also to get a good resolution and separation of peaks. For this we mainly adjusted the oven temperature, the pressure and the carrier gas flow. We must remember that these variables play a first order role in the compound retention time in the column. Oven Temperature, and most important carrier flow, tends to reduce the retention time but in return a less clear separation of certain compounds. A compromise is to find. At an oven temperature of 40°C and a carrier gas flow of 2.7 ml/min, elution of CO<sub>2</sub> is 22 min. This retention time is too much important to follow the crystallization kinetics. We increased the oven temperature to 50°C (up to 180°C) and increased the carrier gas flow between 15 and 50ml/min. the pressure was chosen 23 psi. With these conditions shown in [Table 34](#), we can analyze a sample of gas mixture in less than 7-8 minutes with distinct peaks. The quality of the separation is not affected.



We chose in our analysis to check the reproducibility of results by injecting the same sample twice with an interval of 2 minutes between the first and second injection.

**Table 34 :** Operating conditions of the chromatogram

Injector temperature, °C	200
Detector temperature, °C	220
Filament temperature, °C	270
Oven temperature, °C	50-180
Carrier gas	Helium (He)
Carrier gas pressure, psi	14 or 23
Carrier gas flow rate, ml/min	15-50

In chromatography, for a binary gas mixtures A+B of quantity  $m_T$ , the area of a peak is in general proportional to the amount of injected material  $m_T$ . For a compound (A), peak area (S) that by:

$$S_A = K_A m_A = K_A m_T x_A \quad (109)$$

Where  $x_A$  is the molar fraction of component A and  $m_T$  the mass of all the species. In the classical method of the calibration the proportionality constant  $k_A$  would be determined by injecting a sample even if the amount of A is known. In our sample system, we can not ensure that we take the same amount of gas that the conditions of pressure and temperature change from one experience to another:

$$m_T = \frac{PV}{ZRT} M_T \quad (110)$$

Where  $M_T$  the molar mass of the gas mixtures and Z is the compressibility factor and V is the volume.

We have also chosen to perform relative calibration in using the report of the compositions of a binary gas mixture is analyzed. Finally, the results are independent of initial quantities injected:

$$S_A = k_A n_A = k_A n_T x_A \quad (111)$$

$$\frac{S_A}{S_B} = \frac{k_A}{k_B} \frac{x_A}{x_B} = k \frac{x_A}{x_B} \quad (112)$$

$$S_B = k_B n_B = k_B n_T x_B \quad (113)$$

But, in our experiment, the amount of component cannot be determined after sampling due to the method itself. In fact, the ROLSI instrument is a valve that is opened during a period of time. During this period, the amount of material is proportional to the flow rate, and the flow rate is directly proportional to the pressure. The pressure is not a controlled parameter, but is dependent from equilibrium considerations, or time consideration is the equilibrium is not reached.

The principle of the preparation of the gases is to generate a binary mixture (for example gas A and gas B) with a given mole fraction composition  $x_A$  and  $x_B$  respectively, and to compare the ratio  $(\frac{S_A}{S_B})$  of the surface of the respective chromatograph peak. Once the gas composition is determined, a gas chromatography is performed, and the respective surface areas ratio of gas A and B  $(\frac{S_A}{S_B})$  is measured and correlated to ratio of respective gas composition  $(\frac{x_A}{x_B})$ .

The peak surface area is estimated with an error  $\Delta S/S = 0.05$ .

The result is a calibration curve (Figure 44) which gives estimation of  $(\frac{x_A}{x_B})$  plus or minus 1%.

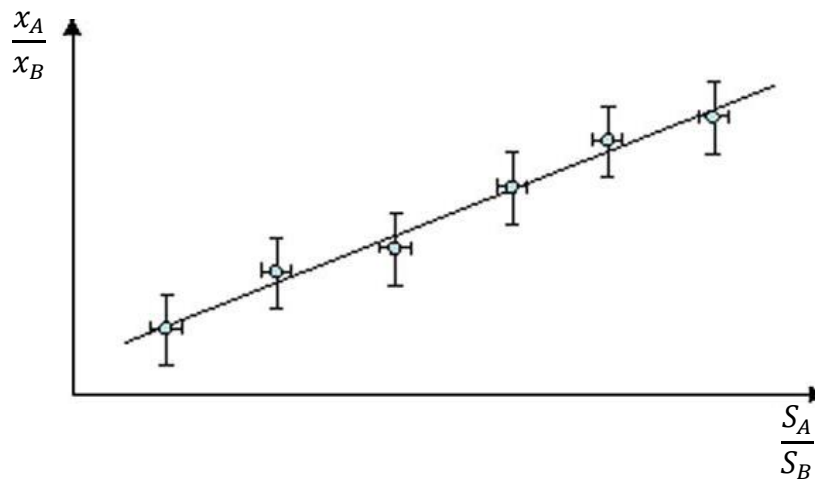


**Figure 44:** Calibration curve of gas chromatograph

For a new sample, the chromatographic analysis allows obtaining the peak areas relative to each compound. To know the composition of the sample, the following system of equations is used.

$$\begin{cases} \frac{x_A}{x_B} = a \frac{S_A}{S_B} + b \\ x_A + x_B = 1 \end{cases} \quad (114)$$

For instances, the calibrations were performed for the A+B gas mixtures. The operating procedure is as follows:

- Initially, the system is emptied by using vacuum pump installed on the circuit is maintained at approximately 279 °K constant temperature by using the cryostat consigned to 278 °K.
- The reactor charged with (A) molecules reaches a certain pressure  $P_1$ . Once the pressure and temperature is stabilized, a gas sampling is performed to verify that the reactor is only filled with gas (A).
- The second gas (B) is subsequently introduced into up to pressure  $P_2$ .
- The gas mixture in the reactor is stirred at  $\sim 400$  rpm. When the pressure and temperature are stabilized in the reactor, the mixture was analyzed by gas chromatography (GC).
- Analysis of the mixture takes place as follows: At first, we purge 10 times the system by pushing the button and opening the Rolsi valve during 0.01s each time. It ensures withdrawing the gas mixtures from the rolsi instrument itself. After waiting 150 seconds, the test sample is injected into the gas chromatograph flow line from a new push on the button to open it during 0.01s. GC analysis takes about 7-9 minutes. Each analysis is done twice to ensure reproducibility of the results. In the end, it takes 20 minutes for a complete analysis.

This calibration can be done from a prepared gas mixture (see section [§6.1.4, Page. 114](#)). In this case, we have to wait a few days for the homogeneity of the gas mixture.

This calibration method compares the areas of the peaks. The different gases used are retained in both the two columns of the chromatograph. Therefore, there is a choice in the peak to exploit. For the three gases, we chose to exploit the second peak, from the Q PoraBOND column that are better than those from the Molsieve 5A column. As an example, [Figure 45](#) shows the peaks for CO<sub>2</sub>-N<sub>2</sub> mixture. Usually, the major molecule is used as reference since it is the peak with the best accuracy (CH<sub>4</sub> as example).

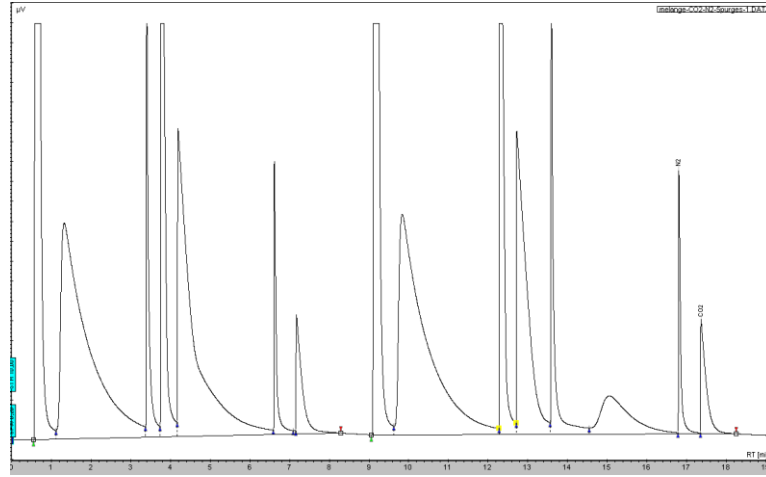


**Figure 45:** Chromatogram of a sample of CO<sub>2</sub>-N<sub>2</sub> mixtures

#### 6.4.3 MASS BALANCE CALCULATION

At any moment, the initial quantity of the gas molecules is distributed between all the phases: gas phase, liquid phase and solid hydrate phase. Thus, in equilibrium, the quantity of gas in the hydrate phase can be determined from a mass balance according to:

$$n_{i,0}^{initial} = n_i^G + n_i^L + n_i^H \quad (115)$$

Where  $n_{i,0}^{initial}$  is the mole number of the gases injected inside reactor, and  $n_i^G, n_i^L, n_i^H$  are the mole numbers of the gaseous component  $i$  ( $i$ : CO<sub>2</sub>, N<sub>2</sub>, hydrocarbon) in the hydrate, the liquid and the gas phase, respectively. We will only consider an aqueous phase for the liquid phase.

The amount of substance of the gases dissolved in the liquid phase is then estimated by means of corresponding gas solubility data into water, whereas the mole number of the gases present in the gas phase is calculated by using an equation of state approach as outlined in the next sections.

- *Calculation of compressibility factor*

The compressibility factor in the gas phase in any equilibrium state can be calculated by means of the classical Eq. (116) combined with a suitable equation of state (EOS), e.g., a classical cubic EOS. For this study, the Soave-Redlich and Kwong (SRK) EOS has been used with parameters from (Danesh, 1998) given in Table 35.

$$Z(T, P, \vec{x}) = \frac{PV}{nRT} \quad (116)$$

with  $n \equiv n^G$  (at each situation) and  $T, P, V$  are the temperature, pressure and phase volume,  $\vec{x} = (x_1, \dots, x_n)$ , represents the vector of the mole fractions of the components in the mixture,  $n$  the total mole number in the gas mixture, and  $R$  the universal gas constant.

**Table 35:** SRK parameters

$j$	$T_c(K)$	$P_c(bar)$	$\omega$	$k(N_2/j)$	$k(CO_2/j)$	$k(CH_4/j)$	$k(C_2H_6/j)$	$k(C_3H_8/j)$	$k(n-C_4H_{10}/j)$
N <sub>2</sub>	126.20	34.00	0.03772	0	-0.03	0.03	0.06	0.09	0.1130
CO <sub>2</sub>	304.21	73.83	0.22362	-0.03	0	0,0933	0,1363	0,1289	0,1430
CH <sub>4</sub>	190.56	45.99	0.01155	0.03	0,0933	0	-0,0078	0,009	0,0056
C <sub>2</sub> H <sub>6</sub>	305.32	48.72	0.09949	0.06	0,1363	-0,0078	0	-0,0022	0,067
C <sub>3</sub> H <sub>8</sub>	369.83	42.48	0.15229	0.09	0,1289	0,009	-0,0022	0	-0,01
<i>n</i> -C <sub>4</sub> H <sub>10</sub>	425.15	37.99	0.2013	0.1130	0,1430	0,0056	0,067	-0,01	0

- *Composition of the gases initial inside reactor*

Before injecting water inside reactor, the mole fraction of each gas in the gas phase  $x_i$  is determined by using gas chromatography analysis.

We recall here that the reactor of total inner volume  $V_R = 2.44L$  (ACACIA system) or  $2.36L$  (SECOHYA system) is initially filled with the gaseous components at the initial temperature  $T_0$  and pressure  $P_0$ .

$$n_0^G = \frac{P_0 V_R}{Z(T, p, y_{j,0}) R T_0} \quad (117)$$

GC analysis provides the gas phase composition only. Each component  $j$  has an initial mole fraction  $x_{ji}$  ( $j$  is CO<sub>2</sub>, N<sub>2</sub>, hydrocarbons). Combined with the measurements of temperature, pressure, and compressibility factor in the gas phase, the initial total mole number in the gas phase  $n_0^G$  is derived from Eq. (117). We also obtain the mole number of each gas

- *Volume of the aqueous phase:*

As mentioned before, the liquid phase contains LiNO<sub>3</sub> as a tracer. Initially the concentration of lithium  $[Li^+]_0$  and the initial volume of liquid  $V_0^L$  are known. During the crystallization and dissociation steps, the concentration of lithium is measured by ion-exchange chromatography after sampling. So, we can calculate the volume of liquid water from a mass balance for the Li<sup>+</sup> ions:

$$V_0^L [\text{Li}^+]_0 = V^L [\text{Li}^+] \Rightarrow V^L = \frac{V_0^L [\text{Li}^+]_0}{[\text{Li}^+]} \quad (118)$$

Where  $V^L$  and  $[\text{Li}^+]$  are the volume of the liquid aqueous phase and the molar concentration of lithium in this phase, *i.e.* in the sample, corresponding to a given step of the crystallization or dissociation.

- *Water mole number in the hydrate phase*

The quantity of water molecules involved in the hydrate structure can be calculated from:

$$n_w^L = \frac{(V_0^L - V^L) \rho_w^\circ}{M_w} \quad (119)$$

$V^L \cong V_w^L$  stands for the volume of the liquid phase in equilibrium,  $\rho_w^\circ$  the liquid water density (about 1kg/L at 4°C), and  $M_w$  is the molar mass of pure water (18g/mole).

- *Mole fraction of the solubility of gases in liquid phase*

The solubility of a gas in a liquid is determined by the equations of phase equilibrium. If a gaseous phase and a liquid phase are at equilibrium, then for any component  $i$  the fugacity in both phases must be the same:

$$f_i^L = f_i^V \quad (120)$$

**The symmetric approach**, called  $\phi\phi$  ( $\phi^v = \phi^L$ ), consists in describing the gas phase and the liquid phase in terms of equations of state (EOS) along with appropriate mixing rules

$$\phi_i^v \gamma_i^v = \phi_i^L x_i^L \quad (121)$$

**The classical or unsymmetrical approach**, called  $\gamma\phi$ , consists of choosing an equation of state (EOS) for the gas phase and a excess model for the liquid phase:

$$\phi_i^v y_i^v P = \gamma_i x_i f_i^{0L} \quad (122)$$

$f_i^0$  is the reference state and can be either the pure liquid or the infinitely diluted compound (Henry's law). In the case of pure liquid,  $f_i^{0L}$  is expressed as function of the saturated vapor pressure of the liquid

$$f_i^{0L} = P_i^{sat} \phi_i^0(T, P_i^{sat}) \exp\left(\frac{v_i^L(P - P_i^{sat})}{RT}\right) \quad (123)$$

$v_i^L$  is the molar volume of the pure liquid component  $i$  ( $i$  = solvent) at saturation. The exponential term is called Poynting correction factor. It represents the deviation between the saturated vapor pressure of component  $i$  and the equilibrium pressure.

For treating the gas solubility in our system, the unsymmetrical approach is used and combined with the unsymmetrical convention (Henry's law approach), which corresponds to infinite dilution reference (i.e. the activity coefficients of the gas molecules into the water equal to unity). The equilibrium condition reads:

$$\phi_i^v y_i^v P = \gamma_i x_i H_i \quad (124)$$

where  $H_i$  is Henry's law constant. It is expressed by means of the following relation:

$$H_i = H_{i,Psat} \exp\left(\frac{v_i^\infty(P - P_i^{sat})}{RT}\right) \quad (125)$$

The so-called solubility models enable the calculation of Henry's law constant. It has to be reminded that the Henry's law constant is determined at the saturated vapour pressure of the pure solvent ( $H_{i,Psat}$ ). Thus, the Poynting factor corrects for the pressure difference between  $P_{sat}$  of the pure solvent (here is the water) and the system pressure  $P$ . The partial molar volume of the gas  $i$  at infinite dilution ( $v_i^\infty$ ) can be calculated from a correlation proposed by (Vidal et al., 1973a, 1973b). However, it is fixed here to  $32 \text{ cm}^3 \cdot \text{mol}^{-1}$  for the majority of the components.

(Holder et al., 1980; Holder and Grigoriou, 1980) proposed the following correlation for Henry's constant at saturation with temperature:

$$H_{i,Psat} = \exp\left(A + \frac{B}{T}\right) \quad (126)$$

The coefficients  $A$  and  $B$  are compiled in Table 36. The temperature is expressed in Kelvins and Henry's constant is given in atmospheres.

**Table 36:** Constants for calculating Henry's constant (Holder et al., 1980)

Gas	A	B	$v_i^\infty$ (Cm <sup>3</sup> /mole)
CH <sub>4</sub>	15.826277	-1559.0631	32
C <sub>2</sub> H <sub>6</sub>	18.400368	-2410.4807	32
C <sub>3</sub> H <sub>8</sub>	20.958631	-3109.3918	32
n-C <sub>4</sub> H <sub>10</sub>	22.150557	-3407.2181	32
CO <sub>2</sub>	14.283146	-2050.3269	32
N <sub>2</sub>	17.934347	-1933.381	32

- *Mole number of gases in the liquid phase:*

From Eq. (124), and Eq. (125), the expression for the mole number  $n_i^L$  of the gas  $i$  dissolved in the liquid phase:

$$n_i^L = \frac{V^L \rho_w^\circ}{M_w} \frac{y_i \phi_i^v P}{H_{i,Psat} \exp(P v_i^\infty / RT)} \quad (127)$$

$V^L \cong V_w^L$  stands for the volume of the liquid phase in equilibrium,  $\rho_w^\circ$  is the density, and  $M_w$  is the molar mass of pure water.  $v_j^\infty = 32 \text{ cm}^3 \text{ mol}^{-1}$  is (an average value from Holder in Table 36) the partial molar volume of the gas  $i$  in the solvent water. In establishing Eq. (127), the activity coefficient of gas in water was in a good approximation neglected and the very good approximations  $n_j^L \ll n_w^L$ , and  $V^L \cong V_w^L$  were applied.

- *Composition of the gases in gas phase*

Eq. (117) has also been used to determine the total amount of substance of the gas phase in a state corresponding to the three phase hydrate-liquid-vapor equilibrium. In the latter case, the initial values of the variables are to be replaced by the corresponding values measured in that equilibrium state, i.e,  $T_0$ ,  $P_0$ ,  $y_{j,0}$  and  $n_0^G$  are to be substituted for  $T$ ,  $P$ ,  $y_j$  and  $n^G$ . The volume of the reactor  $V_R$  has been replaced by the actual value of the gas phase  $V^G$ , which for any given equilibrium state has been approximated by:

$$V^G = V_R - V_{w,0} - V_{sample} \quad (128)$$



Where  $V_{w,0}$  stands for the volume of the liquid water, the reactor is initially loaded with.  $V_{sample}$  is the volume of the liquid sampled for ionic chromatography.

Utilizing the results from the gas chromatographic analysis we got mole fraction of each gas in composition ( $x_i$ ). Combining  $V^G$  and ( $x_i$ , P, T) we can be calculated  $n_i^G$  by means of a suitable equation of state (EOS), here the Soave-Redlich and Kwong (SRK).

- *Composition of hydrate phase*

The hydrate phase calculation comes from a mass balance Eq. (115). The hydration number is also obtained from the quantity of water consumed by the cristallization and also calculated from Eq. (129).

$$n_{HDY} = \frac{m_{Hydrate}}{M_{H2O} \sum n_{Hydrate}} \quad (129)$$

- *A few words about experimental errors*

Evaluation of errors of the calculations was made and written previously (Galfré, 2014; Herri et al., 2011). This last evaluation led to an uncertainty on the gas phase equals to  $\Delta x/x < 3\%$  (determined from GC errors), and to an uncertainty of the hydrate phase of  $\Delta z/z < 6\%$  (See Appendix 3 is presented in section §14. Page. 209). In the present work, another evaluation was performed using Monte Carlo simulations.

Monte Carlo method for evaluating the uncertainties consists in performing a huge number of calculations by taking into account the uncertainties of the inputs. It is usual to consider that the uncertainties follow a Gaussian law. Hence, they are represented by their mean values and standard deviation. A significant number of calculations are then done (about 1000 simulations). Each time, new random values for the inputs are used according to Gaussian law.

In the end, there are as many different outputs as there are simulations. A quick statistical evaluation leads to the mean results (hydrate volume, composition...), and their standard deviations.

To compute each time these 1000 simulations, the following standard deviations of the input data were used:

- $\Delta[\text{Li}^+]/[\text{Li}^+] = 0.1\%$ ,
- $\Delta x_i/x_i = 3\%$ ,
- $\Delta T = 0.2^\circ\text{C}$ ,
- $\Delta P = 0.1 \text{ bar}$ ,
- $\Delta m_w = 0.1 \text{ g}$ ,
- $\Delta m_w (\text{sampling}) = 0.1 \text{ g}$ ,
- $\Delta V_R = 3\%$ ,
- $\Delta Q_w = 10 \text{ kg.m}^{-3}$ ,
- $\Delta Q_{H^{\beta}} = 40 \text{ kg.m}^{-3}$ .

Also, the following assumptions were done:

- $P_w = 1000 \text{ kg/m}^3$ .
- $\rho_{H^{\beta}} = 790 \text{ kg/m}^3$ .

We observed that the molar fraction errors on the hydrate composition were found to be usually inferior to 4%. The standard deviation close to the total dissociation point was calculated to be between 20% and 100%. Indeed, the initial and final  $\text{Li}^+$  concentrations for these points are very close.



## 7. EXPERIMENTALS RESULTS AND DISCUSSIONS

Experimental gas compositions are presented in [Table 37](#). Here are presented experimental results from both procedures (quick and slow crystallization). Each of them are applied to measure the composition of the hydrate formed from different gas mixtures from CO<sub>2</sub>-N<sub>2</sub>-CH<sub>4</sub>-C<sub>2</sub>H<sub>6</sub>-C<sub>3</sub>H<sub>8</sub> ... Corresponding PT results (Pressure and Temperature) are observed carefully in order to investigate the influence of the crystallization rate on the hydrate formation. In a second approach, these results are compared to a thermodynamic modelling (when it is possible). The objective of these simulations is to check the assumption that quick crystallization leads to kinetic equilibria. The simulated results are obtained from our in-house program GasHyDyn.

**Table 37:** Molar composition of the studied gas mixtures and initial conditions of experiments.

Gas mixtures (Exp)	Methods	CO <sub>2</sub>	N <sub>2</sub>	CH <sub>4</sub>	C <sub>2</sub> H <sub>6</sub>	C <sub>3</sub> H <sub>8</sub>	P <sub>i</sub>	T <sub>i</sub>	Reactor volume	Mass water injected
		%	%	%	%	%	MPa	°K	Lite	Gram
		(±0.001)	(±0.001)	(±0.001)	(±0.001)	(±0.001)	(±0.001)	(±0.2)	(±0.001)	(±0.1g)
Gas 1	Quick	82.08	17.92	--	--	--	3.11	278.2	2.44	800.9
Gas 2	Quick	82.81	17.19	--	--	--	3.13	277.9	2.44	800.9
Gas 3	Quick	0.057	--	0.915	0.028	--	3.25	275.8	2.36	801.3
Gas 4	Quick	0.053	--	0.919	0.028	--	2.20	278.0	2.36	799.6
Gas 5	Slow	0.052	--	0.919	0.029	--	4.73	276.4	2.36	800.3
Gas 6	Slow	--	--	84.61	--	15.39	1.73	280.0	2.36	801.1
Gas 7	Slow	--	--	84.61	--	15.39	1.73	280.0	2.36	801.1
Gas 8	Slow	--	--	86.86	--	13.14	1.83	285.0	2.36	800.9
Gas 9	Quick	--	--	85.77	--	14.23	1.81	281.0	2.36	801.2
Gas 10	Quick	--	--	85.81	--	14.19	1.71	280.5	2.36	801.1
Gas 11	Quick	--	--	86.89	--	13.11	1.77	285.1	2.44	800.9
Gas 12	Quick	--	--	86.89	--	13.11	1.77	285.1	2.44	800.9
Gas 13	Slow	--	--	95.02	2.90	02.08	2.78	285.1	2.36	801.1
Gas 14	Slow	--	--	87.72	--	12.28	1.81	284.8	2.36	801.4
Gas 15	Quick	--	--	87.72	--	12.28	1.81	284.8	2.36	778.0
Gas 16	Quick	--	--	86.37	--	13.63	1.78	284.1	2.36	801.4
Gas 17	Slow	--	--	86.37	--	13.63	1.78	284.1	2.36	801.4

In the next sections, tables [Table 38](#), [Table 39](#) and [Table 40](#) present the simulated results (predicted pressures and hydrate compositions) and the mean deviations to experimental results.

## 7.1. CO<sub>2</sub>-N<sub>2</sub> GAS MIXTURES

**Table 38:** CH<sub>4</sub>-SI-V-Lw Equilibrium of CO<sub>2</sub>-N<sub>2</sub> at quick crystallization rate procedure versus predicted results

Experimental Equilibrium Data						Simulation			
T	P	Gas composition		Hydrate composition		S	P	Hydrate composition	
(±0.2)	(±0.01)	Molar gas fraction (±0.001)						Molar gas fraction (±0.003)	
		CO <sub>2</sub>	N <sub>2</sub>	CO <sub>2</sub>	N <sub>2</sub>				
(°C)	(MPa)	(%)	(%)	(%)	(%)		MPa	(%)	(%)
2.3	2.46	0.667	0.333	0.970	0.030	SI	2.53	0.955	0.045
3.1	2.60	0.689	0.311	0.965	0.035	SI	2.69	0.958	0.042
3.3	2.66	0.699	0.301	0.961	0.039	SI	2.73	0.960	0.040
4.3	2.87	0.723	0.277	0.958	0.042	SI	2.99	0.962	0.038
5.2	3.13	0.747	0.253	0.955	0.045	SI	3.22	0.966	0.034
6.0	3.38	0.768	0.232	0.947	0.053	SI	3.48	0.968	0.032
Mean Deviation (%)							3.1	1.0	24.7

The experimental results of CO<sub>2</sub> and N<sub>2</sub> gases mixtures (Table 38, Figure 46 and Figure 58) can be considered as a good case study at thermodynamic equilibrium. The equilibrium pressure is simulated with a precision of 3.1% and the composition of gas in the hydrate phase is simulated with a precision of 1.0 % for CO<sub>2</sub> and of 24.7% for N<sub>2</sub>, respectively. In these cases, the errors on the predicted hydrate compositions are between 10% and 30% for the major species and lower than 50% for the minor species.

The problem in the experimental study is that the calculated hydrate composition is a mean value on the whole hydrate phase. It does not take into account the history of the crystal growth. Hence, it is possible that the thermodynamic model is compared to a situation that is not at thermodynamic equilibrium. Since the simulated results are close to the experimental ones, it can be suggested that the hydrate formation occurs at thermodynamic equilibrium. Maybe the hydrate phase is reorganized to follow at each moment the global thermodynamic equilibrium.

In the end, it can be suggested that the crystallization performed at high driving force could form hydrates at equilibrium. In fact, equilibrium pressures for a CO<sub>2</sub>-N<sub>2</sub> binary mixture are well predicted by the model with a mean deviation 3.1%. The prediction on the composition can be considered as good also, for CO<sub>2</sub> as a major

component. The prediction on  $N_2$  composition, as a minor, is not good but it needs to be noticed that the experimental procedure for minor components does not give accurate measurements.

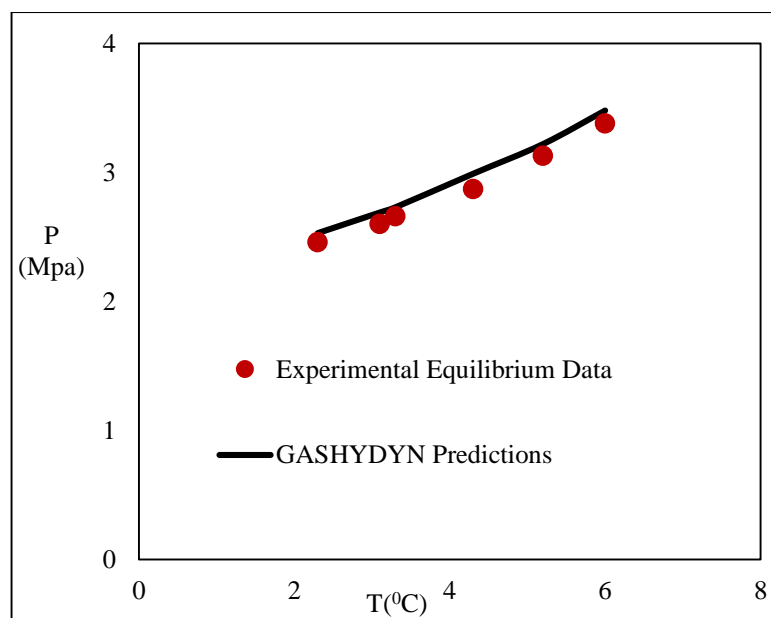


**Figure 46:** Experimental equilibrium data of  $CO_2$ - $N_2$  gas hydrate at high driving force compared with GasHyDyn predictions

As conclusion, in this specific case, the high rate of crystallization does not influence the hydrate composition.

## 7.2. $CO_2$ - $CH_4$ - $C_2H_6$ GAS MIXTURE

In a next run of experimental measurements, gas hydrates were formed from  $CO_2$ - $CH_4$ - $C_2H_6$  ternary gas mixture. Both procedures were used, at low and high crystallization rate.

The experimental data concerning the high crystallization rate are presented on [Table 39](#). The predicted results (PT) are not as accurate as before, with a mean deviation between 6% and 8.9%. The hydrate composition on the major component,  $CH_4$  is correctly predicted (6% deviation), but the two minors,  $CO_2$  and  $C_2H_6$  are poorly (33.6%) and very poorly predicted (143%). It is not surprising since the minor components compositions are more difficult to measure. In this first case, we can

suspect a non-equilibrium formation regime. The predicted composition of the gas hydrate is slightly different from the global composition measured experimentally.

**Table 39:** CH<sub>4</sub>-SI-V-Lw Equilibrium of CO<sub>2</sub>-CH<sub>4</sub>-C<sub>2</sub>H<sub>6</sub> at high crystallization rate procedure versus predicted results.

Experimental Equilibrium Data						GASHYDYN Prediction				
Exp	Hydrate composition					Hydrate composition				
	T ±0.2	P ±0.01	Molar gas fraction (±0.001)			S	P	Molar gas fraction (±0.003)		
			CO <sub>2</sub>	CH <sub>4</sub>	C <sub>2</sub> H <sub>6</sub>			CO <sub>2</sub>	CH <sub>4</sub>	C <sub>2</sub> H <sub>6</sub>
n°	(°C)	(MPa)	%	%	%		(MPa)	%	%	%
1	2.75	3.54	0.07	0.888	0.042	SI	3.11	0.046	0.873	0.081
	3.65	3.81	0.07	0.888	0.042	SI	3.35	0.051	0.858	0.091
	5.15	4.23	0.069	0.891	0.041	SI	3.79	0.054	0.835	0.111
	6.55	4.56	0.07	0.891	0.039	SI	4.33	0.056	0.827	0.117
	7.80	5.12	0.068	0.889	0.042	SI	4.76	0.058	0.814	0.128
	9.25	5.99	0.037	0.897	0.066	SI	5.67	0.068	0.816	0.116
	10.70	6.43	-0.033*	0.945	0.088	SI	6.66	0.069	0.812	0.118
	12.05	6.57	-0.083*	1.07	0.014	SI	7.61	0.067	0.801	0.133
Mean Deviation (%)							8.9	33.6	6.0	143
2**	1.0	2.71	--	--	--	SI	2.57	--	--	--
	1.4	2.76	--	--	--	SI	2.66	--	--	--
	2.0	2.83	--	--	--	SI	2.80	--	--	--
	2.5	2.88	--	--	--	SI	2.88	--	--	--
	2.8	2.89	--	--	--	SI	2.92	--	--	--
	3.3	2.93	--	--	--	SI	3.03	--	--	--
	4.0	3.02	--	--	--	SI	3.15	--	--	--
	5.0	3.06	--	--	--	SI	3.45	--	--	--
	5.8	3.06	--	--	--	SI	3.75	--	--	--
Mean Deviation (%)							6	--	--	--

\*Equilibrium points near total dissociation, hydrate composition errors close to 100%

\*\*Hydrate composition uncertainties ≈ 10% for C<sub>2</sub>H<sub>6</sub> and C<sub>3</sub>H<sub>8</sub>

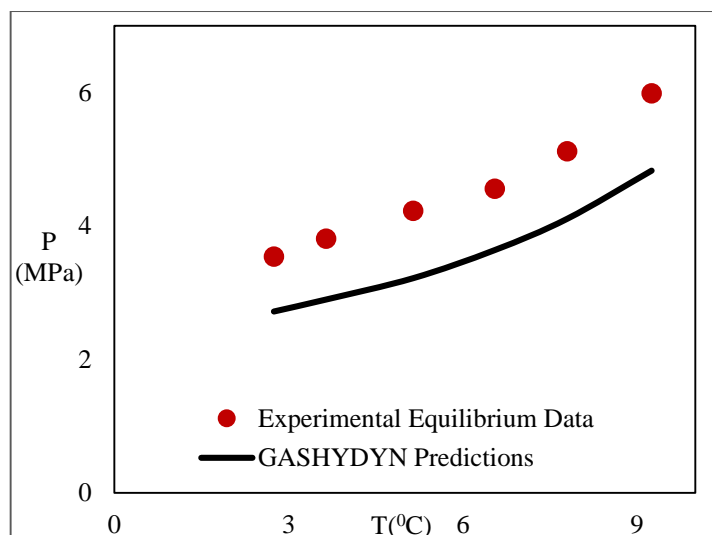


**Figure 47:** Experimental equilibrium data of CO<sub>2</sub>-CH<sub>4</sub>-C<sub>2</sub>H<sub>4</sub> gas hydrate at high driving force compare with GasHyDyn predictions

In second approach are presented data obtained from low rate of crystallization (on Table 40 and Figure 48). First, the final pressure at the lowest temperature is different than at high driving force (30 bars instead of 35 bars). Also, the water conversion is 13% instead of 34%. The cavities occupancy seems to be affected by the speed of crystallization. Concerning the hydrate composition, the hydrate at low crystallization seems to contain more ethane, but is it not obvious at such low molar fractions.

Then, the simulation from the same gas mixture CO<sub>2</sub>-CH<sub>4</sub>-C<sub>2</sub>H<sub>6</sub> gives a pressure and hydrate composition close to the experimental results. Deviation on the pressure is 2%, and the hydrate composition accuracy is lower than 24%. The two minor components, CO<sub>2</sub> and C<sub>2</sub>H<sub>6</sub> are better predicted in comparison to the high crystallization rate experiments.

Since the results for this first ternary mixture performed at low crystallization rate (low driving force) are in better accordance with the simulation, it can be suggested that mixed hydrate formation can form at thermodynamic equilibrium if the crystallization process is very slow.

As reviewed in the §5.5, Page. 95, kinetics control of the hydrate composition would not be a surprise. Indeed, the hydrate crystallization from an initial vapor-liquid equilibrium involves many transfer phenomena. First, the gas dissolution in the aqueous phase is usually a limiting step. Also, the elementary steps of the crystallization, especially the growth, are dependent on the driving force, and in the end on the interface(s) area(s) and mass transfer coefficients which control the instantaneous gas concentration in the liquid phase (and so the driving force for the crystallization). As suggested recently (Herri and Kwaterki 2012), the enclathration



of the gas molecules into the hydrate structure could be significantly affected by kinetics considerations and the final composition of the mixed hydrate could be different than predicted by thermodynamic modeling.

**Table 40:** CH\_SI-V-Lw Equilibrium of CO<sub>2</sub>-CH<sub>4</sub>-C<sub>2</sub>H<sub>6</sub> at low crystallization rate procedure versus predicted results.

Experimental Equilibrium Data					GASHYDYN Prediction				
T ±0.2  (°C)	P ±0.01  (MPa)	Hydrate composition Molar gas fraction (±0.001)			S	P  (MPa)	Hydrate composition Molar gas fraction (±0.003)		
		CO <sub>2</sub>	CH <sub>4</sub>	C <sub>2</sub> H <sub>6</sub>			CO <sub>2</sub>	CH <sub>4</sub>	C <sub>2</sub> H <sub>6</sub>
		%	%	%			%	%	%
6.2	4.17	0.117	0.669	0.214	SI	4.12	0.062	0.811	0.127
4.6	3.78	0.081	0.799	0.12	SI	3.64	0.062	0.843	0.095
4.2	3.56	0.081	0.828	0.091	SI	3.51	0.061	0.846	0.093
3.3	3.18	0.075	0.849	0.076	SI	3.28	0.061	0.869	0.07
2.5	3.04	0.076*	0.854*	0.070*	SI	3.03	0.059	0.871	0.07
1.3*	2.76	0.075	0.862	0.063	SI	2.75	0.057	0.885	0.058
4.2**	3.57	0.062	0.843	0.095	SI	3.47	0.066	0.835	0.099
Mean Deviation (%)						1.8	23.8	5.3	12

\*Equilibrium points near total dissociation, hydrate composition errors close to 100%

\*\*Equilibrium point at dissociation process

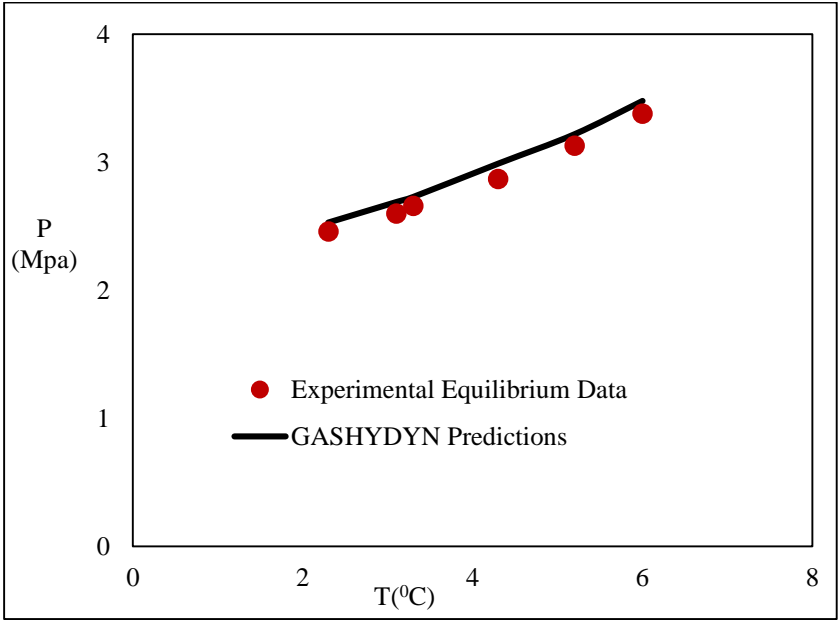


**Figure 48:** Experimental equilibrium data of CO<sub>2</sub>-CH<sub>4</sub>-C<sub>2</sub>H<sub>4</sub> gas hydrate at low driving force compare with GasHyDyn predictions

From our experiments from CO<sub>2</sub>-CH<sub>4</sub>-C<sub>2</sub>H<sub>4</sub> gas mixtures, and comparison between high and low crystallization rate, we have new elements which support the idea that the composition of hydrate could be kinetically controlled.

### 7.3. CH<sub>4</sub>-C<sub>3</sub>H<sub>8</sub> GAS MIXTURES

In the Table 41 and Table 42, are given the experimental results concerning the CH<sub>4</sub>-C<sub>3</sub>H<sub>8</sub> gas mixture, at high and low crystallization rates, respectively. Even if this mixture only involves two molecules, propane is slightly bigger than carbon dioxide, methane or ethane. This could affect significantly the crystallization process.

Results in this part were unfortunately affected by an experimental error due to an unnoticed leak. This leak had obviously a consequence on the pressure and the mass balance calculations. Even if the leak is small, the experiments at low crystallization rate take days to weeks. It is then difficult to compare the experimental results between the two procedures and to the thermodynamic model. However, they will be briefly presented here since some observations are interesting, even if these observations will have to be validated in a further study.

**Table 41:** CH<sub>4</sub>-C<sub>3</sub>H<sub>8</sub> Equilibrium of CH<sub>4</sub>-C<sub>3</sub>H<sub>8</sub> at high crystallization rate procedure.

Exp	Time	Vol Reactor	Conditions		Gas phase		Hydrate phase		
			T	P	Molar gas fraction (±0.001)		hydrate mass	Conversion of mass	nHDY
			±0.2	±0.01	xCH <sub>4</sub>	xC <sub>3</sub> H <sub>8</sub>			
n°	(hours)	(litre)	(oK)	(mPa)	(%)	(%)	gram	(%)	n°
1	0*	2,36	281,00	1,81	0,858	0,142	--	--	--
	186	2,36	274,90	1,40	0,982	0,018	108,57	13,55	6,60
	258	2,36	277,40	1,38	0,972	0,028	90,92	11,40	5,34
	282	2,36	279,15	1,41	0,958	0,042	103,40	13,05	6,17
	306	2,36	280,95	1,48	0,939	0,061	95,64	12,14	6,02
	330	2,36	282,75	1,55	0,922	0,078	94,29	12,04	6,28
	364	2,36	284,60	1,70	0,893	0,107	83,79	10,76	6,44
2	0*	2,36	280,45	1,71	0,858	0,142	--	--	--
	150	2,36	274,90	1,43	0,986	0,014	97,96	12,23	6,36
	294	2,36	275,40	1,33	0,983	0,017	87,66	10,99	5,41
	336	2,36	277,50	1,35	0,971	0,029	83,10	10,48	5,21
	366	2,36	279,25	1,39	0,956	0,044	79,59	10,10	4,73

	408	2.36	281.10	1.44	0.929	0.071	70.19	8.95	3.55
	456	2.36	282.80	1.55	0.899	0.101	50.80	6.51	2.49
	509	2.36	284.95	1.69	0.868	0.132	32.03	4.13	0.81
	574	2.36	286.85	1.84	0.838	0.162	8.87	1.15	1.09
	749	2.36	288.55	1.63**	0.841	0.159	9.86	1.29	0.00
3	0*	2.44	285.05	1.77	0.869	0.131	--	--	--
	129	2.44	276.15	1.38	--	--	--	--	--
	146	2.44	277.75	1.39	--	--	--	--	--
	178	2.44	279.55	1.43	--	--	--	--	--
	240	2.44	281.05	1.49	--	--	--	--	--
	293	2.44	282.80	1.57	--	--	--	--	--
	348	2.44	284.75	1.71	--	--	--	--	--
	408	2.44	285.65	1.83	--	--	--	--	--
	437	2.44	286.45	1.86**	--	--	--	--	--
4	0*	2.44	285.05	1.77	0.869	0.131	--	--	--
	96	2.44	277.55	1.27	--	--	--	--	--
	120	2.44	278.90	1.27	--	--	--	--	--
	144	2.44	280.30	1.30	--	--	--	--	--
	168	2.44	281.50	1.36	--	--	--	--	--
	264	2.44	283.35	1.51	--	--	--	--	--
	288	2.44	285.25	1.61	--	--	--	--	--
	312	2.44	287.10	1.71	--	--	--	--	--
	432	2.44	288.65	1.72**	--	--	--	--	--

\*Equilibrium points without water (only binary gas in reactor)

\*\*Equilibrium points near total dissociation, hydrate composition errors close to 100%

**Table 42:** CH<sub>4</sub>-SI-V-Lw Equilibrium of CH<sub>4</sub>-C<sub>3</sub>H<sub>8</sub> at low crystallization rate procedure.

Exp	Time	Vol Reactor	Conditions		Gas phase		Hydrate phase		
			T ±0.2	P ±0.01	Molar hydrate fraction (±0.001)		hydrate mass	Conversion of mass	nHDY
					xCH <sub>4</sub>	xC <sub>3</sub> H <sub>8</sub>			
n°	(hours)	(litre)	(oK)	(mPa)	(%)	(%)	gram	(%)	n°
1 <sup>b</sup>	0*	2.36	279.95	1.73	0.846	0.154	--	--	--
	144	2.36	281.15	1.70	0.935	0.065	51.56	6.44	4.70
	309	2.36	280.05	1.44	0.942	0.058	52.67	6.63	3.58
	505	2.36	279.20	1.26	0.931	0.069	54.95	6.96	3.18
2 <sup>b</sup>	0*	2.36	279.95	1.73	0.846	0.154	--	--	--
	144	2.36	279.30	1.08	0.902	0.098	90.49	11.53	4.53
	360	2.36	278.25	0.94	0.905	0.095	99.86	12.80	4.57

	552	2.36	277.20	0.83	0.910	0.090	91.08	11.75	3.91
	816	2.36	276.15	0.72	0.912	0.088	90.36	11.72	3.64
	1032	2.36	275.45	0.66	0.912	0.088	92.17	12.03	3.60
	1255	2.36	274.55	0.59	0.914	0.086	95.85	12.59	3.61
	1321	2.36	282.30	0.91**	0.782	0.218	83.91	11.09	3.73
3	0*	2.36	284.95	1.83	0.869	0.131	--	--	--
	96	2.36	284.80	2.38	0.887	0.113	17.09	2.13	13.28 <sup>a</sup>
	422	2.36	282.80	1.69	0.912	0.088	33.05	4.15	2.71
	734	2.36	281.15	1.35	0.913	0.087	34.73	4.39	2.47
	1096	2.36	279.25	1.07	0.913	0.087	43.57	5.54	2.48
	1382	2.36	277.50	0.90	0.921	0.079	53.46	6.85	2.40
	1750	2.36	275.45	0.74	0.933	0.067	57.10	7.36	2.20
	1798	2.36	274.90	0.72	0.936	0.064	57.20	7.42	2.50
	1966	2.36	274.25	0.67	0.939	0.061	65.48	8.54	2.50

\*Equilibrium points without water (only binary gas in reactor)

\*\*Equilibrium point at dissociation process

<sup>a</sup>: this point maybe not at equilibrium P-T

<sup>b</sup>: the experimental with leak reactor

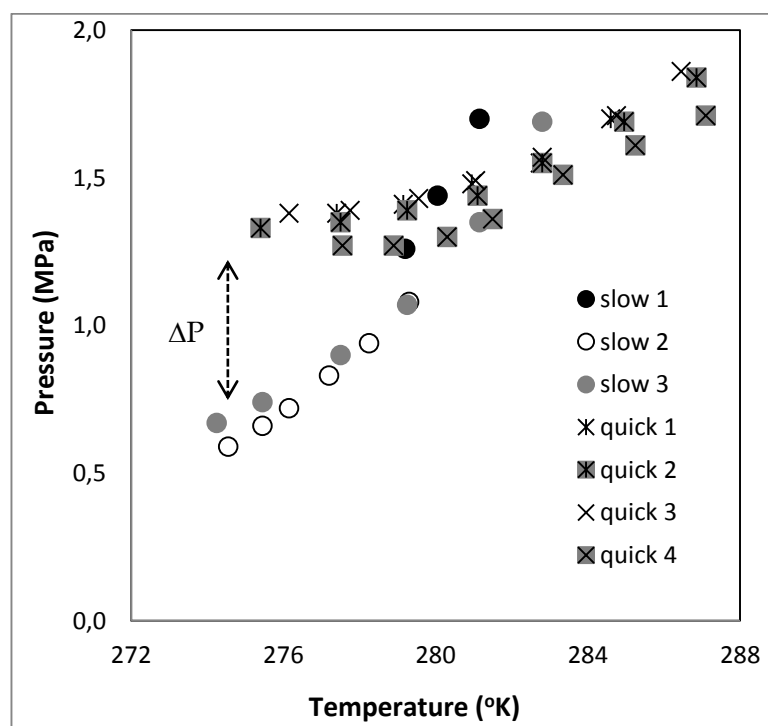


**Figure 49:** Experimental equilibrium data of CH<sub>4</sub>-C<sub>3</sub>H<sub>8</sub> gas hydrate at high and low driving force

Figure 49 shows four results at high crystallization rate and three at low driving force. In both cases, the PT results are consistent. We can see that the pressure at low temperature is significantly different from one procedure to another (7 bars versus 14 bars for quick crystallization). Of course, experiments take more time at low crystallization rate, which could explain the pressure difference. However, a pressure drop of 7 bars is quite significant (too big?), and this should be checked.

Some experiments to investigate the pressure drop due to the leak showed a pressure drop of 4 bars in 13 days at 30 bars in the reactor. It is still too early to draw a final conclusion, but, the thermodynamic modelling could be a tool to investigate  $\text{CH}_4\text{-C}_3\text{H}_8$  equilibria. If a look is taken at the first equilibria observed experimentally (the leak is still not significant, the thermodynamic model is not accurate for structure SI or structure SII in predicting the pressure. So, either we did not observe a thermodynamic equilibrium, or there is both structure of hydrate formed. Nevertheless, a modelling taken into account the mass balance could deepen this question (see chapter §8. Page. 151).

**Table 43:** Experimental and predicted pressures for the first data obtained in each experiments ( $\text{CH}_4\text{-C}_3\text{H}_8$ )

	<b>T</b> <b>(K ±0.2)</b>	<b>P</b> <b>(bars ±0.1)</b>	<b>Ppred</b> <b>(SI)</b>	<b>Ppred</b> <b>(SII)</b>
1	274.90	14	24	6
2	274.90	14.3	25.5	6.6
1b	279.15	17	31.7	7.5
2b	278.30	10.8	20.3	5.2
3b	284.80	18.3	35.4	9.1

#### 7.4. $\text{CH}_4\text{-C}_2\text{H}_4\text{-C}_3\text{H}_8$ GAS MIXTURES

In this last section, an experiment from  $\text{CH}_4\text{-C}_2\text{H}_6\text{-C}_3\text{H}_8$  gas mixture is presented. Unfortunately, this experiment suffered from the same leak problem.

If we compare the results at the same temperature (about 277 K as example), the “equilibrium” pressure are 35.5 bars and 24 bars at quick and slow crystallization rate respectively. A pressure difference of more than 10 bars is quite significant, and we do think that the leak is responsible for such a difference.

As said before, others experiments are needed to confirm this observation.

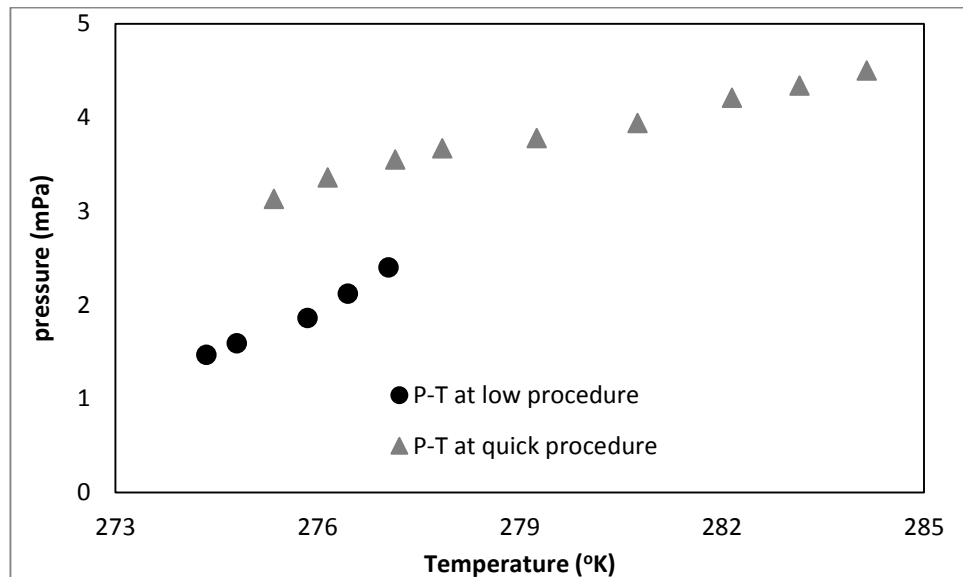


**Figure 50:** Experimental equilibrium data of  $\text{CH}_4\text{-C}_2\text{H}_6\text{-C}_3\text{H}_8$  gas hydrate at low driving force

**Table 44 :** CH<sub>4</sub>-C<sub>2</sub>H<sub>6</sub>-C<sub>3</sub>H<sub>8</sub> Equilibrium of CH<sub>4</sub>-C<sub>2</sub>H<sub>6</sub>-C<sub>3</sub>H<sub>8</sub> at high crystallization rate (Le Quang, 2013)

Exp	Time	Vol Reactor	Conditions		Gas phase			Hydrate phase		
			T ±0.2	P ±0.01	Molar hydrate fraction (±0.001)			hydrate mass	Conversion of mass	nHDY
					xCH <sub>4</sub>	xC <sub>2</sub> H <sub>6</sub>	xC <sub>3</sub> H <sub>8</sub>			
n°	(hours)	(litre)	(oK)	(mPa)	(%)	(%)	(%)	gram	(%)	n°
1	0*	2.36	--	--	--	--	--	--	--	--
	--	2.36	275.35	3.13	0.98	0.003	0.017	--	--	6
	--	2.36	276.15	3.36	0.98	0.003	0.017	--	--	6.2
	--	2.36	277.15	3.55	0.98	0.004	0.016	--	--	7.1
	--	2.36	277.85	3.67	0.98	0.006	0.014	--	--	6.4
	--	2.36	279.25	3.78	0.97	0.008	0.022	--	--	7.7
	--	2.36	280.75	3.94	0.97	0.012	0.017	--	--	8.5
	--	2.36	282.15	4.21	0.96	0.017	0.023	--	--	7.2
	--	2.36	283.15	4.34	0.96	0.019	0.021	--	--	8.2
	--	2.36	284.15	4.5	0.95	0.022	0.028	--	--	9.7

\*Equilibrium points without water (only binary gas in reactor)

**Table 45:** CH<sub>4</sub>-C<sub>2</sub>H<sub>6</sub>-C<sub>3</sub>H<sub>8</sub> Equilibrium of CH<sub>4</sub>-C<sub>2</sub>H<sub>6</sub>-C<sub>3</sub>H<sub>8</sub> at low crystallization rate procedure.

Exp	Time	Vol Reactor	Conditions		Gas phase			Hydrate phase		
			T ±0.2	P ±0.01	Molar hydrate fraction (±0.001)			hydrate mass	Conversion of mass	nHDY
					xCH <sub>4</sub>	xC <sub>2</sub> H <sub>6</sub>	xC <sub>3</sub> H <sub>8</sub>			
n°	(hours)	(litre)	(oK)	(mPa)	(%)	(%)	(%)	gram	(%)	n°
1 <sup>b</sup>	0*	2.36	285.05	2.78	--	--	--	--	--	--
	565	2.36	277.05	2.4	--	--	--	--	--	--
	733	2.36	276.45	2.12	--	--	--	--	--	--
	925	2.36	275.85	1.86	--	--	--	--	--	--
	1164	2.36	274.80	1.59	--	--	--	--	--	--
	1317	2.36	274.35	1.47**	--	--	--	--	--	--

\*Equilibrium points without water (only binary gas in reactor)

\*\*Equilibrium point at dissociation process

<sup>b</sup>: the experimental with leak reactor

## 7.5. CONCLUSION

The two procedures used suggest a kinetic influence on mixed hydrate formation (mostly experiment on  $\text{CO}_2\text{-CH}_4\text{-C}_2\text{H}_6$  gas mixture). Experimental results showed that the enclathration of the heavier molecule (ethane) is more important at low than high crystallization rate. Moreover, the equilibrium pressure for a given temperature and initial gas composition, is different. This observation could not be supported by all the measurements since a leak was detected concerning  $\text{CH}_4\text{-C}_3\text{H}_8$ , and  $\text{CH}_4\text{-C}_2\text{H}_6\text{-C}_3\text{H}_8$  gas mixtures. However, the pressure drop does not seem to be responsible for the big differences observed. New experiments have to be performed to confirm this statement.

Also, the thermodynamic simulations are also in better accordance with the results at slow crystallization.

In the end, the results show that mixed hydrate equilibrium could not be at thermodynamic equilibrium. If the measurements are performed at high crystallization rate the hydrate volume and composition will not be in accordance with the thermodynamic modeling. This observation could have a significant impact on design calculations in which the assumption of thermodynamic equilibrium is made (leading to an over estimation of the hydrates volume in the pipe-lines).

New experimental are scheduled, we will be performed to confirm again the conclusions in this work. The next section of this work, Flash calculation is going to establish in up-grading our simulation software running equilibrium simulation by adding a flash algorithm. The objective is to take into account the history of the crystallization in the modelling work.





## 8. FLASH CALCULATION

### 8.1. INTRODUCTION

So far, mixed hydrate crystallization has been observed from experiments and thermodynamic modeling. If the experiments have been performed at different crystallization rate, there could be some issues and complications. Indeed, a difference in the final state of the system has been discovered, but the exact order of magnitude remains unreliable. That is why the thermodynamic modeling has been used to support these conclusions. The thermodynamic modeling has given good results on  $\text{CO}_2\text{-CH}_4\text{-C}_2\text{H}_6$  experiment (deviation on pressure  $<5\%$ , and  $<24\%$  on hydrate composition). However, it is difficult to draw an ultimate conclusion based on this sole comparison. Actually, the thermodynamic modeling only predicts the composition of the first nucleus in solution (liquid-hydrate equilibrium LHE). Experimentally, this composition can hardly be measured. That is why a significant volume of hydrate is experimentally formed to measure this hydrate composition with more accuracy. But, if we consider that the hydrate composition is not stoichiometric, the measured (and calculated) hydrate composition is only an average value. It is not the case in the thermodynamic modeling. Hence, it is difficult to compare the thermodynamic model with the experimental results, and the crystallization process has to be taken into account in the calculations.

Another issue considered previously (section thermodynamic) is the regression of Kihara parameters. Usually, these parameters are calculated from experimental results (PT data). At best, only pure hydrates are used, for example pure  $\text{CO}_2$  hydrate to compute  $\text{CO}_2$  parameters. However, this is not always possible ([Le Quang, 2013](#); [Le Quang et al., 2016](#)). In this situation, mixed hydrate results can be used. From these results, the objective function can be the error between equilibrium and predicted pressure, as well as the difference between the experimental and predicted hydrate composition. But, two issues arise: the experiments could not be performed at thermodynamic equilibrium, and the measured hydrate composition could be only an average value. To obtain more reliable Kihara parameters, it would be very interesting to be able to predict the hydrate volume, and the hydrate composition, taking into account the non-stoichiometry of the hydrate phase.

At last, the hydrate volume to be formed is essential to determine the amount of kinetic inhibitors (KHI) to use in flow-assurance.

Therefore, flash calculation algorithms have been developed in the hydrate team, to combine both thermodynamic modeling and mass balance while calculating phase equilibria.

## 8.2. STATE OF THE ART

There are not many studies that take into account the crystal growth of mixed clathrate hydrates. Usually, the hydrate phase is considered to be homogeneous, at thermodynamic equilibrium with the surrounding fluid phase. To find such studies, we have to look for kinetic models. Recently, (Herri and Kwaterski, 2012) suggested a kinetic model, already presented in section §5.5 Page.95. More recently, a kinetic flash algorithm has been presented by (Boesen et al., 2014). As a kinetic approach, time is a variable. The driving force is given by the (Per Skovborg and Rasmussen, 1994; P. Skovborg and Rasmussen, 1994). However, this last model does not appeal to thermodynamic equilibrium equations.

### 8.2.1 USUAL FLASH CALCULATIONS

In thermodynamics, flash calculations are thermodynamic equilibrium equations resolution combined with mass balance (and eventually energy balance) equations. Gibbs phase law gives the degree of freedom of a thermodynamic system. Usually, this number is higher than two:

$$var = number\ of\ components - number\ of\ phases + 2 \quad (130)$$

$var = numberofcomponents - numberofphases +$  Among the intensive parameters, pressure (P) and temperature (T) are usually chosen. The volume of the system can also replace one of these two properties. A Flash calculation at given temperature and pressure is often called Flash PT. If there is a heat exchange, the quantity of energy Q can be used (Flash QP, flash QT...). An energy balance is then necessary. More details can be found in the literature on flash calculations (Michelsen, 1990a, 1990b). A basic algorithm is drawn on Figure 51.

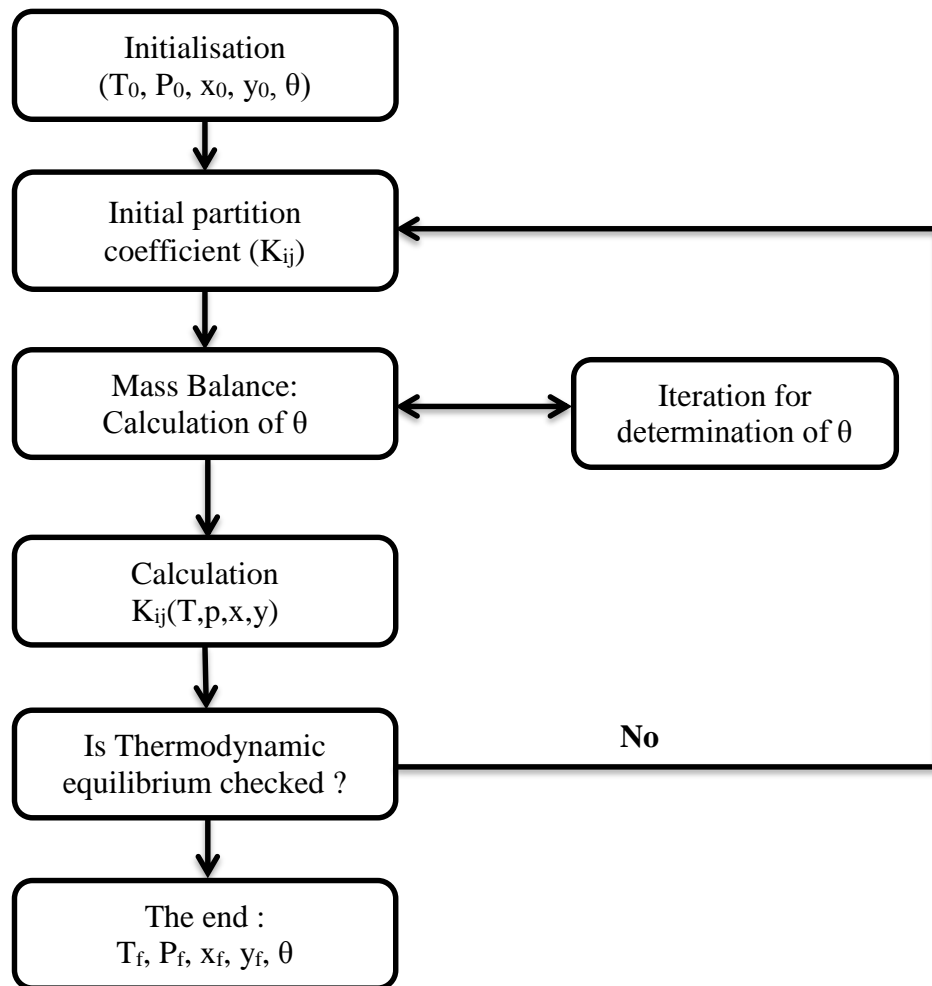


**Figure 51:** Example of Flash algorithm ( $\theta$ =mass flow ratio between phases)

This figure shows that there are two loops in standard flash calculations:

- One loop on mass balance verification ( $\theta$ ),
- One loop on thermodynamic equilibrium ( $K_{ij}$ ).

where symbol  $\theta$  stands for the global mass ratio between the two phases (usually liquid/vapor).

### 8.2.2 FLASH HYDRATE MODELING

In the case of hydrate flash calculations, the algorithm is more complicated, since there are three phases at equilibrium. The third phase (hydrate) decreases the degree of freedom by one. To fit to the experiments of this work, and more extensively to batch experiments, the volume is then considered to be constant. Then, since the temperature is set (cryothermostat), this is the variable for the modeling.

The other issue is the supposed non-stoichiometry of the hydrate crystal. If the solid phase is not homogeneous, the model will have to take into account the crystallization, and the thermodynamic path of the system.

Therefore, the only solution to consider the crystal growth in thermodynamic modeling is to perform successive flash calculation along the crystallization. The basic algorithm is represented on [Figure 52](#). This figure shows that the crystallization is discretized into successive flash calculations. Each step corresponds to a new mass of hydrate. This mass (combined with cavity occupancy) is considered with van der Waals and Platteuw as described in section [§4](#), Page. [57](#). There are two options for the former mass of hydrate:

- It remains the same,
- It is reorganized to be at thermodynamic equilibrium with the surrounding liquid phase.

These two options lead to two different algorithms, two frameworks for the hydrate flash calculations. After presenting the basic algorithm, these two frameworks will be described.

### 8.3. BASIC ALGORITHM

The number of degree of freedom is only one. To compare the further simulations to the previous experiments, the temperature is chosen as variable. The volume is constant, since it is the reactor volume.

The basic algorithm is represented on [Figure 52](#). The objective is to simulate the thermodynamic path of the crystallization, from the initial state (vapor liquid equilibrium, at high temperature), to the final state (hydrate-liquid-vapor equilibrium) at a lower, and final, temperature. [Figure 53](#) shows what is to be simulated. There are two stages: VLE, when the temperature is too high for the hydrate phase to form, and vapor-liquid-hydrate equilibrium (VLHE), at lower temperatures. Point *A* represents the initial state ( $P_0$ ,  $T_0$ ). Point *B* corresponds to the first three phase equilibrium (VLHE) when decreasing the temperature ( $T_B$ ). Step *A* to *B* is the first stage. In the model, this is VLE combined with mass balance. That is to say, a standard vapor-liquid flash calculation

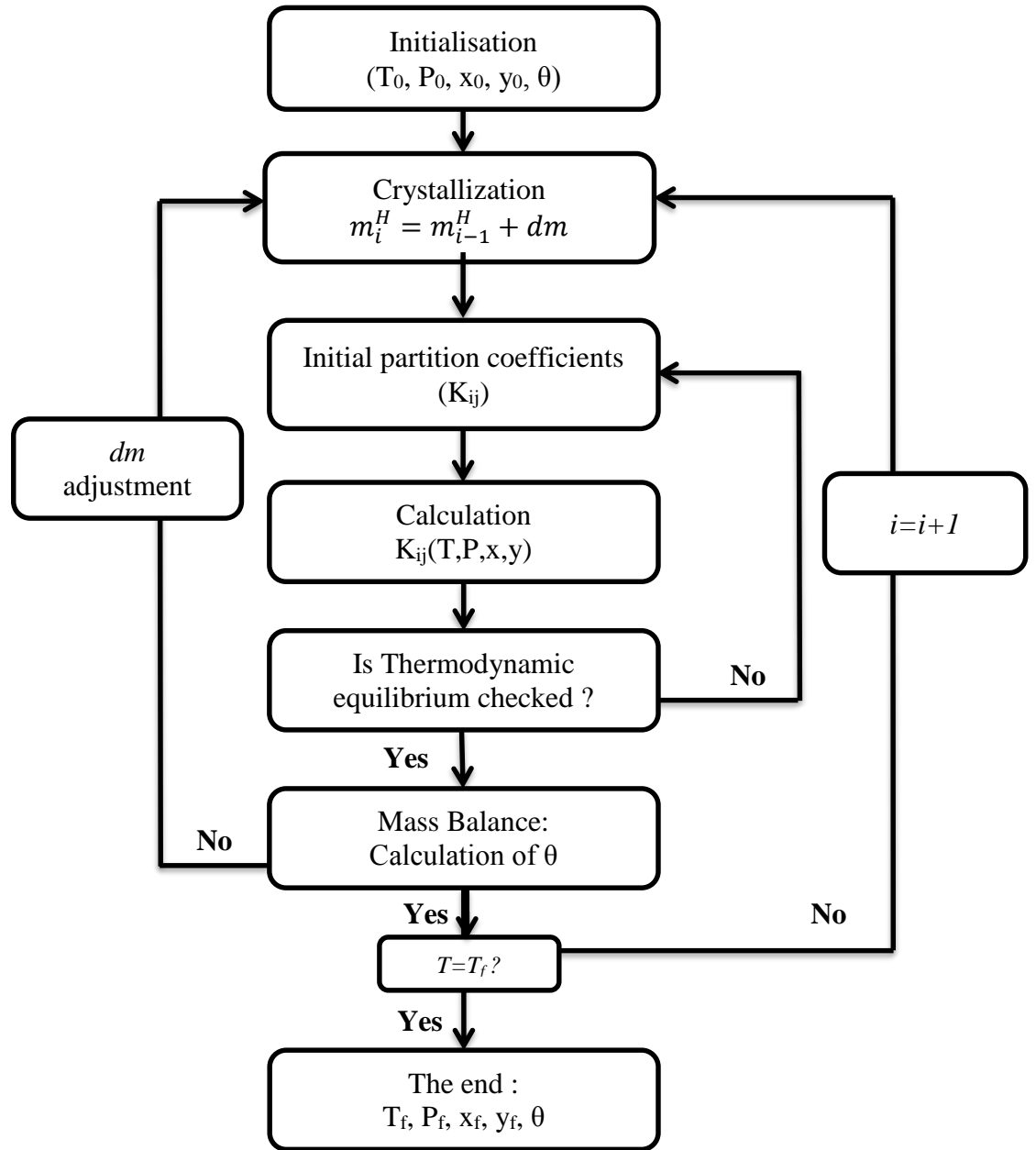


**Figure 52:** Basic hydrate flash algorithm.

Then, the successive  $C_i$  points correspond to the second stage, when the temperature decreases (VLHE, when  $T_C < T_B$ ). Since there is a mass transfer from the gas phase to the hydrate phase (through the liquid phase), the gas molecules are consumed in time. The changes in the gas composition modify the liquid-hydrate equilibrium. This is why there is no longer only one LHE equilibrium curve. Each  $C_i$  point belongs to a different LHE curve. The numbers of  $C_i$  points depends on the discretization of the crystallization. It is an input number, written  $N$  (and  $i \in \{1, \dots, N\}$ ). The temperature step is then:

$$\Delta T = \frac{T_B - T_D}{N} \quad (131)$$

The higher  $N$  is, the more continuous the crystallization is. The lower this is, the more the driving force is significant in the model.

In the end (at final temperature  $T_f = T_D$ ), the system reaches the final state of equilibrium.

The inputs need to account for the total mass of the system. The same procedure as the experimental one is simulated in the modeling. First, “injection” of the gas mixture (gas composition and pressure). The mass of each gas molecule is calculated with the use of an equation of state (SRK). Then, a given mass of water is added. Then, the final temperature is chosen. In the end, the inputs are:

- Initial temperature and pressure ( $T_0$  and  $P_0$ ),
- the “reactor” volume ( $V_R$ ),
- gas mixture composition ( $z_0^G$ ),
- the mass of water ( $m_w$ ),
- the final temperature ( $T_f$ ),
- the iterations number  $N$ .

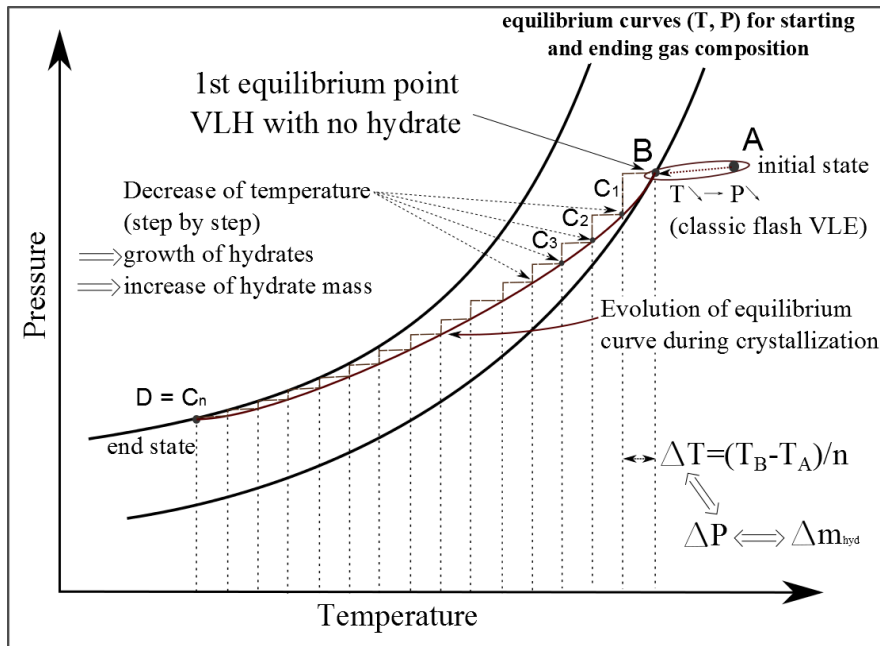


**Figure 53:** Thermodynamic path (Bouillot and Herri, 2016).

#### 8.4. HYDRATE FLASH ALGORITHM WITHOUT CRYSTAL REORGANIZATION

In this section, details on the framework for the hydrate flash calculation without the crystal reorganization are suggested. The detailed algorithm is described on [Figure 54](#).

The first part corresponds to the VLE flash algorithm. In the model, the gas phase is modeled with SRK equation of state (gas density). The vapor-liquid equilibrium is calculated with Henry's law like equation (see also at section §6.4.3. Page. 129). Two loops are used in this first step. The following simultaneous equations are considered:

$$\begin{cases} n_j^0 = n_j^V + n_j^L \\ n_j^L = \frac{V^L \rho_w^0 z_j \varphi_j^G P}{M_w K_{H,j}^\infty} \end{cases} \quad (132)$$

Where  $n$  is the quantity (mole) of molecule  $j$  in phase vapor or liquid or both (superscripts  $V$ ,  $L$  and  $0$ , respectively).  $n_j^V(T, P, z_j, V)$  is calculated with SRK EoS.  $\varphi_j^G$ , the fugacity coefficient of the vapor phase can be set to 1 for hydrocarbon gas mixtures. Since the final adjustment variable is  $P$ , the VLE flash determines the equilibrium pressure of the system (then marked  $P^{VLE}$ ).

After this initial VLE flash calculation, the pressure  $P^{VLE}$  of the system is known. Then, the temperature is decreased to reach the three phase equilibrium, that is to say, VLE flash combined with LHE equations. The output of VLE flash is  $P^{VLE}$ , and the output of LHE is also a pressure (then marked  $P^{LHE}$ ). The three phases equilibrium is reached when  $P^{VLE} = P^{LHE}$ .

From this point, the crystallization begins. System is at three phases equilibrium, but only vapor and liquid phases coexist. As said in introduction, two hypotheses on the hydrate phase can be considered: homogeneous and heterogeneous composition. In this first section, the non-stoichiometric approach is considered.

To reach the final state, the crystal growth is examined. There is a discretization of this growth, depending on the number of iterations  $N$ . If  $N$  is high enough, the growth can be considered as continuous (very low  $\Delta T$ ). Otherwise, the driving force taken into account in the crystallization process is more significant. [Figure 55](#) shows the crystallization modeling.

Since the crystal growth is discretized through  $\Delta T$  step, there is a  $\Delta m^H$  mass of hydrate that corresponds to the previous variation. This mass (more specifically the



mass of water that has crystallized  $\Delta m_w^H$ ) is the new adjustment variation in solving the following simultaneous equation system:

$$\begin{cases} \forall j, n_j^0 = n_j^V + n_j^L + n_j^H \\ p^{VLE} = p^{LHE} \end{cases} \quad (133)$$

$n_j^V$  is calculated using SRK EoS,  $n_j^L$  using Henry's law like equation (section §6.4.3. Page. 129), and  $n_j^H$  from (van der Waals and Platteeuw, 1959) (as described in section §4. Page. 57) combined with assumed  $\Delta m^H$  value. This last calculation is the tricky one. The procedure is the following one.

First, a mass of water that has crystallized ( $\Delta m_w^H$ ) is taken as hypothesis. From this mass, the corresponding volume of hydrate is calculated. To do so, the empty hydrate density is used (the hydrate with no gas molecules inside). This density depends on the hydrate structure. In this thesis, only structure I and II are investigated ( $\rho_I^{H-\beta}$  and  $\rho_{II}^{H-\beta}$ ). (Sloan and Koh, 2007) give an expression for the density of hydrates which is presented in section §2.2.2, Page. 31:

$$\rho^H = \frac{N_w M_w + \sum_{j=1}^C \sum_{i=1}^n \theta_{ij} v_i M_j}{N_{Avo} V_{cell}} \quad (134)$$

Where  $N_w$  is number of water molecule per unit cell (see Table 1),  $N_{Avo}$  the Avogadro's constant,  $M_w$  and  $M_j$  the molecular weights of water and molecule  $j$ ,  $v_i$  the number of type  $i$  cavities by component  $j$ ,  $\theta_{ij}$  the fractional occupation of cavity  $i$  by component  $j$ , and  $V_{cell}$  the volume unit cell (Table 1).

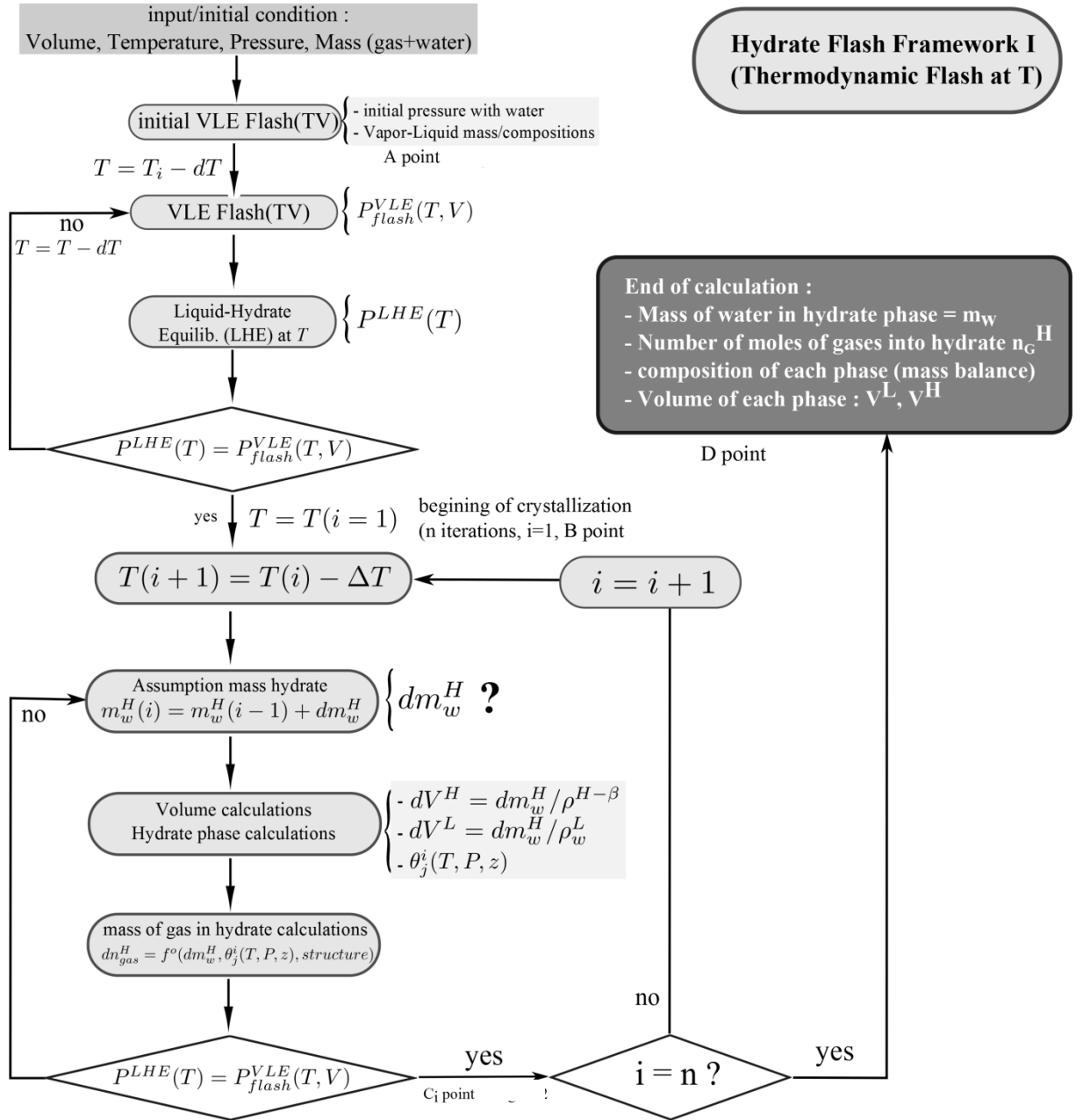


**Figure 54:** Algorithm to perform hydrate flash calculation with no reorganization of the crystal phase (framework I) (Bouillot and Herri, 2016).

For an empty hydrate, this formula becomes:

$$\rho^{H-\beta} = \frac{N_w M_w}{N_{Av} V_{cell}} \quad (135)$$

Values of 790 and 785 kg/m<sup>3</sup> can be obtained for structure I and II respectively. From these values, the crystallized volume of hydrate is:

$$\Delta V^H = \frac{\Delta m_w^H}{\rho^{H-\beta}} \quad (136)$$

From  $\Delta m_w^H$  value, the mass of gas in the hydrate cavities, or  $n_j^H$ , is fully determined (thanks to occupancy  $\theta_{ij}$ ). Also, the volume of the aqueous phase is known ( $V^L = \rho_w^L m_w^L$  by assuming pure water and  $\rho_w^L = 1000 \text{ kg/m}^3$ ), as well as the vapor phase volume ( $V^V = V_R - V^L - V^H$ ).

A “VLE flash” is then performed, and the resulting pressure  $P^{VLE}$  is compared to the predicted LHE pressure ( $P^{LHE}$ ). If  $P^{VLE} \neq P^{LHE}$ , the  $\Delta m_w^H$  value is not correct. There is then an iterative process to find the right hydrate volume, or mass. The objective function is:

$$F_{obj}(dm_w^H) = \frac{|P^{VLE} - P^{LHE}|}{P^{VLE}} \rightarrow 0 (< 10^{-3}) \quad (137)$$

Once the right value of  $\Delta m_w^H$  (or  $dm_w^H$ ) is found, the temperature of the system is decreased of  $\Delta T$ , and the calculations start over until  $T = T_f$ .

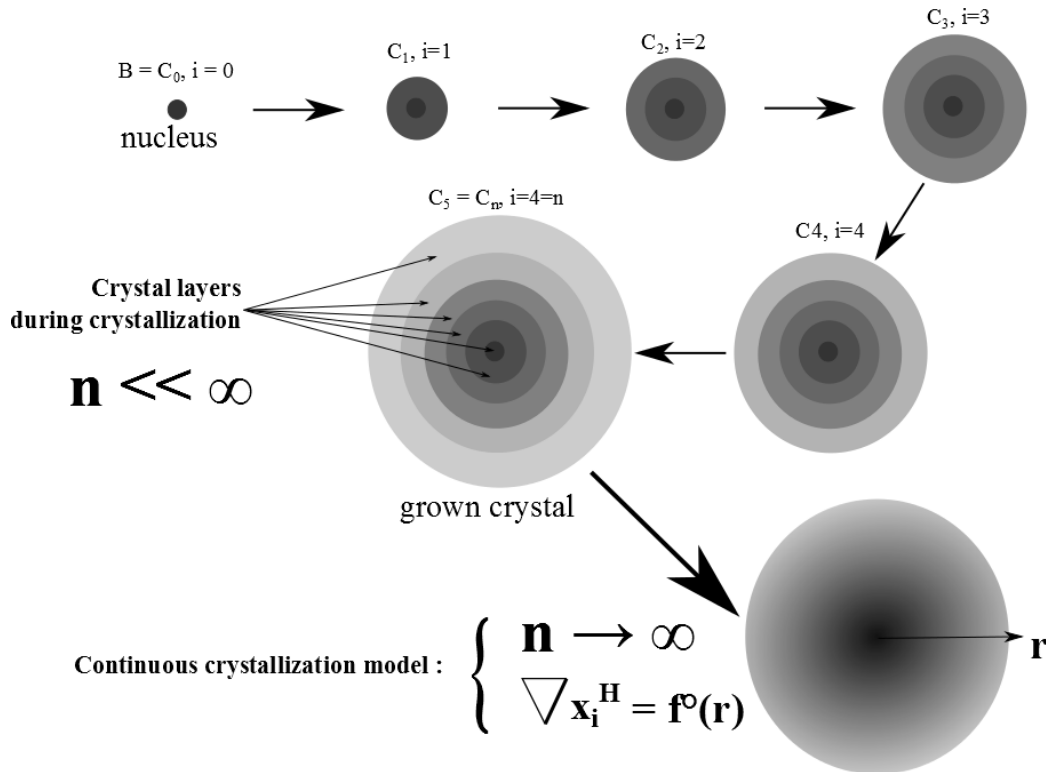


**Figure 55:** Mixed hydrate growth (no reorganization) (Bouillot and Herri, 2016).

The most important hypothesis in this part comes from the calculation of  $\theta_{ij}$  and its use in calculating  $n_j^H$ . Indeed, either the occupancy is calculated from the initial

equilibrium state (before the temperature decrease), or after. The first hypothesis leads to a hydrate phase that is not at thermodynamic equilibrium with the surrounding liquid phase after crystallization, while it is the case in the second hypothesis. Of course, if the number of iteration is infinite, the approaches are the same. In this algorithm, the first approach is chosen (marked framework I). The second (framework II) is investigated in next section.

## 8.5. HYDRATE FLASH ALGORITHM WITH CRYSTAL REORGANIZATION

In this algorithm, then called framework II, the last layer of the hydrate crystal is at thermodynamic equilibrium with the surrounding liquid. To check this assumption, the equilibrium equation has to be validated through the occupancy factor  $\theta$ . Figure 56 presents the algorithm with hydrate reorganization.

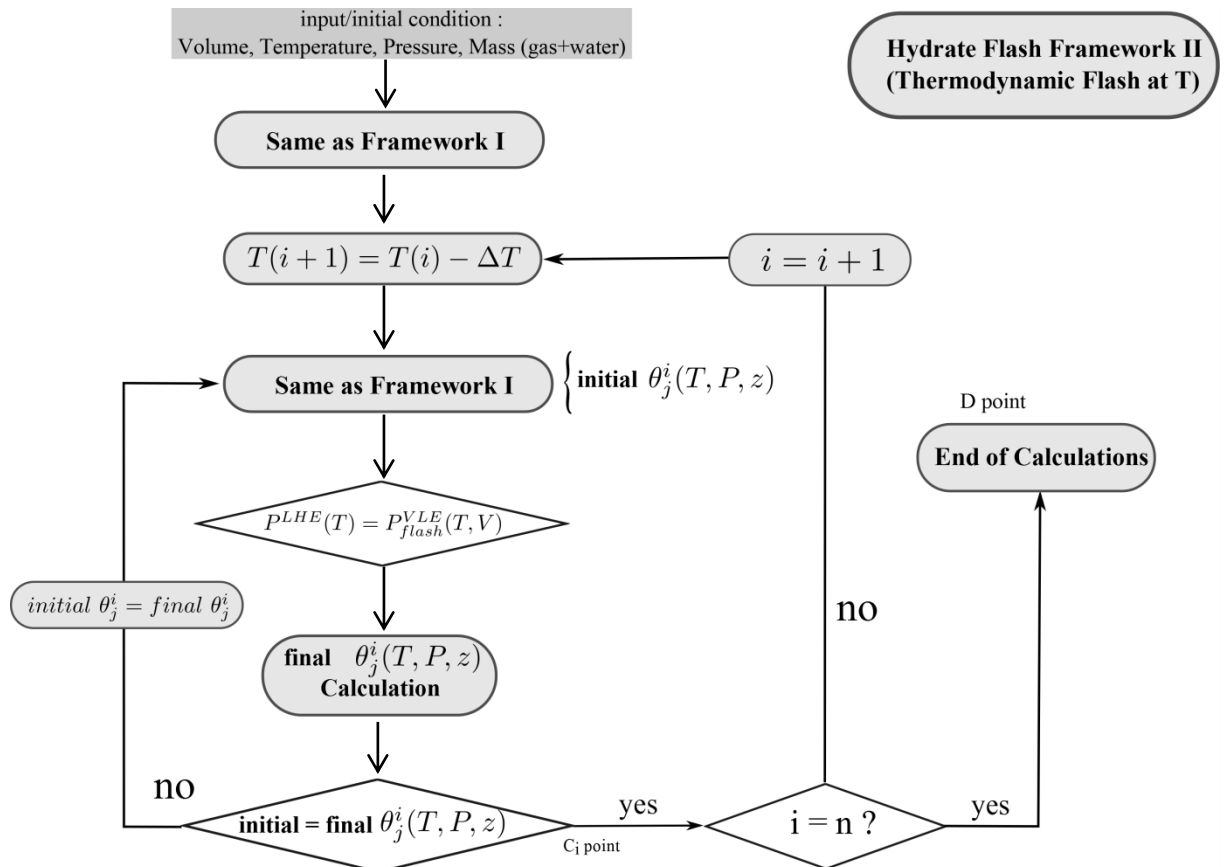


**Figure 56:** Algorithm to perform hydrate flash calculation with reorganization of the hydrate phase during crystallization (framework II) (Bouillot and Herri, 2016).

On this figure, a new loop is added to the initial algorithm. In the end of each iteration  $i$ , the occupancy factor  $\theta_j^i$  is calculated after crystallization (of  $dm_w$ ) and compared before  $dm_w$  adjustment. This way, the LHE equation is validated after

crystallization, for an occupancy factor in accordance with (van der Waals and Platteeuw, 1959) theory at the equilibrium with the fluid phase's compositions.

As with the algorithm with no hydrate phase reorganization, the crystallization is discretized. Figure 53 also represents the thermodynamic path. If the number of iteration is infinite, we can expect that the occupancy factor before and after crystallization is the same. This is why the two algorithms are converging when  $N \rightarrow \infty$ .

If the number of iteration is just 1, there is only one step in the hydrate growth, and the hydrate phase is completely homogeneous. This approach is then called framework II\*, and is represented in Figure 57.

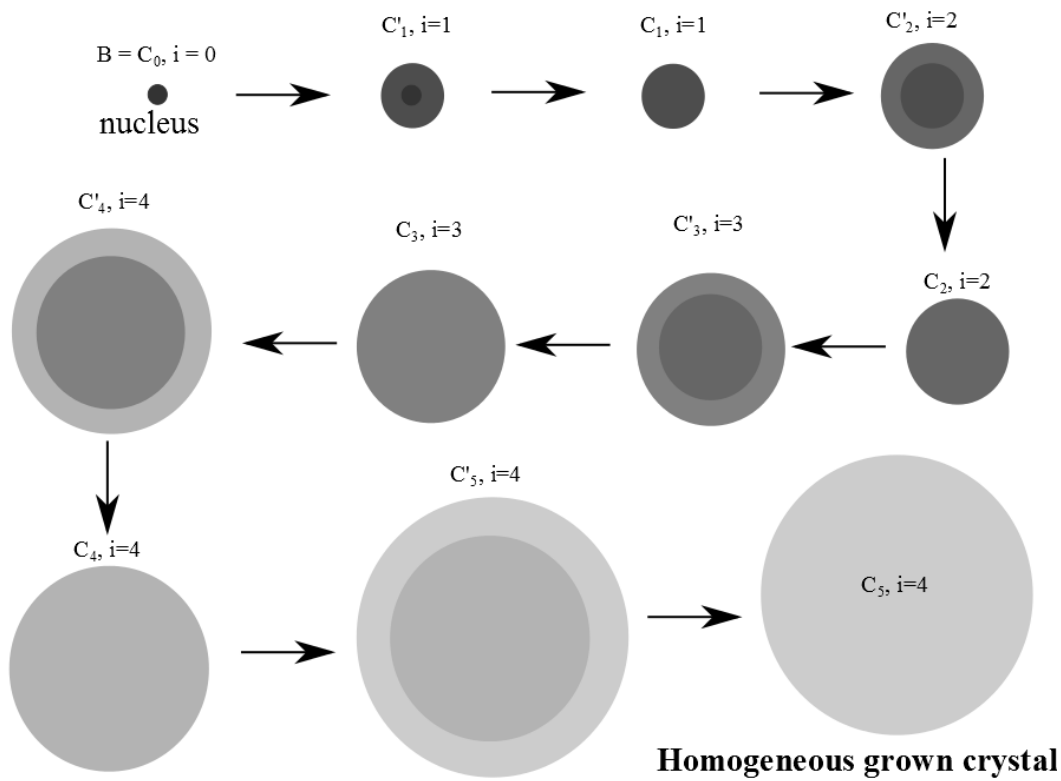


**Figure 57:** Hydrate growth with crystal phase reorganization (framework II\*) (Bouillot and Herri, 2016).

## 8.6. KIHARA PARAMETERS OPTIMIZATION

To investigate the hydrate flash algorithm, an estimation of the Kihara parameters was needed. Since the used code (MATLAB) is different than is the previous modeling work (use of GasHyDyn), the Kihara parameters are also different. Table 46 gives the Kihara parameters obtained from this optimization.

**Table 46:** Quick Kihara parameters optimization of CO<sub>2</sub>, CH<sub>4</sub> and C<sub>2</sub>H<sub>6</sub> on a few experimental data (Adisasmito et al., 1991; Avlonitis, 1988; Dyadin, 1996; Y. A. Dyadin et al., 1996; Yurii A. Dyadin et al., 1996; Englezos and Bishnoi, 1991; Larson, 1955; Le Quang et al., 2016; Nixdorf and Oellrich, 1997; Thakore and Holder, 1987; Yasuda and Ohmura, 2008) (\* data from (Sloan and Koh, 2007))

	$\varepsilon/k$	$\sigma$	$a^*$	RMSE	Nb. Data
CO <sub>2</sub>	171.78	2.978	0.6805	0.02	8
CH <sub>4</sub>	160.70	3.101	0.3834	2.43	14
C <sub>2</sub> H <sub>6</sub>	176.83	3.220	0.5651	0.062	18

## 8.7. RESULTS

To investigate the frameworks and compare them to experimental results, a reference case is used. This baseline is a CO<sub>2</sub>-CH<sub>4</sub>-C<sub>2</sub>H<sub>6</sub> gas mixture, presented previously (Table 19) and published in Fluid Phase Equilibria (Le Quang et al., 2016). It is chosen because it is an experiment at low crystallization rate, supposed to be as close as possible to thermodynamic equilibrium during crystallization.

Then, an investigation of the uncertainty of the model due to Kihara parameters uncertainties is suggested.

In the end of this section, a comparison with experiments at high crystallization rate will be presented.

### 8.7.1. THERMODYNAMIC EQUILIBRIUM

First, the thermodynamic model in the hydrate flash frameworks is compared to the reference case. Table 47 and

Figure 58 show that the thermodynamic model provides results in accordance with the experimental results (RMSE of 0.31 for the pressure, and lower than 0.04 for the hydrate composition). The LHE part of the flash algorithm is accurate in this case, assuming a SI structure. SI structure will then be considered in next sections.

**Table 47:** Experimental versus predicted results for the reference case (CO<sub>2</sub>, CH<sub>4</sub> and C<sub>2</sub>H<sub>6</sub>) from classic thermodynamic calculations assuming a SI structure.

T	P exp	Exp. Gas composition (%mol)			Exp. Hydrate composition (%mol)			P pred	Pred. Hydrate composition (%mol)		
(K)	(bars)	CO <sub>2</sub>	CH <sub>4</sub>	C <sub>2</sub> H <sub>6</sub>	CO <sub>2</sub>	CH <sub>4</sub>	C <sub>2</sub> H <sub>6</sub>	(bars)	CO <sub>2</sub>	CH <sub>4</sub>	C <sub>2</sub> H <sub>6</sub>
279.35	41.7	0.037	0.943	0.02	0.117	0.669	0.214	41.1	0.0569	0.8598	0.0833
277.75	37.75	0.035	0.951	0.014	0.081	0.799	0.12	36.39	0.0579	0.8801	0.0619
277.35	35.6	0.034	0.952	0.014	0.081	0.828	0.091	35.09	0.0566	0.8828	0.0605
276.4	31.8	0.033	0.957	0.01	0.075	0.849	0.076	32.79	0.0567	0.8977	0.0456
275.6	30.4	0.031	0.959	0.01	0.076*	0.854*	0.070*	30.35	0.0546	0.8996	0.0458
274.45	27.6	0.03	0.963	0.007	0.075	0.862	0.063	27.54	0.0534	0.9093	0.0373
RMSE:								0.31	0.0129	0.0383	0.0256

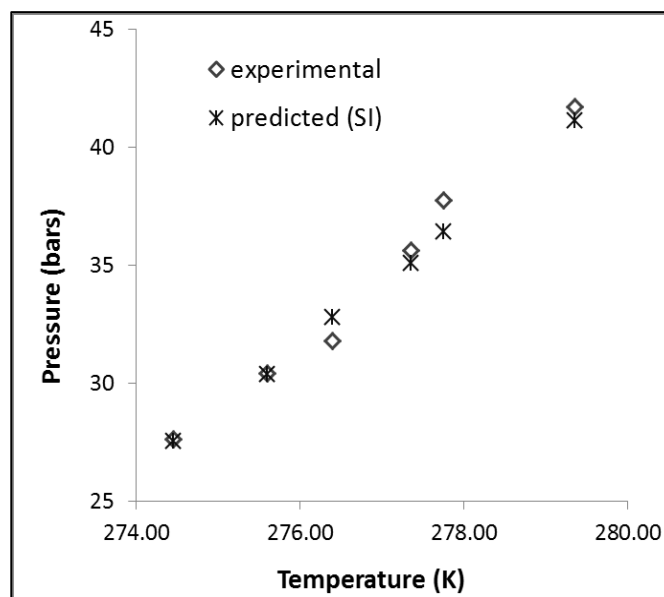


**Figure 58:** PT diagram of experimental and predicted results of the reference case (CO<sub>2</sub>-CH<sub>4</sub>-C<sub>2</sub>H<sub>6</sub>) at different temperatures from the same initial state.

### 8.7.2. FLASH RESULTS

Results obtained for the two frameworks and different iteration numbers  $N$  is suggested in Table 48. Thermodynamic paths for each framework and different number of iterations are presented on Figure 58.

First, all the frameworks provide three phase equilibrium (VLHE) at the same temperature and pressure (280.14 K and 42.63 bars). This means that the first crystal in the bulk should appear in these conditions. At a lower temperature ( $T < 280.14$  K), the crystal phase grows. This is point B on Figure 53.

Then, the temperature is decreased step by step ( $C_i$  points), until it reaches the final temperature  $T_f = 274.5$  K. This is the final experimental temperature.

Figure 58 presents the thermodynamic path (both experimental and predicted) of the crystallization, *i.e.* temperature-pressure states during the crystallization. This figure also provides the thermodynamic LHE curves that are crossed at each step during the crystallization ( $N=7$  and structure SI). This figure is in accordance with Figure 53 and shows a good agreement between the experimental and predicted results concerning the pressure.

More specifically, Table 48 shows that the deviation between experimental and simulated results is under 8% (both hydrate volume and final pressure at the same time).

As expected, framework I and II converge when  $N \rightarrow \infty$  (continuous crystallization, see  $N=100$  as example). Then, using “only” 20 iterations for frameworks I and II allows the calculation of a continuous crystallization (results close to  $N=100$ ) while at the same time presenting a lower time consumption in the calculations.

Then, frameworks I and II provide accurate results in pressure and hydrate volume (<5%). The lower deviation obtained is for framework II for 8 iterations. Concerning influence of  $N$  for framework I, the more the discretization is significant, the lower the deviation is. For framework II, it is the opposite. If a few iterations are used ( $n = 3$ ), the accuracy deteriorates. This can also cause the calculation of negative compositions (too many gas molecules into the hydrate phase, and a negative number in the gas phase).

At last, the framework II\* results are not in better accordance with experimental data. The final pressure is closer, but not the hydrate volume (higher).



**Table 48:** Experimental versus predicted results for the reference case (CO<sub>2</sub>, CH<sub>4</sub> and C<sub>2</sub>H<sub>6</sub>) from classic thermodynamic calculations assuming a SI structure.

	Pf (±0.01)	m <sup>H</sup> <sub>w</sub> (±0.01)	conv. (±0.01)	n <sup>G</sup> (±0.001)	Gas composition (%mol) (±0.001)			n <sup>H</sup> (±0.001)	hydrate composition (%mol) (±0.003)			dev. (%) (±0.01)	
	n (bars)	(g)	%mass	(mol)	×CO <sub>2</sub>	×CH <sub>4</sub>	×C <sub>2</sub> H <sub>6</sub>	(mol)	×CO <sub>2</sub>	×CH <sub>4</sub>	×C <sub>2</sub> H <sub>6</sub>	Exp.	
I	3*	30.03	111.43	13.91	2.166	0.031	0.972	-0.004	1.045	0.073	0.831	0.096	10.6
I	5	29.18	119.38	14.99	2.098	0.031	0.969	0.000	1.117	0.073	0.845	0.082	5.9
I	10	28.90	122.05	15.34	2.076	0.031	0.968	0.001	1.140	0.072	0.849	0.079	4.3
I	20	28.79	123.05	15.47	2.067	0.031	0.968	0.002	1.149	0.072	0.851	0.077	3.7
I	50	28.74	123.51	15.49	2.063	0.031	0.967	0.002	1.153	0.072	0.852	0.077	3.5
I	100	28.74	123.51	15.53	2.064	0.031	0.967	0.002	1.153	0.072	0.852	0.076	3.5
II	8	28.47	125.98	15.86	2.042	0.031	0.966	0.003	1.175	0.071	0.856	0.073	2.0
II	20	28.62	124.55	15.67	2.055	0.031	0.967	0.002	1.162	0.071	0.854	0.075	2.9
II	100	28.68	124.05	15.48	2.059	0.031	0.967	0.002	1.158	0.072	0.853	0.076	3.2
II*	5	27.39	135.94	17.11	1.958	0.031	0.961	0.008	1.263	0.069	0.871	0.061	3.9
II*	20	27.39	135.93	17.10	1.958	0.031	0.961	0.008	1.263	0.069	0.871	0.061	3.9
Exp.	27.60	127.10	15.99	2.009	0.030	0.963	0.007	0.007	1.21	0.075	0.862	0.062	0

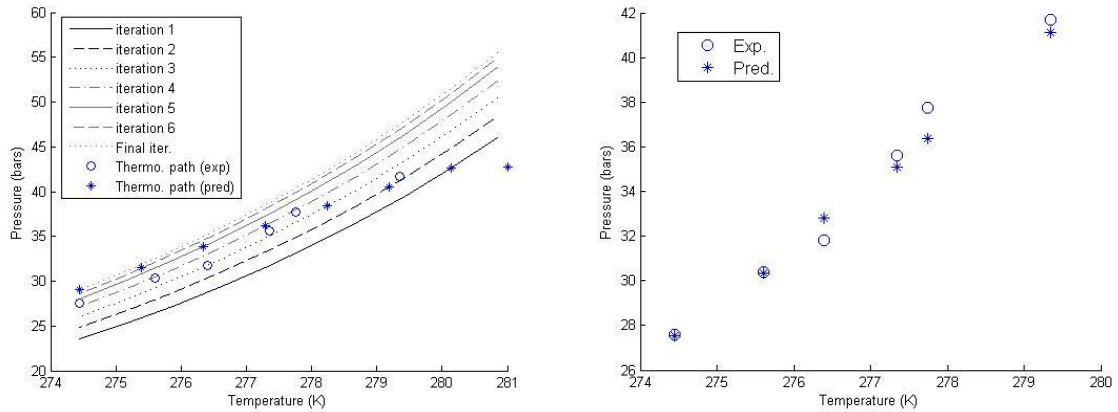


**Figure 59:** Predicted and experimental thermodynamic paths (Pressure vs temperature during crystallization) in the reference case (left: all frameworks at different numbers of iterations; right: framework I,  $N=7$ ).

## 8.8. KIHARA UNCERTAINTIES

Since Kihara parameters are very dependent on the authors as pointed by (Herri et al., 2011), this is interesting to evaluate the influence of their uncertainties. To do this investigation, Monte Carlo simulation were used.

1000 simulations were performed (each time) on the reference case from Gaussian distribution around the mean values of  $\varepsilon/k$  and  $\sigma$ . Standard deviations were taken from 1% to 5%. Framework I with 8 iterations was used.

Table 49 provides the obtained results. This demonstrates that a small difference (5%) can have a significant effect on the final pressure and hydrate volume (standard deviations of 42% and 125% respectively).

Since the models deviations from experimental results are usually under 5%, it can be concluded that the frameworks are in good accordance with the experiments.

**Table 49:** Influence of the Kihara parameters uncertainties on the flash hydrate results (framework I, reference case).

	Pf	$\sigma(\text{Pf})$	$\sigma(\text{Pf})$	V <sup>H</sup>	$\sigma(\text{V}^{\text{H}})$	$\sigma(\text{V}^{\text{H}})$
uncert.	bars	bars	%	mL	mL	%
1%	30.6	4.7	15.36	162	56	34.57
2%	31.20	8.06	25.83	152.3	98	64.35
3%	31.55	10.4	32.96	145.7	128.5	88.19
5%	32.05	13.4	41.81	138.6	172.9	124.75

## 8.9. MIXED HYDRATE CRYSTALLIZATION

In this last section, more experimental results are compared to simulated results. These experimental data were obtained at high crystallization rate from CO<sub>2</sub>-CH<sub>4</sub> and CO<sub>2</sub>-CH<sub>4</sub>-C<sub>2</sub>H<sub>6</sub> gas mixtures (Le Quang et al., 2016). The objective is to investigate if the results at high crystallization rate can be simulated with good accordance with hydrate flash frameworks.

Experiments at high crystallization rate are expected to occur at non-thermodynamic equilibrium. This is why framework II\* should not be the best approach. Table 48 provides the aforementioned results.

Surprisingly, all frameworks give quite accurate results compared to experiments. Expect framework II\* (as expected), final pressure deviations are below 5%. Concerning the final hydrate volume (or  $m_w^H$ ), the deviation from the experimental results is higher, but within the 3% uncertainty ( $\pm$  standard deviation  $\sigma$ ) on the kihara parameters (or within 1% uncertainty at  $\pm$  variance). Since a kinetic effect on the hydrate crystallization was anticipated, higher deviations were prophesied.

In conclusion, it seems that CO<sub>2</sub>-CH<sub>4</sub> gas mixtures are not very much affected by kinetics. Also, framework I with 5 iterations provides the best results. This framework, combined with this number of iterations, was not the best as compared to the reference case at slow driving force. This could validate that a higher driving force is closer to framework I with no hydrate reorganization. Nevertheless, the results are more than adequate, and it would probably not be the same for other mixtures where kinetics could be predominating.

**Table 50:** Framework I ( $n=5$  and 20) and II\* predictions compared to experimental results at quick crystallization (gas 1-2 from CO<sub>2</sub>-CH<sub>4</sub> mixtures and 3-4-5 from CO<sub>2</sub>-CH<sub>4</sub>-C<sub>2</sub>H<sub>6</sub> mixtures) and slow crystallization (reference case of the present study)

Experimental					Framework I, n=20			
Gas	T <sub>f</sub> (°C)	P <sub>f</sub> (bar)	V <sup>H</sup> (mL)	m <sub>w</sub> <sup>H</sup> (g)	Pf pred (bar)	m <sub>w</sub> <sup>H</sup> pred (g)	dev P <sub>f</sub> (%)	dev m <sub>w</sub> <sup>H</sup> (%)
	(±0.1)	(±0.1)	(±0.04)	(±0.04)	(±0.1)	(±0.04)	(±0.1)	(±0.1)
Gas 1	3.4	33.3	268.4	212.0	31.6	256.0	5.0	21.0
Gas 2	2.2	29.1	217.8	172.1	28.19	186.11	3.1	8.2
Gas 3	2.2	30.7	--	--	31.59	139.9	2.9	--
Gas 4	1.0	27.1	--	--	26.21	43.1	3.3	--
Gas 5	2.75	35.4	345.3	272.8	33.87	333.5	4.3	22.0
Gas 6	1.3	27.6	160.9	127.1	28.79	123.1	4.3	3.2
Framework I, n=5					Framework II*			
Gas	T <sub>f</sub> (°C)	P <sub>f</sub> (bar)	V <sup>H</sup> (mL)	m <sub>w</sub> <sup>H</sup> (g)	Pf pred (bar)	m <sub>w</sub> <sup>H</sup> pred (g)	dev P <sub>f</sub> (%)	dev m <sub>w</sub> <sup>H</sup> (%)
	(±0.1)	(±0.1)	(±0.04)	(±0.04)	(±0.1)	(±0.04)	(±0.1)	(±0.1)
Gas 1	31.7	255.5	5.0	21.0	31.3	259.0	5.9	22.0
Gas 2	28.26	185.4	2.9	7.8	28.1	187.9	3.4	9.2
Gas 3	32.0	135.9	4.2	--	29.95	155	2.4	--
Gas 4	26.2	43.0	3.3	--	25.53	49.3	5.8	--
Gas 5	33.88	333.1	4.3	22.0	32.3	349.5	8.8	28.0
Gas 6	29.2	119.4	5.8	6.1	27.39	135.9	0.08	6.9

## 8.10. CONCLUSION

In this last chapter, a preliminary approach through flash calculation has been suggested. Since it is a hard task to perform experiments at low crystallization rate (very long experiments, subjects to apparatus issues), the modeling work can suggest another comprehensive approach of hydrate crystallization.

The chosen approach has been a thermodynamic flash modeling. The model presents different possible algorithms to take into account different mixed hydrate growths (crystal phase reorganization, heterogeneous crystal or homogeneous crystal phase).

In frameworks I and II, the crystallization is discretized in mass of hydrate. Crystal growth is supposed to occur at local thermodynamic equilibrium with the surrounding liquid (itself at thermodynamic equilibrium with the surrounding gas phase). That is to say, successive thermodynamic equilibria between liquid and the last layer of the hydrate phase are considered. These equilibria are considered before layer crystallization for framework I, and after for framework II. The discretization corresponds to the aforementioned layers of the hydrate crystal. As a consequence, the final clathrate is non-stoichiometric.

In a slightly different physical approach with a single iteration (framework II\*), the hydrate phase is completely homogeneous (local composition = global composition). To accomplish this, the crystal composition is homogenized during crystallization at each step.

The simulation results, compared to a reference case (experiment at low crystallization rate from  $\text{CO}_2\text{-CH}_4\text{-C}_2\text{H}_6$  gas mixture), are pretty accurate. All the frameworks provide deviations on final pressure and hydrate volume under 5%. Frameworks I and II give better results in terms of crystallized mass of water while framework II\* seems to be better at predicting the final pressure. Also, a study on the uncertainties due to Kihara parameters uncertainties showed that the experimental results are within the margin of error for the models (about 15% and 35% uncertainties on pressure and volume for 1% uncertainty on Kihara parameters). Concerning the discretization of the crystallization, a number above 20 iterations for the crystal growth is enough (frameworks I and II). As suspected, frameworks I and II converge when the iteration number is infinite.

It is important to notice and underline that these flash calculations are only based on thermodynamic equilibria. If different paths are investigated, then no kinetic considerations exist such as mass transfer limitation at gas/liquid interface ([Herri et al., 1999a, 1999b](#)), or possible diffusion effects at the liquid/hydrate interface ([Herri and Kwaterski, 2012](#)). These considerations might be necessary to model hydrate

crystallization at high driving force, where the final pressure could to be significantly affected.

In the end, the presented frameworks provide a usefull tool for industry and academia to predict with a more realistic accuracy the final pressure. They also give good orders of magnitude concerning the hydrate volume to be formed. For gas mixtures that do not show important kinetic effects (such as  $\text{CO}_2\text{-CH}_4$ ), predictions are still accurate and within the same uncertainties.

If the kinetic effects of the crystallization rate on the final state of mixed hydrate crystallization have not been proved yet from the experiments performed in this thesis, the modeling of the mixed hydrate growth supports the hypothesis of this work. This is also encouraging for future works.



## 9. CONCLUSION

In this thesis, an experimental and modeling work have been carried out to study the influence of the crystallization rate on mixed clathrate hydrate formation. Since the beginning of the study, mixed hydrates were suspected not to form at thermodynamic equilibrium. Could mixed hydrate formation could be the results of kinetic phenomena? This suggestion has a significant impact on the water conversion and hydrate volume, two properties of high interest.

Therefore, two experimental protocols to mixed hydrate formation have been presented: under low (cooling 0.2°C/day) and high rate of crystallization (cooling 10°C in one day). Experiments in an instrumented batch reactor have been performed according to the two methods of crystallization. With this apparatus, the gas and hydrate compositions could be measured, as well as the final pressure and water conversion. Gas mixtures have been chosen to be representative of the oil industry (from N<sub>2</sub>, CO<sub>2</sub>, CH<sub>4</sub>, C<sub>2</sub>H<sub>6</sub> and C<sub>3</sub>H<sub>8</sub>).

Then, a modeling approach, from classic van der Waals and Platteuw method, has been used to validate the assumption, as well as to investigate different hypothesis. Moreover, in order to be able to calculate the hydrate volume, a flash calculation approach has been used according to two different hypotheses (homogeneous and heterogeneous hydrate crystal)

First, in the case of a binary mixture like N<sub>2</sub>/CO<sub>2</sub>, the thermodynamic modeling is accurate, and the hydrate formation does not seem to be significantly affected by the crystallization rate.

In the case of a ternary mixture like CO<sub>2</sub>/CH<sub>4</sub>/C<sub>2</sub>H<sub>6</sub>, differences between the results have been observed in terms of hydrate composition, hydrate volume and final pressure, from a same mixture and initial state. The final pressure at low crystallization rate has been found to be lower than at high crystallization rate. The occupancy of the hydrate cavities is fore significant.

Experiments on CH<sub>4</sub>/C<sub>3</sub>H<sub>8</sub> gas mixtures have shown the same results. However, an experimental problem occurred (a leak in the reactor), and the results could not be used properly. Same remark on CH<sub>4</sub>-C<sub>2</sub>H<sub>6</sub>-C<sub>3</sub>H<sub>8</sub> gas mixture.

In the end, the modeling approach taking into account a mass balance has been chosen to study mixed hydrate formation from fundamental point of view, using experimental results of this work (CO<sub>2</sub>/CH<sub>4</sub>/C<sub>2</sub>H<sub>6</sub>), and from a previous experimental work.



Two frameworks for thermodynamic flash calculations considering mixed hydrate have been presented. Two hypotheses have been suggested: heterogeneous crystal composition due to the gas consumption during the hydrate growth and the change of thermodynamic equilibrium; or homogeneous crystal due to a reorganization of the solid phase during growth.

In the end, results were quite accurate when comparing to experimental data at slow crystallization (predicted pressure and hydrate volume within 7% accuracy). This accuracy deteriorates a bit when comparing to high rate experiments (<20%).

One conclusion could be that mixed hydrate could form at thermodynamic equilibrium at low crystallization rate. This case corresponds to steady-state processes in oil production, for example. In the case of high crystallization rate, mixed hydrate formation is likely to form a non-homogeneous crystal whose composition could be driven by kinetics.

At last, estimation of the hydrate volume to be formed is possible, helping to determine the amount of kinetic inhibitors (KHI) to use in flow-assurance issues.

Also, the modeling approach suggests a new comprehensive view of mixed hydrate crystallization that could be useful to determine essential thermodynamic parameters such as Kihara parameters. A kinetic modeling is also a significant perspective to this work.

## 10. LIST OF SYMBOLS

<b>A</b>	A particular type of guest molecule, or coefficient used in temperature correlation of dimensionless eNRTL-interaction energy parameters $\tau_{mm'}$ and $\tau_{m'm}$ of molecule-molecule interactions. $[A_1]=K$ , $[A_3]=K^{-1}$ , $A_0$ and $A_2$ , dimensionless
<b>AA</b>	Anti-Agglomerant
<b>EQ</b>	a state of equilibrium
<b><math>A_s</math></b>	Surface area of hydrate crystal, $[A_s]=m^2$
<b><math>A_\phi</math></b>	Debye-Hückel constant, dimensionless
<b>KHI</b>	Kinetic Hydrate Inhibitor
<b>B</b>	Coefficient used in temperature correlation of dimensionless eNRTL interaction energy parameters $\tau_{CA,m}$ , $\tau_{m,CA}$ , $\tau_{AC,AC'}$ , $\tau_{AC',AC}$ , $\tau_{CA,CA'}$ , $\tau_{CA',CA}$ accounting for interactions where ion-pairs are involved. $[B_1]=K$ , $B_0$ and $B_2$ , dimensionless
<b><math>B_I</math></b>	Rate of primary nucleation, $[B_I]=(\text{mol of nuclei})s^{-1}m^{-3}$
<b><math>B_{II}</math></b>	Rate of primary nucleation, $[B_{II}]=(\text{mol of nuclei})s^{-1}m^{-3}$
<b>C</b>	Langmuir constant of a guest molecule in a given cavity, $[C]$ depends on corresponding concentration/concentration dependent variable in relation to which it is defined, for example $[C_f]=Pa^{-1}$ , whereas $[C_x]$ is dimensionless, or heat capacity $[C]=JK^{-1}$ , or concentration $[C]=mol.m^{-3}$
<b><math>C_p, C_v</math></b>	Mass heat capacity at constant pressure, at constant volume, $[C]=Jkg^{-1}K^{-1}$
<b><math>\Delta</math></b>	Finite difference between two values of a quantity
<b><math>\Delta_\alpha^\beta</math></b>	Finite difference between two values of a quantity for a process from a given initial state $\alpha$ to a final state $\beta$
<b>D</b>	Diffusivity of gas in solvent, $[D]=m^2s^{-1}$
<b>d</b>	Molar transfer coefficient, appearing in Eq. (98), $[d]=mol m^{-2}s^{-1}$
<b><math>d_p</math></b>	Mean diameter of gas bubbles in a liquid $[d_p]=m$
<b>z</b>	Compressibility factor
<b>e</b>	Elementary charge, $e=(1.602176565\pm0.000000035)\times10^{-19}C$
<b>eNRTL</b>	Electrolyte NRTL (Non-Random-Two-Liquid) model for the excess Gibbs energy
<b>EOS</b>	Equation of state
<b>SRK</b>	Soave-Redlich and Kwong

$f$	Fugacity, $[f] = \text{Pa}$
$F$	Flow rate per mole of cavities, $[F] = \text{s}^{-1}$ , or flow rate $[F] = \text{moles}^{-1}$
$G$	Growth rate, $[G] = \text{ms}^{-1}$ , or Gibbs energy, $[G] = \text{J}$ , or Boltzmann kind factor in eNRTL model, dimensionless, depending on the context
$I$	Inonic strength, dimensionless
$h$	Thickness of the gas/liquid interface $[h] = \text{m}$
$H$	Enthalpy, $[H] = \text{J}$
$k$	Rate (kinetic) constant, $[k]$ can depend the choice for the generalised concentration variable $\zeta$ . With $\zeta = x$ , $[k] = \text{s}^{-1}$ , or polytropic coefficient, dimensionless
$k_1$	Rate (kinetic) constant for primary nucleation, in Eq.(41), $[k_1] = \text{mols}^{-1} \text{m}^{-3}$
$k_L$	Rate (kinetic) of gas transfer at the gas/liquid $[k_L] = \text{????}$
$k_B$	Boltzmann's constant $k_B = (1.3806488 \pm 0.0000013) \times 10^{-23} \text{ J K}^{-1}$
$k_H^\infty$	Henry's constant at saturation pressure of the pure solvent, i.e., at infinite dilution of the dissolved species, $[k_H^\infty] = \text{Pa}$
$K$	Ratio of the intrinsic kinetic constant and the Grow rate, $[K] = \text{m}^{-1}$
$l$	Diameter of spherically assumed crystal or clusters, $[l] = \text{m}$
$m$	Molality of a chemical species, $[m] = \text{mol kg}^{-1}$
$\bar{m}$	Stoichiometric molality of a component, i.e., based on component particles by disregarding possible dissociation reactions. The quantity is defined by the ratio between the amount of substance of the component and the mass of the solvent, $[\bar{m}] = \text{mol kg}^{-1}$
$\mu$	Chemical potential of a species or component, $[\mu] = \text{J mol}^{-1}$
$M$	Molar mass, $[M] = \text{g mol}^{-1}$
$M_i$	Momentum of order $i$ of a function $f$ of one variable $x$ $M_i = \int_0^\infty x^i f(x) dx$
$n$	Amount of substance, i.e. mole number, $[n] = \text{mol}$
$N$	Number in general, dimensionless
$N_{\text{cav}}$	Number of different types of cavities, dimensionless
$N_g$	Number of different types of guest species, dimensionless
$N_p$	Concentration in number of particles of a population $[N_p] = \text{m}^{-3}$
$N_{\text{Av}}$	Avogadro's number, $N_{\text{Av}} = (6.02214129 \pm 0.00000027) \times 10^{23} \text{ mol}^{-1}$

NRTL Non-Random-Two-Liquid model for the excess Gibbs energy

- $\nu$  Stoichiometric coefficient, or number of water molecules per number of guest molecules in a cage of a given type  $I$  (hydration number), dimensionless
- $p$  Pressure,  $[p] = \text{Pa}$
- $\phi$  Osmotic coefficient []
- $r$  a) Rate of the enclathration or declathration,  $[r] = \text{mol s}^{-1}$  or  $[r] = \text{s}^{-1}$  and b) distance between the centre of the cavity and the guest molecule  $[r] = \text{nm}$ , and c) gas constant,  $r = 1000 \cdot R / M$ ,  $[r] = \text{J} \cdot \text{kg}^{-1} \cdot \text{K}^{-1}$

RMSE An simple root mean square error

- $R$  Universal molar gas constant,  $R = (8.314472 \pm 0.000015) \text{J K}^{-1} \text{mol}^{-1}$ , or radius of a cavity, assumed to be of spherical geometry,  $[R] = \text{nm}$
- Re Reynolds' number of the crystal particle, dimensionless
- Sc Schmidt's number, dimensionless
- S Supersaturation, dimensionless, or given set (here of indices) in general
- Sh Sherwood's number of the crystal particle, dimensionless
- $S_{\text{cav}}$  Set of indices counting the different types of cavities
- $S_{\text{g}}$  Set of indices counting the guest molecules
- $S_{\text{p}}$  Concentration in total surface of particles of a population  $[S_{\text{p}}] = \text{m}^2 \text{m}^{-3}$
- $T$  Absolute temperature,  $[T] = \text{K}$
- VLE The vapor-liquid equilibrium
- VLH Vapor-Liquid-Hydrate
- VLHE Vapor-Liquid-Hydrate equilibrium
- $V$  Volume,  $[V] = \text{m}^3$
- $\bar{w}$  Stoichiometric weight fraction of a chemical component, i.e. weight fraction based on component particles (disregarding dissociation reactions), dimensionless
- $x$  Mole fraction of a chemical species, dimensionless; here mainly used to designate the mole fraction of guest species dissolved in the liquid phase in the immediate vicinity of the hydrate surface
- $y$  Mole fraction of a chemical species, dimensionless; here mainly used to designate the mole fraction of guest species in the gas phase
- $\bar{x}$  Stoichiometric mole fraction of a chemical component, i.e. weight fraction based on component particles (disregarding dissociation reactions), dimensionless

$X$	Effective mole fractions of species, dimensionless
$Y$	Ionic charge fractions, dimensionless
$z$	Coordination number of a cavity, dimensionless, or charge number, positive for cations, negative for anions, zero for neutral species, dimensionless
#	Number

## Subscripts

Exp	experimental result
A, A', A''	Anionic species $A^{ z_A  -}$
bulk	Referring to the bulk phase
C, C', C''	Cationic species $C^{z_C +}$
CA	Binary salt $C_{\nu_C} A_{\nu_A}$ , composed of $\nu_C$ cations, $C^{z_C +}$ , and $\nu_A$ anions, $A^{ z_A  -}$
Calc	Calculated
cav	Referring to type of cavity
cryst	During crystallisation
d	Referring to declathration process, corresponding to the deconstruction of cages at the outer surface of the hydrate crystal under simultaneous liberation of guest species
e	Referring to enclathration process, corresponding to the formation of cages at the outer surface of the hydrate crystal under simultaneous inclusion of guest species
eq	Referring to a state of equilibrium
exp data	Referring to experimental data
$f$	Indicating reference fugacity used as concentration dependent quantity $[f]$ (Pa)
fus	Property referring to the process of fusion
g	Referring to type of guest species
Gas	referring to a gas phase
Hyd	referring to clathrate hydrate, or semi clathrate hydrate
int	Interface between the integration layer and the diffusion layer
i	iteration number, or initial state, or index of cavity (1,2,3)
$i$	Index identifying a particular type of cavity
$j, l$	Index characterising chemical species or chemical component (depending on the context), or guest specie

$k$	Indicating components (molecular and strong electrolyte components)
Liq	referring to liquid phase
LC	Local Composition model
LR	Property referring to Long Range contribution
$m$	Referring to molar or partial molar quantity of a given extensive quantity
$m$	1) Referring to molecular species (as well as $m'$ ), or 2) indicating the reference to the molality as reference frame for the composition variable, depending on the context
$p$	Referring to a crystal particle, used in combination with the dimensionless parameters $Re$ , $Sc$ , $Sh$ , or total surface of particle $S$ , or referring to property at constant pressure
$q$	Index used for counting data points
Solid	referring to a solid phase
SR	Property referring to Short Range contribution
$w$	Water molecule
$x$	Indicating the reference to the mole fraction as reference frame for the composition variable
$\zeta$	Referring to generalised concentration variable in the definition of the respective quantity, $[\zeta]$ depending on the particular choice of the composition variable and hence, it can not be generally assigned
$\pm$	Mean ionic quantity
0	Indicating reference conditions for temperature and pressure, $T_0 = 273.15$ K and $p_0 = 0$ MPa, in the context of gas hydrate reference properties
$\langle \rangle$	corresponding to a cluster or crystal state
$( )$	corresponding to a "liquid state

### Superscripts

- Indicating a concentration quantity which is based on the overall or apparent composition, i.e., where the possible dissociation of the components in solution is disregarded in contrast to concentration quantities based on true chemical species
- \* Indicating the unsymmetric convention for normalisation of activity coefficients, i.e., the pure component reference frame for the solvent component and the infinitely dilution reference frame for the solute components and the solute species, respectively, or corresponding to the critical nuclei
- Pure component state

$\infty$	State of infinite dilution of a/all the solute species in the solution
$\beta$	Hypothetical reference phase for the hydrate phase corresponding to empty lattice
$\beta - \varphi$	Referring to the difference between any phase and the reference phase b
G	Gas/Vapour phase
H	Hydrate phase
I	Ice phase
L	Liquid phase
$L_w$	Liquid aqueous phase (depending on the context either an aqueous phase consisting of pure water or a liquid mixed aqueous phase composed of an aqueous solution of a single binary electrolyte)
$\pi$	Any given phase in general
ref	Reference state/frame in general
S	Solid phase in general
$\sigma$	Liquid-vapour saturation conditions
V	Vapour phase

## Greek letters

$a$	Spherical hard core radius in Kihara potential $[a] = \text{pm}$ , or coefficients in correlation of Henry's constant as function of temperature, or activity coefficient, dimensionless, or the mass transfer surface area per volume of liquid $[a] = \text{m}^{-1}$
$\alpha$	Nonrandomness factor []
$b$	Coefficient occurring in empirical temperature correlation for $\Delta_{\beta}^{L_w} C_{p,m,w}^{\circ}(T, p_0)$ , $[b] = \text{J K}^{-2} \text{mol}^{-1}$
$c$	Molar volume concentration, here in particular used to express the concentration of cavities of a given type per unit of volume, $[c] = \text{mol dm}^{-3}$ , or constant used for calculating the effective mole fractions $X$ in eNRTL equations. $c_j$ to be set to zero for $j \in S_m$ , and to $ z_j $ for $j \in S_c \cup S_A$ , respectively
$\varepsilon$	Dielectric constant, $[\varepsilon] = \text{As V}^{-1} \text{m}^{-1}$ , or characteristic energy, $[\varepsilon] = \text{J}$ , depending on the context, or Kihara parameter, maximum attraction potential, $[\varepsilon] = \text{J}$ , or energy dissipation rate, $[\varepsilon] = \text{W m}^{-3}$
$\varepsilon_G$	Gas holdup (i.e. volume gas fraction) in a liquid phase, dimensionless $[\varepsilon_G] = \text{m}^3 \text{m}^{-3}$

$\gamma$	Activity coefficient, dimensionless, or specific energy of surface $[\gamma] = \text{J m}^{-2}$ , or isentropic coefficient, dimensionless
$\nu$	Kinematic viscosity, $[\nu] = \text{m}^2 \text{s}^{-1}$ $\nu(\Theta \in [0-100^\circ\text{C}]) = 3.274 \cdot 10^{-14} \Theta^4 - 9.132 \cdot 10^{-12} \Theta^3 + 9.898 \cdot 10^{-10} \Theta^2 - 5.520 \cdot 10^{-8} \Theta + 1.778 \cdot 10^{-6}$
$\eta$	Dynamic viscosity $[\eta] = \text{Pa.s}$ $\eta(\Theta \in [0-100^\circ\text{C}]) = 3.245 \cdot 10^{-11} \Theta^4 - 9.061 \cdot 10^{-9} \Theta^3 + 9.845 \cdot 10^{-7} \Theta^2 - 5.521 \cdot 10^{-5} \Theta + 1.778 \cdot 10^{-3}$
$\omega$	Intermolecular interaction potential, $[\omega] = \text{J}$
$\sigma$	Core distance at which attraction and repulsion between a guest host-pair balance each other, or surface tension $[\sigma] = \text{N} \cdot \text{m}^{-1}$
$\sigma_{\text{rel}}$	Root mean square deviation (relative) []
$\Gamma$	Surface concentration, here particularly used for describing the number of moles, i.e., amount of substance, of active cavities of a given type per unit of surface area, $[\Gamma] = \text{mol m}^{-2}$
$\rho$	(Mass) density, $[\rho] = \text{kg m}^{-3}$
$\Theta$	Celsius temperature $[\Theta] = ^\circ\text{C}$
$\theta$	Fraction of sites occupied (by a particular species and for a specific type of cavity as indicated by additional subscripts, dimensionless
$\tau$	Energetic interaction coefficient []
$\zeta$	Generalised concentration variable, $[\zeta]$ depending on the particular choice of the composition variable and hence, it can not be generally assigned
$\Delta$	Difference
$\Phi$	Solid volume fraction in a liquid, dimensionless, $[\Phi] = \text{m}^3 \text{m}^{-3}$
$\psi$	Activation coefficient for nucleation, number between 0 and 1
$\mu$	Chemical potential, $[\mu] (\text{Jmol}_1)$
$\psi$	Activation coefficient for nucleation, number between 0 and 1





## 11. REFERENCES

- Adamson, A.W., Jones, B.R., 1971. Physical adsorption of vapors on ice. IV. Carbon dioxide. *Journal of Colloid and Interface Science* 37, 831–835. doi:10.1016/0021-9797(71)90364-X
- Adisasmito, S., Frank, R.J., Sloan, E.D., 1991. Hydrates of carbon dioxide and methane mixtures. *J. Chem. Eng. Data* 36, 68–71. doi:10.1021/je00001a020
- Adisasmito, S., Sloan, E.D., 1992. Hydrates of hydrocarbon gases containing carbon dioxide. *J. Chem. Eng. Data* 37, 343–349. doi:10.1021/je00007a020
- Al-Otaibi, F., Clarke, M., Maini, B., Bishnoi, P.R., 2011. Kinetics of structure II gas hydrate formation for propane and ethane using an in-situ particle size analyzer and a Raman spectrometer. *Chemical Engineering Science* 66, 2468–2474. doi:10.1016/j.ces.2011.03.012
- Ananthaswamy, J., Atkinson, G., 1984. Thermodynamics of concentrated electrolyte mixtures. 4. Pitzer-Debye-Hueckel limiting slopes for water from 0 to 100. degree. C and from 1 atm to 1 kbar. *Journal of Chemical and Engineering Data* 29, 81–87.
- Armenante, P.M., Kirwan, D.J., 1989. Mass transfer to microparticles in agitated systems. *Chemical Engineering Science* 44, 2781–2796. doi:10.1016/0009-2509(89)85088-2
- Avlonitis, D., 1988. Multiphase equilibria in oil-water hydrate forming systems. *Mémoire de*.
- Baba-Ahmed, A., Guilbot, P., Richon, D., 1999. New equipment using a static analytic method for the study of vapour-liquid equilibria at temperatures down to 77 K. *Fluid Phase Equilibria* 166, 225–236. doi:10.1016/S0378-3812(99)00294-0
- Baldi, G., Conti, R., Alaria, E., 1978. Complete suspension of particles in mechanically agitated vessels. *Chemical Engineering Science* 33, 21–25. doi:10.1016/0009-2509(78)85063-5
- Barrer, R.M., Edge, A.V.J., 1967a. Selective Clathration during the Formation of Gas Hydrates. *Separation Science* 2, 145–154. doi:10.1080/01496396708049922
- Barrer, R.M., Edge, A.V.J., 1967b. Gas Hydrates Containing Argon, Krypton and Xenon: Kinetics and Energetics of Formation and Equilibria. *Proceedings of the Royal Society of London A: Mathematical, Physical and Engineering Sciences* 300, 1–24. doi:10.1098/rspa.1967.0154
- Becker, R., Döring, W., 1935. The kinetic treatment of nuclear formation in supersaturated vapors. *Ann. Phys* 24, 752.

- Belandria, V., Eslamimanesh, A., Mohammadi, A.H., Richon, D., 2011. Gas Hydrate Formation in Carbon Dioxide + Nitrogen + Water System: Compositional Analysis of Equilibrium Phases. *Ind. Eng. Chem. Res.* 50, 4722–4730. doi:10.1021/ie101635k
- Boesen, R.R., SØRENSEN, H., PEDERSEN, K.S., 2014. New approach for hydrate flash calculations. *Proceedings of the 8th International Conference on Gas Hydrates (ICGH8)*.
- Botsaris, C.A.E., 1975. Differential descent methods for function minimization.
- Bouchemoua, A., Fezoua, A., Ouabbas, Y., Chauvy, F., Cameirao, A., Herri, J.-M., 2009. CO<sub>2</sub> capture by gas mixtures hydrate crystallisation, in: XII<sup>e</sup> Congrès de La Société Française de Génie Des Procédés Pour Relever Les Défis Industriels Du XXI<sup>e</sup> Siècle A La Croisée Des Sciences et Des Cultures. Société Française de Génie des Procédés.
- Bouillot, B., Herri, J.-M., 2016. Framework for clathrate hydrate flash calculations and implications on the crystal structure and final equilibrium of mixed hydrates. *Fluid Phase Equilibria, Special Issue: Gas Hydrates and Semiclathrate Hydrates* 413, 184–195. doi:10.1016/j.fluid.2015.10.023
- Burnol, A., Thinon, I., Ruffine, L., Herri, J.-M., 2015. Influence of impurities (nitrogen and methane) on the CO<sub>2</sub> storage capacity as sediment-hosted gas hydrates – Application in the area of the Celtic Sea and the Bay of Biscay. *International Journal of Greenhouse Gas Control* 35, 96–109. doi:10.1016/j.ijggc.2015.01.018
- Burton, W.K., Cabrera, N., Frank, F.C., 1951. The Growth of Crystals and the Equilibrium Structure of their Surfaces. *Philosophical Transactions of the Royal Society of London A: Mathematical, Physical and Engineering Sciences* 243, 299–358. doi:10.1098/rsta.1951.0006
- Cameirao, A., Le Ba, H., Darbouret, M., Herri, J.-M., Peytavy, J.-L., Glénat, P., 2012. Chord length distributions interpretation using a polydispersed population: Modeling and experiments. *Journal of Crystal Growth, 6th National Congress on Industrial Crystallization (CRISTAL-6)* 342, 65–71. doi:10.1016/j.jcrysgr.2011.05.028
- Carroll, J., 2014. *Natural Gas Hydrates: A Guide for Engineers*. Gulf Professional Publishing.

- Chakoumakos, B.C., Rawn, C.J., Rondinone, A.J., Stern, L.A., Circone, S., Kirby, S.H., Ishii, Y., Jones, C.Y., Toby, B.H., 2003. Temperature dependence of polyhedral cage volumes in clathrate hydrates. *Can. J. Phys.* 81, 183–189. doi:10.1139/p02-141
- Chassefière, E., Dartois, E., Herri, J.-M., Tian, F., Schmidt, F., Mousis, O., Lakhli, A., 2013. CO<sub>2</sub>–SO<sub>2</sub> clathrate hydrate formation on early Mars. *Icarus* 223, 878–891. doi:10.1016/j.icarus.2013.01.001
- Chen, C.-C., Britt, H.I., Boston, J.F., Evans, L.B., 1982. Local composition model for excess Gibbs energy of electrolyte systems. Part I: Single solvent, single completely dissociated electrolyte systems. *AIChE J.* 28, 588–596. doi:10.1002/aic.690280410
- Chen, C.-C., Evans, L.B., 1986. A local composition model for the excess Gibbs energy of aqueous electrolyte systems. *AIChE J.* 32, 444–454. doi:10.1002/aic.690320311
- Child, W.C., 1964. Thermodynamic Functions for Metastable Ice Structures I and II. *J. Phys. Chem.* 68, 1834–1838. doi:10.1021/j100789a027
- Cournil, M., Gohar, P., 1989. Thermodynamic model of supersaturated liquid solutions: Application to the homogeneous nucleation of potassium sulfate. *Journal of Colloid and Interface Science* 132, 188–199. doi:10.1016/0021-9797(89)90228-2
- Cournil, M., Herri, J.-M., 2003. Asymptotic models for gas–liquid crystallization in two-film systems. *AIChE J.* 49, 2030–2038. doi:10.1002/aic.690490813
- Danesh, A., 1998. PVT and phase behaviour of petroleum reservoir fluids. Elsevier.
- Darbouret, M., Cournil, M., Herri, J.-M., 2005. Rheological study of TBAB hydrate slurries as secondary two-phase refrigerants. *International Journal of Refrigeration* 28, 663–671. doi:10.1016/j.ijrefrig.2005.01.002
- De Roo, J.L., Peters, C.J., Lichtenthaler, R.N., Diepen, G. a. M., 1983. Occurrence of methane hydrate in saturated and unsaturated solutions of sodium chloride and water in dependence of temperature and pressure. *AIChE J.* 29, 651–657. doi:10.1002/aic.690290420
- Deaton, W.M., Frost, E.M.J., 1946. Gas Hydrates and Their Relation to the Operation of Natural-Gas Pipe Lines (No. BM-Mon-8). Bureau of Mines, Amarillo, TX (USA). Helium Research Center.
- Delsemme, A.H., Miller, D.C., 1971. Physico-chemical phenomena in comets—III. *Planetary and Space Science* 19, 1229–1257. doi:10.1016/0032-0633(71)90180-2
- Delsemme, A.H., Miller, D.C., 1970. Physico-chemical phenomena in comets—II. *Planetary and Space Science* 18, 717–730. doi:10.1016/0032-0633(70)90053-X

- Delsemme, A.H., Wenger, A., 1970. Physico-chemical phenomena in comets—I. Planetary and Space Science 18, 709–715. doi:10.1016/0032-0633(70)90052-8
- Dharmawardhana, P.B., Parrish, W.R., Sloan, E.D., 1980. Experimental Thermodynamic Parameters for the Prediction of Natural Gas Hydrate Dissociation Conditions. Ind. Eng. Chem. Fund. 19, 410–414. doi:10.1021/i160076a015
- Douzet, J., Kwaterski, M., Lallemand, A., Chauvy, F., Flick, D., Herri, J.-M., 2013. Prototyping of a real size air-conditioning system using a tetra-n-butylammonium bromide semiclathrate hydrate slurry as secondary two-phase refrigerant – Experimental investigations and modelling. International Journal of Refrigeration 36, 1616–1631. doi:10.1016/j.ijrefrig.2013.04.015
- Duc, N.H., Chauvy, F., Herri, J.-M., 2007. CO<sub>2</sub> capture by hydrate crystallization – A potential solution for gas emission of steelmaking industry. Energy Conversion and Management 48, 1313–1322. doi:10.1016/j.enconman.2006.09.024
- Dunning, W.J., 1955. p. 159, “Chemistry of the Solid State”, ed. Garner, W.E. Butterworths, London.
- Dyadin, Y., 1996. Gas hydrates: thermodynamics and structural aspects. Presented at the 2nd International conference on natural gas hydrates, Toulouse, FRANCE (02/06/1996), pp. 625–632.
- Dyadin, Y.A., Larionov, E.G., Mikina, T.V., Starostina, L.I., 1996. Clathrate hydrate of xenon at high pressure. Mendeleev Communications 6, 44–45. doi:10.1070/MC1996v006n02ABEH000571
- Dyadin, Y.A., Larionov, E.G., Mirinskij, D.S., Mikina, T.V., Starostina, L.I., 1996. Hydrate formation in the krypton - water and xenon - water systems up to 10 kbar. Presented at the 2nd International conference on natural gas hydrates, Toulouse, FRANCE (02/06/1996), pp. 59–66.
- Englezos, P., Bishnoi, P.R., 1991. Experimental study on the equilibrium ethane hydrate formation conditions in aqueous electrolyte solutions. Ind. Eng. Chem. Res. 30, 1655–1659. doi:10.1021/ie00055a038
- Englezos, P., Kalogerakis, N., Dholabhai, P.D., Bishnoi, P.R., 1987a. Kinetics of formation of methane and ethane gas hydrates. Chemical Engineering Science 42, 2647–2658. doi:10.1016/0009-2509(87)87015-X
- Englezos, P., Kalogerakis, N., Dholabhai, P.D., Bishnoi, P.R., 1987b. Kinetics of gas hydrate formation from mixtures of methane and ethane. Chemical Engineering Science 42, 2659–2666. doi:10.1016/0009-2509(87)87016-1

- Englezos, P., Ngan, Y.T., 1993. Incipient equilibrium data for propane hydrate formation in aqueous solutions of sodium chloride, potassium chloride and calcium chloride. *J. Chem. Eng. Data* 38, 250–253. doi:10.1021/je00010a017
- Falabella, B.J., 1975. A study of natural gas hydrates.
- Falabella, B.J., Vanpee, M., 1974. Experimental Determination of Gas Hydrate Equilibrium below the Ice Point. *Ind. Eng. Chem. Fund.* 13, 228–231. doi:10.1021/i160051a012
- Fan, S.-S., Guo, T.-M., 1999. Hydrate Formation of CO<sub>2</sub>-Rich Binary and Quaternary Gas Mixtures in Aqueous Sodium Chloride Solutions. *J. Chem. Eng. Data* 44, 829–832. doi:10.1021/je990011b
- Farkas, L., 1927. Keimbildungsgeschwindigkeit in übersättigten Dämpfen. *Z. phys. Chem* 125, 236–242.
- Fidel-Dufour, A., Gruy, F., Herri, J.M., 2005. Experimental characterization and modelling of the rheological properties of methane hydrate slurries during their crystallisation in a water in dodecane emulsion under laminar flowing. *Chemical Engineering Science* 61, 505–515.
- Fray, N., Marboeuf, U., Brissaud, O., Schmitt, B., 2010. Equilibrium Data of Methane, Carbon Dioxide, and Xenon Clathrate Hydrates below the Freezing Point of Water. Applications to Astrophysical Environments. *J. Chem. Eng. Data* 55, 5101–5108. doi:10.1021/je1006604
- Galfré, A., 2014. Captage du dioxyde de carbone par cristallisation de clathrate hydrate en présence de cyclopentane : Etude thermodynamique et cinétique (phdthesis). Ecole Nationale Supérieure des Mines de Saint-Etienne.
- Galfré, A., Kwaterski, M., Brântuas, P., Cameirao, A., Herri, J.-M., 2014. Clathrate Hydrate Equilibrium Data for the Gas Mixture of Carbon Dioxide and Nitrogen in the Presence of an Emulsion of Cyclopentane in Water. *J. Chem. Eng. Data* 59, 592–602. doi:10.1021/je4002587
- Galloway, T.J., Ruska, W., Chapplelear, P.S., Kobayashi, R., 1970. Experimental Measurement of Hydrate Numbers for Methane and Ethane and Comparison with Theoretical Values. *Ind. Eng. Chem. Fund.* 9, 237–243. doi:10.1021/i160034a008
- Green, D., Perry, R., 2007. *Perry's Chemical Engineers' Handbook*, Eighth Edition. McGraw Hill Professional.

- Guilbot, P., Valtz, A., Legendre, H., Richon, D., 2000. Rapid on-line sampler-injector: a reliable tool for HT-HP sampling and on-line GC analysis. *Analisis* 28, 426–431.
- Gutt, C., Asmussen, B., Press, W., Johnson, M.R., Handa, Y.P., Tse, J.S., 2000. The structure of deuterated methane-hydrate. *The Journal of Chemical Physics* 113, 4713–4721. doi:10.1063/1.1288789
- Hachikubo, A., Miyamoto, A., Hyakutake, K., Abe, K., Shoji, H., 2002. High pressure cell experiments for gas hydrate formation processes, in: *Fourth International Conference on Gas Hydrates, Japan*. p. 357–360.
- Handa, Y.P., Tse, J.S., 1986. Thermodynamic properties of empty lattices of structure I and structure II clathrate hydrates. *J. Phys. Chem.* 90, 5917–5921. doi:10.1021/j100280a092
- Herri, J.-M., 1996. Etude de la formation de l'hydrate de méthane par turbidimétrie *in situ* (phdthesis). Université Pierre et Marie Curie - Paris VI; Ecole Nationale Supérieure des Mines de Saint-Etienne.
- Herri, J.-M., Bouchemoua, A., Kwaterski, M., Brântuas, P., Galfré, A., Bouillot, B., Douzet, J., Ouabbas, Y., Cameirao, A., 2014. Enhanced Selectivity of the Separation of CO<sub>2</sub> from N<sub>2</sub> during Crystallization of Semi-Clathrates from Quaternary Ammonium Solutions. *Oil & Gas Science and Technology – Revue d'IFP Energies nouvelles* 69, 947–968. doi:10.2516/ogst/2013201
- Herri, J.-M., Bouchemoua, A., Kwaterski, M., Fezoua, A., Ouabbas, Y., Cameirao, A., 2011. Gas hydrate equilibria for CO<sub>2</sub>-N<sub>2</sub> and CO<sub>2</sub>-CH<sub>4</sub> gas mixtures—Experimental studies and thermodynamic modelling. *Fluid Phase Equilibria* 301, 171–190. doi:10.1016/j.fluid.2010.09.041
- Herri, J.-M., Chassefière, E., 2012. Carbon dioxide, argon, nitrogen and methane clathrate hydrates: Thermodynamic modelling, investigation of their stability in Martian atmospheric conditions and variability of methane trapping. *Planetary and Space Science, Solar System science before and after Gaia* 73, 376–386. doi:10.1016/j.pss.2012.07.028
- Herri, J.M., Gruy, F., Pic, J.S., Cournil, M., Cingotti, B., Siquin, A., 1999a. Interest of *in situ* turbidimetry for the characterization of methane hydrate crystallization: Application to the study of kinetic inhibitors. *Chemical Engineering Science* 54, 1849–1858. doi:10.1016/S0009-2509(98)00433-3

- Herri, J.-M., Kwaterski, M., 2012. Derivation of a Langmuir type of model to describe the intrinsic growth rate of gas hydrates during crystallisation from gas mixtures. *Chemical Engineering Science* 81, 28–37. doi:10.1016/j.ces.2012.06.016
- Herri, J.-M., LeBa, H., Cameirao, A., Darbouret, M., Peytavy, J.-L., Glenat, P., 2009. Interpretation and modeling of chord length distribution from FBRM results during gas hydrate formation and agglomeration from water-in-oil emulsion, in: *ABSTRACTS OF PAPERS OF THE AMERICAN CHEMICAL SOCIETY. AMER CHEMICAL SOC 1155 16TH ST, NW, WASHINGTON, DC 20036 USA.*
- Herri, J.M., Pic, J.S., Gruy, F., Cournil, M., 1999b. Methane hydrate crystallization mechanism from in-situ particle sizing. *AIChE J.* 45, 590–602. doi:10.1002/aic.690450316
- Herslund, P.J., Thomsen, K., Abildskov, J., von Solms, N., Galfré, A., Brântuas, P., Kwaterski, M., Herri, J.-M., 2013. Thermodynamic promotion of carbon dioxide-clathrate hydrate formation by tetrahydrofuran, cyclopentane and their mixtures. *International Journal of Greenhouse Gas Control* 17, 397–410. doi:10.1016/j.ijggc.2013.05.022
- Hester, K.C., Huo, Z., Ballard, A.L., Koh, C.A., Miller, K.T., Sloan, E.D., 2007. Thermal Expansivity for sI and sII Clathrate Hydrates. *J. Phys. Chem. B* 111, 8830–8835. doi:10.1021/jp0715880
- Holder, G.D., Corbin, G., Papadopoulos, K.D., 1980. Thermodynamic and molecular properties of gas hydrates from mixtures containing methane, argon, and krypton. *Industrial & Engineering Chemistry Fundamentals* 19, 282–286.
- Holder, G.D., Grigoriou, G.C., 1980. Hydrate dissociation pressures of (methane + ethane + water) existence of a locus of minimum pressures. *The Journal of Chemical Thermodynamics* 12, 1093–1104. doi:10.1016/0021-9614(80)90166-4
- Holder, G.D., Hand, J.H., 1982. Multiple-phase equilibria in hydrates from methane, ethane, propane and water mixtures. *AIChE J.* 28, 440–447. doi:10.1002/aic.690280312
- Holder, G.D., Kamath, V.A., 1982. Experimental determination of dissociation pressures for hydrates of the cis- and trans-isomers of 2-butene below the ice temperature. *The Journal of Chemical Thermodynamics* 14, 1119–1128. doi:10.1016/0021-9614(82)90034-9



- Ikeda, T., Mae, S., Yamamuro, O., Matsuo, T., Ikeda, S., Ibberson, R.M., 2000. Distortion of Host Lattice in Clathrate Hydrate as a Function of Guest Molecule and Temperature. *J. Phys. Chem. A* 104, 10623–10630. doi:10.1021/jp001313j
- Ikeda, T., Yamamuro, O., Matsuo, T., Mori, K., Torii, S., Kamiyama, T., Izumi, F., Ikeda, S., Mae, S., 1999. Neutron diffraction study of carbon dioxide clathrate hydrate. *Journal of Physics and Chemistry of Solids* 60, 1527–1529. doi:10.1016/S0022-3697(99)00165-1
- Jeffrey, G.A., 1984. Hydrate inclusion compounds. *Journal of inclusion phenomena* 1, 211–222.
- Jhaveri, J., Robinson, D.B., 1965. Hydrates in the methane-nitrogen system. *The Canadian Journal of Chemical Engineering* 43, 75–78.
- John, V.T., Holder, G.D., 1982a. Contribution of second and subsequent water shells to the potential energy of guest-host interactions in clathrate hydrates. *J. Phys. Chem.* 86, 455–459. doi:10.1021/j100393a008
- John, V.T., Holder, G.D., 1982b. Hydrates of methane + butane below the ice point. *J. Chem. Eng. Data* 27, 18–21. doi:10.1021/je00027a004
- John, V.T., Papadopoulos, K.D., Holder, G.D., 1985. A generalized model for predicting equilibrium conditions for gas hydrates. *AIChE J.* 31, 252–259. doi:10.1002/aic.690310212
- Jones, C.Y., Marshall, S.L., Chakoumakos, B.C., Rawn, C.J., Ishii, Y., 2003. Structure and Thermal Expansivity of Tetrahydrofuran Deuterate Determined by Neutron Powder Diffraction. *J. Phys. Chem. B* 107, 6026–6031. doi:10.1021/jp020513n
- Kashchiev, D., 1984. The kinetic approach to nucleation. *Cryst. Res. Technol.* 19, 1413–1423. doi:10.1002/crat.2170191102
- Kashchiev, D., Firoozabadi, A., 2003. Induction time in crystallization of gas hydrates. *Journal of Crystal Growth* 250, 499–515. doi:10.1016/S0022-0248(02)02461-2
- Kashchiev, D., Firoozabadi, A., 2002a. Driving force for crystallization of gas hydrates. *Journal of Crystal Growth* 241, 220–230. doi:10.1016/S0022-0248(02)01134-X
- Kashchiev, D., Firoozabadi, A., 2002b. Nucleation of gas hydrates. *Journal of Crystal Growth* 243, 476–489. doi:10.1016/S0022-0248(02)01576-2
- Katz, J.L., Spaepen, F., 1978. A kinetic approach to nucleation in condensed systems. *Philosophical Magazine Part B* 37, 137–148. doi:10.1080/01418637808226648
- Katz, J.L., Wiedersich, H., 1977. Nucleation theory without Maxwell Demons. *Journal of Colloid and Interface Science* 61, 351–355. doi:10.1016/0021-9797(77)90397-6

- Klauda, J.B., Sandler, S.I., 2005. Global Distribution of Methane Hydrate in Ocean Sediment. *Energy Fuels* 19, 459–470. doi:10.1021/ef049798o
- Kobayashi, R., Katz, D.L., others, 1949. Methane hydrate at high pressure. *Journal of Petroleum Technology* 1, 66–70.
- Kubota, H., Shimizu, K., Tanaka, Y., Makita, T., 1984. THERMODYNAMIC PROPERTIES OF R13 (CCIF<sub>3</sub>), R23 (CHF<sub>3</sub>), R152a (C<sub>2</sub>H<sub>4</sub>F<sub>2</sub>), AND PROPANE HYDRATES FOR DESALINATION OF SEA WATER. *Journal of Chemical Engineering of Japan* 17, 423–429. doi:10.1252/jcej.17.423
- Kvenvolden, K.A., 1993. Gas hydrates—geological perspective and global change. *Rev. Geophys.* 31, 173–187. doi:10.1029/93RG00268
- Kvenvolden, K.A., Claypool, G.E., Threlkeld, C.N., Dendy Sloan, E., 1984. Geochemistry of a naturally occurring massive marine gas hydrate. *Organic Geochemistry* 6, 703–713. doi:10.1016/0146-6380(84)90091-3
- Larson, S.D., 1955. Phase Studies of the Two-Component Carbon Dioxide-Water System. Involving the Carbon Dioxide Hydrate, University of Illinois.
- Le Quang, D., 2013. Equilibre des hydrates de gaz en présence d'un mélange d'hydrocarbures gazeux. Saint-Etienne, EMSE.
- Le Quang, D., Le Quang, D., Bouillot, B., Herri, J.-M., Glenat, P., Duchet-Suchaux, P., 2016. Experimental procedure and results to measure the composition of gas hydrate, during crystallization and at equilibrium, from N<sub>2</sub>-CO<sub>2</sub>-CH<sub>4</sub>-C<sub>2</sub>H<sub>6</sub>-C<sub>3</sub>H<sub>8</sub>-C<sub>4</sub>H<sub>10</sub> gas mixtures. *Fluid Phase Equilibria, Special Issue: Gas Hydrates and Semiclathrate Hydrates* 413, 10–21. doi:10.1016/j.fluid.2015.10.022
- Leba, H., Cameirao, A., Herri, J.-M., Darbouret, M., Peytavy, J.-L., Glénat, P., 2010. Chord length distributions measurements during crystallization and agglomeration of gas hydrate in a water-in-oil emulsion: Simulation and experimentation. *Chemical Engineering Science* 65, 1185–1200. doi:10.1016/j.ces.2009.09.074
- Makogon, T., Sloan, J., E., 1995. Phase Equilibrium for Methane Hydrate from 190 to 262K. *J. Chem. Eng. Data* 40, 344–344. doi:10.1021/je00017a901
- Makogon, T.Y., Sloan, E.D.J., 1994. Phase Equilibrium for Methane Hydrate from 190 to 262 K. *J. Chem. Eng. Data* 39, 351–353. doi:10.1021/je00014a035
- Marshall, D.R., Saito, S., Kobayashi, R., 1964. Hydrates at high pressures: Part I. Methane-water, argon-water, and nitrogen-water systems. *AIChE J.* 10, 202–205. doi:10.1002/aic.690100214

- McKoy, V., Sinanoğlu, O., 1963. Theory of Dissociation Pressures of Some Gas Hydrates. *The Journal of Chemical Physics* 38, 2946–2956. doi:10.1063/1.1733625
- McLeod, H.O., Campbell, J.M., 1961. Natural Gas Hydrates at Pressures to 10,000 psia. *Journal of Petroleum Technology* 13, 590–594. doi:10.2118/1566-G-PA
- Mehta, A.P., Sloan, E.D., 1996. Improved thermodynamic parameters for prediction of structure H hydrate equilibria. *AIChE J.* 42, 2036–2046. doi:10.1002/aic.690420724
- Mehta, V.D., Sharma, M.M., 1971. Mass transfer in mechanically agitated gas—liquid contactors. *Chemical Engineering Science* 26, 461–479. doi:10.1016/0009-2509(71)83019-1
- Mersmann, A., Angerhöfer, M., Gutwald, T., Sangl, R., Wang, S., 1992. General prediction of median crystal sizes. *Separations Technology* 2, 85–97. doi:10.1016/0956-9618(92)80011-2
- Michelsen, M.L., 1990a. A method for incorporating excess Gibbs energy models in equations of state. *Fluid Phase Equilibria* 60, 47–58. doi:10.1016/0378-3812(90)85042-9
- Michelsen, M.L., 1990b. A modified Huron-Vidal mixing rule for cubic equations of state. *Fluid Phase Equilibria* 60, 213–219. doi:10.1016/0378-3812(90)85053-D
- Miller, B., Strong, E.R., 1946. Hydrate storage of natural gas. *American Gas Association Monthly* 28, 63–67.
- Miller, S.L., Smythe, W.D., 1970. Carbon Dioxide Clathrate in the Martian Ice Cap. *Science* 170, 531–533. doi:10.1126/science.170.3957.531
- Mohammadi, A.H., Afzal, W., Richon, D., 2008a. Gas hydrates of methane, ethane, propane, and carbon dioxide in the presence of single NaCl, KCl, and CaCl<sub>2</sub> aqueous solutions: Experimental measurements and predictions of dissociation conditions. *The Journal of Chemical Thermodynamics* 40, 1693–1697. doi:10.1016/j.jct.2008.06.015
- Mohammadi, A.H., Afzal, W., Richon, D., 2008b. Experimental Data and Predictions of Dissociation Conditions for Ethane and Propane Simple Hydrates in the Presence of Methanol, Ethylene Glycol, and Triethylene Glycol Aqueous Solutions. *J. Chem. Eng. Data* 53, 683–686. doi:10.1021/jc700527d
- Mohammadi, A.H., Richon, D., 2010a. Clathrate hydrate dissociation conditions for the methane+cycloheptane/cyclooctane+water and carbon dioxide+cycloheptane/cyclooctane+water systems. *Chemical Engineering Science* 65, 3356–3361. doi:10.1016/j.ces.2010.02.027

- Mohammadi, A.H., Richon, D., 2010b. Ice–Clathrate Hydrate–Gas Phase Equilibria for Air, Oxygen, Nitrogen, Carbon Monoxide, Methane, or Ethane + Water System. *Ind. Eng. Chem. Res.* 49, 3976–3979. doi:10.1021/ie901820u
- Mohan, R., Kaytancioglu, O., Myerson, A.S., 2000. Diffusion and cluster formation in supersaturated solutions of ammonium sulfate at 298 K. *Journal of Crystal Growth* 217, 393–403. doi:10.1016/S0022-0248(00)00528-5
- Mooijer-Van den Heuvel, M.M., 2004. Phase Behaviour and Structural Aspects of Ternary Clathrate Hydrate Systems. The Role of Additives (Dissertation). TU Delft, Delft University of Technology.
- Muromachi, S., Nagashima, H.D., Herri, J.-M., Ohmura, R., 2013. Thermodynamic modeling for clathrate hydrates of ozone. *The Journal of Chemical Thermodynamics* 64, 193–197. doi:10.1016/j.jct.2013.05.020
- Myerson, A.S., Lo, P.Y., 1990. Diffusion and cluster formation in supersaturated solutions. *Journal of Crystal Growth* 99, 1048–1052. doi:10.1016/S0022-0248(08)80079-6
- Nagashima, H.D., Fukushima, N., Ohmura, R., 2016. Phase equilibrium condition measurements in carbon dioxide clathrate hydrate forming system from 199.1 K to 247.1 K. *Fluid Phase Equilibria*, Special Issue: Gas Hydrates and Semiclathrate Hydrates 413, 53–56. doi:10.1016/j.fluid.2015.09.020
- Nixdorf, J., Oellrich, L.R., 1997. Experimental determination of hydrate equilibrium conditions for pure gases, binary and ternary mixtures and natural gases. *Fluid Phase Equilibria* 139, 325–333. doi:10.1016/S0378-3812(97)00141-6
- Noguera, C., Fritz, B., Clément, A., Baronnet, A., 2006a. Nucleation, growth and ageing scenarios in closed systems I: A unified mathematical framework for precipitation, condensation and crystallization. *Journal of Crystal Growth* 297, 180–186. doi:10.1016/j.jcrysgro.2006.08.049
- Noguera, C., Fritz, B., Clément, A., Baronnet, A., 2006b. Nucleation, growth and ageing scenarios in closed systems II: Dynamics of a new phase formation. *Journal of Crystal Growth* 297, 187–198. doi:10.1016/j.jcrysgro.2006.08.048
- Ogienko, A.G., Kurnosov, A.V., Manakov, A.Y., Larionov, E.G., Ancharov, A.I., Sheromov, M.A., Nesterov, A.N., 2006. Gas Hydrates of Argon and Methane Synthesized at High Pressures: Composition, Thermal Expansion, and Self-Preservation. *J. Phys. Chem. B* 110, 2840–2846. doi:10.1021/jp053915e

- Ohgaki, K., Takano, K., Sangawa, H., Matsubara, T., Nakano, S., 1996. Methane Exploitation by Carbon Dioxide from Gas Hydrates—Phase Equilibria for CO<sub>2</sub>-CH<sub>4</sub> Mixed Hydrate System—. *Journal of Chemical Engineering of Japan* 29, 478–483. doi:10.1252/jcej.29.478
- Parrish, W.R., Prausnitz, J.M., 1972. Dissociation Pressures of Gas Hydrates Formed by Gas Mixtures. *Ind. Eng. Chem. Proc. Des. Dev.* 11, 26–35. doi:10.1021/i260041a006
- Patil, S.L., 1987. Measurement of multiphase gas hydrate phase equilibria: Effect of inhibitors and heavier hydrocarbon components.
- PIC, J.-S., HERRI, J.-M., Cournil, M., 2000. Mechanisms of Methane Hydrate Crystallization in a Semibatch Reactor: Influence of a Kinetic Inhibitor: Polyvinylpyrrolidone. *Annals of the New York Academy of Sciences* 912, 564–575.
- Pitzer, K.S., 1980. Electrolytes. From dilute solutions to fused salts. *Journal of the American Chemical Society* 102, 2902–2906.
- Pitzer, K.S., 1977. Electrolyte theory-improvements since Debye and Hückel. *Accounts of Chemical Research* 10, 371–377.
- Pitzer, K.S., 1973. Thermodynamics of electrolytes. I. Theoretical basis and general equations. *J. Phys. Chem.* 77, 268–277. doi:10.1021/j100621a026
- Rawn, C.J., Rondinone, A.J., Chakoumakos, B.C., Circone, S., Stern, L.A., Kirby, S.H., Ishii, Y., 2003. Neutron powder diffraction studies as a function of temperature of structure II hydrate formed from propane. *Can. J. Phys.* 81, 431–438. doi:10.1139/p03-022
- Reamer, H.H., Selleck, F.T., Sage, B.H., 1952. Some Properties of Mixed Paraffinic and Olefinic Hydrates. *Journal of Petroleum Technology* 4, 197–202. doi:10.2118/952197-G
- Ribeiro Jr., C.P., Lage, P.L.C., 2008. Modelling of hydrate formation kinetics: State-of-the-art and future directions. *Chemical Engineering Science* 63, 2007–2034. doi:10.1016/j.ces.2008.01.014
- Roberts, O.L., Brownscombe, E.R., Howe, L.S., Ramser, H., 1940. Constitution diagrams and composition of methane and ethane hydrates. *Oil Gas J* 39, 37–41.
- Robinson, D.B., Metha, B.R., 1971. Hydrates In the PropaneCarbon Dioxide- Water System. *Journal of Canadian Petroleum Technology* 10. doi:10.2118/71-01-04

- Rondinone, A.J., Chakoumakos, B.C., Rawn, C.J., Ishii, Y., 2003. Neutron Diffraction Study of Structure I and Structure II Trimethylene Oxide Clathrate Deuterate. *J. Phys. Chem. B* 107, 6046–6050. doi:10.1021/jp027127q
- Schmitt, B., 1986. La surface de la glace: structure, dynamique et interactions: implications astrophysiques (Theses). Université Scientifique et Médicale de Grenoble.
- Seo, Y.-T., Kang, S.-P., Lee, H., Lee, C.-S., Sung, W.-M., 2000. Hydrate phase equilibria for gas mixtures containing carbon dioxide: A proof-of-concept to carbon dioxide recovery from multicomponent gas stream. *Korean J. Chem. Eng.* 17, 659–667. doi:10.1007/BF02699114
- Shpakov, V.P., Tse, J.S., Tulk, C.A., Kvamme, B., Belosludov, V.R., 1998. Elastic moduli calculation and instability in structure I methane clathrate hydrate. *Chemical Physics Letters* 282, 107–114. doi:10.1016/S0009-2614(97)01241-4
- Skovborg, P., Rasmussen, P., 1994. A mass transport limited model for the growth of methane and ethane gas hydrates. *Chemical Engineering Science* 49, 1131–1143. doi:10.1016/0009-2509(94)85085-2
- Skovborg, P., Rasmussen, P., 1994. Comments on: hydrate dissociation enthalpy and guest size. *Fluid Phase Equilibria* 96, 223–231. doi:10.1016/0378-3812(94)80098-7
- Sloan, E.D., 2005. A changing hydrate paradigm—from apprehension to avoidance to risk management. *Fluid Phase Equilibria, PPEPPD 2004 Proceedings* 228–229, 67–74. doi:10.1016/j.fluid.2004.08.009
- Sloan, J.E.D.S., 1998. *Clathrate Hydrates of Natural Gases*, Second Edition, Revised and Expanded. CRC Press.
- Sloan, J.E.D.S., Koh, C., 2007. *Clathrate Hydrates of Natural Gases*, Third Edition. CRC Press.
- Sparks, K.A., Tester, J.W., 1992. Intermolecular potential energy of water clathrates: the inadequacy of the nearest-neighbor approximation. *J. Phys. Chem.* 96, 11022–11029. doi:10.1021/j100205a075
- Sridharan, K., Sharma, M.M., 1976. New systems and methods for the measurement of effective interfacial area and mass transfer coefficients in gas—liquid contactors. *Chemical Engineering Science* 31, 767–774. doi:10.1016/0009-2509(76)80049-8
- Stackelberg, M. v, Müller, H.R., 1951. On the Structure of Gas Hydrates. *The Journal of Chemical Physics* 19, 1319–1320. doi:10.1063/1.1748038

- Sum, A.K., Koh, C.A., Sloan, E.D., 2009. Clathrate hydrates: from laboratory science to engineering practice. *Industrial & Engineering Chemistry Research* 48, 7457–7465.
- Svandal, A., Kvamme, B., Grànàsy, L., Pusztai, T., Buanes, T., Hove, J., 2006. The phase-field theory applied to CO<sub>2</sub> and CH<sub>4</sub> hydrate. *Journal of Crystal Growth*, The 16th American Conference on Crystal Growth and Epitaxy ACCGE 16 The 12th Biennial Workshop on OMVPE OMVPE 12 287, 486–490. doi:10.1016/j.jcrysgr.2005.11.071
- Takeya, S., Kida, M., Minami, H., Sakagami, H., Hachikubo, A., Takahashi, N., Shoji, H., Soloviev, V., Wallmann, K., Biebow, N., Obzhairov, A., Salomatin, A., Poort, J., 2006. Structure and thermal expansion of natural gas clathrate hydrates. *Chemical Engineering Science* 61, 2670–2674. doi:10.1016/j.ces.2005.11.049
- Takeya, S., Nagaya, H., Matsuyama, T., Hondoh, T., Lipenkov, V.Y., 2000. Lattice Constants and Thermal Expansion Coefficient of Air Clathrate Hydrate in Deep Ice Cores from Vostok, Antarctica. *J. Phys. Chem. B* 104, 668–670. doi:10.1021/jp993344o
- Tee, L.S., Gotoh, S., Stewart, W.E., 1966a. Molecular Parameters for Normal Fluids. Kihara Potential with Spherical Core. *Ind. Eng. Chem. Fund.* 5, 363–367. doi:10.1021/i160019a012
- Tee, L.S., Gotoh, S., Stewart, W.E., 1966b. Molecular Parameters for Normal Fluids. Lennard-Jones 12-6 Potential. *Ind. Eng. Chem. Fund.* 5, 356–363. doi:10.1021/i160019a011
- Thakore, J.L., Holder, G.D., 1987. Solid vapor azeotropes in hydrate-forming systems. *Ind. Eng. Chem. Res.* 26, 462–469. doi:10.1021/ie00063a011
- Thiam, A., 2008. L'étude des conditions thermodynamiques et cinétiques du procédé de captage de CO<sub>2</sub> par formation d'hydrates de gaz: Application au mélange CO<sub>2</sub>-CH<sub>4</sub> (phdthesis). Ecole Nationale Supérieure des Mines de Saint-Etienne.
- Tohidi, B., Burgass, R.W., Danesh, A., Todd, A.C., 1993. Hydrate Inhibition Effect of Produced Water: Part 1—Ethane and Propane Simple Gas Hydrates. Society of Petroleum Engineers. doi:10.2118/26701-MS
- Tonnet, N., Herri, J.-M., 2009. Methane hydrates bearing synthetic sediments—Experimental and numerical approaches of the dissociation. *Chemical Engineering Science* 64, 4089–4100. doi:10.1016/j.ces.2009.05.043
- Tse, J.S., 1987. *J. de Physique (Paris)*, Colloq. C1.

- Udachin, K.A., Ratcliffe, C.I., Ripmeester, J.A., 2002. Single Crystal Diffraction Studies of Structure I, II and H Hydrates: Structure, Cage Occupancy and Composition. *Journal of Supramolecular Chemistry*, Special Issue to Honor the Memory of Professor Yuri Dyadin 2, 405–408. doi:10.1016/S1472-7862(03)00049-2
- Uno, K., Sarashina, E., Arai, Y., Saito, S., 1975. Application of the Perturbation Theory to the Calculation of Henry's Constants for Normal Fluids. *Journal of Chemical Engineering of Japan* 8, 201–206. doi:10.1252/jcej.8.201
- Unruh, C.H., Katz, D.L., 1949. Gas Hydrates of Carbon Dioxide-Methane Mixtures. *Journal of Petroleum Technology* 1, 83–86. doi:10.2118/949983-G
- van der Waals, J.H. van der, Platteeuw, J.C., 1959. Clathrate Solutions, in: Prigogine, I. (Ed.), *Advances in Chemical Physics*. John Wiley & Sons, Inc., pp. 1–57.
- Verma, D.P.S., Nash, D.T., Schulman, H.M., 1974. Isolation and in vitro translation of soybean leghaemoglobin mRNA. *Nature* 251, 74–77. doi:10.1038/251074a0
- Verma, V.K., 1974. Gas hydrates from liquid hydrocarbon-water systems.
- Verma, V.K., 1971. A method of calculation for two-dimensional and axisymmetric boundary layers.
- Vidal, J., Allieu, Y., Fassio, B., Adrey, J., Goalard, C., 1973a. Réduction du spondylolisthésis par le matériel de Harrington. *Proceedings of the SICOT* 646–647.
- Vidal, J., Goalard, C., Escare, P., Allieu, Y., 1973b. Normalisation d'une prothèse de toute l'extrémité supérieure du fémur. *J Chir* 106, 125–134.
- Volmer, M., 1929. Über Keimbildung Und Keimwirkung Als Spezialfälle Der Heterogenen Katalyse. *Zeitschrift für Elektrochemie und angewandte physikalische Chemie* 35, 555–561. doi:10.1002/bbpc.192900026
- Volmer, M., Weber, A., 1926a. Keimbildung in übersättigten Gebilden. *Z. phys. Chem* 119, 277–301.
- Volmer, M., Weber, A., 1926b. Nucleation in super-saturated products. *Zeitschrift fuer Physikalische Chemie, (Fed. Republic of Germany)* 119, 277–301.
- Volmer, M., Weber, A., 1926c. Nucleus formation in supersaturated systems. *Z. Phys. Chem* 119.
- Volmer, M., Weber, A., 1926d. Novel growth mechanism in heteroepitaxial semiconductor growth. *Z. Phys. Chem* 119, 277.
- Vysniauskas, A., Bishnoi, P.R., 1985. Kinetics of ethane hydrate formation. *Chemical Engineering Science* 40, 299–303. doi:10.1016/0009-2509(85)80070-1



- Vysniauskas, A., Bishnoi, P.R., 1983. A kinetic study of methane hydrate formation. *Chemical Engineering Science* 38, 1061–1072. doi:10.1016/0009-2509(83)80027-X
- Wilke, C.R., Chang, P., 1955. Correlation of diffusion coefficients in dilute solutions. *AIChE J.* 1, 264–270. doi:10.1002/aic.690010222
- Yang, S.O., Cho, S.H., Lee, H., Lee, C.S., 2001. Measurement and prediction of phase equilibria for water + methane in hydrate forming conditions. *Fluid Phase Equilibria, Proceedings of the 14th symposium on thermophysical properties* 185, 53–63. doi:10.1016/S0378-3812(01)00456-3
- Yasuda, K., Ohmura, R., 2008. Phase Equilibrium for Clathrate Hydrates Formed with Methane, Ethane, Propane, or Carbon Dioxide at Temperatures below the Freezing Point of Water. *J. Chem. Eng. Data* 53, 2182–2188. doi:10.1021/jc800396v
- Zettlemoyer, A.C., 1969. *Nucleation*. Dekker New York.

## 12. APPENDIX 1: CALCULATION OF THE VOLUME OF REACTOR

### Theory

The gas introduced into the reactor (in this case, N<sub>2</sub>) then waiting until the gas is stability in reactor (pressure and temperature not change). The quantity of gas initial can be calculated by equation is given below:

$$n_0 = \frac{P_0 V_r}{Z_0 R T_0} \quad (138)$$

After inject water the first time,

$$n_1 = \frac{P_1 (V_r - V_w)}{Z_1 R T_1} \quad (139)$$

We have a relationship between  $n_1$  and  $n_0$  are presented:

$$n_1 = n_0 - n_{diss} \quad (140)$$

So we have to determine mole number of gas solubility in water ( $n_{diss}$ ) through the application of Henry's law.

**Henry's law:**

$$H_i = H_{i,Psat} \exp\left(\frac{v_i^\infty (P - P_i^{sat})}{RT}\right) \text{ With } H_{i,Psat} = \exp\left(A + \frac{B}{T}\right) \quad (141)$$

### Calculating the compressibility factor:

For this study we chose an equation of state type Soave-Redlich-Kwong, together with those of Peng and Robinson & Trebble-Bishnoi, is among the most widely used in the field of hydrates. The state equation is of the form:

$$P = \frac{RT}{V-b} - \frac{a}{V.(V+b)} \quad (142)$$

Where V is the molar volume and both coefficients *a* and *b* depends on the nature of the gas and temperature such that:

$$a = 0.4278 \frac{R^2 T_c^2}{P_c} \cdot \left[ 1 + (0.480 + 1.875\omega - 0.176\omega^2) \cdot \left( 1 - \sqrt{\frac{T}{T_c}} \right) \right]^2 \quad (143)$$

$$b = 0.08664 \frac{RT_c}{P_c} \quad (144)$$

After some arithmetic manipulations on the equation of state easy to show that the compressibility factor Z is a solution of the cubic equation:

$$Z^3 - Z^2 + (A - B^2 - B)Z - AB = 0 \quad (145)$$

with

$$A = \frac{aP}{R^2 T^2}, \quad B = \frac{bP}{RT} \quad (146)$$

The calculation of the compressibility factor Z was conducted using the constants reported in Table 51 is given below:

**Table 51:** Constants necessary for the calculation of the compressibility factor

Gas	PC (MPa)	TC (°K)	ω (--)
N <sub>2</sub>	3,35	126,2	0,040

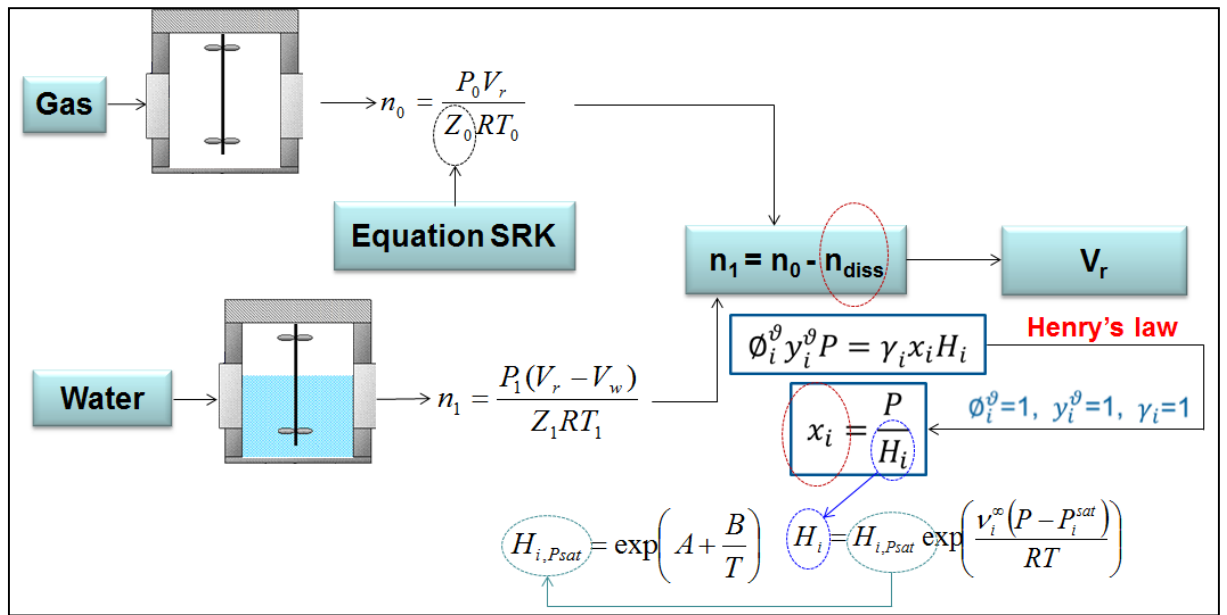


**Figure 60:** Schematic of the calculation of the Volume of Reactor

## Measurements

Initially, the cleaning of reactor equipment then the reactor is evacuated by a vacuum pump in 40÷50 minutes.

### Step 1: Injection of N<sub>2</sub> gas

The N<sub>2</sub> gas is injected until the pressure reach up to 20 bars. Then waiting the pressure and temperature are stability (not change), after that, to mark the number of values.

### Step 2: Injection of water (H<sub>2</sub>O)

The stirrer is stopped, the water used in our experiments is deionized water and introduce into reactor by using a HPLC pump (JASCO). Each time, we injected about 400 gam ( $m_{H_2O} = 400.84$  gam). Then waiting the pressure and temperature are stability (not change), after that, to mark the number of values.

### Step 3: Injection of water (H<sub>2</sub>O) at second time

Do the same step 2.

The Experimental is slooped three times to finish (see data on [Table 52](#)).

## Results

In these experiments, the gas compositions are presented in [Table 52](#). In the experimental results, we present details on the mass of the water infection each time, as well as results on P-T (Pressure and Temperature) obtained from experiments.

**Table 52:** Experiment data

Exp 1			Exp 2			Exp 3		
H <sub>2</sub> O (gram)	P <sub>0</sub> (bar)	T <sub>0</sub> (°C)	H <sub>2</sub> O (gram)	P <sub>0</sub> (bar)	T <sub>0</sub> (°C)	H <sub>2</sub> O (gram)	P <sub>0</sub> (bar)	T <sub>0</sub> (°C)
0	21,4	20,4	0	11,2	20,6	0	16,1	17,7
400,84	25,7	20,5	406,75	13,5	20,7	400,84	19,3	18,4
801,68	31,9	20,5	807,52	16,8	20,9	801,68	24	18,7
1202,52	42,2	20,5	1208,39	22,2	21	1202,55	31,9	19

For the calculation of the volume of the reactor, we chose an equation of state type Soave-Redlich-Kwong, together with those of Peng and Robinson & Trebble-Bishnoi, also, we used the equation of Henry's which to determine mole number of gas solubility in water ( $n_{diss}$ ). The final results are given below on [Table 53](#):

**Table 53:** The results of the calculation

P (mPa)	T (°K)	n mole	n <sub>diss</sub> mole	X <sub>diss</sub> mole	H <sub>i</sub> , P <sub>sat</sub>	H <sub>i</sub>
2.14	293,55	2,14085981	0	1,62624E-16	84807,5814	1,2988E+17
2.57	293,65	2,14085981	1,5618E-17	7,01942E-19	84998,0078	3,6138E+19
3.19	293,65	2,14085981	1,1467E-20	2,57687E-22	84998,0078	1,2219E+23
4.22	293,65	2,14085981	3,1208E-26	4,6753E-28	84998,0078	8,909E+28

P <sub>sat</sub> (mPa)	Z (SRK)	V (N <sub>2</sub> ) (lite)	m <sub>water</sub> (gam)	n <sub>water</sub> (mole)	Z (PGL)	Z(SRK)-(PGL)	Evaluation
0	0,9991585	0,0024396	0	0	0,9991585	1,11E-16	should be =0
0	0,9992961	0,0020388	400,84	22,250001	1,0024321	0,003136	should be =0
0	0,9996353	0,001638	801,68	44,500002	0,9996353	9,995E-09	should be =0
0	1,0006332	0,0012371	1202,52	66,750003	0,9987862	0,001847	should be =0

n <sub>init</sub>	2,100125438	variable
V <sub>r</sub>	0,002439647	variable

So, the result of the volume of the reactor is  $V_r = 2,44L$  (ACACIA system), also we do the same with SECOHYA system and the result obtained  $V=2.36L$  (SECOHYA system)

### 13. APPENDIX 2: CALIBRATION OF GAS CHROMATOGRAPHY

- $CO_2-N_2$  gas mixture

#### Theory

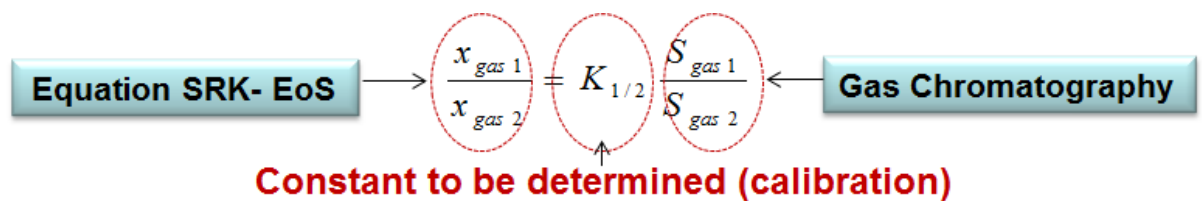


**Figure 61:** Schematic of calibration of Gas Chromatography (GC)

Calibration of the GC is the quantity calculated by the equation below:

$$\frac{x_{gas1}}{x_{gas2}} = K_{1/2} \frac{S_{gas1}}{S_{gas2}} \quad (147)$$

Where the peak area ratio of the gas1 and gas2 ( $\frac{S_{gas1}}{S_{gas2}}$ ) is obtained from results GC, and the molefraction ration of the gas1 and gas2 ( $\frac{x_{gas1}}{x_{gas2}}$ ). We can use SRK-EOS equations

#### Measurements

Initially, the cleaning of reactor equipment then the reactor is evacuated by a vacuum pump in 40÷50 minutes.

Step 1: Injection of  $N_2$  gas

The  $N_2$  gas is injected until the pressure reach up to 6 bars. Then waiting the pressure and temperature are stability (not change), after that, to mark the number of values.

Step 2: Injection of  $CO_2$

The stirrer is stopped; the second gas, CO<sub>2</sub> is injected into reactor. Then waiting the pressure and temperature are stability (not change), after that, to mark the number of values.

Step 3: Injection of CO<sub>2</sub>

Do the same step 2

The Experimental is slooped several times until the pressure reach up to 40÷45 bars.  
(See [Table 54](#))

**Table 54:** Experiment results

Exp n°	P (bar)	T (0C)	S <sub>N2</sub>	S <sub>CO2</sub>
N2	6,2	5,2	12111,6	0
1	11,2	5,15	11344,6	11153,6
	16,1	5,35	11722,3	23561,3
	20,6	5,5	11469,9	35082,1
	25,6	5,45	11051,5	47588,8
	30,5	5,5	11245	63922,6
	35,2	5,5	10799	77865,1
	40,5	5,2	10376,6	95846,3
	44,3	5,05	9711,9	105058,5
N2	4,2	5,8	8668,9	0
2	7,5	5,65	9285,9	8565,2
	11,4	5,75	8359,5	17252,9
	15,1	5,8	8360,1	27056,5
	18,9	5,8	8894,5	40029,9
	22,8	5,8	8490,9	50334,7
	26,7	5,25	8377,5	62451
	30,7	5,2	8749,8	80312,5
	34,7	5,2	7938,7	87747,4
	38,6	5,2	8289,3	108756,1
CO2	6,6	5,35	0	15124,9
3	11,2	5,35	10037	16984
	16	5,5	21049,7	17262,8
	21,4	5,2	35714	18907,2
	28,1	5,2	52678,2	19186,3
	36,5	5,3	81148,1	21263,3
	40,7	5,25	93885,8	21568,3
	46	5,3	112882,3	22608,3
CO2	4,1	5,05	0	5991,5
4	8	5,1	6311	7482,9
	13,2	5,25	14896,7	7761,8

17,1	5,3	21962	8078,6
20,6	5,35	28925,6	8392,9
23,4	5	44691,5	11166,6
26,7	5,05	54963,1	11753,1
29,4	5,15	67052,8	12776,6
32,1	5,15	80049	13789,2
34,3	5,15	89183	14203,2
37	5,25	86014,3	12595,5
39,7	5,25	102246,2	13836,6
41,6	5,25	108124,7	13892,8
44,2	5,25	123596,9	14936,4
46,4	5	118037,9	13642,5

## Results

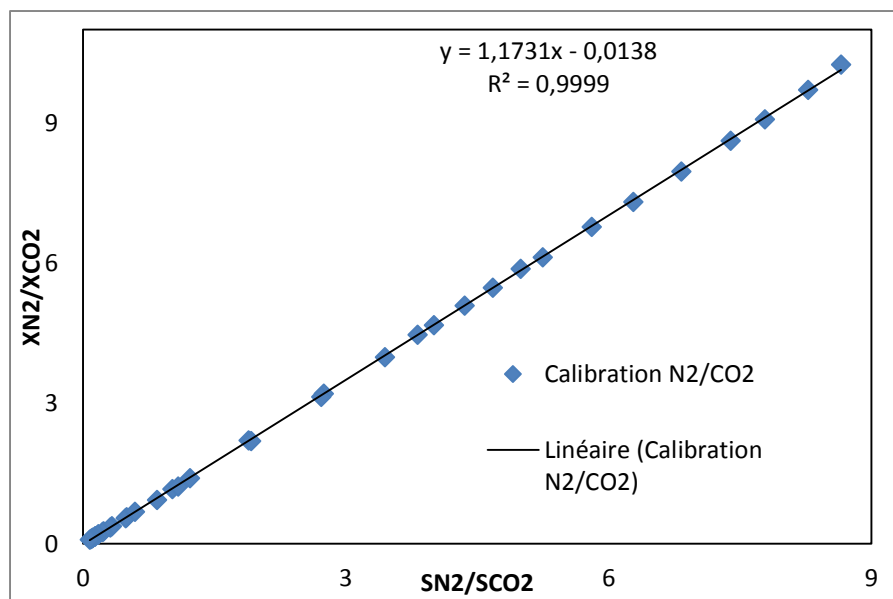


**Figure 62:** Calibration curve of gas chromatograph of CO<sub>2</sub>-N<sub>2</sub> gas mixture

The result is given certainty between the point on curve ( $y = 1.1731x - 0.0138$ ) compare with in fact is 3.2%.

Do the same method with other gas mixtures in our experiments.



- $CH_4$ - $C_3H_8$  gas mixture

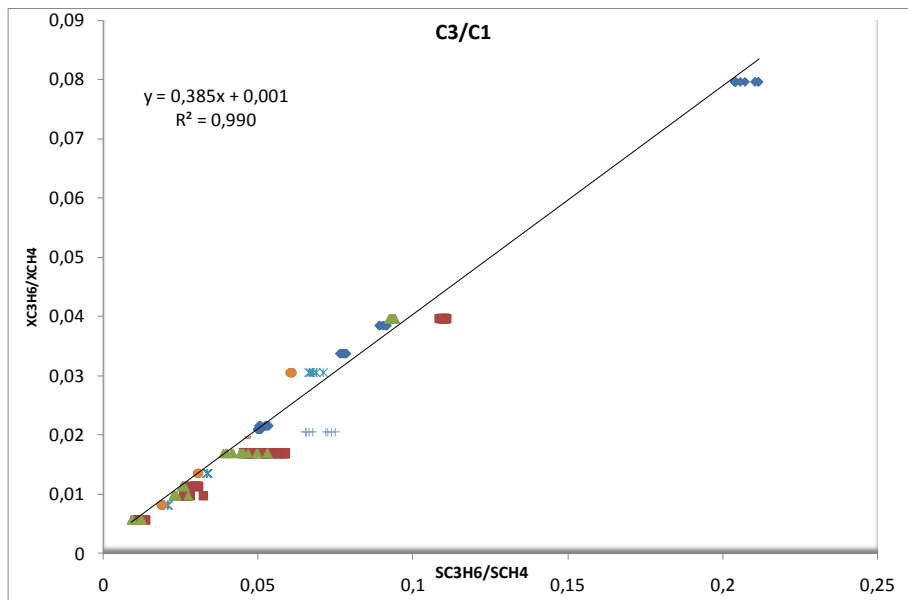


**Figure 63:** Calibration curve of gas chromatograph of  $CH_3$ - $C_3H_8$  gas mixture

- $CO_2$ - $CH_4$  gas mixture

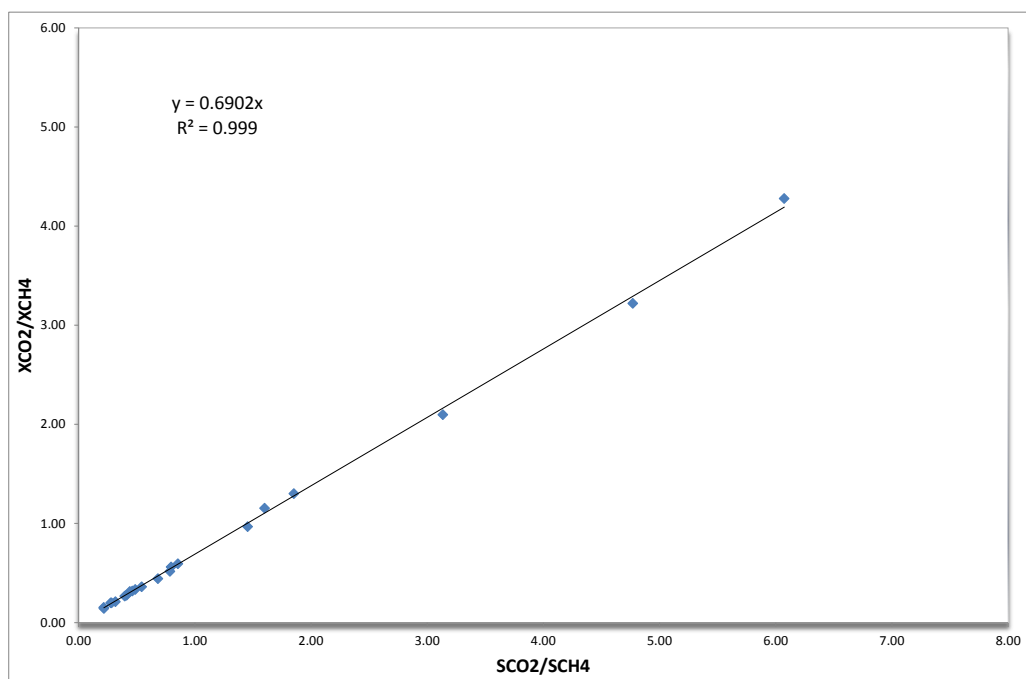


**Figure 64:** Calibration curve of the gas chromatograph for CO<sub>2</sub>-CH<sub>4</sub>

- C<sub>2</sub>H<sub>6</sub>-C<sub>3</sub>H<sub>8</sub> gas mixture

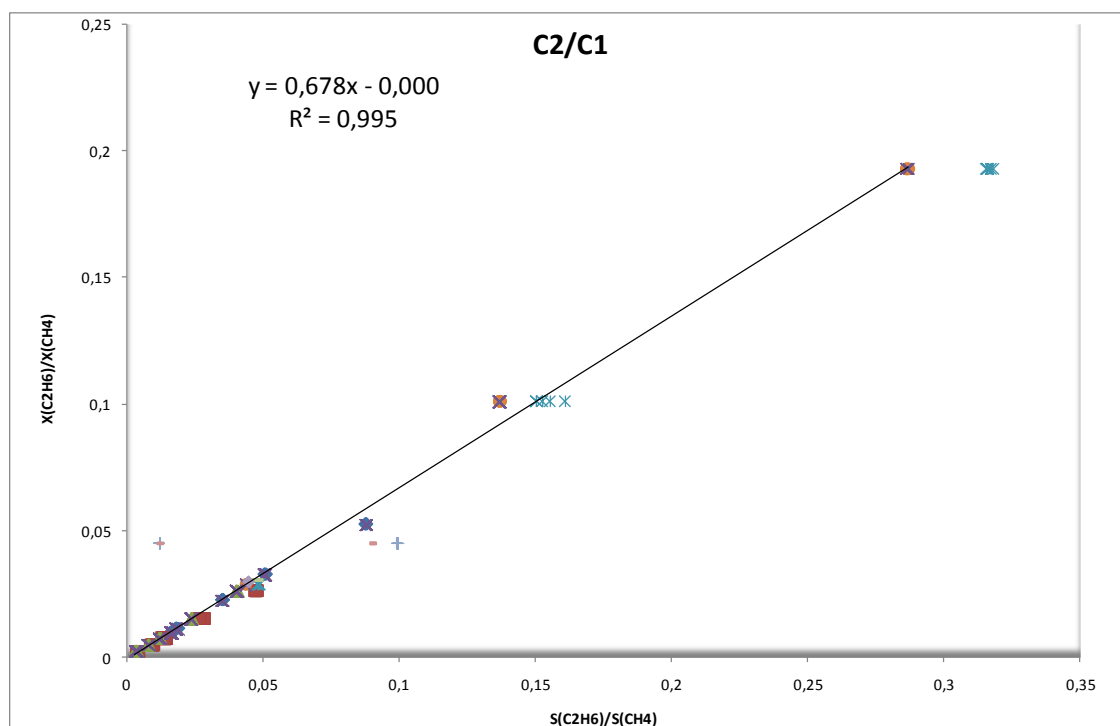


**Figure 65:** Calibration curve of the gas chromatograph for C<sub>2</sub>H<sub>6</sub>-CH<sub>4</sub>



## 14. APPENDIX 3: EVALUATION OF ERRORS CALCULATION

- *Evaluation of the initial quantity of gases in the reactor from pressure balance.*

The principle of the preparation of the gases is to generate a binary mixture (for example CO<sub>2</sub> and N<sub>2</sub>) with a given molar composition (y(A) and y(B)) by the following procedure:

- 0- Temperature is controlled to T value
- 1- After vacuuming, a volume V of reactor (temperature T), inject the first gas (A) into the reactor up to a pressure P1
- 2- Inject second gas (B) to a pressure P2
- 3- Back calculate the molar composition n<sub>A</sub>, n<sub>A+B</sub> and n<sub>B</sub> = n<sub>A+B</sub>-n<sub>A</sub> by using the following algorithm (Figure 66)

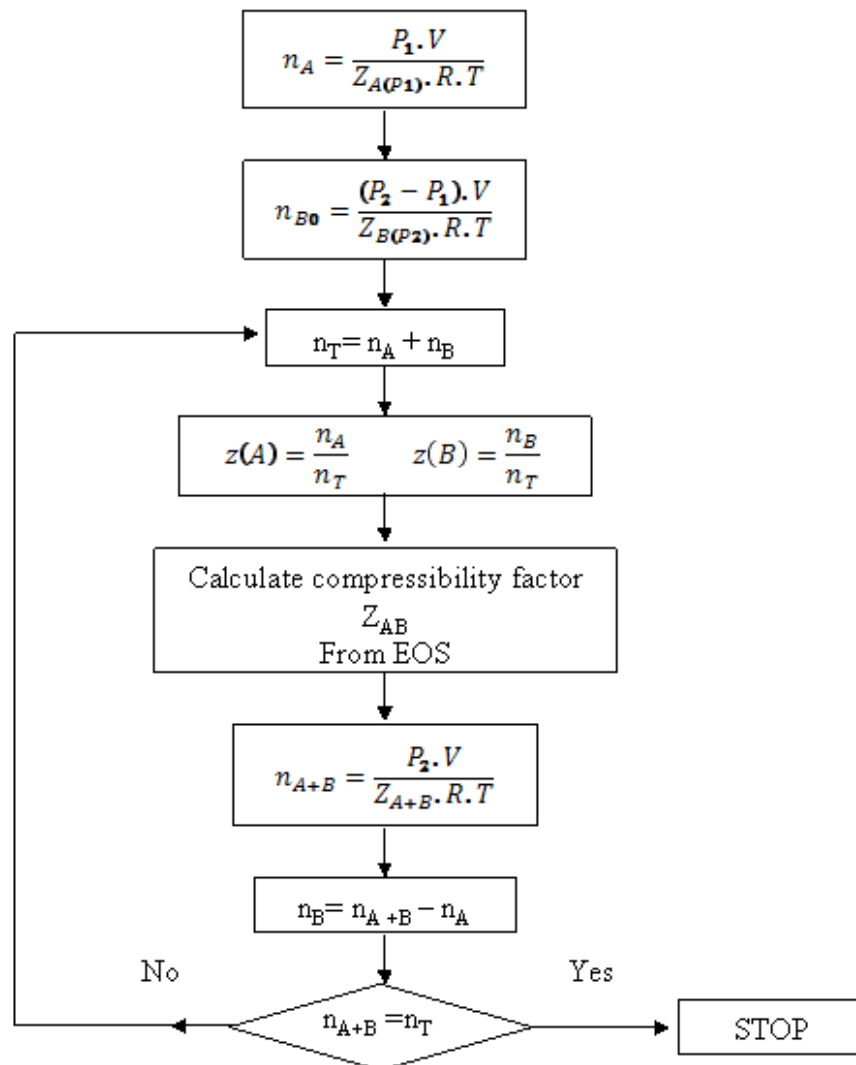


**Figure 66:** Algorithm of calculation on the molar composition

## Calculation of error

After convergence, the gas composition is calculated from

$$n_A = \frac{P_1 V}{Z_{A(P1)} RT} \quad n_{A+B} = n^G = \frac{P_2 V}{Z_{A+B(P2)} RT} \quad n_B = \frac{P_2 V}{Z_{A+B(P2)} RT} - n_A \quad (148)$$

So, a direct evaluation of error on  $n_A$  and  $n_{A+B}$  gives

$$\frac{\Delta n_A}{n_A} = \frac{\Delta P_1}{P_1} + \frac{\Delta V}{V} + \frac{\Delta Z_{A(P1)}}{Z_{A(P1)}} + \frac{\Delta T}{T} \quad (149)$$

and

$$\frac{\Delta n_{A+B}}{n_{A+B}} = \frac{\Delta P_2}{P_2} + \frac{\Delta V}{V} + \frac{\Delta Z_{A+B(P2)}}{Z_{A+B(P2)}} + \frac{\Delta T}{T} \quad (150)$$

So finally

$$\frac{\Delta n_B}{n_B} = \frac{1}{y(B)} \frac{\Delta n_{A+B}}{n_{A+B}} + \frac{y(A)}{y(B)} \frac{\Delta n_A}{n_A} \quad (151)$$

The error on evaluation of pressure is  $\Delta P = 0.01 \text{ mPa}$

The error on evaluation of reactor is volume  $\Delta V = 0.001 \text{ lite}$

The error on the valuation of compressibility factor is not evaluated here, and considered as negligible compared to other

The error on temperature is  $\Delta T = 0.02 \text{ }^\circ\text{K}$

In regard to the precision of the instrument, the error is mainly due to the precision in the evaluation of the pressure:

$$\frac{\Delta n_A}{n_A} \approx \frac{\Delta P_1}{P_1} \quad \text{and} \quad \frac{\Delta n_{A+B}}{n_{A+B}} \approx \frac{\Delta P_2}{P_2} \quad \text{and} \quad \frac{\Delta n_B}{n_B} \approx \frac{1}{y(B)} \frac{\Delta P_{A+B}}{P_{A+B}} + \frac{y(A)}{y(B)} \frac{\Delta P_A}{P_A} \quad (152)$$

- *Evaluation of the error on  $y^{(A)}$  and  $y^{(B)}$  from gas chromatography*

After sampling of the gas phase, once  $\frac{S(A)}{S(B)}$  has been determined by gas chromatography, the value of  $\frac{y(A)}{y(B)}$  is determined from the previous calibration curve:

$$a = \frac{y(A)}{y(B)} \text{ and } y(A) + y(B) = 1; \text{ so } y(A) \left(1 + \frac{1}{a}\right) = y(A) \frac{1+a}{a} \text{ and } y(A) = \frac{a}{1+a} \quad (153)$$

So, the error on the evaluation of  $y^{(A)}$  (or  $y^{(B)}$ ) is

$$\frac{\Delta y(A)}{y(A)} = \frac{\Delta y(B)}{y(B)} = \frac{2\Delta a}{a} \quad (154)$$

and value of 2%

- *Evaluation of the error  $err_j^G$  of the mole number of gas in the gas phase at time t.*

At time t, the composition of the gas is given from gas chromatography ( $\Delta y/y = 0.02$ ) and pressure measurement ( $\Delta P = 0.01 \text{ mPa}$ ).

$$n^G = \frac{P V_R}{Z(T, p, y_j) R T} \text{ and } n_j^G = n^G y_j \quad (155)$$

$$\frac{\Delta n_j^G}{n_j^G} = \frac{\Delta n^G}{n^G} + \frac{\Delta y_j}{y_j} \text{ and } \frac{\Delta n^G}{n^G} \approx \frac{\Delta P}{P} \quad (156)$$

With  $\Delta P = 0.01 \text{ mPa}$  and  $\Delta y/y = 0.02$ , we obtain an estimation of the error that is always superior to 2%, inferior to 3% as soon as the pressure is superior to 0.5 mPa, and inferior to 2.5% as soon as the pressure is superior to 1 MPa. In our experiments, pressure is always superior to 1 MPa, and we will retain that

$$err_j^G = \frac{\Delta n_j^G}{n_j^G} = 0.025 \quad (157)$$

- *Evaluation of the error on the calculation of the gas mole number consumption between two steps at phase at time t1 and t2*

We evaluate the error on the calculation of  $n_{j0}^G - n_j^G$  that is the quantity of gas that has been transferred to solution, i.e. dissolution and crystallisation.

$$n_{j0}^G - n_j^G = \frac{P_0 V_R}{Z(T, P_0, y_{j0})RT} y_{j0} - \frac{P V_R}{Z(T, P, y_j)RT} y_j \quad (158)$$

In a good approximation, we can write

$$n_{j0}^G - n_j^G \approx \frac{V_R}{\bar{Z}RT} (P_0 y_{j0} - P y_j) \quad (159)$$

with

$$\bar{Z} = \frac{Z(T, P_0, y_{j0}) + Z(T, P, y_j)}{2} \quad (160)$$

Secondly, in consideration that the evaluation of the mole number is first order depend on the precision of pressure P and composition z, we can write:

$$d(n_{j0}^G - n_j^G) = \frac{V_R}{\bar{Z}RT} (dP_0 y_{j0} + P_0 dy_{j0} - dP y_j - P dy_j) \quad (161)$$

So

$$\Delta(n_{j0}^G - n_j^G) = \frac{V_R}{\bar{Z}RT} (\Delta P_0 (y_{j0} + y_j) + (P_0 + P)(\Delta y)) \quad (162)$$

$$\frac{\Delta(n_{j0}^G - n_j^G)}{n_{j0}^G - n_j^G} < \left( 2 \frac{\Delta P_0}{P_0} + 2(\Delta y) \right) < 5\% \quad (163)$$

The same calculation can be done for the total amount of gas:

$$\frac{\Delta(n_0^G - n^G)}{n_0^G - n^G} = 2 \frac{\Delta P_0}{P_0} \quad (164)$$

- Evaluation of the error  $err_j^L$  of the mole number of gas in the liquid phase at time  $t$

Gas composition of the liquid phase is determined from a Henry correlation (see in the mole number of gas in the liquid phase at method calculation of mass balance).

$$n_j^L = \frac{V^L \rho_w^\circ}{M_w} \frac{y_j \phi_j^G P}{K_{H,j}^\infty \exp(P v_j^\infty / RT)} \quad (165)$$

In a first approximation, we can write that:

$$\frac{\Delta n_j^L}{n_j^L} = \frac{\Delta V^L}{V^L} + \frac{\Delta K_{H,j}^\infty}{K_{H,j}^\infty} + \frac{\Delta P}{P} \quad (166)$$

With

$$V^L = \frac{V_0^L [Li^+]_0}{[Li^+]} \quad (167)$$

and so

$$\frac{\Delta V^L}{V^L} = \frac{\Delta V_0^L}{V_0^L} + \frac{\Delta [Li^+]_0}{[Li^+]_0} + \frac{\Delta [Li^+]}{[Li^+]} \quad (168)$$

$\frac{\Delta V_0^L}{V_0^L} \ll 0.001$  because it is determined from mass measurement, with precision of 0.01g and total mass of water around 1 kg.

$\frac{\Delta [Li^+]}{[Li^+]} \ll 0.001$  in reason of the precision of the ionic chromatography

So, we can give an evaluation of

$$\frac{\Delta n_j^L}{n_j^L} \approx \frac{\Delta K_{H,j}^\infty}{K_{H,j}^\infty} + \frac{\Delta P}{P} \quad (169)$$



Without an evaluation of the precision of the Henry constant, we will overestimate it to 10%, so that  $err_j^L = \frac{\Delta n_j^L}{n_j^L} \approx 0.1$ . We will see after there is no consequence on the evaluation of the mole number of gas in the hydrate phase (see following) because of low quantity of gas in the liquid phase in respect to the quantity in the gas phase and hydrate phase;

- *Evaluation of error of the mole number of gas in the hydrate phase.*

The mole number of gas in the hydrate phase is calculated from a mass balance from Eq. (115)

$$n_j^H = n_j^L + n_j^G - n_{j,0} \quad (170)$$

In a first approximation, because of the very low solubility of gases in water, we have also

$$n_j^L \ll n_j^H \text{ and } n_j^H \approx n_j^G - n_{j,0} \quad (171)$$

So, from Eq. (163) we obtain

$$\frac{\Delta n_j^H}{n_j^H} \approx \frac{\Delta(n_j^G - n_{j,0})}{n_j^G - n_{j,0}} < 5\% \quad (172)$$

- *Evaluation of the error on the calculation of composition (molar fraction) of gas in the hydrate*

In a first approximation that assumes the quantity of gas in liquid is negligible compared to other quantities (hydrate and gas phases), we can write:

$$x_j^H = \frac{n_j^H}{\sum_i n_i^H} = \frac{n_j^H}{n_0^G - n^G} \quad (173)$$

and

$$dx_j^H = \frac{dn_j^H}{n_0^G - n^G} - \frac{1}{(n_0^G - n^G)^2} n_j^H d(n_0^G - n^G) \quad (174)$$

that gives

$$\Delta x_j^H = \frac{\Delta n_j^H}{n_0^G - n^G} + \frac{n_j^H}{n_0^G - n^G} \frac{\Delta(n_0^G - n^G)}{n_0^G - n^G} \quad (175)$$

with Eq. (163)

$$\frac{\Delta(n_0^G - n^G)}{n_0^G - n^G} = 2 \frac{\Delta P_0}{P_0} \quad (176)$$

we get

$$\Delta x_j^H = \frac{n_j^H}{n^H} 0.05 + \frac{n_j^H}{n^H} 0.01 \quad (177)$$

So, finally, the evaluation is:

$$\frac{\Delta x_j^H}{x_j^H} < 0.06 \quad (178)$$





NNT: **2016LYSEM002**

Quang-Du LE

## INVESTIGATION OF NON-EQUILIBRIUM CRYSTALLIZATION OF MIXED GAS CLATHRATES HYDRATES: AN EXPERIMENTAL STUDY COMPARED TO THERMODYNAMIC MODELING WITH AND WITHOUT FLASH CALCULATIONS

Speciality: Process engineering

Keywords: Gas Hydrates, Thermodynamic, Kinetic, Crystallization, CO<sub>2</sub> capture and storage, Flow assurance, Phase equilibria, Flash calculations

### Abstract:

The scientific goal of this thesis is based on the acquisition of experimental data and the modeling of the composition of clathrates gas hydrate. The domains of application concern the gas separation and storage, water purification, and energy storage using change phase materials (PCMs).

Our research team has recently demonstrated that the composition of gas hydrates was sensitive to the crystallization conditions, and that the phenomenon of formation was out of thermodynamic equilibrium.

During this thesis, we have investigated several types of crystallization, which are based on the same initial states. The goal is to point out the differences between the initial solution composition and the final solution composition, and to establish a link between the final state and the crystallization rate.

Depending on the rate of crystallization (slow or fast), the acquisition time of experimental data lasted from a few days to several weeks. The experimental tests were performed inside a stirred batch reactor (autoclave, 2.44 or 2.36 L) cooled with a double jacket. Real-time measurements of the composition of the gas and the liquid phases have been performed, in order to calculate the composition of the hydrate phase using mass balance calculations. Depending on the crystallization mode, we have identified several variations of the composition of the hydrate phase and final hydrate volume.

We have established a successful thermodynamic model, which indicates the composition of the hydrate phase and hydrate volume in thermodynamic equilibrium state using a gas mixture which had never been used before in the literature. So this thermodynamic model has required an extremely slow experimental test. These tests were also long in order to be sure of the thermodynamic equilibrium state.

We are currently establishing a kinetics model in order to model the deviations from the reference point of equilibrium of our experimental tests which were carried out at a high crystallization rate.

NNT: **2016LYSEM002**

Quang-Du LE

# INVESTIGATION DE LA CRISTALLISATION HORS-ÉQUILIBRE DES CLATHRATES HYDRATES DE GAZ MIXTES: UNE ÉTUDE EXPÉRIMENTALE COMPARÉE À LA MODÉLISATION THERMODYNAMIQUE AVEC ET SANS CALCULS FLASH

Spécialité: Génie des Procédés

Mots clefs: Clathrate hydrates, Captage et Stockage du CO<sub>2</sub>, Thermodynamique, Cinétique, Cristallisation, Flow assurance, Phase équilibrais, Calculs flash.

## Résumé :

L'activité scientifique du sujet porte sur l'acquisition de données expérimentales et la modélisation de la composition des clathrates hydrates de gaz. Les domaines d'application concernent la séparation et le stockage de gaz, la purification de l'eau, et le stockage d'énergie par matériaux à changement de phase.

L'équipe a mis en évidence il y a quelques années que la composition des hydrates de gaz était sensible aux conditions de cristallisation, et que le phénomène de formation se produisait en dehors de l'équilibre thermodynamique.

Le travail de thèse a permis d'explorer plusieurs modes de cristallisation à partir de solutions de même composition initiale pour observer les différences concernant l'état final, compositions notamment, et les relier à la vitesse de cristallisation.

Suivant le mode de cristallisation, lent ou rapide, l'acquisition des données expérimentales peut prendre de quelques jours à plusieurs semaines. Les expériences sont réalisées en réacteur pressurisé dans lequel nous mesurons en ligne la composition de la phase gaz et de la phase liquide, pour calculer par bilan de matière la composition de la phase hydrate.

Nous avons bien mis en évidence des variations dans la composition de la phase hydrate suivant le mode de cristallisation. Nous avons dû établir un modèle thermodynamique donnant la composition de la phase hydrate à l'équilibre pour des mélanges de gaz qui n'avaient jamais été traité par la littérature, et qui ont donc nécessité des campagnes de mesure extrêmement lentes et donc longues pour être sûr de l'état thermodynamique à l'équilibre.

Nous sommes en cours d'établir un modèle cinétique pour modéliser les écarts à cet état d'équilibre de référence pour nos expériences réalisées à vitesse de cristallisation rapide.